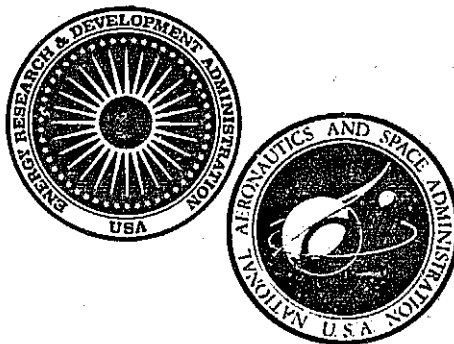


## **General Disclaimer**

### **One or more of the Following Statements may affect this Document**

- This document has been reproduced from the best copy furnished by the organizational source. It is being released in the interest of making available as much information as possible.
- This document may contain data, which exceeds the sheet parameters. It was furnished in this condition by the organizational source and is the best copy available.
- This document may contain tone-on-tone or color graphs, charts and/or pictures, which have been reproduced in black and white.
- This document is paginated as submitted by the original source.
- Portions of this document are not fully legible due to the historical nature of some of the material. However, it is the best reproduction available from the original submission.

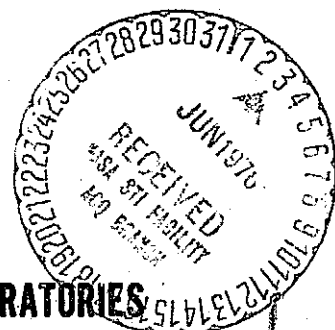
588  
NASA CR-134941  
VOLUME II



**ENERGY CONVERSION ALTERNATIVES STUDY**  
**-ECAS-**  
**WESTINGHOUSE PHASE I FINAL REPORT**  
**Volume II — MATERIALS CONSIDERATIONS**

by  
D.E. Thomas, et al

**WESTINGHOUSE ELECTRIC CORPORATION RESEARCH LABORATORIES**



Prepared for

**NATIONAL AERONAUTICS AND SPACE ADMINISTRATION**  
**ENERGY RESEARCH AND DEVELOPMENT ADMINISTRATION**  
**NATIONAL SCIENCE FOUNDATION**

**NASA Lewis Research Center**  
**Contract NAS 3-19407**

(NASA-CR-134941-Vol-2) ENERGY CONVERSION  
ALTERNATIVES STUDY (ECAS), WESTINGHOUSE  
PHASE 1. VOLUME 2: MATERIALS  
CONSIDERATIONS Final Report (Westinghouse  
Research Labs.) 306 p HC \$9.75 CSCI 10B G3/44

N76-23693

Unclas  
28167

1. Report No. NASA CR-134941 Volume II		2. Government Accession No.		3. Recipient's Catalog No.	
4. Title and Subtitle ENERGY CONVERSION ALTERNATIVES STUDY (ECAS), WESTINGHOUSE PHASE I FINAL REPORT VOLUME II - MATERIALS CONSIDERATIONS				5. Report Date February 12, 1976	
				6. Performing Organization Code	
7. Author(s) D. E. Thomas, et al				8. Performing Organization Report No. Westinghouse Report No. 76-9E9-ECAS-RLv.2	
9. Performing Organization Name and Address Westinghouse Electric Corporation Research Laboratories Pittsburgh, PA 15235				10. Work Unit No.	
				11. Contract or Grant No. NAS 3-19407	
12. Sponsoring Agency Name and Address Energy Research and Development Administration National Aeronautics and Space Administration National Science Foundation Washington, D. C.				13. Type of Report and Period Covered Contractor Report	
				14. Sponsoring Agency Code	
15. Supplementary Notes Project Managers: W. J. Brown, NASA Lewis Research Center, Cleveland, OH 44135 D. T. Beecher, Westinghouse Research Laboratories, Pittsburgh, PA 15235					
16. Abstract Extensive studies were carried out on materials behavior of importance in advanced energy conversion systems using coal or coal-derived fuels. Fireside corrosion and erosion of boiler and heat exchanger materials are treated. Specific materials recommendations are made for critical components of the nine advanced energy conversion system studied.					
17. Key Words (Suggested by Author(s)) materials      erosion      helium temperature      steam stress      gas turbine corrosion      liquid-metal				18. Distribution Statement  Unclassified - Unlimited	
19. Security Classif. (of this report) Unclassified		20. Security Classif. (of this page) Unclassified		21. No. of Pages 296	22. Price* -

\* For sale by the National Technical Information Service, Springfield, Virginia 22161

## ACKNOWLEDGMENTS

Section 3 entitled "Materials Considerations" was centered in the Westinghouse Research Laboratories and directed by D. E. Thomas.

Those making significant contributions were:

- F. G. Arcella, who assembled the information on materials for use in the presence of cesium and potassium vapor. (Subsection 3.7)
- F. J. Harvey, who assembled the information on materials exposed to helium in closed-cycle gas turbine systems. (Subsection 3.6)
- D. M. Moon, who assembled the information on materials exposed to high temperature combustion products in gas turbines, combustors and boilers. (Subsections 3.4, 3.5, 3.6 and 3.12)
- B. R. Rossing, who assembled the information on material for open- and closed-cycle MHD systems. (Subsection 3.9 and 3.10)
- T. Vojnovich, who assembled the information on materials for fuel cells. (Subsection 3.11)
- R. E. Witkowski, who assembled the information on materials for liquid-metal MHD systems. (Subsection 3.8)



## TABLE OF CONTENTS

NASA Report No.  
NASA CR-134941

Volume I	Section 1	INTRODUCTION AND SUMMARY
	Section 2	GENERAL ASSUMPTIONS
Volume II	Section 3	MATERIALS CONSIDERATIONS
Volume III	Section 4	COMBUSTORS, FURNACES, AND LOW-BTU GASIFIERS
Volume IV	Section 5	OPEN RECUPERATED AND BOTTOMED GAS TURBINE CYCLES
Volume V	Section 6	COMBINED GAS-STEAM TURBINE CYCLES
Volume VI	Section 7	CLOSED-CYCLE GAS TURBINE SYSTEMS
Volume VII	Section 8	METAL VAPOR RANKINE TOPPING-STEAM BOTTOMING CYCLES
Volume VIII	Section 9	OPEN-CYCLE MHD
Volume IX	Section 10	CLOSED-CYCLE MHD
Volume X	Section 11	LIQUID-METAL MHD SYSTEMS
Volume XI	Section 12	ADVANCED STEAM SYSTEMS
Volume XII	Section 13	FUEL CELLS

# EXPANDED TABLE OF CONTENTS

## Volume II

	<u>Page</u>
ACKNOWLEDGMENTS . . . . .	i
TABLE OF CONTENTS . . . . .	ii
SUMMARY . . . . .	viii
3. MATERIALS CONSIDERATIONS . . . . .	3-1
3.1 Introduction . . . . .	3-1
3.1.1 Purpose, Organization and Use . . . . .	3-1
3.1.2 Materials Application Rating System . . . . .	3-2
3.2 Corrosion and Erosion of Material in Combustion Gases. .	3-4
3.2.1 Gas Turbine Materials . . . . .	3-4
3.2.1.1 Contaminant Levels in Coal Derived Fuels..	3-4
High-Btu Gas . . . . .	3-4
Medium-Btu Gas . . . . .	3-5
Distillate from Coal-Derived Liquids . . .	3-5
Low-Btu Gas . . . . .	3-5
3.2.1.2 Recommended Materials for Gas Turbine	
Vaness and Blades . . . . .	3-20
Ceramic Materials . . . . .	3-23
Chromium-Based Alloys . . . . .	3-25
Uncoated Nickel- and Cobalt-Based	
Superalloys . . . . .	3-27
Oxidation- and Hot-Corrosion Resistant	
Coatings . . . . .	3-31
3.2.2 Heat Exchanger Materials . . . . .	3-38
3.2.2.1 Corrosion, Erosion, and Fouling of Heat	
Exchanger Materials . . . . .	3-38
3.2.2.2 Experimental Studies of In-Bed Corrosion	
and Erosion . . . . .	3-44

## EXPANDED TABLE OF CONTENTS (Continued)

	<u>Page</u>
Pressurized Bed Tests of In-Bed Boiler Tube Materials . . . . .	3-45
Corrosion Studies of Boiler Tube Materials at Atmospheric Pressure and Low Fluidized Velocities . . . . .	3-45
Long-Term Corrosion Tests at Atmospheric Pressure to Assess the Effect of Limestone Additions on Corrosion of Boiler Tube Materials . . . . .	3-49
3.3 Material Considerations in Steam Boilers Utilizing Coal and Coal-Derived Fuels . . . . .	3-59
3.3.1 Introduction . . . . .	3-59
3.3.2 Selection of Candidate Alloys . . . . .	3-61
3.3.3 Stress Rupture Performance . . . . .	3-63
3.3.4 Oxidation Performance . . . . .	3-65
3.3.5 Conclusions . . . . .	3-69
3.4 Materials Considerations in Advanced Steam Systems . . .	3-71
3.4.1 Introduction . . . . .	3-71
3.4.2 Main Transfer Piping and Casing . . . . .	3-72
3.4.3 Turbine Rotors . . . . .	3-75
3.4.4 Blading . . . . .	3-80
3.4.5 Summary . . . . .	3-80
3.5 Material Considerations in Open-Cycle Gas Turbines/ Recuperated- or Combined-Cycle Systems . . . . .	3-81
3.5.1 Introduction . . . . .	3-81
3.5.2 Turbine Blade Material . . . . .	3-81
3.5.3 Turbine Vane Alloys . . . . .	3-93
3.5.4 Summary . . . . .	3-95
3.6 Material for Closed-Cycle Gas Turbine Systems . . . . .	3-95
3.6.1 Corrosion Behavior of High-Temperature Materials in Impure Helium . . . . .	3-95

# EXPANDED TABLE OF CONTENTS (Continued)

	<u>Page</u>
3.6.1.1 Introduction . . . . .	3-95
3.6.1.2 Thermodynamic Considerations . . . . .	3-98
3.6.1.3 Gas-Solid Reactions in Dragon Reactor Coolant . . . . .	3-103
3.6.1.4 Mechanical Property Interaction . . . . .	3-107
3.6.1.5 Effect of Concentration of Impurities . . . . .	3-109
3.6.1.6 Gas Solid Reactions in Water Vapor- Helium Atmospheres . . . . .	3-111
3.6.1.7 Summary of Corrosion Behavior in Impure Helium . . . . .	3-113
3.6.2 Selection of Heat Transfer Materials for Closed- Cycle Gas Turbine Systems . . . . .	3-114
3.6.3 Material Selection for Closed-Cycle Helium Gas Turbines . . . . .	3-117
3.7 Materials for Potassium and Cesium Vapor Rankine Cycle Components . . . . .	3-123
3.7.1 Liquid-Metal Boiler . . . . .	3-125
3.7.2 Metal Vapor Turbine . . . . .	3-131
3.7.3 Liquid-Metal Loop . . . . .	3-137
3.7.4 Metal Vapor Condenser/Steam Generator . . . . .	3-139
3.7.5 Cover Gas System . . . . .	3-140
3.7.6 Shaft Seal and Bearings . . . . .	3-142
3.7.7 Instrument Subsystem . . . . .	3-145
3.7.8 Summary of Prime Materials Selected for Liquid- Metal Rankine Cycle Components . . . . .	3-145
3.8 Materials for Sodium Lithium MHD System Components . . . . .	3-146
3.8.1 Heat Source-Alkali Metal/Accelerating Gas Combustion System Heat Exchanger . . . . .	3-147
3.8.1.1 Potential Problems Area . . . . .	3-148
3.8.2 MHD Generator Including Mixer, Duct and Nozzle. . . . .	3-148
3.8.2.1 Structural Materials . . . . .	3-148

## EXPANDED TABLE OF CONTENTS (Continued)

	<u>Page</u>
3.8.2.2 MHD Duct Electrodes and Insulators . . . .	3-153
3.8.2.3 Potential Problem Areas . . . . .	3-154
3.8.3 Liquid-Metal Loop Including the Separator and Diffuser . . . . .	3-155
3.8.3.1 Potential Problem Areas . . . . .	3-157
3.8.4 Gas System Including the Steam Generator . . . .	3-157
3.8.4.1 Potential Problem Areas . . . . .	3-159
3.8.5 Closed-Cycle Liquid-Metal MHD Materials Selection Summary . . . . .	3-159
3.8.6 Instrument Subsystem . . . . .	3-161
3.8.6.1 Cover Gas/Accelerating Gas Impurity Monitors . . . . .	3-161
3.8.6.2 Liquid-Metal Impurity Monitors . . . . .	3-162
3.8.6.3 Alkali-Metal Vapor Detectors . . . . .	3-162
3.8.6.4 Steam Generator Leak Detection/Leak Location Devices . . . . .	3-162
3.8.6.5 Potential Problem Areas . . . . .	3-163
3.8.6.6 Instrument Subsystem Summary . . . . .	3-165
3.9 Materials for Open-Cycle MHD Systems . . . . .	3-165
3.9.1 Background . . . . .	3-165
3.9.2 Combustor Materials . . . . .	3-169
3.9.3 Generator Materials . . . . .	3-171
3.9.3.1 Electrodes . . . . .	3-171
3.9.3.2 Insulators . . . . .	3-178
3.9.3.3 Coal-Fired MHD Generator Materials . . . .	3-183
3.9.4 Air Preheater Materials . . . . .	3-192
3.9.4.1 High-Temperature Air Preheaters . . . . .	3-192
3.9.4.2 Materials Requirements for MHD Air Preheater	3-195
3.9.4.3 Mechanical Properties of Preheater Materials	3-197
3.9.4.4 Corrosion Resistance of Preheater Materials	3-198

# EXPANDED TABLE OF CONTENTS (Continued)

	<u>Page</u>
3.9.5 Other High-Temperature Components . . . . .	3-202
3.9.5.1 Diffuser . . . . .	3-202
3.9.5.2 High-Temperature Ducting . . . . .	3-203
3.9.5.3 High-Temperature Valves . . . . .	3-203
3.9.6 Heat Recovery and Seed Recovery Materials . . . .	3-204
3.9.6.1 Corrosion of Downstream Metallic Components	3-205
3.9.7 Magnet Materials . . . . .	3-208
3.9.8 Summary . . . . .	3-209
3.10 Materials for Closed-Cycle MHD Systems . . . . .	3-209
3.10.1 High-Temperature Heat Exchanger . . . . .	3-211
3.10.2 Closed Cycle Loop Materials . . . . .	3-212
Structural Metals . . . . .	3-214
Ceramics and Insulator Materials . . . . .	3-215
3.10.3 Selection of Closed-Cycle MHD Loop Materials . .	3-217
Diffuser and Nozzle . . . . .	3-218
Heat Recovery Materials . . . . .	3-219
3.10.4 Summary . . . . .	3-219
3.11 Materials for Fuel Cells . . . . .	3-219
3.11.1 Background . . . . .	3-221
3.11.2 Performance and Material Requirements . . . . .	3-224
3.11.3 High-Temperature Solid Electrolyte Fuel Cell . .	3-225
3.11.3.1 Materials Problems . . . . .	3-236
3.11.3.2 Development Needs . . . . .	3-237
3.11.4 Molten Carbonate Fuel Cells . . . . .	3-237
3.11.4.1 Materials Problems . . . . .	3-240
3.11.4.2 Development Needs . . . . .	3-241
3.11.5 Acid and Alkaline Fuel Cells . . . . .	3-242
3.12 Compilation of Composition and Mechanical Properties . .	3-255
3.13 Comparison of Materials Problems Associated with Advanced	
Energy Conversion Systems . . . . .	3-257
3.13.1 Summary Materials Application Evaluation . . . .	3-257
3.13.2 Comparison of Materials Ratings . . . . .	3-266
3.14 References . . . . .	3-277

## SUMMARY

Extensive studies, reported here, were carried out on materials behavior of importance in advanced energy conversion systems using coal and coal-derived fuels. The areas of materials behavior receiving particular attention in this regard are: fireside corrosion and erosion in boiler and heat exchanger materials, oxidation and hot corrosion of gas turbine materials, liquid metal corrosion and mass transport, high temperature steam corrosion, compatibility of materials with coal slag and MHD seed, reaction of materials with impure helium, allowable stresses for boiler and heat exchanger materials, environmental effects on mechanical properties, and liquid metal purity control and instrumentation. Such information was then utilized in recommending materials for use in the critical components of the power systems, and at the same time to identify materials problem areas and to evaluate qualitatively the difficulty of solving these problems.

Specific materials recommendations for critical components of the advanced systems under study are contained in summary tables which also include estimates of the difficulty of solving the materials application problems posed. Using the materials application rating system described in the report, overall rating of the advanced systems from a materials point of view resulted in the following ranking in the order of increasing difficulty. (Page numbers indicate the location of summary tables.)

- (1) Open Cycle Gas Turbine Systems (p. 3-96)
- (2) Combined Cycle Gas Turbine Systems (p. 3-97)
- (3) Closed-Cycle Helium Gas Turbine Systems (p. 3-122)
- (4) Liquid Metal MHD Systems (p.3-160)
- (5) Advanced Steam Systems (p. 3-82)
- (6) Liquid Metal Rankine Systems (p. 3-145)
- (7) Fuel Cell Systems (p. 3-248)
- (8) Closed-Cycle MHD Systems (p. 3-220)
- (9) Open-Cycle MHD Systems (p. 3-210)



### 3. MATERIALS CONSIDERATIONS

#### 3.1 Introduction

##### 3.1.1 Purpose, Organization and Use

This section includes a summary of the state-of-the-art of materials for the critical components of the advanced energy conversion systems under study, materials recommendations for the critical components, and an assessment of the difficulty of demonstrating that the recommended materials are in fact satisfactory for the application.

This section is organized along the following lines. There is, first, Subsection 3.2 dealing with the corrosion-erosion behavior of materials in combustion gases of interest in the overall system study. Since a common denominator in this study is the use of coal and coal-derived fuels it was considered appropriate to treat corrosion-erosion behavior in one place. Thus, this subsection is supportive of the remaining subsections. Similarly, Subsection 3.3 is devoted to steam boiler materials that are pertinent to a number of the advanced cycle systems. This is followed by Subsection 3.4, dealing with open-cycle gas turbine materials, and is applicable both to advanced open-cycle gas turbine systems and to other advanced systems having a gas turbine subsystem. There follow Subsections 3.6 to 3.11, dealing with materials for the critical components peculiar to specific advanced systems. Finally, Subsection 3.12 contains tabulated and graphical presentations of static and time-dependent mechanical property data for the materials discussed in the other subsections.

For the reader who wishes to use this section for reference purposes while reading the system analysis sections, it is suggested that the summary tables in the pertinent subsection be consulted first for the materials recommended for each critical component. Further information

relating to the selection, including alternate materials, may then be located in the text of that subsection or in one of the supporting subsections (3.2, 3.3, and 3.12).

### 3.1.2 Materials Application Rating System

A system of qualitatively rating materials applications has been adopted in this section. Four categories are used:

- (A) Established Materials Applications
- (B) Near Term Materials Applications
- (C) Development Materials Applications
- (D) Speculative Materials Applications

While these category titles are almost self-explanatory, it is useful to refer to Table 3.1, which contains qualitative statements relating to the relative credibility of selected candidate materials, the sufficiency of the existing data base, how far the projected service conditions are from the existing data base, the amount and kind of additional materials work that is needed, the quality of the R&D rationale by which it is hoped to achieve the desired result, and finally the probability of success. It is important to note that the rating refers to a particular material in a particular application, and not to the material per se. Thus, a well-developed, commercially available material may receive a low rating by virtue of questions about its utility in a severe application.

The materials-application ratings provide a qualitative measure of the difficulty of demonstrating the utility of a material in a particular application. It will be one of the purposes during Tasks II and III of the study to expand upon the factors involved in the ratings so that quantitative estimates of development times and costs can be provided.

Table 3.1 — Materials Application Rating Criteria

Materials Application Rating	Selection Status	Data Base	Extrapolation from Data Base	Materials Work Required	R&D Program Characteristics	
					Rationale	Success Probability
Established (A)	Firm selections can be made. Materials are commercially available in form required.	Sufficient	None	Minimal, routine applications engineering	Not applicable	Not applicable
Near Term (B)	A number of candidate materials are identified. Candidates are commercial or near commercial.	Incomplete	Short extrapolations from existing data base are involved	Confirmatory testing and minimal R&D	Straight-forward	Virtually certain
Developmental (C)	A number of candidate materials are identified. Candidates may be developmental	Incomplete Important gaps exist	Large extrapolations from existing data required	Considerable R&D is required	A credible rationale exists. Alternative avenues are evident.	Good to excellent
Speculative (D)	Only a small number of candidate materials can be suggested	Sparse or Absent	Highly speculative or not possible	Extensive R&D is required	Rationale is not clear, or requires a breakthrough or serendipity	Fair to poor

3-3

REPRODUCIBILITY OF THE  
ORIGINAL PAGE IS POOR

### 3.2 Corrosion and Erosion of Materials in Combustion Gases

#### 3.2.1 Gas Turbine Materials

##### 3.2.1.1 Contaminant Levels in Coal-Derived Fuels

In order to evaluate materials for various energy conversion systems, one first has to consider the nature and concentrations of the contaminants in coal-derived fuels, which can cause accelerated oxidation and corrosion of selected materials. In this study, the following coal-derived fuels are to be considered for the cycle analysis:

- High-Btu gas
- Medium-Btu gas
- Low-Btu gas
- Distillate from coal-derived liquids.

High-Btu Gas -- Somers (Reference 3.1) has calculated the chemical composition of the high-Btu gas produced from coals. He states that the high-Btu gases produced from three coals, specified by NASA, will not appreciably differ in chemical composition. He gives the following composition for the high-Btu pipeline quality gas irrespective of the coal used:

CO <sub>2</sub>	0.39% (by volume)
CO	0.08%
H <sub>2</sub> <sup>A</sup>	2.49%
N <sub>2</sub>	2.81%
S	0.00%
CH <sub>4</sub>	94.23%

Thus, the high-Btu coal gas will be free of any detrimental contaminants which could cause accelerated hot corrosion of materials, and hence the limiting factor in the use of materials will be only oxidation. In this respect, the combustion gases produced by burning high-Btu gas will be similar to those produced by burning natural gas or clean diesel oils such as ASTM GT-2.

Medium-Btu Gas -- The medium-Btu gas produced by commercial Koppers-Totzek gasifiers will have a composition (Reference 3.1):

CO <sub>2</sub>	6.01%
CO	55.90%
H <sub>2</sub>	37.39%
N <sub>2</sub>	0.70%

The raw gas before desulfurization would contain about 10% water and 0.3 to 0.4% hydrogen sulfide and carbonyl sulfide (COS). It is assumed, however, that this gas will be cleaned up to essentially zero sulfur before it is used in advanced energy conversion systems. Thus, the combustion gases produced by burning cleaned-up medium-Btu gas will be essentially free of alkali elements, sulfur-bearing species, and particulate matter. The limiting factor for materials, therefore, will again be oxidation only.

Distillate from Coal-Derived Liquids -- According to Somers (Reference 3.1), the Illinois No. 6 coal with 3.9% sulfur will give PAMCO (Pittsburgh and Midway Coal Co.) solids with ~1% sulfur. These solids can be liquefied for use as a liquid fuel. Similarly, liquids from the H-coal process will contain 0.2 to 0.4% sulfur. Distillate products from these liquid fuels with negligible traces of alkali elements and sulfur will be used to fire gas turbines. The distillates, therefore, can be assumed similar to clean diesel oils (ASTM GT-2) in the sense that combustion gases produced from them should not cause any hot corrosion of selected gas turbine materials.

Thus the maximum use temperature for various gas turbine materials utilizing high- or medium-Btu gases, or distillates from coal, will be limited by oxidation only, and no hot corrosion is expected in these systems.

Low-Btu Gas -- The low-Btu gas from coals is not cleaned to the extent that the high- and medium-Btu gases are cleaned; and therefore, the low-Btu gas will contain significant amounts of detrimental contaminants, such as sodium, potassium, sulfur, chlorine, and particulate matter,

---

\*Pittsburgh and Midway Coal Co. solvent refined coal.

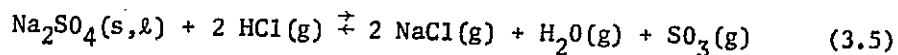
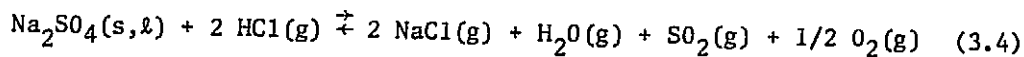
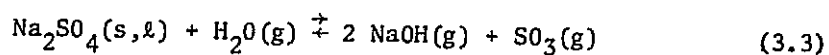
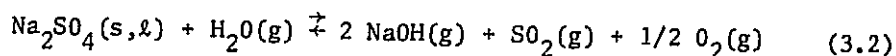
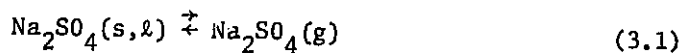
carried over from the coals. The chemical nature and concentration of these contaminants will depend upon the initial contaminant levels in feedstocks (e.g., coal and dolomite), the particular coal-gasification process used, and the method and extent of gas cleanup employed. For example, the sulfur level in the low-Btu gas will greatly depend upon the desulfurization process used. It is estimated (Reference 3.2) that low-Btu gas from Westinghouse fluidized bed gasification process will contain between 200 and 500 ppm hydrogen sulfide after high-temperature desulfurization. The raw gas, however, before any desulfurization takes place may contain up to ten times as much hydrogen sulfide.

Hamm (Reference 3.2) has calculated the basic chemical composition of the low-Btu gases produced from three coals specified by NASA. However, the material behavior in combustion gases produced by burning these low-Btu gases depends not so much on the basic constituents (e.g., carbon monoxide, carbon dioxide, nitrogen, etc.), as on the detrimental contaminants levels, as long as the combustion gases are highly oxidizing. These detrimental contaminants, mainly sodium, potassium, chlorine, sulfur, and particulate matter, are carried over from coal and dolomite feedstocks into the gases. The following section, abstracted from the work of Jansson and Sverdrup (Reference 3.3), discusses the nature of these contaminants and their estimated concentrations.

Sodium and potassium exist as clay minerals in coal and dolomite, and as sodium and potassium chlorides (NaCl and KCl) in saline ground water filling pores or cracks in coal and rock beds. The high volatility of sodium chloride makes it likely that entrained saline water will release sodium (as gaseous chloride) to the coal gases. In addition, alkalis and chlorine will be released from alkali-containing clay minerals in coal and dolomite at gasification temperatures. The exact paths of alkali compound reactions in gasification systems will depend on pressure, temperature, time, chemical composition of clay minerals, and the nature of the surrounding gas phase. At present, no reliable experimental data exist on the extent of alkalis and chlorine release from coal and dolomite,

and hence the nature of the alkali-containing species and their concentrations in low-Btu gas cannot be calculated. However, it is well recognized now that sodium, sulfur, and chlorine in combustion gases in a gas turbine could cause deposition of liquid sodium sulfate ( $\text{NaSO}_4$ ) and/or chloride salts on turbine components resulting in their accelerated corrosion. Jansson (Reference 3.3) has performed several mass balance and thermochemical calculations to estimate the minimum concentration of sodium in the fuel which would cause deposition of liquid sodium salts on turbine components at different sulfur and chlorine levels and cause hot corrosion of turbine materials. The results of these calculations are summarized below.

Sodium sulfate deposit stability in a combustion gas environment involves the five reaction processes:



For an oil-fired gas turbine where the primary sources of alkali contaminants are sodium chloride (or sea salt) in the fuel and in the air, the first three reactions are of primary importance, i.e., straight volatilization of sodium sulfate, and the action of water vapor to form sodium hydroxide vapor. The gaseous sulfur oxides suppress the formation of sodium hydroxide vapors in accordance with reactions given by Equations 3.2 and 3.3.

Figure 3.1 (Reference 3.3) shows three curves which relate the conditions where sodium sulfate deposits will form for three different levels of sodium contaminants (as sodium chloride) in gas turbine fuel oil. This oil, with an average composition  $\text{CH}_{1.85}$ , was taken to contain 1% sulfur, and conversion of sulfur dioxide to the equilibrium levels of sulfur trioxide was assumed to occur at all temperatures. Volatilization of the sodium sulfate and decomposition of this sulfate by either Equation 3.2 or 3.3 determine the position of each of the three curves.

The four rectangles in Figure 3.1 show the static pressure and temperature ranges for the first- and second-stage vanes and rotating blades in a large gas turbine operating at a gas inlet temperature of 1400°K (2060°F). Condensed sodium sulfate is stable for conditions to the right of the relevant concentration curves. The figure shows that at any component temperature, an increased pressure can lead to deposit formation (strictly an effect of increased partial pressure). Interpolation between the concentration curves (in a logarithmic fashion) shows that to avoid all formation of liquid sodium sulfate in any part of the first- and second-stage turbine components, the sodium concentration in the fuel oil must be less than 0.26 ppm. This level varies with the sulfur and water vapor content of the fuel. Figure 3.2 summarizes the effects of variations in sulfur content and water vapor level in the combustion gases on the tolerance to sodium (sodium levels that avoid the formation of liquid sodium sulfate) on turbine components. It is clear from the curves in Figure 3.2 that increased sulfur in fuel reduces the sodium tolerance, while a relatively small increase in sodium tolerance can be achieved by an increase in water vapor level.

When a low-Btu gas is burned, instead of fuel oil, with air and expanded in a large industrial gas turbine, the stability of a condensed sodium sulfate deposit on turbine components is largely determined by the gaseous hydrogen chloride concentration in the gas through reactions, Equations 3.4 and 3.5. Here, hydrogen chloride gas helps to remove sulfate deposits. Figures 3.3 and 3.4 show the conditions for solid and liquid sodium sulfate stability on turbine components for the coal



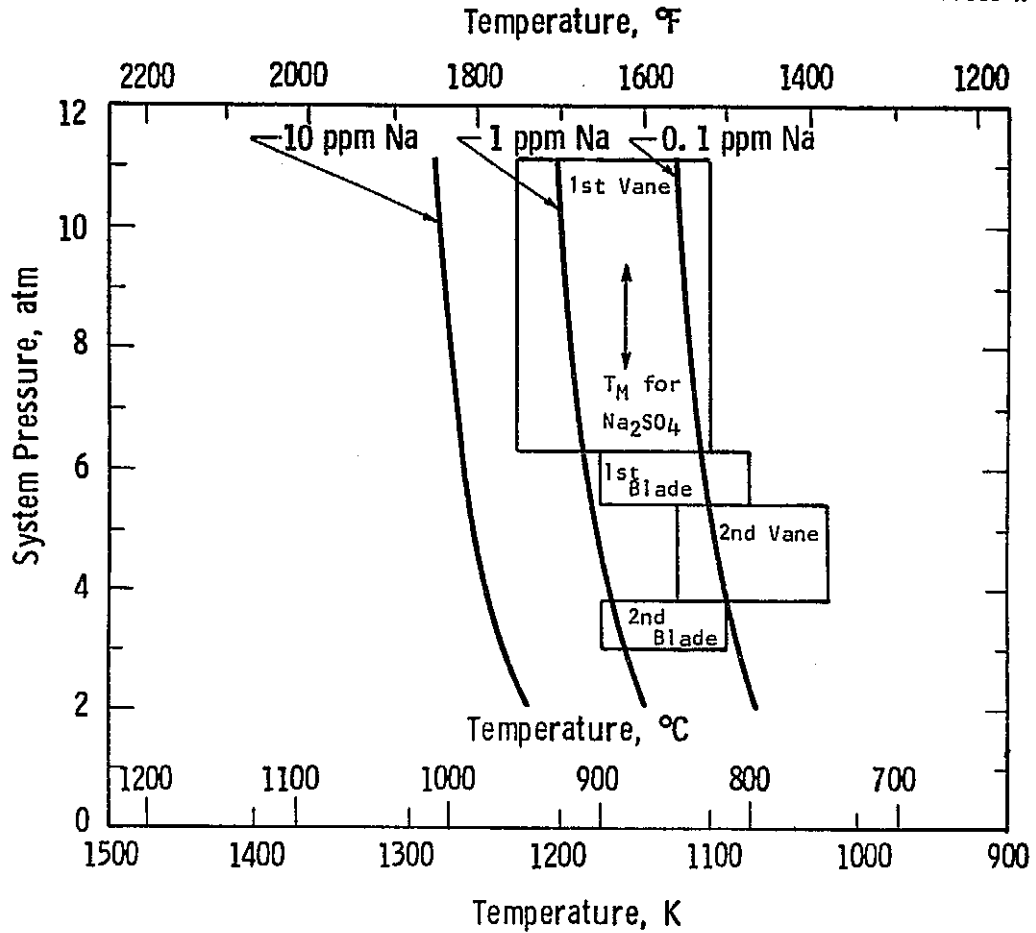


Figure 3.1 - Conditions for sodium sulfate deposit stability (to the right of the different concentration curves) on the first and second stages of a large industrial gas turbine burning gas turbine fuel oil contaminated with sodium chloride at the indicated sodium levels (1% sulfur in oil).

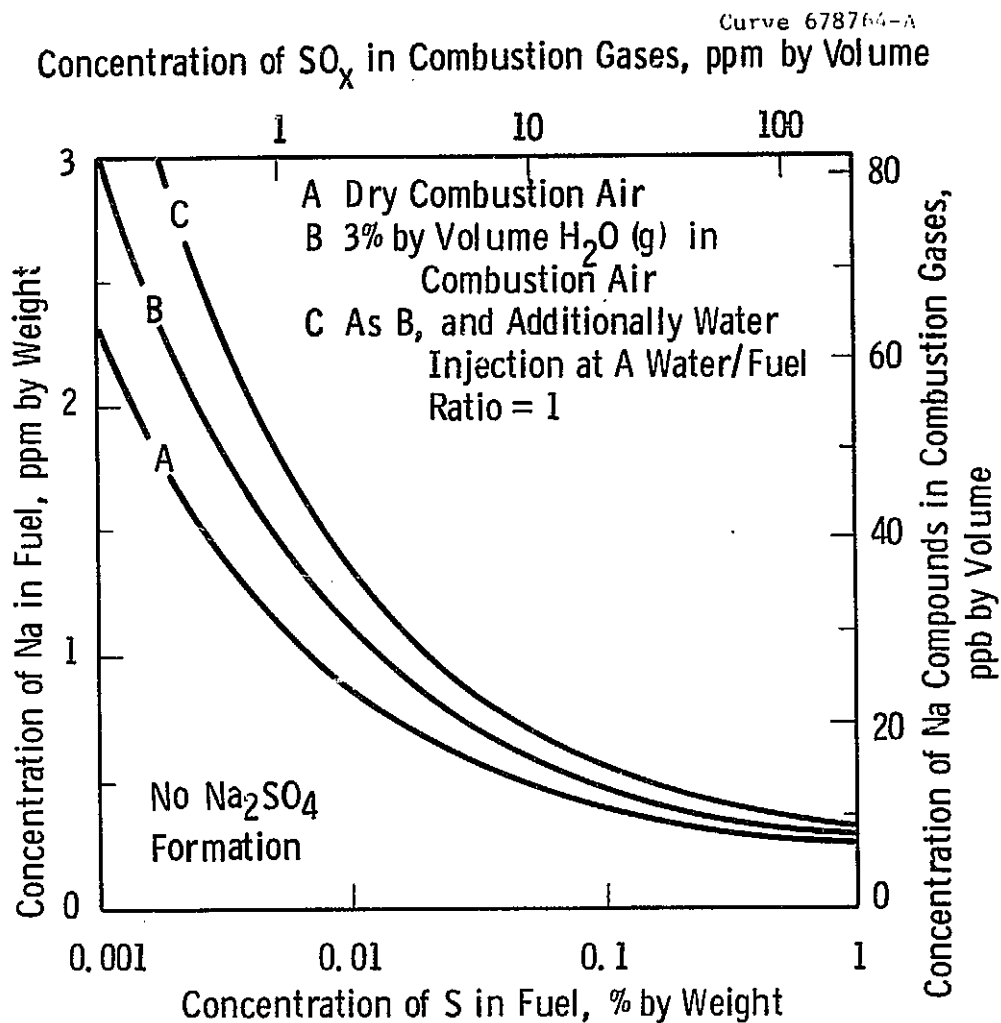


Figure 3.2 — Effect of humidity in combustion gases and of S in  $\text{CH}_{1.85}$  gas turbine fuel oil on the tolerance to Na (levels that avoid the formation of  $\text{Na}_2\text{SO}_4$  (l) on turbine components).

REPRODUCIBILITY OF THE  
ORIGINAL PAGE IS POOR

Curve 678540-A

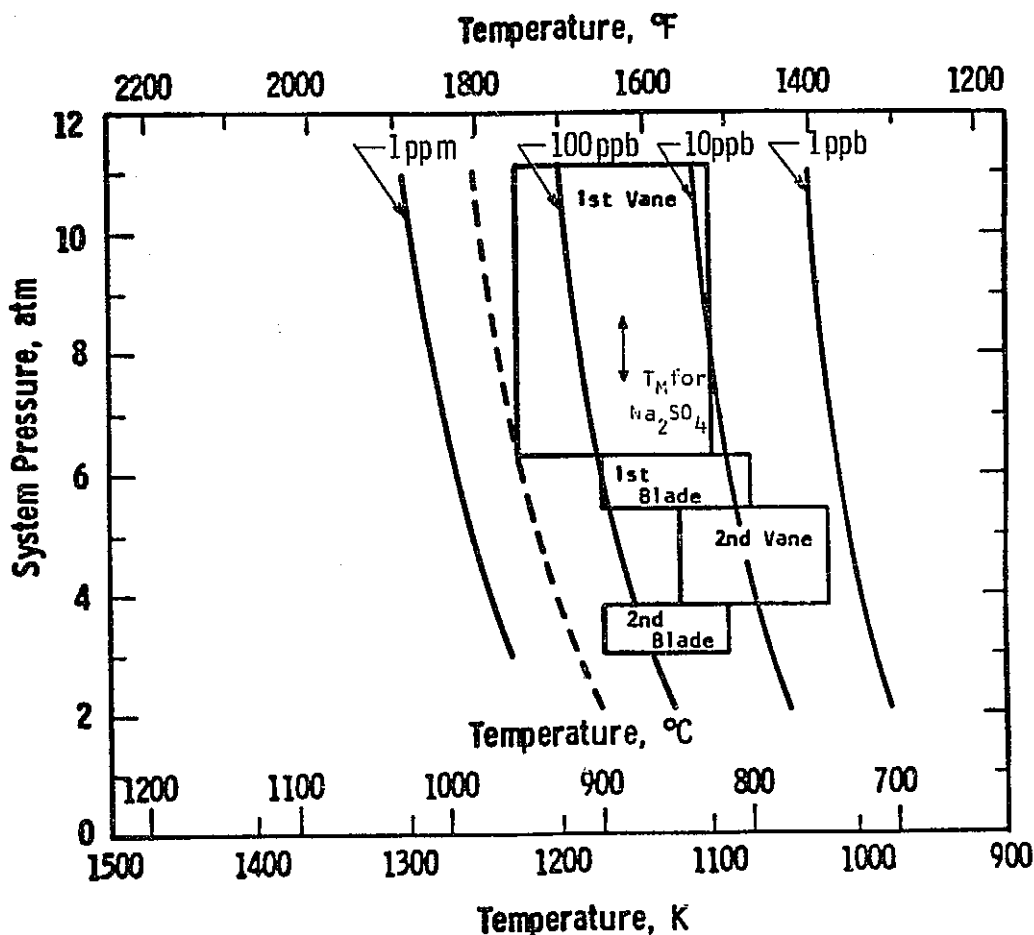


Figure 3.3 — Conditions for sodium sulfate stability (to the right of the different concentration lines) on the first and second stages of a large industrial gas turbine burning coal gas that contains 4.2 ppm by volume of chlorine compounds and also sodium contaminants at the indicated volume concentration levels. The heavy broken line represents the estimated sodium concentration shown in Figure 3.5.

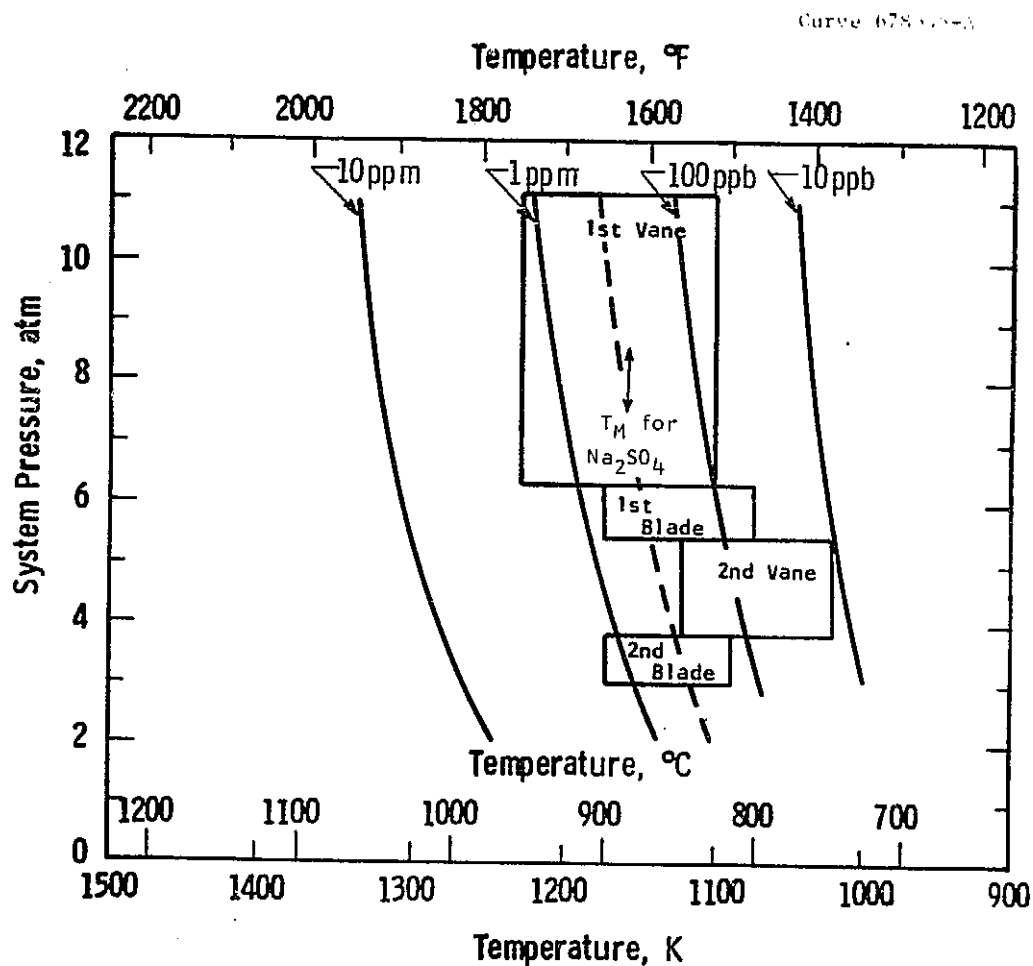


Figure 3.4 — Conditions for sodium sulfate stability (to the right of the different concentration lines) on the first and second stages of a large industrial gas turbine burning coal gas that contains 33.4 ppm by volume of chlorine compounds and also sodium contaminants at the indicated volume concentration levels. The heavy broken line represents the estimated sodium concentration shown in Figure 3.5.

gas combustion products (effective composition assumed to be 12.25% oxygen, 5.40% water, and 124 ppm sulfur dioxide + sulfur trioxide by volume), at chlorine contaminant levels of 4.2 ppm and 33.4 ppm, respectively, by volume. Increasing the chlorine contaminant level results in a shift of the different sodium tolerance levels towards higher temperatures, i.e., the allowable levels of sodium (so as not to cause formation of liquid sodium sulfate) in the coal gas increase with increasing chlorine concentration. In this respect, higher chlorine concentrations in coal gas may be beneficial. For maximum sodium tolerance, the calculations (Reference 3.3) suggest that the chlorine level should be maximized and sulfur level minimized as far as possible in the coal gas. Also, the hydrogen chloride vapor is much more effective than the water vapor in raising the sodium tolerance levels, but this has a negative effect as will be discussed on page 3-17.

As mentioned earlier, the composition of low-Btu gas with respect to contaminant levels (mainly sodium, potassium, sulfur, and chlorine) remains essentially uncharacterized, and hence it is difficult to state with certainty whether the sodium, sulfur, and hydrogen chloride vapor levels in low-Btu gases from the three coals specified by NASA will cause deposition of liquid sodium sulfate on turbine components. Jansson (Reference 3.3), however, has estimated the concentrations of various contaminant species, assuming that only 1% of the alkalis and 100% of the chlorine present in coal and dolomite feedstock are released into the low-Btu gas. Based on these assumptions, the contaminant levels in low-Btu gas produced by the Westinghouse fluidized bed coal gasification system and in the combustion gases in a gas turbine utilizing this coal gas are shown in Figure 3.5. The contaminant levels are calculated for a coal containing 3.59% sulfur, and 0.52% sodium oxide and 1.80% potassium oxide (both in the ash), and a dolomite containing 0.070 and 0.217% sodium and potassium, respectively. In performing the above calculations, it was assumed that the combined chlorine content of coal and dolomite ranged between 100 and 800 ppm. These levels of contaminants represent Illinois No. 6 coal fairly well. As in Figures 3.3 and 3.4, the calculated values of sodium compounds and sulfur dioxide

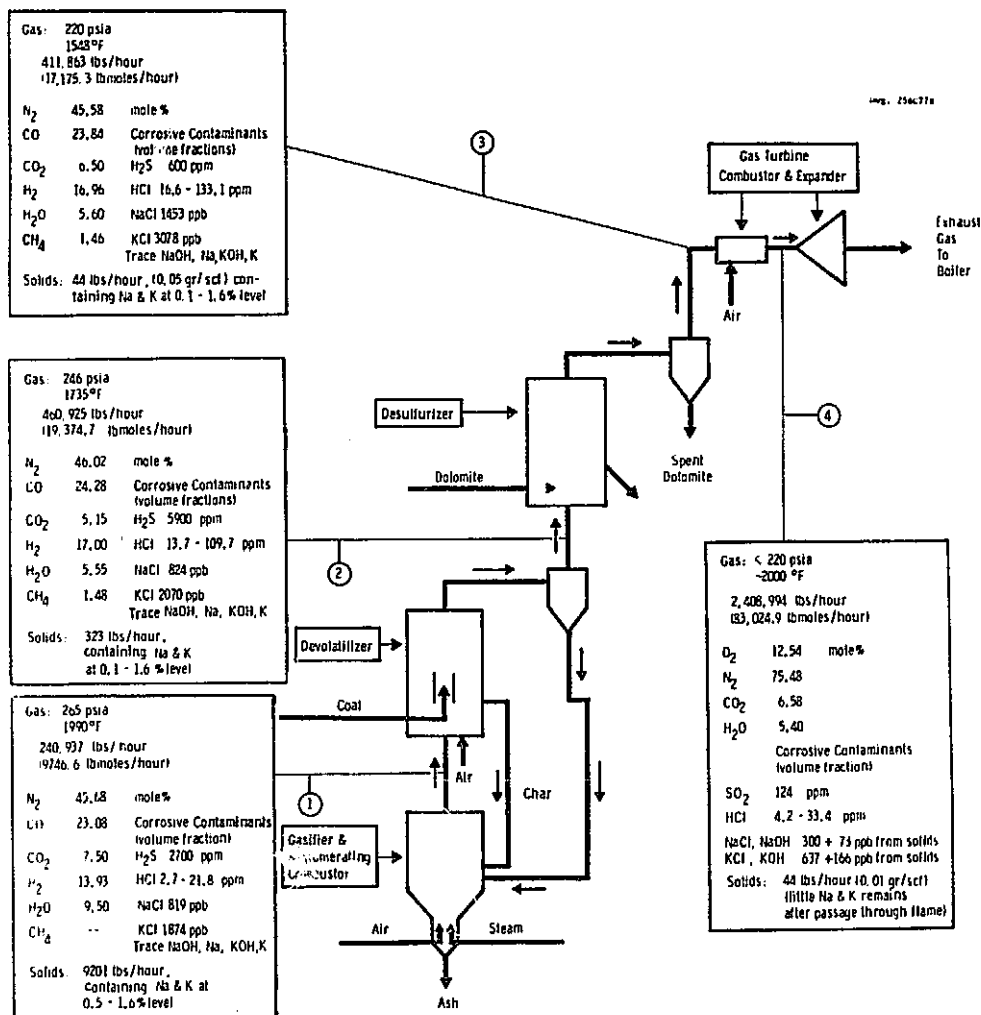


Fig. 3.5 — Summary of gas chemistry and corrosive contaminant levels at selected points of the system.

in the combustion gases will be sufficient to produce sodium sulfate solid and/or liquid deposits on all parts of the first-stage components for chlorine contaminant levels below 4.2 ppm. A chlorine contaminant level of 33.4 ppm makes liquid sodium sulfate unstable over the highest temperature portions of the first- and second-stage vanes and the first-stage blades, but it does not altogether eliminate the possibility of liquid sodium sulfate formation on these turbine components.

Even though, at present, there is no experimental verification or justification for the assumption used in calculating the contaminant levels in low-Btu gas -- namely, that only 1% of the alkalis and 100% of the chlorine present in coal and dolomite are released during gasification, it can be safely said that alkalis, chlorine, and sulfur species will definitely be present in low-Btu gas. In the absence of a knowledge of the actual contaminant levels in low-Btu gas, it is considered safer in recommending gas turbine materials to assume that these levels will be significant enough to cause hot corrosion of turbine components.

In addition to the deposition of liquid sodium sulfate as discussed above, potassium sulfate ( $K_2SO_4$ ) could also condense on turbine components at temperatures up to about 1228°K (1750°F), the exact temperature limit being determined by the chlorine and sulfur content of the gases (Reference 3.4). The potassium sulfate, however, will be solid at these temperatures [(melting point 1342°K (1956°F))], and if no interaction is assumed between sodium and potassium compounds, then this solid potassium sulfate should be relatively innocuous to turbine materials. But, in reality, potassium and sodium compounds, predominantly sulfates and chlorides, could form very low melting eutectic compounds. Figure 3.6 shows the liquidus temperatures in the sodium-potassium-sulfur-oxygen-chlorine system, and indicates that liquid compounds are possible in this system at as low a temperature as 7890°K (960°F). These molten alkali compounds can attack the protective oxide scales on gas turbine materials, just as liquid sodium sulfate does, to cause their accelerated corrosion. At present, vapor pressure data over these

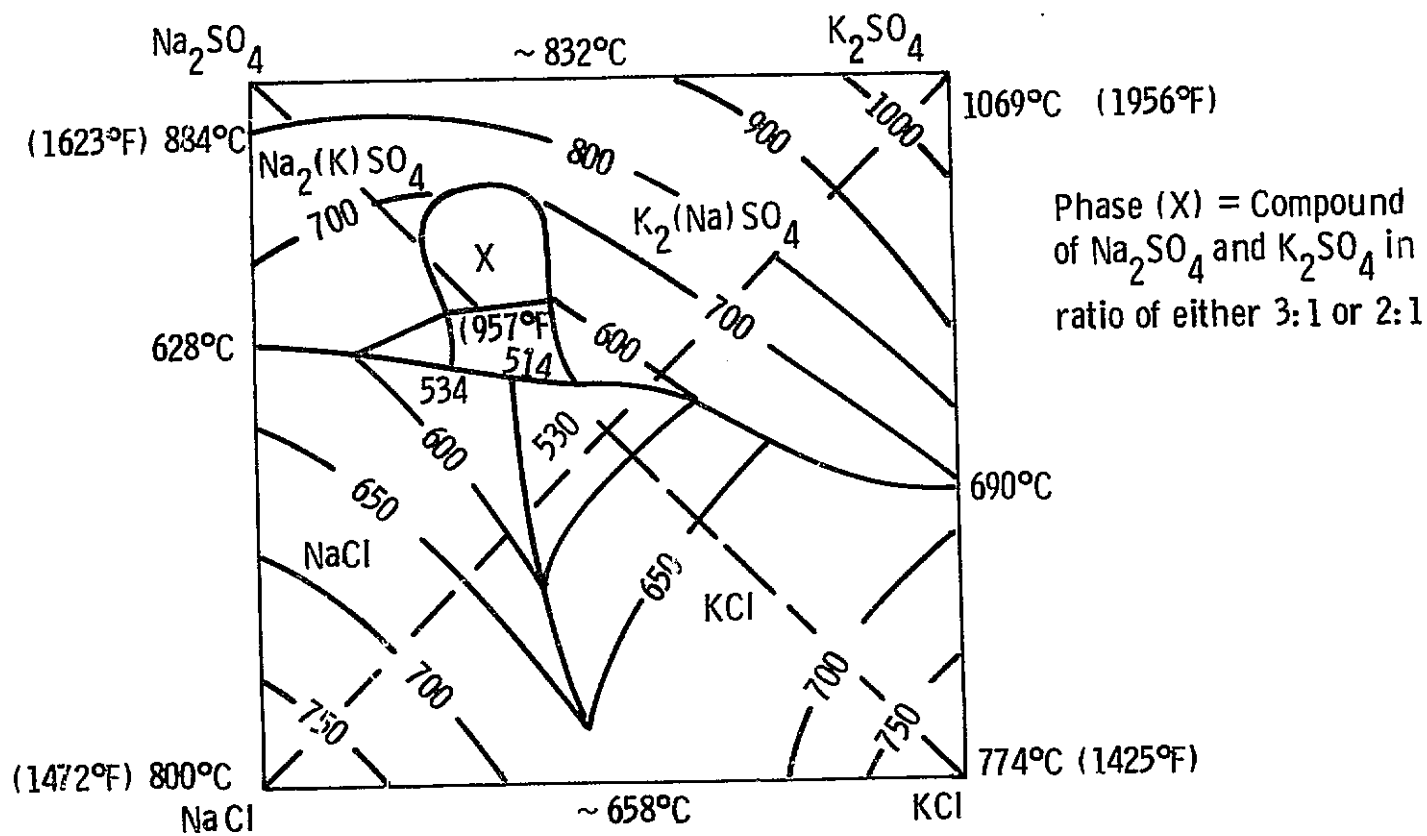
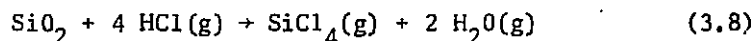
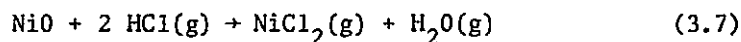
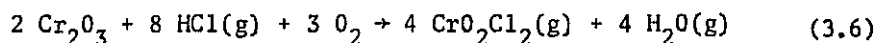


Fig. 3.6 — Projection of liquidus surface of  $\text{Na}_2\text{SO}_4$ - $\text{K}_2\text{SO}_4$ - $\text{KCl}$ - $\text{NaCl}$  system showing temperature contours (after Akopov, E.K. and Bergman A.G.-Zhur. Obshchei Khim, 1954, 24. pp 1524-1532).



complex eutectic compounds are not available, but it seems certain that the formation of these compounds will lower the alkali tolerance levels from those illustrated in Figures 3.3 and 3.4 for sodium only. The actual alkali tolerance level will again be influenced by sulfur and chlorine concentrations in the low-Btu gas.

As illustrated earlier, chlorine as hydrogen chloride vapor has a beneficial effect in increasing the tolerance level for alkalis. On the other hand, the presence of hydrogen chloride vapor in the combustion gases can result in the accelerated oxidation of gas turbine materials because of the volatilization of the protective oxide scales formed on superalloys and silicon-based ceramics as gaseous chloride or oxychloride, by reactions of the following types:



For example, for the combustion gases with composition shown in Figure 3.5, the partial pressure of chromium oxychloride vapor by reaction, Equation 3.6, would be about 5.06 MPa ( $5 \times 10^{-8}$  atm) at 100 ppm hydrogen chloride vapor. The extent and severity of such attack under actual operating conditions will depend upon the hydrogen chloride vapor partial pressure in the combustion gases, the gas velocity, and on the relative rates of formation of the protective oxide and of the gaseous chloride or oxychloride. Thus, chlorine in low-Btu coal gas plays both a beneficial and a detrimental role as far as materials performance is concerned, and the total effect can only be determined by experiments under coal-gas burning conditions. Until now, no such experiments have been reported in the literature.

In addition to the detrimental effects of alkalis, chlorine, and sulfur on materials performance, the situation is further complicated

by the presence of particulate matter in the low-Btu gas. This particulate matter will consist mostly of coal ash and/or sorbent particles such as dolomite. These particulates could cause severe erosive damage of gas turbine vane and blade materials. The extent of such erosive damage will depend upon the particle size, shape, velocity, impingement angle, and concentration. For example, Table 3.2 shows the estimated erosion losses in each blade passage at a projected ash concentration of  $22.95 \text{ mg/m}^3$  ( $0.01 \text{ gr/scf}$ ) with the particle size distribution indicated therein (Reference 3.5). The catch efficiencies reported in Table 3.2 are the estimated fractions of available gas-borne particles in the size range 1-to-10  $\mu\text{m}$  that strike the surface of a blade in the gas stream. The erosion losses shown are estimated for an ash with average density of  $2.5 \text{ g/cm}^3$  in coal gas combustion products flowing at  $294.8 \text{ kg/s}$  ( $650 \text{ lb/s}$ ) at  $1144^\circ\text{K}$  ( $1600^\circ\text{F}$ ) and  $1.013 \text{ MPa}$  ( $10 \text{ atm}$ ) pressure through a 60-blade first stage. For a 57.07% service factor, these volumetric erosion loss rates are equivalent to surface recession rates of about  $96.6 \text{ pm/s}$  ( $1.2 \text{ mils/yr}$ ) at  $152.4 \text{ m/s}$  ( $500 \text{ ft/s}$ ) and  $8.05 \text{ pm/s}$  ( $10 \text{ mils/yr}$ ) at  $304.8 \text{ m/s}$  ( $1000 \text{ ft/s}$ ), values that are representative of entrance and exit velocities in typical industrial gas turbine design. It appears from these projected erosion rates that the particulate loading and size of the coal gas must be reduced to levels even below those assumed above, or that exit velocities must be reduced by enlarging the turbine. Particularly, efforts should be made to clean up the low-Btu gas to reduce the concentration of particulates of above  $2 \mu\text{m}$  size as much as possible, since larger particles even in smaller fractions can cause severe erosion.

The overall material wastage, however, will necessarily depend on the synergistic effects of corrosion and erosion, whereby the protective oxide scales on turbine hardware could conceivably be removed by the erosive effect of particulate matter. Establishing the interaction between hot-corrosion inducing contaminants and the erosive attack that can be expected is difficult in the absence of experimental data under coal-burning gas turbine conditions. Furthermore, if liquid alkali sulfate-chloride films form on turbine hardware, these films could

Table 3. 2- Particle Size Distribution of Ash and Estimated Erosion Losses

Size ( $\mu\text{m}$ )	Vol. Fract. (%)	Ash Flow Rate (mg/s)	Catch Efficiency (%)		Blade Loss ( $10^{-9} \text{ cm}^3/\text{s}$ )	
			500 ft/s	1000 ft/s	500 ft/s	1000 ft/s
0-1	80	70	0	0.05	0	9.4
1-2	12.5	11	0.1	0.3	0.6	8.7
2-5	6.25	5.5	5.5	14	20	202
5-10	1.25	1.1	33	55	23.1	156
TOTAL	100	87.6	0.8	1.7	43.7	376.1

accumulate large amounts of particulates forming thick deposits on the component surfaces. These deposits have the potential to impair seriously the aerodynamic performance of the turbine.

In summary, using low-Btu gas to fire gas turbines could result in severe hot corrosion, chlorination, and erosion attack on turbine materials; and, therefore, the materials recommendations presented in the next section are those believed to offer the highest probability of meeting the demanding requirements imposed by the low-Btu gas. It is also recommended, however, that efforts be made to clean the low-Btu gas with respect to detrimental contaminants, (e.g., sodium, potassium, chlorine, sulfur, and particulate matter). One approach to reducing these contaminant levels would be to adjust the various coal gasification parameters (e.g., temperature, pressure, and mass flow rates) in such a way as to reduce the release of these contaminants from coal and dolomite feedstock into the gas.

In order to specify turbine materials for use with low-Btu gas, the vast literature on hot corrosion of superalloys and coatings has been reviewed. However, much of the data on conditions for hot corrosion attack in combustion gases seem contradictory. What helps

create this impression as that what appears to be one type of attack can originate in different ways (e.g., sulfidation/oxidation attack which is initiated by gaseous sulfidation and followed by oxidation could also be caused by temporary reduction of a sulfate phase when exposed to carbon or other reducing agents). Another such factor is that the nature of the total deposit system or of its interactions with oxide scale components is not always recognized. Of special importance probably is the fact that liquid alkali sulfate-chloride deposit on turbine components could cause mechanical failure of the protective scales as suggested by Hancock (Reference 3.6). Furthermore, the experimental data on the extent of hot corrosion attack of various materials differ from laboratory to laboratory, depending upon the particular rig and fuel used. The materials recommendations for use with low-Btu gas are, therefore, based on experience with heavy residual oils and operations in marine environments, where hot corrosion attack is usually observed.

#### 3.2.1.2 Recommended Materials for Gas Turbine Vanes and Blades

It is clear from the discussion in Section 3.2.1.1 that oxidation will be the limiting factor for materials in gas turbines utilizing clean fuels, e.g., high- and medium-Btu gases, and distillate from coals, whereas hot corrosion and erosion would be the limiting factor for gas turbines burning low-Btu gas. Based on the literature data on the oxidation and hot corrosion of various materials and on Westinghouse experience with gas turbines over the last 75 years, the choice of materials for use in gas turbines at different temperatures is shown in Tables 3.3 and 3.4 for clean fuels and for low-Btu gas, respectively. The materials are ranked A, B, C, or D, depending upon whether their use is established, near term, developmental, or speculative at different temperatures and in different fuels. The ranking system is explained in detail in Subsection 3.1.

The experimental data on oxidation and hot corrosion of various gas turbine materials are vast, and no effort will be made to present a

Table 3.3 — Gas Turbine Materials Suitable for Use with Clean Fuels,  
(e.g., High- and Medium-Btu Gas and Distillate from Coals)

Maximum Material Temperature	Material	Rating*
1500°F	Uncoated superalloys, e.g., U-500, U-520	A
1600°F	Uncoated superalloys, e.g., X-45, U-700	A
1700°F	Uncoated superalloys, e.g., Mar-M-509, IN-738, IN-792, FSX-418	A
1800°F	(i) Directionally solidified alloys, e.g., Mar-M-421, coated with a diffusion aluminide coating.	A
	(ii) Superalloys, e.g., Mar-M-509, IN-792 coated with NiCrAlY overlay coating.	A
	(iii) Chromium-coated IN-738 or U-710 alloy.	B
1950°F	(i) NiCrAlY coated mechanically-alloyed (with Y <sub>2</sub> O <sub>3</sub> ) IN-792 alloy.	B
	(ii) Rare-earth (Hf, Y, Ce)-modified nickel-base superalloys such as B-1900, IN-100.	B
2050°F	(i) TD-NiCr coated with a NiCrAlY overlay coating.	A
	(ii) WAZ-16 alloy coated with a NiCrAlY overlay coating.	B
	(iii) Directionally solidified eutectic alloy, e.g., Ni <sub>3</sub> Al-Ni <sub>3</sub> Cb, coated with a NiCrAlY overlay coating.	B
	(iv) Fiber (W-Re-Hf-C, W-Hf-C, or W-3ThO <sub>2</sub> )- reinforced Mar-M-200 composite coated with a NiCrAlY overlay coating.	C
	(v) Chromium-base alloys, e.g., Cr-7 Mo-1 Cb-.1 Y, coated with a nitridation-resistant coating such as Li-doped Cr-Cr <sub>2</sub> O <sub>3</sub> -Y <sub>2</sub> O <sub>3</sub> .	C
2200°F	(i) Commercial hot-pressed silicon nitride.	B
	(ii) Commercial hot-pressed silicon carbide.	B
2400°F	(i) Silicon nitride hot-pressed with Y <sub>2</sub> O <sub>3</sub> .	C
	(ii) Silicon carbide sintered with boron.	C
2500°F	(i) Advanced hot-pressed or sintered silicon nitride.	D
	(ii) Advanced hot-pressed or sintered silicon carbide.	D
	(iii) Advanced hot-pressed silicon nitride coated with silicon carbide.	D

\* This is a partial rating based on corrosion/erosion behavior only at a particular temperature. For overall ratings and materials recommendations including working fluid compatibility, mechanical properties, etc., see the appropriate subsection of Section 3.

Table 3.4 — Gas Turbine Materials Suitable for Use with Low-Btu Gas

<u>Maximum Material Temperature</u>	<u>Material</u>	<u>Rating*</u>
1500°F	Superalloys such as U-500, U-520 coated with a chromium diffusion or CoCrAlY overlay coating.	A
1600°F	(i) Superalloys such as X-45 or U-710, coated with a NiCoCrAlY overlay coating.	A
	(ii) Superalloy such as U-710 coated with a chromium diffusion coating.	A
1800°F	(i) Superalloys such as Mar-M-509, IN-792 or IN-739 coated with a Pt-modified NiCoCrAlY overlay coating.	B
	(ii) Superalloys such as IN-738 coated with a chromium coating.	B
1950°F	Pt-modified CoCrAlY overlay coating on WAZ-16 alloy.	B
2050°F	(i) WAZ-16 alloy coated with a Pt-modified CoCrAlY overlay coating.	C
	(ii) Directionally solidified eutectic alloy e.g., Ni <sub>3</sub> Al-Ni <sub>3</sub> Cb, coated with a Pt-modified CoCrAlY overlay coating.	C
	(iii) Chromium-base alloys, e.g., Cr-7 Mo-1 Cb-.1 Y, coated with Li-doped Cr-Cr <sub>2</sub> O <sub>3</sub> Y <sub>2</sub> O <sub>3</sub> .	C
	(iv) Graded SiC or ZrO <sub>2</sub> coating on WAZ-16 alloy.	D
2200°F	(i) Commercial hot-pressed silicon nitride.	B
	(ii) Commercial hot-pressed silicon carbide.	B
2400°F	(i) Silicon nitride hot-pressed with Y <sub>2</sub> O <sub>3</sub> .	C
	(ii) Silicon carbide sintered with boron.	C
2500°F	(i) Advanced hot-pressed or sintered silicon nitride.	D
	(ii) Advanced hot-pressed or sintered silicon carbide.	D
	(iii) Advanced hot-pressed silicon nitride coated with silicon carbide.	D

\* This is a partial rating based on corrosion/erosion behavior only at a particular temperature. For overall ratings and material recommendations, including working fluid compatibility, mechanical properties, etc., see the appropriate subsection of Section 3.

complete review of these data. The gas turbine materials recommended in Tables 3.3 and 3.4, however, fall into four categories: ceramics, chromium alloys, coatings, and uncoated superalloys. A brief summary of relevant oxidation and hot corrosion data on these materials is presented in the following sections.

#### Ceramic Materials

The ceramic materials, mainly hot-pressed silicon nitride ( $\text{Si}_3\text{N}_4$ ) and hot-pressed or sintered silicon carbide ( $\text{SiC}$ ), are contemplated for use as gas turbine vane and blade materials at temperatures from 1367 to 1644°K (2000 to 2500°F). At these temperatures, alkali sulfates are not stable and, hence, should not condense on these ceramic materials. Thus the use of ceramic materials at these high temperatures is limited by oxidation and erosion only in low-Btu gas, and no hot-corrosion attack is expected.

The oxidation/erosion data for commercially available hot-pressed silicon nitride and silicon carbide are summarized in Figure 3.7, which shows the average surface recession in 0.9 Ms (250 hr) as a function of temperature in a gas turbine environment burning ASTM GT-2 diesel oil at 303.9 kPa (3 atm) pressure (References 3.7, 3.8). The data are presented on an Arrhenius-type plot, even though experimental data are available only at two temperatures. The data show that commercial hot-pressed silicon nitride and silicon carbide could experience rather large surface recessions above approximately 1478°K (2200°F). The projected recessions at 1478°K (2200°F) for 36 Ms (10,000 hr) operation are approximately 0.355 to 0.584 mm (14 to 23 mils) for silicon nitride and silicon carbide, respectively. Thus, the use of the commercially available silicon nitride and silicon carbide would probably be limited to about 1478°K (2200°F).

Progress is being made, however, in improving both silicon nitride and silicon carbide materials to increase their oxidation/erosion resistance in addition to their mechanical properties. These ceramic materials are now being experimentally formed by using alternative

Curve 679699-A

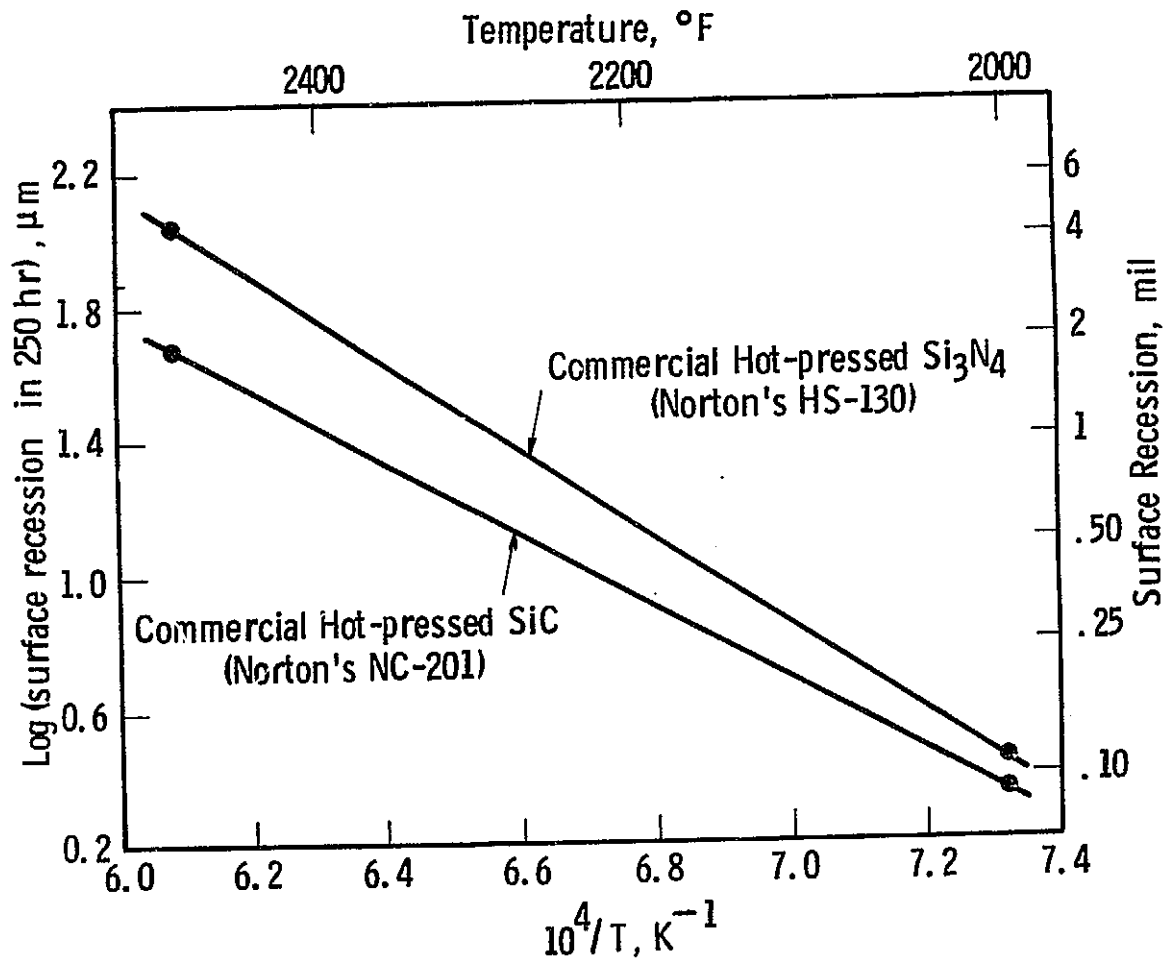


Figure 3.7 - Estimated surface recessions for hot-pressed silicon nitride and silicon carbide in a gas turbine environment in 250 hr.



hot-pressing additives, and also by employing alternative powder consolidation techniques such as sintering. Preliminary results show that hot-pressing silicon nitride with yttrium oxide ( $Y_2O_3$ ) instead of magnesium oxide (MgO) which is used in commercial silicon nitride, could improve its oxidation resistance and other properties to make it suitable for use at temperatures up to about 1589°K (2400°F). The use of ceramic materials above this temperature will require large improvements even in present experimental materials. One approach may be to use silicon carbide-coated silicon nitride, since silicon carbide exhibits much greater resistance to oxidation/corrosion in a gas turbine environment.

#### Chromium-Based Alloys

Chromium-based alloys, e.g., Cr-7 Mo-1 Cb-0.1 Y-0.1 C, Cr-7 Mo-1 Cb-0.1 Y-0.08 B, or Cr-1.8 Ta-0.1 Y-0.06 C-0.05 B, can be used as gas turbine materials, provided they are protected against embrittlement due to nitridation. A lithium-doped  $Cr-Cr_2O_3-Y_2O_3$  coating has shown great promise in preventing nitridation of chromium-based alloys (Reference 3.9). This coating is produced by first codepositing chromium and lithium on the surface of the alloy by electrolysis in a fused salt bath, and then plasma-spraying a powdered mixture of chromium and yttrium oxide. The additions of lithium and yttrium oxide aid in the stabilization of the basically chromium oxide coating and also reduce its oxidation rate. In addition to protecting chromium-based alloys against embrittlement, this coating also affords excellent oxidation resistance at temperatures up to about 1422°K (2100°F). The oxidation behavior of this coating on a Cr-7 Mo-TaC alloy is summarized in Figure 3.8. The data, extrapolated to 36 Ms (10,000 hr), predict a coating recession of only 15.2 to 30.4 mm (0.6 to 1.2 mil) at 1422°K (2100°F). The data also reveal, however, that the oxidation rate increases with an increasing cooling rate, and, therefore, the resistance of the coating to thermal cycling will have to be improved. Thus, chromium-based alloys might be considered for use as gas turbine materials with clean fuels, provided they are protected with a coating of the type Li-Cr- $Cr_2O_3-Y_2O_3$  with sufficient resistance to thermal cycling.

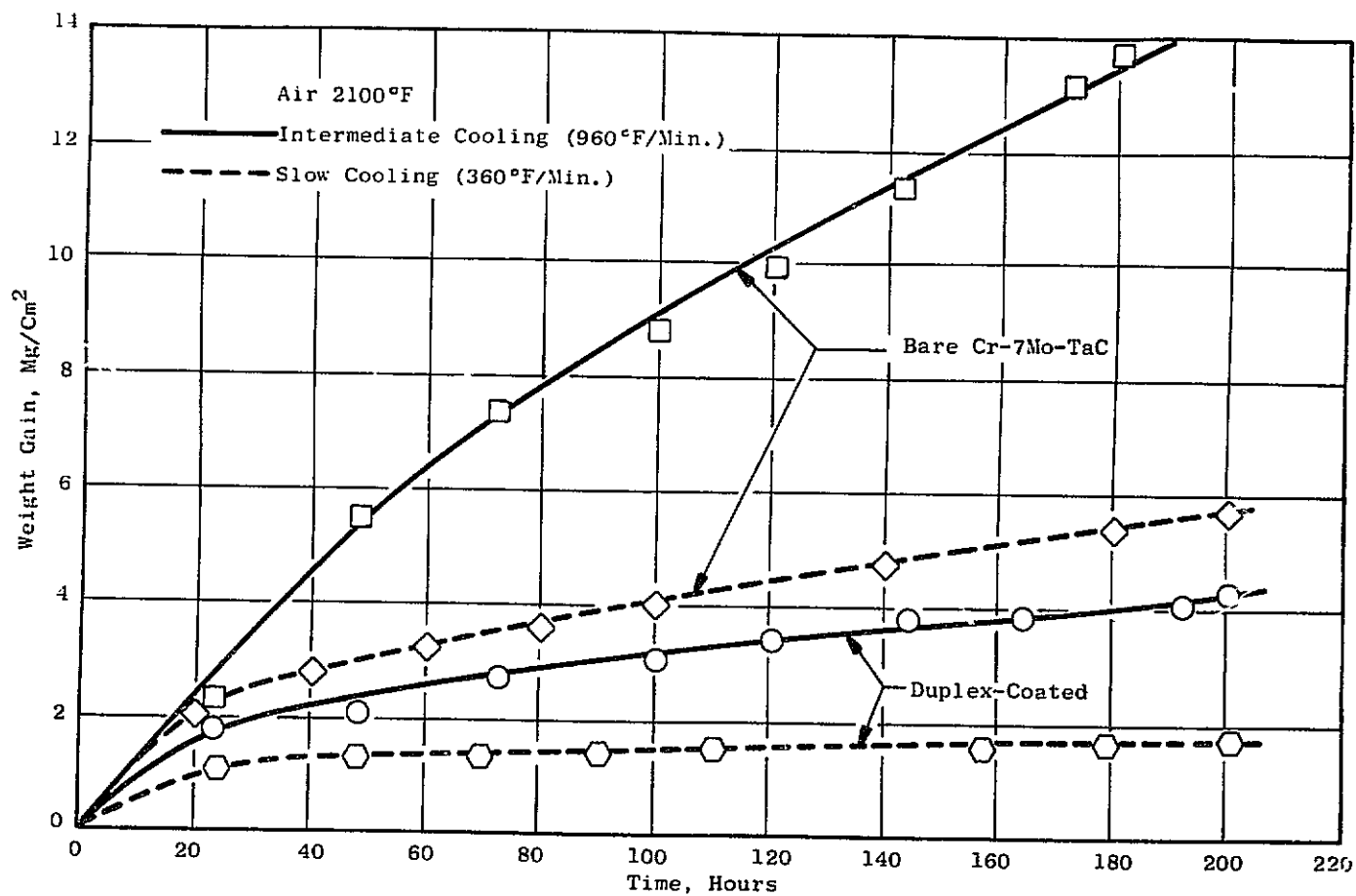


Figure 3.8 — Oxidation behavior of chromided plus plasma-sprayed (90 Cr-10 Y<sub>2</sub>O<sub>3</sub>) coating and the substrate Cr-based alloy in air at 2100°F.

This coating has also shown excellent resistance to hot corrosion attack by liquid sulfates (Reference 3.10), and, hence, coated chromium-based alloys may also be used in gas turbines burning low-Btu gas. Considerable further work is required, however, to substantiate the laboratory data by experiments in an actual gas turbine environment.

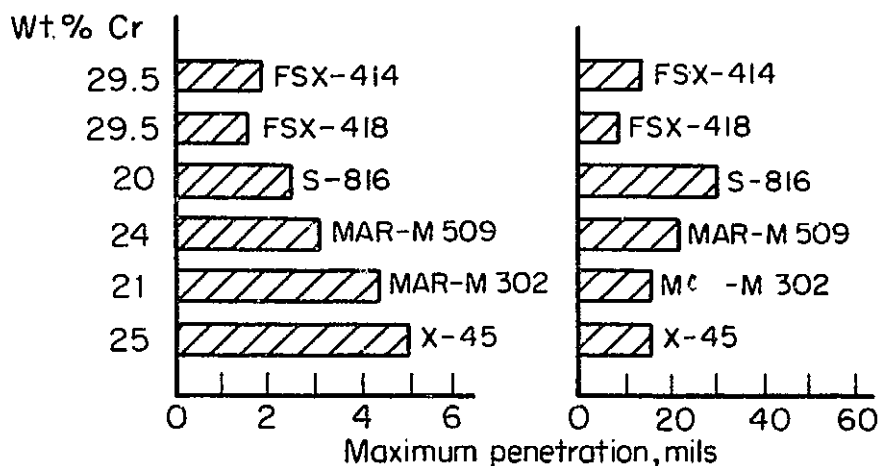
#### Uncoated Nickel- and Cobalt-Based Superalloys

As mentioned earlier, the experimental data on oxidation and hot corrosion behavior of nickel- and cobalt-based superalloys are vast and often vary from laboratory to laboratory. The materials selected for use in oxidizing and hot-corrosive environments are those believed to offer the highest performance among a multitude of available alloys. The oxidation and hot corrosion data on these selected materials are summarized below.

The relative rates of oxidation and hot corrosion of several cobalt-based alloys are shown in Figure 3.9 (Reference 3.11). The oxidation data are for 1366°K (2000°F) in a rig burning clean natural gas, while the hot corrosion data are for 1144°K (1600°F) in a rig burning residual oil with 3% sulfur and 325 ppm sodium chloride.

The corrosion and oxidation rate data for several of the selected alloys are shown in Figure 3.10, as a function of temperature (Reference 3.12). The amount of metal recession after 540 ks (150 hr) of exposure is plotted against surface temperature under conditions of normal oxidation and under hot corrosion conditions using ASTM GT-3 fuel with 5 ppm sodium and 2 ppm vanadium in the fuel. The curves show that alloys like U-500, IN-713, IN-738, and X-45 can be used in an oxidizing gas turbine environment at temperatures up to about 1200°K (1700°F), but they will require protective coatings in a hot corrosion environment to prevent excessive metal recessions.

In 1970, the National Materials Advisory Board sponsored a round-robin test of the hot corrosion behavior of several alloys at 1088 to 1255°K (1500 to 1800°F) in a gas turbine combustion environment contaminated by sulfur and sea salt (Reference 3.13). Ranking of the



(a) Hot corrosion in  
600hr. exposure  
@ 1600 °F in a  
rig burning  
residual oil with  
3% S and 325 ppm  
NaCl

(b) Oxidation in  
600hr. exposure  
@ 2000 °F in a  
rig burning  
clean natural  
gas

Figure 3.9 —Relative hot-corrosion and oxidation resistance of selected cobalt-based alloys in 600 hr.

Curve 642993-A

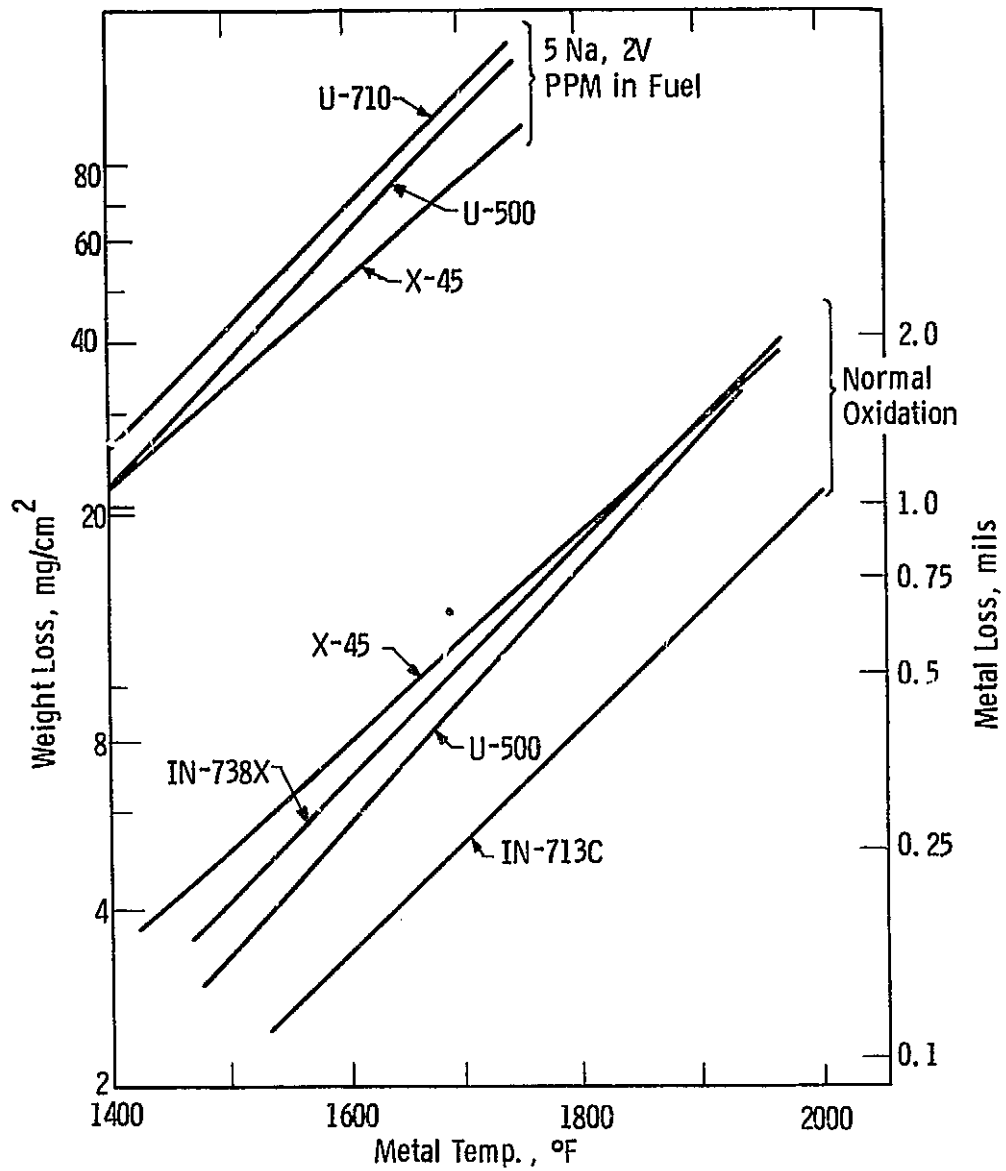


Figure 3.10 — Corrosion rate of several alloys when burning 3-CT fuel compared to normal oxidation in 150 hr.

Table 3.5 — Results of "Round Robin" Test Organized by National Materials Advisory Board

Alloy	Ranking of Alloys by Participant														
	A	B	C	D	E	F	G	H	I	J	K	L	M	N	O
U-500	1	2	2	2	1	3	1	1	3	3	3	3	1	3	1
IN-738	2	1	1	3	3	2	3	2	2	2	1	2	3	1	2
MAR-M 421	3	3	3	4	4	1	2	4	1	5	2	1	2	2	3
U-700	4	4	4	1	2	4	4	3	4	1	4	4	4	4	4
Alloy 713 C	5	6	5	5	6	5	5	5	5	6	6	5	5	5	5
IN-100	6	5	6	6	5	6	6	6	6	4	5	6	6	6	6
No. of alloys not ranked according to average	1	3	1	4	5	3	2	3	3	6	4	3	2	2	1
Total no. of places removed from average	1	3	1	7	7	5	3	3	5	11	5	5	3	3	1

RELIABILITY OF THE  
TEST IS POOR

alloys by 15 U.S. laboratories (including Westinghouse) is shown in Table 3.5. U-500 and IN-738 were ranked far superior to the others tested. Corrosion studies at Westinghouse (Reference 3.14) show that IN-738 is better than U-500, and as good as U-710 when subjected to a variety of contaminant-temperature conditions. The comparative hot corrosion rates of several alloys are shown in Figure 3.11 (Reference 3.15).

Based on these data and their current usage in gas turbines, it is believed that uncoated U-500 and U-520 can be used in clean fuels up to about 1089°K (1500°F), X-45 and U-700 up to 1144°K (1600°F), and Mar-M-509, IN-738, IN-792, and FSX-418 up to about 1200°K (1700°F). Above 1200°K (1700°F), protective coatings will be required.

Reactive elements such as cerium, lanthanum, or yttrium, or fine dispersions of reactive oxides, such as thorium dioxide ( $\text{ThO}_2$ ), yttrium oxide, cerium dioxide ( $\text{CeO}_2$ ), and possibly even aluminum oxide ( $\text{Al}_2\text{O}_3$ ), have been found to increase the oxidation resistance of both nickel- and cobalt-based alloys (which form either chromium oxide or aluminum oxide scales) under cyclic conditions, apparently by improving the oxide adhesion and preventing spalling (Reference 3.16). Alloys modified with these rare earth elements (e.g., modified B-1900 and IN-100) could therefore be used up to about 1339°K (1950°F) in gas turbines with clean fuels, though their oxidation behavior in an actual gas turbine environment at these high temperatures remains to be verified and the effect of such additions on mechanical properties measured.

In hot-corrosive environments such as would be produced by burning low-Btu gas, however, it is considered safer to recommend using coatings on nickel- and cobalt-based superalloys for use even at as low a temperature as 1089°K (1500°F). These coatings are discussed below.

#### Oxidation- and Hot-Corrosion Resistant Coatings

The recommended coatings for various superalloys, dispersion-hardened alloys, composites, and directionally solidified eutectics can be classified into the following three categories:

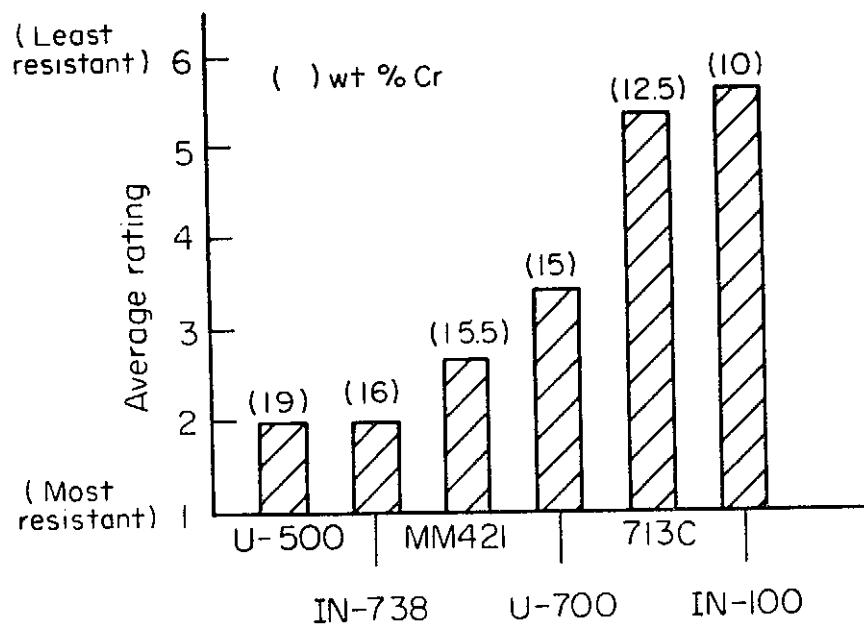


Figure 3.11 — Average relative hot-corrosion resistance of selected nickel-based superalloys.

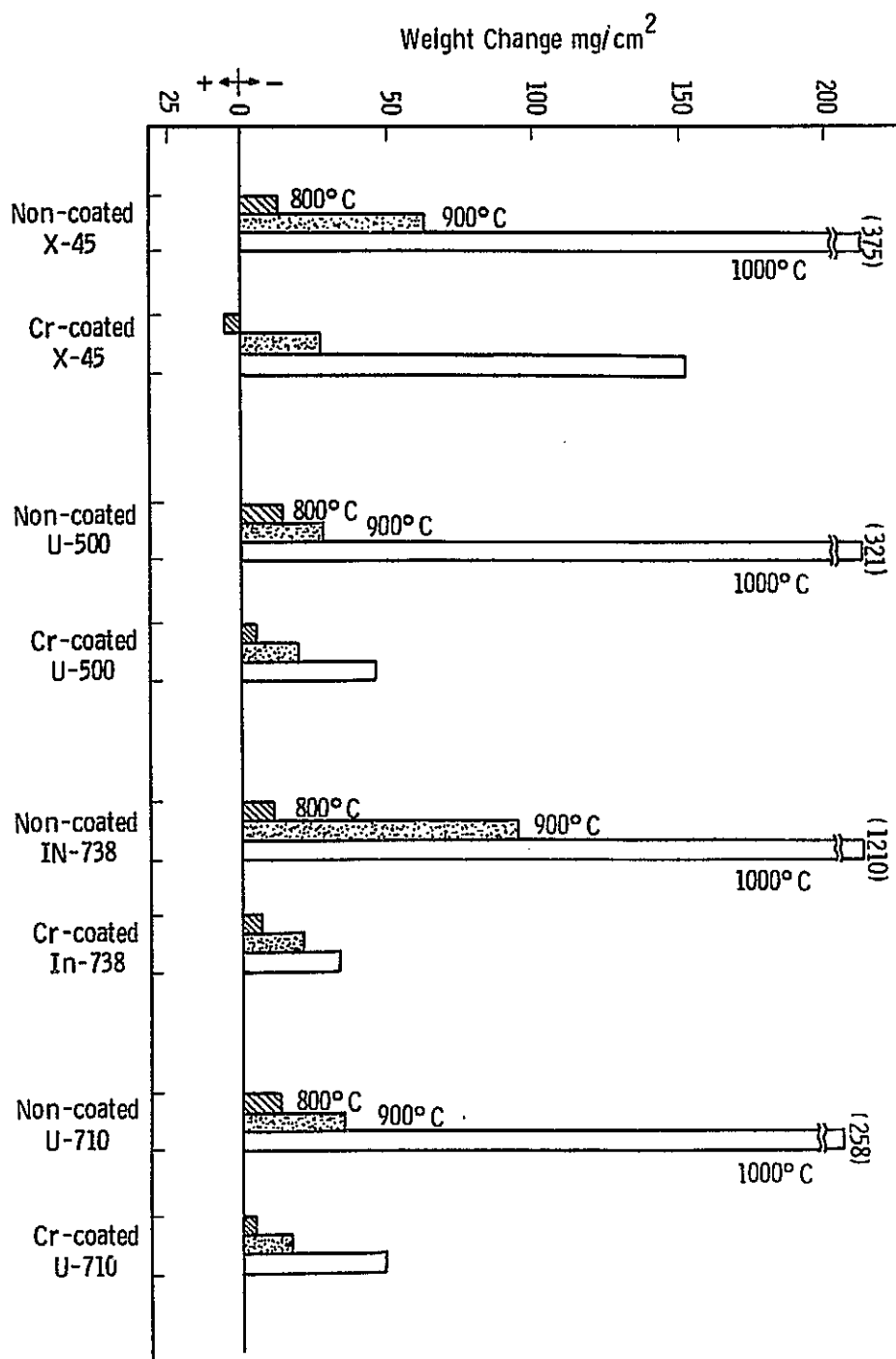


### (1) Diffusion Chromium Coatings

Chromium coatings have been used successfully for conferring oxidation and hot-corrosion resistance in industrial turbines (Reference 3.17). These coatings are produced by a pack cementation process. The hot-corrosion resistance of chromium-coated X-45, IN-738X, U-500, and U-710, in combustion gases obtained by burning heavy residual oil (containing 35 ppm vanadium, 6-7 ppm sodium) with 500 ppm sodium chloride added to it, is illustrated in Figure 3.12 at temperatures of 1073, 1173, and 1273°K (up to 1832°F) (Reference 3.18). From these data it is clear that the diffusion chromium coatings can be used both with clean fuels and with low-Btu gas up to about 1255°K (1800°F). It has been found advantageous to cover these chromium coatings with a thin outer layer of iron or nickel, which appears to control the rate of outward diffusion of chromium to form a protective scale; the barrier metals are not themselves oxidized (Reference 3.13).

### (2) Diffusion Aluminide Coatings

Aluminide coatings, usually formed by a pack cementation process by diffusing aluminum into the surfaces of nickel- and cobalt-based alloys, improve their oxidation resistance. The subject of aluminide coatings for superalloys has been reviewed by Jackson and Hall (Reference 3.19), the Materials Advisory Board Committee on coatings (Reference 3.20), Lindblad (Reference 3.21), and Goward (Reference 3.22). Since these coatings form a surface intermetallic near 50% aluminum, and since upon oxidation this intermetallic compound forms a surface layer of tenacious aluminum oxide, aluminide coatings are currently the most widely used protection system for superalloys. They offer adequate long-time protection in oxidizing atmospheres to a maximum temperature of approximately 1255°K (1800°F), depending upon the particular substrate alloy. The failure times of an aluminide coating on WI-52 alloy in burner-rig tests using clean fuel are shown in Figure 3.13 (Reference 3.23) as a function of temperature. The life of these aluminide coatings at higher temperatures is limited by oxide spalling in cyclic conditions, and also by the interdiffusion of aluminum into the



Curve 679714-8

Figure 3.12 — Corrosion rates of Cr-coated X-45, U-500, In-738 and U-710 in heavy residual oil with 500 ppm NaCl, for 100 hr.

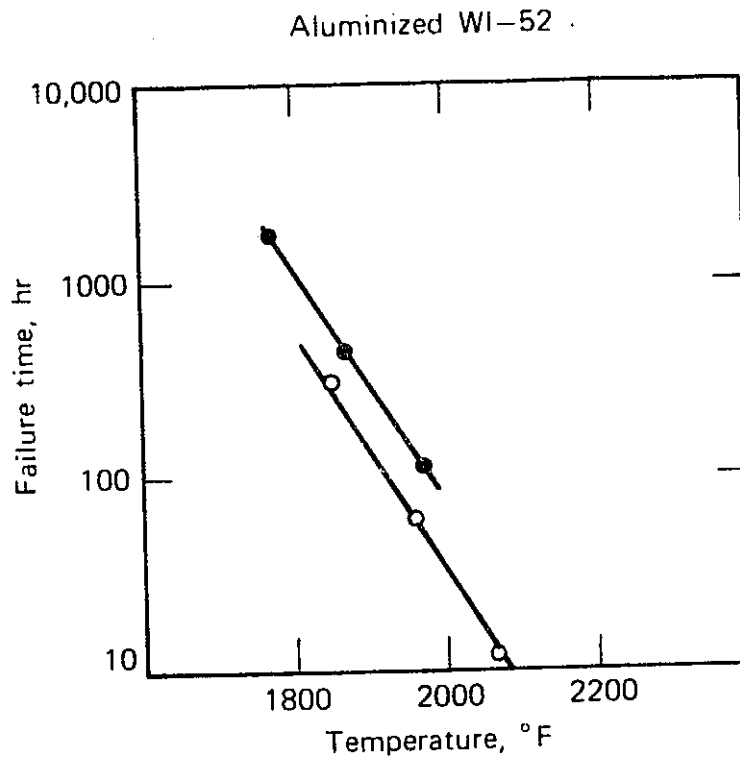


Figure 3.13 — Aluminide coating (on WI-52 alloy) life at various temperatures in burner-rig tests using different rigs and failure criteria (1 hr cycles followed by air-blast quench, o = visual failure; • = metallographic failure. (Reference 3.23)

Table 3.6 — Cyclic Oxidation Behavior of MCrAlY-Type Overlay Coatings (Reference 3.24)

<u>Coating Type</u>	<u>Hours Tested (No. of Cycles)</u>	<u>Total Wt. Change (mg/cm<sup>2</sup>)</u>
<u>2200°F</u>		
NiCrAlY/Pt	100	0.56
NiCoCrAlY	20	1.27
NiCrAlY	100	- 4.5
<u>2100°F</u>		
NiCrAlY/Pt	40	3.1
NiCoCrAlY	100	- 3.5
NiCrAlY	100	- 4.4
<u>2000°F</u>		
NiCrAlY/Pt	500	0.58
NiCoCrAlY	500	0.52
NiCrAlY	500	1.24

Composition and Thickness of Above Coatings

NiCrAlY/Pt: Ni-18 Cr-12 Al-0.3 Y (5 mil)+ Pt  
(0.25 mil)

NiCoCrAlY : Co-33 Ni-18 Cr-15 Al-0.6 Y (5 mil)

NiCrAlY : Ni-18 Cr-12 Al-0.3 Y (5 mil)

substrate causing formation of undesirable solid solutions. Use of a substrate alloy such as yttrium oxide-containing IN-792 will increase the adherence of the aluminide coating, and hence it is suggested that aluminide coatings may be used up to about 1311°K (1900°F) on this alloy. Use of barrier layers to prevent diffusion of aluminum into the substrate alloy is also extensively being studied (Reference 3.24). No barriers, however, have been successful in increasing the long-term temperature of aluminide coatings beyond about 1311°K (1900°F).

### (3) MCrAlY-Type Overlay Coatings

The MCrAlY coatings (M = nickel and/or cobalt) also rely on aluminum oxide or aluminum oxide-rich surface scales to provide protection against oxidizing and hot-corrosive environments. These coatings offer the best promise for providing superalloys, dispersion-strengthened superalloys, composites, and directionally solidified eutectics (e.g., Ni<sub>3</sub>Al - Ni<sub>3</sub>Cb) with protection to several hundred degrees higher than that offered by aluminide coatings. These coatings are usually applied as overlays by electron beam vapor deposition, though in some cases cladding may be used.

The MCrAlY type coatings are a family of compositions within the system MCrAlY, with different gas turbine manufacturers developing and testing different compositions. The MCrAlY coatings are further modified with the inclusion of platinum for use at higher temperatures in hot-corrosive environments. A detailed evaluation of MCrAlY and MCrAlY/Pt coatings has recently been reported by Felten et al. (Reference 3.24). In their study, coatings were applied on directionally solidified eutectics; the results they obtained, however, illustrate the great potential of these coatings on any substrate system, and also give an indication of the highest temperature at which these coatings can be used.

Felten et al. evaluated coatings under conditions of cyclic oxidation. The results on various coatings are summarized in Table 3.6. Based on their results, and on additional work done with similar coatings at Westinghouse, it is felt that in clean fuels, NiCrAlY coating can be

used successfully to about 1394°K (2050°F). In hot-corrosive environments, however, such as would be expected in burning low-Btu gas, NiCoCrAlY type coatings should be used up to about 1144°K (1600°F). Above this temperature, Pt-modified CoCrAlY coating is recommended. These coatings are still under development, and their detailed evaluation in a hot-corrosive environment at temperatures up to 1394°K (2050°F) is currently in progress at Westinghouse. Preliminary results with a CoCrAlY coating on cobalt-based alloys project a surface recession of about 2.82 pm in 36 Ms (4 mils in 10,000 hr) of operation with ASTM GT-2 fuel containing 10 ppm sodium and 0.5% sulfur. Detailed, long-term evaluation of these coatings in gas turbine environments is required before making firm recommendations.

### 3.2.2 Heat Exchanger Materials

The following types of boilers are being considered in the ECAS study:

- (i) Atmospheric fluidized bed boiler
- (ii) Pressurized fluidized bed boiler
- (iii) Atmospheric conventional boiler
- (iv) Pressurized supercharged boiler
- (v) Pressurized fired heater.

The fuels to be used for these boilers are either pulverized coals, or high- or low-Btu gases obtained from the three coals specified by NASA. Even though the boiler tubes may contain steam, liquid metals, or inert gases, their fire-side corrosion behavior will be similar. The following discussion of fire-side corrosion, therefore, applies to all heat transfer materials (e.g., in-bed boiler tubes, convection heater, superheaters, etc.) which will be used in conjunction with the above boilers.

#### 3.2.2.1 Corrosion, Erosion, and Fouling of Heat Exchanger Materials

The performance of fluidized bed combustion boilers with immersed heat transfer surfaces depends on the resistance to corrosion,

erosion, and fouling of the heat transfer surface in the fluidized bed or in the freeboard. Short-term experimental data (Reference 3.25) on tubes immersed in fluidized beds of limestone or dolomite and burning various coals show that conventional boiler tube materials might be suitable for use in fluidized bed combustion boiler designs without encountering exceptional corrosion, erosion, or fouling problems.

Fire-side metal loss from heat transfer tubes may occur through abrasion, fouling, and corrosion. A great deal of information on fire-side corrosion is available from conventional boiler experience (Reference 3.26). Although metal erosion in a conventional coal-fired boiler is not as severe as that in the gas turbine, the ash-erosion problem does exist in the conventional boilers and must not be ignored even though the ash particles may be exceedingly fine. The hard nature of pulverized coal-ash makes the particles particularly erosive. Where the ash particles accumulate, as at the turns formed by baffles within boiler tanks, erosion is a potential problem. External erosion of the in-bed tubes in the fluidized bed may result from the vigorous particle motion which continuously scours the surface of the tubes. Erosion, per se, is not considered important in the fluid bed application where the maximum gas velocity in the boilers is 4.573 m/s (15 ft/s), and the particle velocity is considerably less than the gas velocity due to the high frequency of inelastic particle collisions in the bed. The vigorous particle motion may be beneficial in scrubbing off deposits formed on heat transfer surfaces.

Corrosion will occur predominantly by chemical attack with different mechanisms such as surface oxidation, removal of the protective scale on metal surfaces through chemical reactions with corrosives, and direct chemical attack on metal surfaces. The alkali compounds, chlorine and sulfur present in coals, will again be the detrimental contaminants as discussed for the gas turbine materials.

The concentrations of alkali metals appearing in the fluidized bed combustion gas will be limited by the feed rate of coal and dolomite to the fluidized bed system and the rate at which alkalis can be liberated from the stone and char particles during their stay in the bed.

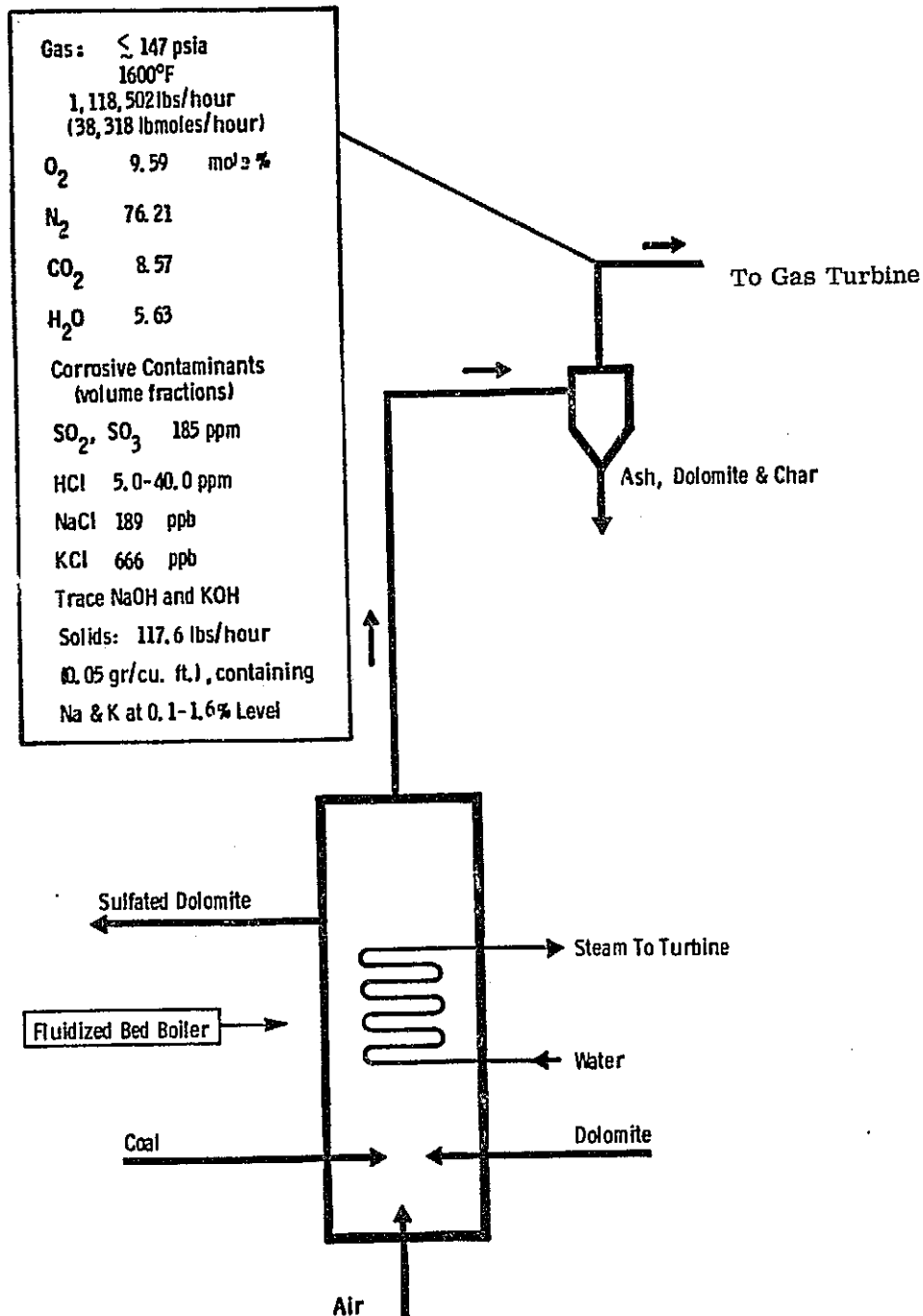


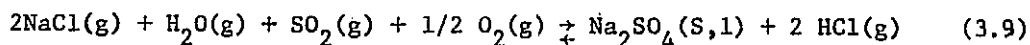
Figure 3.14 — Summary of gas chemistry and corrosive contaminant levels in the combustion gas stream directed to the gas turbine.



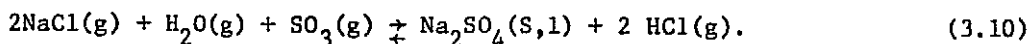
A summary of gas chemistry and corrosive contaminant levels in the gases leaving a fluidized bed combustor is shown in Figure 3.14. The contaminant levels are calculated for a coal containing 3.59% sulfur and 0.52% sodium oxide and 1.80% potassium oxide (both in the ash), and a dolomite containing 0.070 and 0.217% sodium and potassium, respectively. The combined chlorine content of coal and dolomite is assumed to range between 100 and 800 ppm in the above calculations. These levels of contaminants represent Illinois No. 6 coal fairly well. This is a working estimate which assumes complete release of chlorine from coal and dolomite and a 1% release of sodium and potassium. The actual alkali release may be appreciably lower, resulting in correspondingly lower levels of volatile alkali compounds in the coal and combustion gases.

Figure 3.14 shows that, at the probable chlorine levels for U.S. coals and with the assumption that all chlorine produces hydrochloric acid vapors that can react with alkali compounds, the predominant volatile alkali species are the chlorides. Hydroxides and metal vapors are calculated to exist only at trace levels (i.e., at two to three orders of magnitude lower concentration than the chlorides).

The gaseous environment of a fluidized bed combustor system thus principally consists of oxygen, nitrogen, carbon dioxide, and water vapor, with minor concentrations of hydrogen chloride, sodium chloride, potassium chloride, sodium dioxide, and sulfur trioxide. The three principal classes of reactions that can occur in this gas phase are oxidation, sulfidation, and hydrogen chloride and alkali chloride effects. Another class of corrosion reaction that may be possible is hot corrosion, since alkali sulfate deposition could conceivably occur by reactions such as



and



679977-B

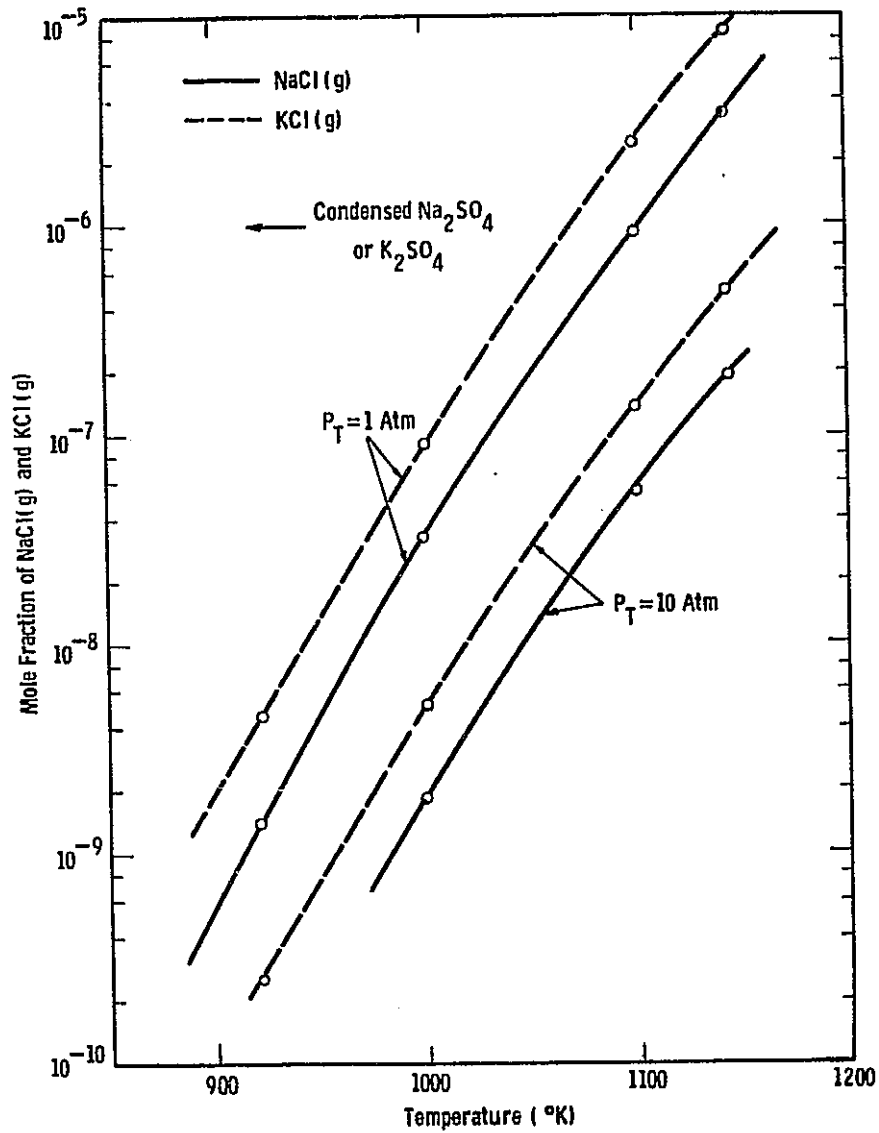


Figure 3.15 — Minimum NaCl(g) and KCl(g) required to condense  $\text{Na}_2\text{SO}_4$  or  $\text{K}_2\text{SO}_4$  in a gas mixture containing 10%  $\text{O}_2$ , 5%  $\text{H}_2\text{O}$ , 200 ppm  $\text{SO}_2$  and 50 ppm HCl.

Similar reactions can also be written for deposition of potassium sulfate. The minimum mole fractions of sodium chloride and potassium chloride vapor required for condensation of sodium sulfate or potassium sulfate are shown in Figure 3.15 as a function of temperature. The concentrations of oxygen and water vapor used in the calculation are 10 and 5%, respectively, while those of sulfur dioxide and hydrogen chloride are 200 and 50 ppm, respectively. At the minimum projected levels of sodium chloride and potassium chloride in fluidized bed combustor gases, condensation will not occur at 1144°K (1600°F); at temperatures lower than 1050°K (1431°F), however, condensation can occur. Although condensation is thermodynamically favored under these latter conditions, it may not necessarily occur, because of kinetic limitations. The hot corrosion of heat exchanger materials in a fluidized bed by liquid alkali sulfates is, therefore, not likely to occur; but, the condensation of alkali chlorides on heat transfer surfaces in fluid bed combustors burning high-chlorine-content coals can lead to accelerated corrosion. Chlorine has been known to contribute significantly to the fouling and corrosion of tubing when present in the coal in concentrations higher than 0.3%.

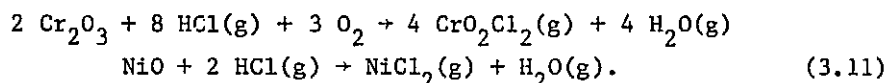
Dainton and Elliott (Reference 3.32) immersed a stainless steel probe in an atmospheric fluidized bed burning a coal of both high chlorine and sulfur content (Cl-0.86 wt %, S - 1.06 wt %) at a temperature of 978°K (1300°F) and found for metal surface temperatures above 866°K (1100°F) there was no deposit or corrosion attack in 432 ks (120 hr). At lower temperatures sodium chloride deposited.

Giddon (Reference 3.29) in comparable experiments found that the deposition rate of sodium chloride was related to the chlorine content of the coal. He also found a maximum rate of deposition, for each particular coal, to be in the metal temperature range of 783 to 868°K (950 to 1100°F). He found no corrosion attack after 540 ks (150 hr) of testing in a low chlorine (0.3 wt%) coal.

Comprehensive and systematic studies of corrosion attack and deposition on boiler tube materials by the National Coal Board in pressurized and atmospheric beds combusting coal with dolomite resulted in the conclusion that high-chlorine coals, which allow deposition of sodium chloride, cause accelerated corrosion attack of the alloys, including the austenitic stainless steels.

Conventional boiler tube materials can operate in the combustion atmosphere of a fluidized bed boiler with acceptable levels of corrosion attack, unless there is deposition of alkali chlorides. The formation of alkali chloride as liquid or solid will result in accelerated corrosion attack of the heat transfer tube materials unless the surface temperatures are held to less than 811°K (1000°F).

The presence of chlorides in the combustion gases can also result in an accelerated oxidation because of the volatilization of the protective oxide scales formed on various alloys as gaseous chloride or oxychloride, by reactions such as:



The extent and severity of such attack under actual operating conditions will depend upon the hydrogen chloride partial pressure in the combustion gases, the gas velocity, and the relative rates of formation of the protective oxide and of the gaseous chloride or oxychloride.

### 3.2.2.2 Experimental Studies of In-Bed Corrosion and Erosion

The corrosion and deposit problems on heat transfer materials in conventional pulverized-coal-fired boilers are well documented (References 3.26, 3.27) and the heat transfer materials for use up to metal temperatures of about 866°K (1100°F) are readily available. Recently, experimental studies (References 3.30, 3.31) were also conducted on the corrosion, erosion, and fouling of boiler tube materials in fluidized bed combustors; the results are summarized below.

### Pressurized Bed Tests of In-Bed Boiler Tube Materials (Reference 3.30)

In this study, the highest temperature of the fluidized bed was 1072°K (1470°F), and the highest pressure was 506.5 kPa (5 atm). The investigation was performed on a U.K. coal with a U.K. dolomite, and by combusting a U.S. coal with a U.S. dolomite in a 1.219 by 0.6096 m (48 by 24 in ) pressurized fluidized bed at 303.9 to 506.5 kPa (3 to 5 atm) pressure. The U.K. coal chosen was Welbeck coal, with 0.53 wt% chlorine and 1.25 wt% sulfur; the U.S. coal was Humphrey No. 7, with 0.08 wt% chlorine and 2.75 wt% sulfur. Specimens of seven boiler tube materials, all steels, welded together into continuous tubes, were immersed in the bed and air-cooled to the temperature range 600 to 1072°K (620 to 1470°F). The test specimens were descaled and weight losses examined after each run of roughly 360 ks (100 hr) duration at a fluidizing velocity of 0.6096 m/s (2 ft/s).

The results are presented in Table 3.7. In all cases visual observation indicated that the color, adherence, and type of deposits depended on the material and temperature of the specimens. Metallographic examinations found no evidence of intergranular penetration in any of the tested specimens, and the higher weight losses of the low-alloy ferritic steel specimens were associated with a general surface roughening. The nonuniformity of the weight losses can, in some instance, be related to the position of the specimens relative to the coal-feeding nozzles.

### Corrosion Studies of Boiler Tube Materials at Atmospheric Pressure and Low Fluidizing Velocities (Reference 3.30)

U.S. Humphrey No. 7 coal was combusted in a 0.3048 m (12 in ) rig at 0.9144 m/s (3 ft/s) fluidizing velocity with and without limestone addition. Specimens of tube form and coupon were used in the bed and in the freeboard. The results from 1.8 Ms (500 hr) tests without limestone addition are summarized in Table 3.8. There was no marked difference between these results and those of similar tests under pressurized conditions reported above. The high-chromium alloys again appeared satisfactory, while the medium-carbon and 2-1/4% Cr-1% Mo steels suffered intolerably high rates of metal loss. In all instances substantially less metal wastage was observed for the tubes and coupons located in the freeboard than for those in the bed.

Table 3.7 — Average Tube Specimen Weight Loss under Pressurized  
Operation Condition,  $\mu\text{g}/\text{cm}^2\text{-h}$

TUBE MATERIAL															
TEMPERATURE RANGE, °F(a)		12% Cr		RF 36 <sup>(d)</sup>		SF 316 <sup>(d)</sup>		PE 16 <sup>(d)</sup>		Esshete <sup>(d)</sup> 1250		1% Cr 1/2% Mo		2 1/4% Cr 1% Mo	
Series B(b)	Series U(c)	B	U	B	U	B	U	B	U	B	U	B	U	B	U
1350- 1460	<u>1470</u> <u>1450</u>	-	-	16	<u>145</u> <u>63</u>	15	<u>166</u> <u>80</u>	7	<u>50</u> <u>37</u>	50	<u>223</u> <u>207</u>	-	-	-	-
1320- 1380	1280- 1380	5	18	8	48	8	54	5	36	28	210	-	-	-	-
1040- 1220	1100- 1180	5	15	4	28	4	23	3	13	5	48	-	-	-	-
730- 920	830- 1090	6	29	13	29	11	33	6	17	9	-	373	254	445	319
660- 990	620- 920	2	18	4	9	4	22	3	8	5	15	24	99	35	151

- (a) Temperature ranges are the temperature differences between the ends of the composite tubes.
- (b) Series B is the result obtained from combusting a U.K. coal and a U.K. dolomite.
- (c) Series U is the result obtained from combusting a U.S. coal and a U.S. dolomite.
- (d) Analysis of metal specimens: RF 36/18 Cr-12 Ni-1 Nb-69 Fe; SF 316/17 Cr-12 Ni-2.5 Mo- 2 Mn-66.5 Fe; PE 16/18 Cr-37 Ni-5 Mo-1.2 Ti-1.2 Al-37 Fe; Esshete 1250/15 Cr-10 Ni-1 Mo-6 Mn-1 Nb-67 Fe.

Table 3.8 —Summary of Rate of Metal Loss- $\mu\text{g}/\text{cm}^2\text{h}$   
Duration 500 h

LOCATION	NOMINAL TEMPERATURE OF SPECIMEN °F	RATE OF WEIGHT LOSS - $\mu\text{g}/\text{cm}^2\text{h}$							
		Type 347 Austenitic Steel	Type 316 Austenitic Steel	Esshete 1250	12% Cr Ferritic Steel	2-1/4% Cr Ferritic Steel	Medium C Steel	Nimonic PE 16	
BED Tubes	735		2 <1	2 <1 <1	1 2	34 29 33	73 35 36		
			2 1	2 2 1	5 8	81 64 87	65 67 132		
	1095	4 2	4 3 3	5 5 3		459 793 365			
	1290	3 3	5 4 4	6 9 2	2 3 5			3 3 5	
	Coupons	-	-	-	-	-	-	-	
	FREEBOARD Tubes	755		<1 <1	<1 <1 <1	<1 2	29 23 23	36 21 18	
1285		1 1 2	1 1 2	2 5 6	1 1 3			1 1 2	
Coupons	-	-	-	-	-	-	-		

Table 3.9— Observed Rate of Weight Losses on Specimens  
Duration - 500 h

NOMINAL TEMPERATURE (°F)	RATE OF WEIGHT LOSS ( $\mu\text{g}/\text{cm}^2/\text{h}$ )					
	Type 347 austenitic steel	Type 316 austenitic steel	Esshete 1250	12% Cr ferritic	2-1/4% Cr ferritic	Medium C steel
750	7	2	2	3	30	41
	4	4	2	4	53	55
	1		1	4	96	614
	8		5	4	111	80
			4			
			7			
930	7	4	6	6		301
	3	4	9	6	A <sup>(a)</sup>	A
	9	6	7	9		
			7	8		
			11			
1110	6	3	6	2		
		3	7	3		
		2	7	2		
		4	9	2	A	A
		4	8	5		
1290	13	6	11	3		
	3	8	12	4		
	8	8	12	4		
	4	14	21	4		
	12	13	22	5		
	15	10	19	6		

(a) Specimens suffer internal attack on the steam side, possible by  $\text{Cl}^-$  and  $\text{O}_2$  in the steam supply, so data require additional correction.



Long-Term Corrosion Tests at Atmospheric Pressure to Assess  
the Effect of Limestone Addition on Corrosion of Boiler  
Tube Materials (Reference 3.30)

Four series of tests with duration of operation up to 3.6 Ms (1000 hr) were run. At the same time, the particle size of limestone and the combustion conditions were changed to evaluate their respective effects on corrosion. The available data using U.S. Humphrey No. 7 coal without limestone addition at a fluidizing velocity of 2.4384 m/s (8 ft/s) are presented in Table 3.9. Again, the data show that the austenitic steels perform satisfactorily; and of the chrome-ferritic steels, the 12% chromium steel behaves the best. The low-chromium steels suffer much higher weight losses. The conclusions of this study can be summarized as follows:

- The austenitic steels give very small weight loss [ $< 10 \mu\text{g}/\text{cm}^2$  after 1.8 Ms (500 hr) operation] at all tested temperatures for lower-chlorine-content coals and at fluidizing velocities up to 2.4384 m/s (8 ft/s). Increasing the fluidizing velocity increases the rate of weight loss.
- A high-chlorine coal is unlikely to cause corrosion of an austenitic steel heat transfer surface immersed in a fluidized bed if the metal temperature is kept above the dew point temperature of sodium chloride in the gas. The sodium chloride dew point temperature is determined mainly by the chlorine content of the coal and the bed temperature which determines its vapor pressure. The dew point would rise as the bed temperature is increased, thus increasing the temperature range over which metal corrosion is likely.
- The chrome-ferritic and medium-carbon steels are more susceptible to attack, as shown by their greater weight loss rates, although the rate tends to decrease with increasing operation time.
- Metallographic examination revealed no intergranular penetration or pitting under normal operating conditions.
- Substantially less corrosion was found on the specimens situated in the freeboard than on those in the bed.

Table 3.10 - Summary of Weight Loss Measurements in 1000-Hour  
Pressurized Bed Tests (Reference 3.33)

Alloy	Temperature °F	Weight loss μg/cm <sup>2</sup> h	Previous measurements in fluidized beds
1% Chrome	390-700	100	No data
2½% Chrome	(a) 700-1000 (b) 500-1250	260 400	{180 to 230 μg/cm <sup>2</sup> h @ 930°F } {570 to 970 μg/cm <sup>2</sup> h @ 1110°F }
12% Chrome	(a) 970-1220 (b) 1240-1430	160 170	{7 to 14 μg/cm <sup>2</sup> h @ 1290°F } {790 to 1000 μg/cm <sup>2</sup> h @ 1560°F }
18% Chrome (AISI 321)	(a) 1150-1380 (b) 1430-1530	70 40	{10 - 20 μg/cm <sup>2</sup> h @ 1290°F } For {10. - 70 μg/cm <sup>2</sup> h @ 1560°F } AISI 316
21% Chrome (Incoloy 800)	1380-1520	45	No data

### Pressurized Bed Tests at Higher Temperatures

These tests by NCB (Reference 3.33) differed from the pressurized bed tests performed previously in that the maximum bed temperature was much higher [1228 vs 1072°K (1750 vs 1470°F)] than previously. The bed pressure was 0.4826 mPa (70 psig) and the fluidizing gas velocity was 0.762 m/s (2.5 ft/s). Four tests totalling 734.4 ks (204 hr) operation were performed. The maximum specimen temperature of 1088°K (1500°F) in the tests was actually not very different from that of the previous pressurized bed tests [1072°K (1470°F)] or that of previous atmospheric-pressure tests [1122°K (1560°F)].

The main results of this study, which refer only to a test duration of about 3.60 Ms (1000 hr), are compared in Table 3.10, with those of work performed previously on the same materials. The report authors conclude that all the materials would have acceptable long-term corrosion performance at least up to the temperature levels at which they would be used in conventional boiler practice. For operation at high metal temperatures [1088°K (1500°F)], Incoloy 800 appears to give acceptable corrosion performance, but AISI 321 does not. Much longer-term testing, however, under precisely controlled conditions, would be needed to obtain definitive data on corrosion rates.

#### 3.2.2.3 Materials Recommendations for Various Heat Transfer Tubes

Based on current materials usage in conventional pulverized-fuel-fired boilers, experimental studies in fluidized bed boilers described in a previous section, and literature oxidation/corrosion data, the recommended materials suitable for heat transfer tubes are shown in Table 3.11. The temperatures given are the metal temperatures rather than the gas or bed temperatures, which may be several hundred degrees higher than the metal temperatures, depending upon the location of the heat transfer tubes. Furthermore, the materials specified in Table 3.11 can be used with either gaseous fuels derived from coals or with pulverized coals specified by NASA, since the fire-side corrosion data presently available are not

Table 3.11 — Materials Suitable for Use in Heat Transfer Equipment  
Using Coal Gas or Pulverized Coal

<u>Maximum Material Temperature</u>	<u>Material</u>	<u>Rating*</u>
750°F	(i) SA 213-T22 (2-1/4 Cr-1 Mo Steel)	A
	(ii) SA 210-A1 (Carbon steel)	A
1000°F	(i) SA 213-T22 (2-1/4 Cr-1 Mo Steel)	B
	(ii) SA 213-T9 (9 Cr-1 Mo steel)	A
	(iii) SA 213-TP-304H (304 stainless steel)	A
1200°F	(i) 304 or 316 austenitic stainless steel	A
	(ii) Incoloy 800 (21% Cr)	A
	(iii) 17-14 Cu Mo stainless steel	B
1400°F	(i) Incoloy 800	B
	(ii) Inco clad 671 on Incoloy 800	A
	(iii) Haynes Alloy 188	B
	(iv) 50/50 Cr-Ni type alloys, IN-589 and IN-657	B
1600°F	(i) Haynes Alloy 188	B
	(ii) Inco clad 671 on Incoloy 800	B
	(iii) 50/50 Cr-Ni type alloys, IN-589 and IN-657	B
1800°F	(i) Inco clad 671 on Haynes Alloy 188	C
	(ii) CoCrAlY clad - Haynes Alloy 188	C
	(iii) TD-NiCr, TD-NiCrAlY or TD-NiCrFe alloy	C
	(iv) 50/50 Cr-Ni-type alloys, IN-589 and IN-657	C

\*This is a partial rating based on fire-side corrosion considerations only. For overall ratings and materials recommendations, including working fluid compatibility, mechanical properties, and so on, see the appropriate subsection of Section 3.

detailed enough to allow specification of different materials for use with different coals. Hence, the materials recommended are those which are considered to offer the highest probability of providing long life under most demanding conditions. It must be emphasized that the information in Table 3.11 refers only to the fire-side compatibility of the materials listed. Other factors that must be taken into account, such as compatibility with the working fluid, mechanical properties, and so on, are dealt with in the appropriate subsection dealing with specific systems and components, where materials selections are presented.

At metal temperatures up to 672°K (750°F), carbon steel (e.g., SA 210-A1), or 2-1/4 Cr-1 Mo steel (SA 213-T22) is recommended, since their use as tubes in conventional boilers is fairly well established. These steels have also shown adequate performance in short-term fluidized bed combustor tests, as discussed in Section 3.2.2.2.

At temperatures higher than 672°K (750°F), higher chromium content is considered necessary in any boiler tube material to provide protection against oxidation, sulfidation, and any coal-ash corrosion. For this reason, the steels specified for use up to 811°K (1000°F) contain 2-1/4, 9, or 18% chromium. The austenitic stainless steel (SA 213-TP-304 H) may be necessary at these temperatures to provide protection against high-sulfur coal such as Illinois No. 6.

For boiler tubes at temperatures up to 922°K (1200°F), stainless steels such as 304 or 316, and 17-14 Cu Mo, and an iron-based superalloy, Incoloy 800, are recommended. These materials show adequate resistance in short-term fluidized bed boiler tests described earlier, and these have also been used successfully in conventional coal-fired boilers.

At temperatures higher than about 922°K (1200°F), the corrosion data on fluidized bed boilers showed that even austenitic stainless steels may not be able to provide long-term life. At these temperatures, therefore, heat transfer tubes will have to be made of a high-temperature superalloy. Incoloy 800 containing 21% chromium could be used up to about 1033.2°K (1400°F), but at still higher temperatures, even this may

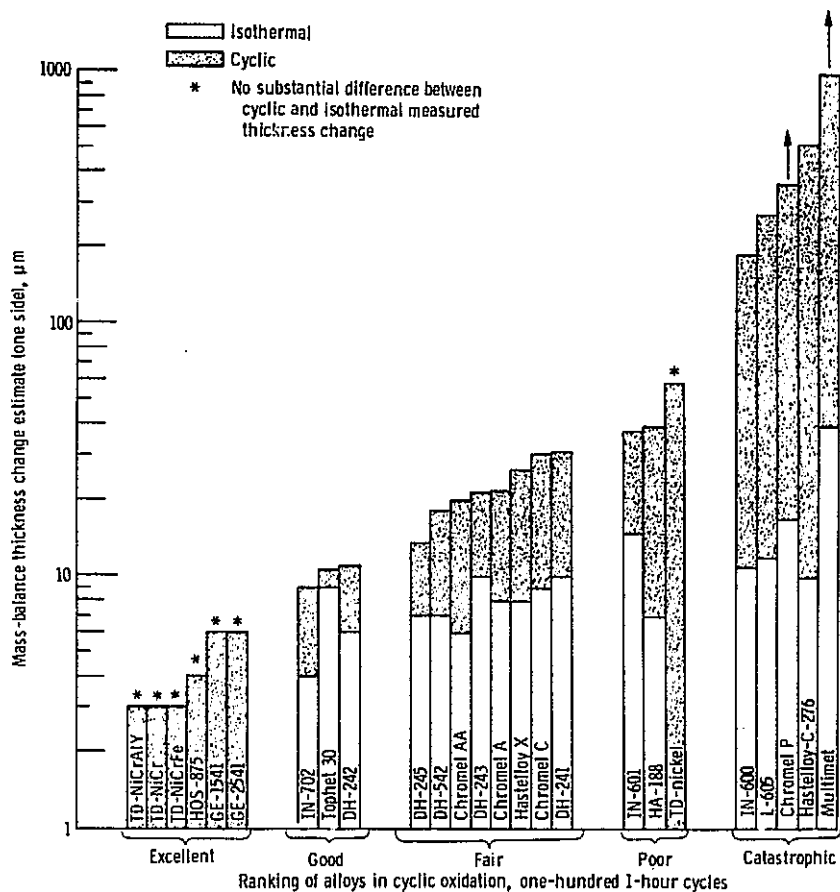


Figure 3.16 — Comparison of cyclic and isothermal oxidation for 100 hr in still air at 1150°C.

have to be protected with a coating to provide adequate resistance against sulfidation and ash-corrosion.

Recently, Barrett and Lowell (Reference 3.34) studied the isothermal and cyclic oxidation of 25 high-temperature nickel-, cobalt-, and iron-based sheet alloys for 360 ks (100 hr) in air at 1422°K (2100°F). Even though we do not anticipate using the boiler tube materials at such high temperatures, their data reveal the relative ranking of various sheet alloys with respect to oxidation. These data are summarized in Figure 3.16, which shows that TD-NiCrAlY, TD-NiCr, and TD-NiCrFe offer the best protection against high-temperature oxidation. Decker and Richards (Reference 3.35), from their experiments in simulated coal- and oil-fired conditions at 922°K (1200°F), have also concluded that 50-50 and 60-40 chromium-nickel alloys offer the best resistance against environmental attack. Their results are confirmed by the trials of 12 different cast alloys in 75 superheater tube supports at Consolidated Edison Company of New York, which used Bunker 'C' fuel oil with a vanadium content ranging from 100 to 400 ppm, sodium from 20 to 80 ppm, and sulfur from 1.5 to 4%. Gas temperatures in the area of the bracelet supports were in the range 978 to 1255°K (1300 to 1800°F). The data summarized in Figure 3.17 show that only the 50-50 and 60-40 chromium-nickel alloys survived a service life of 43.2 Ms (12,000 hr), each with only negligible corrosion. Several similar service trials have been documented (Reference 3.36) which demonstrate the corrosion-resistance of 50-50 and 60-40 chromium-nickel alloys in oil-fired installations at metal temperatures above 922°K (1200°F). In coal-fired plants there is only limited experience with the use of 50-50 or 60-40 chromium-nickel alloys to resist coal-ash corrosion at higher metal temperatures, though there is evidence that alloys with high-chromium content are beneficial (Reference 3.37). Both 50-50 and 60-40 chromium-nickel alloys, however, have demonstrated adequate resistance to oil-ash attack at temperatures up to 1172°K (1650°F) in oil refinery heaters and marine boilers (Reference 3.36). Two new improved alloys of 50-50 chromium-nickel type, IN-589 and IN-657, have recently been developed by the International

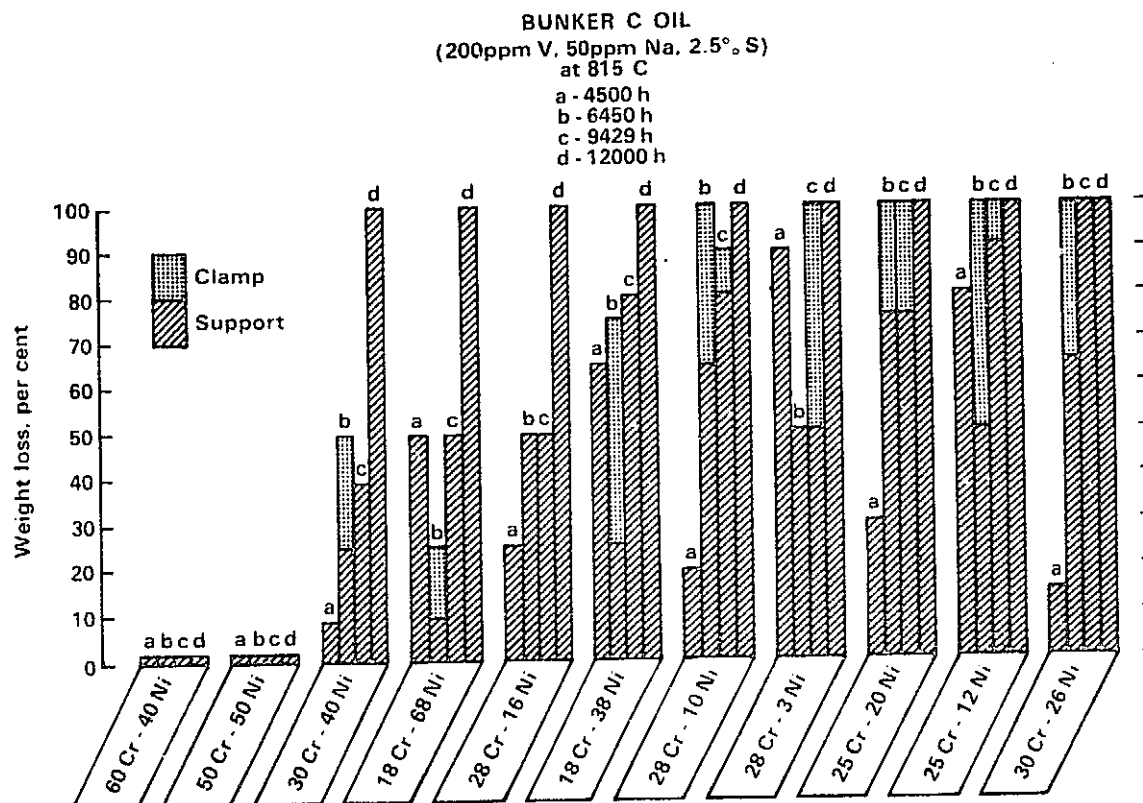


Figure 3.17 — Fuel-oil ash corrosion of tube supports at Consolidated Edison Company of New York.



Nickel Company, and these alloys are recommended for use up to about 1255°K (1800°F). Long-term corrosion data on these alloys under coal-burning conditions are required to firm up the useful upper temperature limit.

A 50-50 chromium-nickel-type Inconel alloy 671 cladding on Incoloy alloy 800 substrate (known as Inco Clad 671/800H) has also shown excellent resistance to oxidation, carburization, and coal-ash corrosion (Reference 3.38). The results of the cyclic oxidation tests performed at 1255°K (1300°F) on Inco Clad 617/800H specimens coated with sodium sulfate, shown in Figure 3.18, indicate that this material could be used as boiler tubes up to 1255°K (1800°F). The resistance of Inco Clad 671/800H to fuel-ash corrosion has been demonstrated by test installations in power-plant steam superheaters up to temperatures of 841°K (1055°F) (Reference 3.38), but their long-term corrosion behavior at higher temperatures still needs to be studied. The cladding of Inconel 671 (basically 50-50 nickel-chromium) should, however, provide adequate corrosion resistance up to 1255°K (1800°F), and from this viewpoint only the Inco Clad 671/800H is recommended for boiler tubes for use up to 1255°K (1800°F).

In addition to the nickel-chromium alloys discussed above, a cobalt-based alloy, Haynes 188, is also recommended for boiler tubes which would carry liquid sodium or potassium. Haynes 188 is currently being considered for use as a combustor material for gas turbines and possesses excellent resistance against oxidation and sulfidation. The oxidation rate of this alloy is estimated at about 16.1 pm/s at 1366°K (20 mil/yr at 2000°F) from intermittent 360 ks (100 hr) tests in dry air (Reference 3.39). Recent work at Westinghouse has shown metal recession rates of 0.6 and 4 mil in 250 hr at 1172 and 1366°K (1650 and 2000°F), respectively, for Haynes Alloy 188 when exposed to combustion gases from turbine diesel oil at 303.9 kPa (3 atm) pressure. Thus, even though long-term data are still lacking under coal-burning conditions, it is considered that Haynes Alloy 188 could be used for boiler tubes up to about 1144°K (1600°F). At still higher temperatures, it will have to be protected with a high-chromium cladding such as

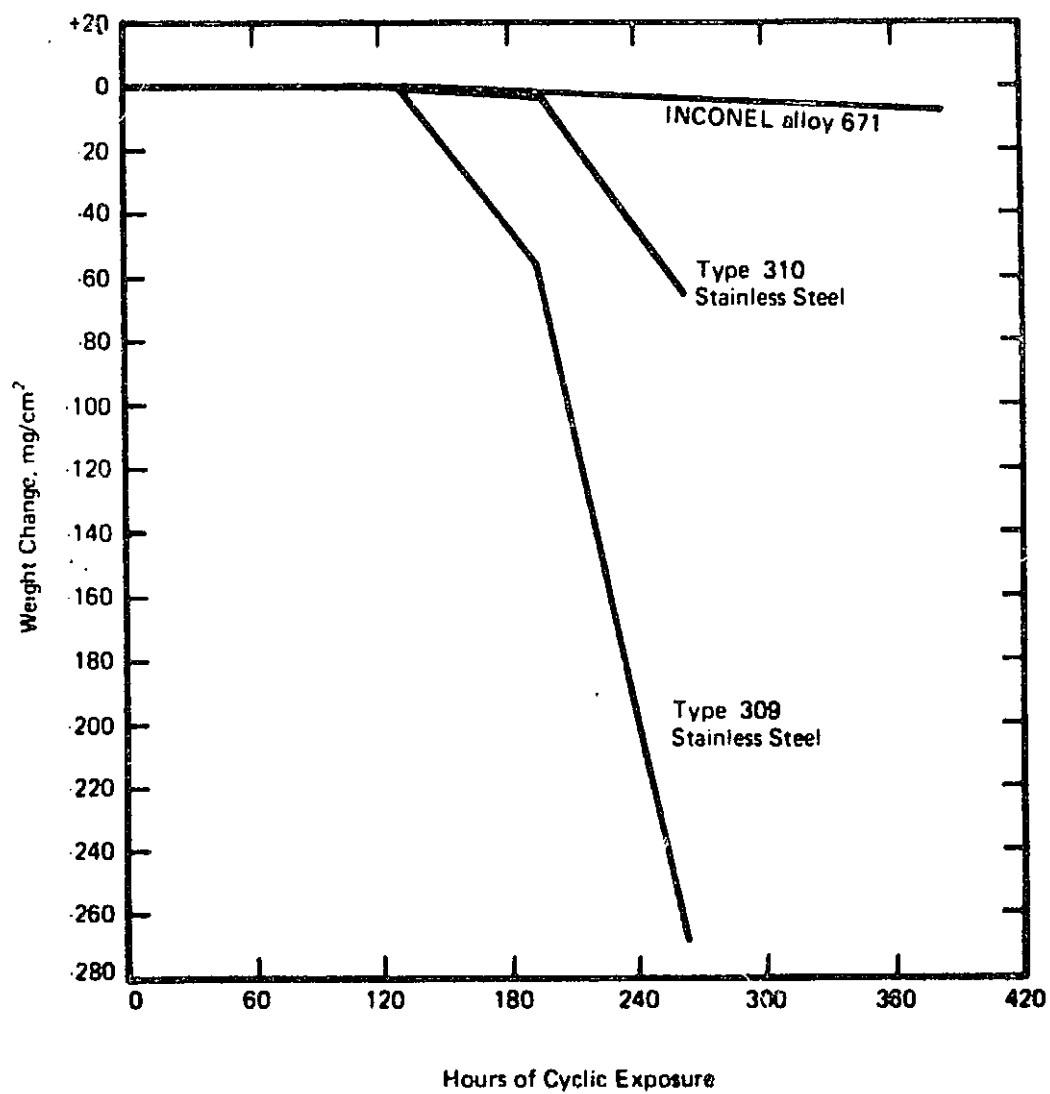


Figure 3.18 — Cyclic oxidation-resistance at 1800°F of specimens coated with sodium sulfate.

Inco Clad 671 or CoCrAlY. In summary, the materials recommendations for boiler tubes for use at high temperatures are based on their potential performance under coal-burning conditions, though actual corrosion data under these conditions still need to be obtained.

### 3.3 Material Considerations in Steam Boilers Utilizing Coal and Coal-Derived Fuels

#### 3.3.1 Introduction

The operating life of materials at elevated temperatures is limited by corrosion/oxidation, by creep (beyond some allowable limit), or by rupture. The selection of materials for piping and tubing in a high-temperature steam environment must possess the following characteristics of steam-side behavior (Reference 3.40).

- Excellent creep and stress rupture properties
- Resistance to oxidation (steam-side corrosion)
- Good thermal stability (i.e., limited microstructural change with time at temperature)
- Strength at elevated temperature
- Good weldability and freedom from brittle fracture in the weld area
- Material must be available in pipe and tube form.

The need for excellent creep and stress rupture properties and for thermal stability is of the utmost importance. The material must exhibit sufficient long-term, high-temperature strength to allow the use of reasonable wall thicknesses and freedom from embrittlement due to microstructural changes. Careful attention must be paid to the accelerated downward slope of the stress rupture curves as the temperature increases. Heavy-walled pipes enhance stiffness and tridimensional stress and increase the possibility of developing severe thermal stress across the wall with rapid temperature changes. For tubing the wall thickness is directly related to the heat transfer rates attainable. Greater wall thicknesses increase the thermal stresses and increase the tendency for cracking and catastrophic failures.

The use of higher alloyed material presents potential difficulties in fabrication in the processing of both the pipes and the tubes, and, perhaps more important, in joining (welding) during installation. Higher alloy materials tend to develop crack-sensitive regions during welding, which may lead to premature failure. Careful attention must be paid to the suggested welding parameters, preheat, postheat, electrode composition, heat input, joint design, and so on.

Materials for high-temperature steam usage must also be characterized by resistance to oxidation at operating temperatures. The use of ferritic alloys is limited to about 811°K (1000°F) operating temperature because of excessive oxidation, poor stress rupture properties, and the instability of the carbide phase at temperatures above 811°K (1000°F).

Even though the ferritic steels are less expensive, easier to fabricate, and possess good reliability, the use of austenitic steels and/or nickel- and cobalt-based superalloys are required for higher temperature and pressure.

The importance of close control of the water/steam chemistry in a steam power generation system cannot be overemphasized. Potentially deleterious species, such as caustics and chlorides, along with hydrogen and oxygen, can be found in various concentrations in "high purity" steam. The exact behavior of candidate alloys with respect to these species cannot be completely addressed at this time.

In general, the candidate alloys possess good oxidation resistance at the selected temperature. Specific data based on the performance of candidate alloys in high-temperature steam are not available. The corrosion and stress-corrosion cracking resistance of the alloys under evaluation appears to be good. The combination of nickel and chromium in the alloy generally confers resistance to an oxidizing solution. Resistance to reducing solutions is supplied by the nickel and molybdenum content. As was the case with oxidation resistance data, specific corrosion and stress corrosion data are not available. The effect of hydrogen diffusion on the ductility of ferritic steels is known. The

embrittling phenomenon is referred to as "methanation." No problem occurs when the hydrogen diffuses freely through the metal. Severe embrittlement develops when the hydrogen reacts with carbon in the metal to form internal pockets of methane. The internal pressure increases until a void is formed; subsequently a brittle rupture occurs. Once again, specific data are not available on the effect of hydrogen on the reduction in percent elongation for the candidate alloys. In general, all iron-, nickel-, and cobalt-based alloys exhibit some degree of ductility loss because of hydrogen pickup, but no drastic reduction in elongation is anticipated for any of the recommended alloys.

### 3.3.2 Selection of Candidate Alloys

The development and subsequent utilization of alloys for steam applications usually center around oxidation and corrosion resistance, while creep and rupture performance is treated solely as a design problem. Unfortunately, as operating temperature and stress levels increase, the creep and stress rupture properties become the limiting factor for many materials. Available data on stress rupture behavior of many materials at high temperature for extended times are limited. The utilization of elevated temperature tensile data provides only limited information since these tests show only the effect of temperature on a short-time basis. Stress rupture tests measured the effect of long-term load-bearing characteristics of material.

The evaluation of candidate materials for high-temperature steam usage is based on stress rupture performance and oxidation resistance. Only alloys currently available in tubular form and exhibiting good weldability were considered as candidate alloys. The candidate materials (Table 3.12) are composed of austenitic stainless steels and nickel- and cobalt-based alloys. Available high-temperature data on the majority of these materials are limited. The information that is available is based on laboratory tests, and the results must be treated as such. This type of data is useful as a preliminary screening method, but the final selection should be after performance data from actual service (pilot-scale facility) have been obtained.

Table 3.12 — Alloys Evaluated

<u>Iron - Chromium - Nickel Alloys</u>	
304 (18Cr/8Ni)	321 (18Cr/10Ni/Ti)
310 (25Cr/20Ni)	347 (18Cr/10Ni/Cb)
316 (16Cr/13Ni/3Mo)	15 Cr/15Ni
18 Cr/11 Ni	20 Cr/35 Ni
20 Cr/25 Ni	
20 Cr/25 Ni/Nb	Hastelloy C-4
Inconel 600	Hastelloy C-276
Inconel 601	Hastelloy G
Inconel 604	Nimonic 80
Inconel 617	Nimonic 80A
Inconel 625	Nimonic 90
Inconel 671	RA-600
Inconel 722	Unitemp Waspalloy
Inconel X-750	Armco 20-45-5
Inco Clad 671/800	17-14 CuMo
Pyromet 625	Croloy 15-15N
Pyromet 680	IN-102
Hastelloy X	18-18-3-1
	Incoloy 807
	Incoloy 800
<u>Cobalt Based Alloy</u>	
Haynes 188	Jesop Saville G-32
Haynes 25	Allegheny 5816
Crucible WF 11	

### 3.3.3 Stress Rupture Performance

Long-term stress rupture data are extremely important when one judges the potential performance of candidate alloys for high-temperature applications. Materials considered for piping and tubing applications must support high internal pressures at high temperatures. Their design strength is usually determined by either the stress rupture or creep strength. Oxidation losses affect the net metal wall thickness, which at the end of the design life should be sufficient to support the applied stresses. As the environmental temperature to which a material is exposed increases, the time required for it to rupture at a given stress level decreases. Materials employed at elevated temperature, therefore, must possess higher stress rupture properties, or design compromises must be made to lower the operating stress level.

The maximum allowable working stress for code-approved material can be found in the ASME Boiler and Pressure Vessel Code, Section 1, which covers carbon, low-alloy (chromium-molybdenum) and high-alloy steels (18 Ni-10 Cr). At operating conditions of 922, 978, 1033, and 1089°K (1200, 1300, 1400, and 1500°F) and 24.1325 to 34.79 kPa (3500 to 5000 psi), none of the materials currently code approved appear usable. None of the higher alloyed austenitic stainless steels or super-alloys (nickel- or cobalt-based) are covered by the ASME Boiler and Pressure Vessel Code. To determine the maximum allowable working stress for candidate materials not covered by the ASME Code, a value equal to 67% of the rupture stress at 360 Ms (100,000 hr) at the specified temperature was employed (Reference 3.41). A review of published data indicated the lack of long-term [360 Ms (100,000 hr)] stress rupture data.

Graphical extrapolation of short-term [3.6 to 36 Ms (1000 to 10,000 hr)] stress rupture data, along with the development of Larson-Miller plots, was employed to obtain 360 Ms (100,000 hr) stress rupture values.

Reliable extrapolation of short-term stress rupture data can only be performed when it is certain that no microstructural change

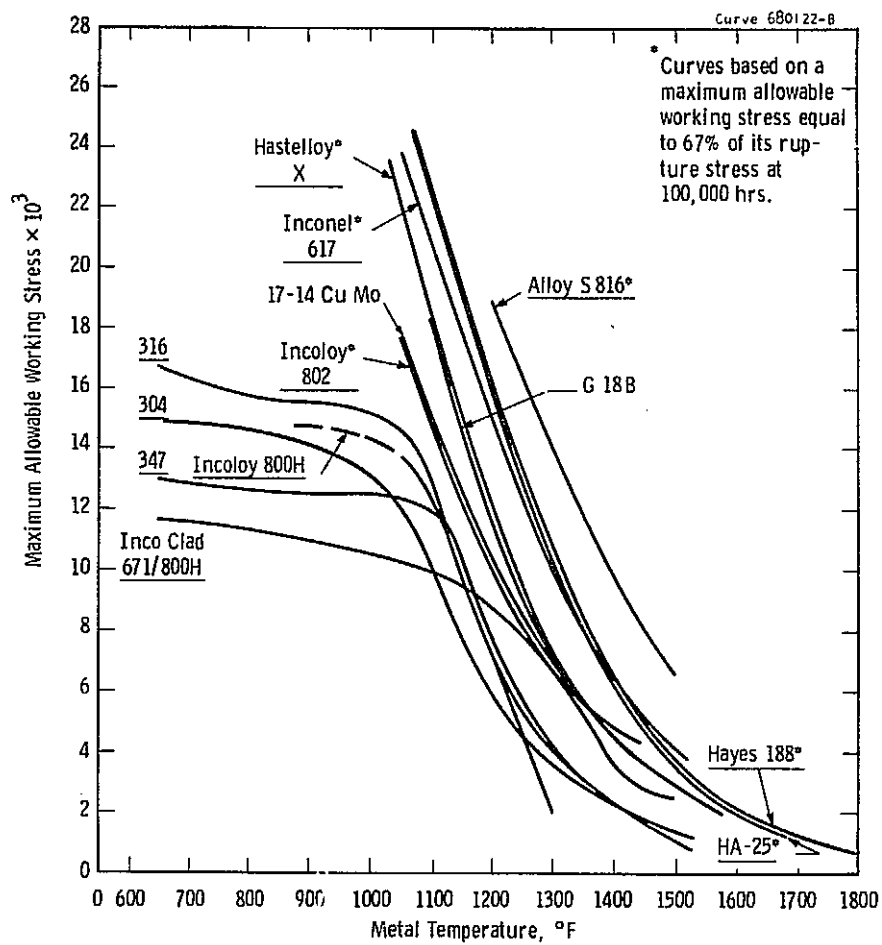


Fig. 3. 19--Maximum allowable stress for candidate tube materials



occurs in the region of the extrapolation. Microstructural changes, such as precipitation of an embrittling phase, could cause a drastic reduction in the stress rupture properties. The tendency for structural change increases with time and temperature. Insufficient data are currently available to determine what high-temperature alloys, if any, undergo microstructural change at high temperatures for extended exposures. Within the context of this evaluation, therefore, no microstructural change is assumed in the region of extrapolation.

Larson-Miller plots were developed for the potentially applicable tubing alloys, using available data (References 3.42 to 3.45) (Refer to Section 3.12). These plots were employed to develop a working curve illustrating maximum allowable working stress as a function of metal temperature (Figure 3.19).

#### 3.3.4 Oxidation Performance

The alloys considered for service in high-temperature steam are iron-chromium-nickel alloys and cobalt-based superalloys. The most extensive research into the performance of austenitic materials in high-temperature steam was conducted by the ASME Research Committee on High-Temperature Steam Generation. The final findings of this work are collected into one volume (Reference 3.47) which lists the reference of all previous publications of this committee. The work was conducted at temperatures up to 1089°K (1500°F).

Evaluation of the scale deposit after exposure indicates a duplex structure with an inner and an outer layer. The inner layer should be considered for corrosion rate comparisons as this is the depth of penetration in from the original tube surface. The authors point out that it was impossible to evaluate the scaling behavior in a sensible manner due to small scale thicknesses. They also report exfoliation of the outer scale and irregular intrusions of the inner layer. Table 3.13 summarizes the results of this investigation. The values appear to be average scale thicknesses and do not take into

Table 3.13 Oxidation Layer Thickness

Material	Steam Temperature F	Exposure Time Months	Thick n e s s		Total Scale Layer Mils	Ratio Inner/Total Scale Layer	Material	Steam Temperature F	Exposure Time Months	Thick n e s s		Total Scale Layer Mils	Ratio Inner/Total Scale Layer		
			Inner Scale Layer Mils	Outer Scale Layer Mils						Inner Scale Layer Mils	Outer Scale Layer Mils				
9Cr-1Mo	1100	6	2.4	2.1	4.5	0.53	Type 310	1200	12	1.9	0.3	2.2	0.86		
		12	3.2	3.7	6.9	0.464			18	0.2	0.1	0.3	0.67		
		12	3.6	3.7	7.5	0.48			1350	12	0.4	0.2	0.6	0.67	
		18	3.8	4.0	7.8	0.487				18	3.2	0.6	3.8	0.84	
		24	5.0	5.4	10.4	0.48				16-25-6	1200	6	0.2	1.3	1.5
	1200	6	4.8	5.7	10.5	0.457	12	1.5	1.1			2.6	0.58		
		12	6.0	7.0	13.0	0.46	18	2.4	1.8			4.2	0.57		
		12	5.6	5.7	11.3	0.495	1350	6	0.2			0.8	1.0	0.25	
		18	6.5	8.0	14.7	0.44		12	1.1			1.0	2.1	0.52	
		24	7.2	7.2	14.4	0.50		18	1.3	1.3	2.6	0.50			
Type 304	1200	12	4.6	1.0	5.6	0.82	1500	6	0.3	1.3	1.6	0.20			
		18	1.4	1.2	2.8	0.50		12	1.6	1.1	2.7	0.59			
		36	5.0	1.6	6.6	0.75		17-14 CuMo	1200	6	0.2	1.8	2.0	0.10	
		36	5.5	1.4	6.9	0.80				12	5.5	0.9	6.4	0.86	
		1350	12	1.8	1.6	3.4				0.53	18	2.1	1.9	4.0	0.53
	18		2.6	1.9	4.5	0.58	1350			6	0.3	1.7	2.0	0.15	
	36		3.8	1.5	5.3	0.71				12	5.0	1.0	6.0	0.83	
	1500	36	2.0	2.8	4.8	0.42		18	4.4	3.1	7.5	0.59			
		12	2.8	1.6	4.4	0.64	1500	6	0.3	1.7	2.0	0.15			
		Type 321	1200	6	3.6	1.7	5.3	0.68	15-15N	1200	12	3.6	2.7	6.3	0.57
12				1.9	0.7	2.6	0.73	18			3.3	1.5	4.8	0.69	
18				(1.9)	(1.8)	(3.7)	(0.51)	1350			-	-	-	-	-
(1.6)	(0.6)			(2.2)	(0.73)	12	4.0				1.0	5.0	0.80		
(3.3)	(1.0)			(4.3)	(0.77)	18	7.0				1.0	8.0	0.88		
36	2.2			1.0	3.2	0.69	1500				-	-	-	-	-
Type 321	1350	6	3.0	0.7	3.7	0.81	Inconel	1200	12	1.1	0.3	1.4	0.78		
		12	1.1	0.8	1.9	0.58			18	3.0	1.0	4.0	0.75		
		18	5.0	0.5	5.5	0.91			1350	12	1.6	0.4	2.0	0.80	
		36	3.5	1.0	4.5	0.78				18	2.1	0.3	2.4	0.88	
		36	5.8	1.1	6.9	0.84				Incoloy	1200	12	2.3	0.8	3.1
	1500	12	5.0	1.1	6.1	0.82	18	4.0	0.8			4.8	0.83		
		18	3.1	0.8	3.9	0.79	1350	12	2.0			0.7	2.7	0.74	
		Type 347	1200	6	0.1	0.7	0.8	0.13	18			3.0	0.5	3.5	0.86
				12	0.4	0.6	1.0	0.40	Type 316			1200	12	4.1	1.8
				18	0.3	0.4	0.7	0.43		18	3.6		1.5	5.1	0.71
36	3.0			1.0	4.0	0.75	1350	6		1.7	1.0		2.7	0.63	
36	2.7			0.5	3.2	0.84		12		3.1	1.4		4.5	0.69	
1350	6			1.3	0.6	1.9		0.68		18	3.5		1.8	5.3	0.66
	12	1.8	0.4	2.2	0.82	12		3.0		1.2	4.2		0.71		
	18	5.3	2.5	7.8	0.68	18		1.9		2.0	3.9		0.49		
	36	4.6	1.8	6.4	0.72										
Type 316	1200	12	4.1	1.8	5.9	0.70	1500	12		3.0	1.2		4.2	0.71	
		18	3.6	1.5	5.1	0.71		18		1.9	2.0		3.9	0.49	
		1350	6	1.7	1.0	2.7		0.63	1500	12	3.0	1.2	4.2	0.71	
			12	3.1	1.4	4.5		0.69		18	1.9	2.0	3.9	0.49	
			18	3.5	1.8	5.3		0.66		1500	12	3.0	1.2	4.2	0.71
			18	3.0	1.2	4.2		0.71			18	1.9	2.0	3.9	0.49
18	1.9		2.0	3.9	0.49										

REPRODUCIBILITY OF THE  
ORIGINAL PAGE IS POOR

account the irregular oxide spikes which occur in the molybdenum-containing steels as well as in the other alloys. The highly alloyed Type 310, Incoloy 800, and Inconel 600 exhibited the slowest scaling rate at the lower temperatures tested, 922 to 1005°K (1200 and 1350°F), but again there were deeper oxide spikes in these materials.

The steam pressure in these tests was 13.789 MPa (2000 psi) but tests at lower pressures did not affect the observed scaling rates. The scale on the austenitic alloys was found to increase heat transfer (Reference 3.47), presumably because of the irregular surfaces produced.

In addition to the alloys listed in Table 3.13, chromium-molybdenum ferritic steels were evaluated. Results at temperatures up to 922°K (1200°F) indicated large total scale buildups [0.504 to 0.762 mm (20 to 30 mil)]. Two other alloys, IN-102 and 18-18-3W-1Nb, were included in the study of mechanical properties (Reference 3.47). All but the last two failed by creep or rupture at 1089°K (1500°F) and 13.789 MPa (2000 psi) stress. For these materials this is a high operating stress and temperature, especially when considered along with the nitrogen pickup and sigma embrittlement which occurs at this temperature and in nitrogen-bearing environments. For this type of service these materials are considered risky. There probably will be some nitrogen present in the steam for use in this plant as it is not intentionally removed as is oxygen.

Work in Sweden (Reference 3.48) at temperatures up to 1079°K (1482°F) showed essentially the same results as those found in the ASME testing, in that the higher alloyed materials performed better. They ranked their alloys, after testing for time to 18 Ms (5000 hr), in the order: 16-75 (Inconel 600), 20-25 niobium, 20-35 (Incoloy 800), 20-25, 18-11, 15-15 (these are nominal chromium-nickel values). The one important feature is that the niobium stabilized 20-25 material appears to be better than the unstabilized 20-35 material. In this work, which used weight gain as a measure of oxidation, there were penetrations of the corrosion product into the metal below the average depth of attack.

Incoloy 800 is the material that is presently used for gas-cooled reactor steam generator and superheater applications (Reference 3.49). However, the temperatures here are of the order of 978°K (1300°F) or less, and at 1075°K (1475°F) some acceleration in corrosion occurs. Both Incoloy 800 and Inconel 600 have been shown to have good corrosion properties in steam at higher temperatures, as mentioned previously. If air corrosion data are used to give an idea of steam corrosion, then Incoloy 801 and 802 may also be considered to be good. These two alloys are higher titanium (801) and higher carbon (802) modifications of Incoloy 800 and have hot air corrosion properties approaching those of Inconel 600, while having the slightly superior creep strength of Incoloy 800. The creep strengths are low on all of these alloys, the stress to produce rupture in 360 Ms (100,000 hr) being of the order of 15.16 MPa (2200 psi). This would require very low differential pressures across the tube wall or very thick-walled tubes. Inconel 601 has a creep strength similar to that of Inconel 600 and offers better oxidation resistance (Reference 3.50). Inconel X-750 (Reference 3.51) offers the same oxidation properties as Inconel 600, with high strength up to 978°K (1300°F), but this would probably drop at 1033°K (1400°F) to give very little improvement over Inconel 600. Inconel 625 (Reference 3.52) offers better oxidation resistance and higher creep strength than does Inconel 600. The stress to produce rupture at 360 Ms (100,000 hr) is 20.685 MPa (3000 psi), double that of Inconel 600.

The use of air oxidation data to predict steam data is not entirely satisfactory, as the attack can be greater in steam environments (Reference 3.53).

Incoloy 807 has been recommended as the steam generator material for high-temperature gas-cooled reactor (HTGR) steam generation (Reference 3.54). The operating conditions of this reactor were 1223 to 1037°K (1741 to 1407°F) at 6.078 MPa (60 atm) pressure. There is no readily available information on this alloy which is a British (Wiggin) alloy containing: 40% nickel, 8% cobalt, 5% tungsten, 20.5% chromium, 1% manganese, 1% niobium, 0.75% silicon, 0.55% titanium, 0.50% aluminum, 0.1% carbon, and the balance iron.

### 3.3.5 Conclusions

Based on the ASME Boiler Code for ferrous tubing up to and including 0.127 m (5 in) od, the following formula can be used to determine the diameter-to-thickness ratio for each candidate alloy based on its maximum allowable working stress.

$$t = \frac{PD}{2S + P}$$

where

t = the minimum required wall thickness, in

P = the maximum allowable working pressure, psi

D = outside diameter of the tube, in

S = the maximum allowable stress value at the operating temperature of the metal, psi.

As discussed previously, the maximum allowable working stress will be equal to 67% of the rupture stress at 360 Ms (100,000 hr). Using the curves shown in Figure 3.19 and the above equation, the D/t ratio for candidate alloys was calculated. The D/t ratio provided a number by which alloy recommendations at specified temperatures could be made.

Table 3.14 summarized the recommendations for tubing material based on allowable working stress. The fire-side and steam-side corrosion behavior (Tables 3.11 and 3.13, respectively) was also factored into the final selection.

At temperatures of 811°K (1000°F) and operating pressures of 16.546, 24.132, 31.026, and 34.473 MPa (2400, 3500, 4500, and 5000 psi) the austenitic stainless steel (5A213-TP-304H) is required to meet the strength requirement. Fire-side and water-side performance should present no problem.

With operating at lower pressures [2.413, 4.137, 4.329, and 7.584 MPa at 811°K (350, 600, 625, and 1100 psi at 1000°F)] the low-alloy 2-1/4 Cr-1 Mo steel (SA213-T22) is recommended. The operating performance of this material is well established with conventional boilers.

Table 3.14 - Boiler Tubing Alloy Recommendations (Based on Stress and Fireside/Steam Side Corrosion)

Pressure (psi)	1000°F	Temperatures 1200°F	1400°F
350	2-1/4 Cr-1 Mo (A)	--	347 SS (A) Inco Clad 671/800H (B) Incoloy 802 (B)
450	--	--	As above
600	2-1/4 Cr-1 Mo (A)	304 SS (A) Incoloy 800H (A) Incoloy 802 (A)	As above
625	As above (A)	--	--
1100	As above (A)	304 SS (A) Incoloy 800H (B) Incoloy 802 (B)	Inco clad 671/800H (B) Incoloy 802 (B) Inconel 617 (B)
1300	--	As above	--
1800	--	As above	--
2000	--	316 SS (A) 347 SS (A) Incoloy 802 (B)	--
2200	--	As above	Incoloy 802 (C) Inconel 617 (C)
2400	304 SS (A) Incoloy 800H (A)	304 SS (A) Incoloy 800H (B) Incoloy 802 (B)	Incoloy 802 (C) Inconel 617 (C) HA 188 (C)
3500	304 SS (A) Incoloy 800H (A)	304 SS (B) Incoloy 800H (B) Incoloy 802 (B)	Inconel 617 (C) HA 188 (C) S 816 (D)
4500	As above (B)	Incoloy 802 (C) Inconel 617 (C)	As above (D)
5000	As above (B)	As above (C)	As above (D)

REPRODUCIBILITY OF THE  
ORIGINAL PAGE IS POOR

At temperatures of 922°K (1200°F) and operating pressures of 31.026 and 34.474 MPa (4500 and 5000 psi) high strength materials such as Incoloy 802 are required. As the operating pressure drops at 922°K (1200°F), the conventional austenitic stainless steels (SA213-TP-304H) will do the job.

Operation at 1033°K (1400°F) and moderate pressures [2.413, 3.103, 4.137, 7.584, 15.168, and 16.547 MPa (350, 450, 600, 1100, 2200, and 2400 psi)] indicates the need for higher alloyed iron-nickel, cobalt, and nickel-based materials. Materials such as Incoloy 800H, Incoloy 802, Inco Clad-671/800H, and Haynes 188 can be employed. For higher pressures at 1033°K (1400°F) the need for ultrahigh-strength materials exist. Alloys such as Allegheny S816, Inconel 617, Haynes 188, IN589, and IN657 are needed.

Available oxidation data for the higher nickel-content alloys, along with the cobalt base, is limited, although many of these alloys were originally developed for utilization as high-temperature oxidation resistance materials.

This brief review suggests that the concept of advanced steam systems is feasible from an existing materials standpoint, but additional data must be generated for the potentially usable alloys before a firm conclusion can be reached. These data must be generated early in the life of the project to enable long-term exposure data to be accumulated.

### 3.4 Materials Considerations in Advanced Steam Systems

#### 3.4.1 Introduction

In the previous two sections, the materials problems associated with steam boilers have been considered. Materials for boiler tubes are recommended, taking into account fire-side corrosion, steam corrosion, and creep strength. Since these recommendations cover all of the numerous types of boilers being utilized in the advanced steam concept,

the boiler materials recommendations will not be repeated in this section. Instead, this section will discuss the material problems associated with the transfer piping that transports the steam from the boilers to the steam turbine, the casing or pressure vessel in which the steam turbine is housed, and the steam turbine itself.

#### 3.4.2 Main Transfer Piping and Casing

The major material consideration in main transfer piping and casing materials are similar to those previously considered for boiler tubes. The design of these components is dictated by the design allowables on stress set by the ASME pressure vessel codes. At the temperatures and pressures usually encountered in steam turbines, these design allowables are determined by the stress rupture strength of the material. While rupture strength is a necessary consideration for main piping, the large size of this component [(typically 254 mm (10 in) id with a 101.6 mm (4 in) wall thickness] introduces additional requirements on the material selection. Because of the heavy wall thicknesses required, particularly for the advanced steam conditions contemplated in the present study, heavy section weldability and thermal fatigue resistance are of primary concern.

For present day steam plants operating at either 24.1325 MPa/811°K/811°K (3500 psi/1000°F/1000°F) or 1616.65 MPa/811°K/811°K (2400 psi/1000°F/1000°F) extruded and fabricated 2-1/4 Cr-1 Mo (SA-213-T22) is the standard piping and high-temperature casing material. The material has been successfully used for many years and has an excellent service record.

For advanced steam conditions containing steam temperatures higher than 839°K (1050°F), 2-1/4 Cr-1 Mo will not have sufficient strength, and higher strength austenitic materials will be required.

The only austenitic material having an adequate data base for strength, metallurgical stability, heavy section welding, and some experience in this application is Type 316 stainless steel. This



material was used successfully in the Eddystone Plant for both main transfer piping and inner cylinder on the superpressure element designed to operate in 922°K/34.475 MPa (1200°F/5000 psi) steam (References 3.55 and 3.56). As can be seen from Table 3.15, assuming an area represented by a 254 mm (10 in) id pipe is required from flow considerations, at 922°K/34.475 MPa (1200°F/5000 psi) steam conditions, a 109.2 mm (4.3 in) wall thickness would be required with Type 316 stainless steel. In view of the stiffness and fabrication difficulties of this heavy section piping, some design options can be exercised to reduce the wall thickness. By using multiple transfer pipes to obtain the same total area [101.6 to 127 mm to (4 to 5 in) id pipes], the required wall thickness can be reduced by a factor of two. This is the design option used in the construction of the Eddystone Plant (References 3.55 and 3.56).

For higher temperature steam conditions, [1033°K (1400°F)], Type 316 stainless steel with a design allowable stress of 17.23 MPa (2.5 ksi) clearly does not have sufficient strength, and without some form of cooling, alternative materials must be considered.

As with the boiler tube application, ASME boiler code cases have not been presented for a majority of materials that can be used above 922°K (1200°F). For the purpose of this study, the design allowable stresses have been calculated for these materials by taking 67% of the average 360 Ms (100,000 hr) rupture strength. When it became necessary to extrapolate data to obtain the 360 Ms (100,000 hr) rupture strength, the Larson-Miller parameter technique was used.

By substituting Kromarc 58 stainless steel with a higher design allowable stress over Type 316, a somewhat reduced section size results at 922°K/34.475 MPa (1200°F/5000 psi), however, and even with the use of multiple piping at 1033°K (1400°F) a large wall thickness is required (Reference 3.58).

Also, while some experience has been obtained on Kromarc 58 as a wrought pipe in steam turbines, very little experience exists using the alloy as a casting required for inner casings and nozzle blocks.

Table 3.15 -- Pipe Wall Thicknesses as a Function of  
Material and Steam Conditions

Pressure/Temp. psi °F	10 in. id Wall Thickness	Material	Rating
2400/1000	1.8	2-1/4 Cr-1 Mo	A
3500/1000	3.0	2-1/4 Cr-1 Mo	A
5000/1000	4.3	2-1/4 Cr-1 Mo	A
5000/1000	2.0	316	A
2400/1200	1.8	316	A
3500/1200	3.0	316	A
5000/1200	4.3	316	A
3500/1400	39.0	316	
5000/1200	3.2	KROMARC 58	B
3500/1400	18.3	KROMARC 58	
3500/1400	3.5	IN617	B
		HA188	B
5000/1400	5.8	HA188	C
5000/1400	3.3	S816	C

To further reduce wall thickness, higher strength material will be required. A summary of the available materials has already been discussed in the section on boiler tube material.

Both HA188 and IN617 have adequate strength for the 1033°K/24.2 MPa (1400°F/3500 psi) case. The wall thickness at 1033°K/34.475 MPa (1400°F/5000 psi), however, becomes excessive, and the higher strength S816 appears a more reasonable alloy. At the present time, almost no heavy section welding and fabrication experience exists for any of these alloys. Obviously, much development work will be required before they are used for this application.

#### 3.4.3 Turbine Rotors

The high-temperature turbine rotor represents probably the most critical material problem encountered in designing a turbine to operate at the high temperatures and pressures being considered in this program. The present high-temperature rotor steel (chromium-molybdenum-vanadium) used for conventional 811°K/24.2 MPa (1000°F/3500 psi) turbines is limited to temperatures below 866°K (1100°F). Above this temperature, the alloy loses most of its strength because of the dissolution and coarsening of the carbide phases. At higher temperature,  $\gamma'$  ( $\text{Ni}_3\text{Al}$  types), iron- or nickel-based superalloys, strengthened with a more stable precipitate, will be required. The major problems in the use of nickel-based superalloy is in the high cost and the limited size forging commercially available.

In order to reduce the amount and size of the superalloy required in the turbine, a design philosophy of isolating the high temperatures in separate elements has been adopted. This same design philosophy was used in the construction of the Eddystone turbine (Reference 3.56). The Eddystone turbine, which was designed for an initial steam pressure of 34.475 MPa and 922°K (5000 psig and 1200°F), utilized a small superpressure element which reduced the steam conditions to 811°K/17.24 MPa (1000°F/2500 psi) which then could exhaust to a plant made up of standard ferritic steel components.

Several superpressure rotors were manufactured for the Eddystone turbine, utilizing a number of different materials. The rotor which eventually was placed into service was made out of DISCALLOY, an iron based superalloy which had been developed at Westinghouse for gas turbine applications. An alloy of similar composition, A286, has continued to be a major material for discs in the aerospace industry. The DISCALLOY rotor was forged from a 7030 kg (15,500 lb) electric arc melted ingot and had a final machined weight of 1588 kg (3500 lb). The rotor was essentially a 3.658 m (12 ft) long shaft having a main body 0.5588 m (22 in) diameter by 0.6096 m (24 in) long into which blades were fastened. As a backup to this forging, rotors were also made from the ferritic materials chromium-molybdenum-vanadium and AISI 422. The design life of these rotors was calculated to be rather limited, however, and periodic replacements would have been necessary if these materials had been used.

Since the time of construction of the Eddystone Plant in mid-1950, gas turbines have continued to be the prime users of large forgings of superalloys. In order to improve the quality of the product, the air-melting practice used on the Eddystone turbine has been replaced by vacuum-induction melting (VIM) an electrode which is subsequently vacuum-arc remelted (VAR) (Reference 3.59). More recently, the use of electroslag remelting (ESR) has been applied to the manufacture of large ingots for disk forgings. The state of technology in gas turbines has evolved using these processing techniques so that ingots of roughly 11,340 kg (~25,000 lb) have been produced from alloys such as Incoloy 901, Inconel 718, and Inconel 706. The major problems presented by processing these large ingots are the segregation of alloying elements that occurs during solidification, carbide freckling, and ingot cracking produced by the high thermal stresses resulting from differential cooling. In order to control both ESR and VIM-VAR processing problems, ingot diameters are limited to about 0.762 m (~30 in) diameter with the near-term production capability to increase this to 1.016 m (40 in) if some way to control segregation is discovered. While there has been some work done on

understanding freckling, the problem has not been sufficiently researched so that alloy development free of ingot freckles is possible. Until this has been done, ingots will be limited to nearly present-day sizes.

Using either VIM-VAR or ESR technology, it is possible today to manufacture high-quality rotors of A286 for use as superpressure rotors [operating at 922°K (1200°F)] of somewhat larger size than the Eddystone turbine. For higher temperature service [1033°K (1400°F)], however, this alloy does not have sufficient strength. Unfortunately, the only alloys with which large ingots and forgings have been produced to date, Incoloy 901, Inconel 718, and Inconel 706, do not have the required strength to operate at 1033°K (1400°F) (Figure 3.20). For 1033°K (1400°F) service an alloy of the strength level of Waspalloy will have to be used. Although there is very little experience to date on large ingots of WASPALLOY, its relatively dilute alloy content is such that no serious problems are anticipated with freckling. Assuming no major technological problems are encountered, Waspalloy rotors of around 9072 kg (~20,000 lb), should be feasible.

Another technique that could possibly be used if larger forgings of A286 or Waspalloy are needed would be to return to the air melted ingot technology used at Eddystone. This process will allow production of ingots weighing up to 45.36 Mg (50 tons), but ingot segregation and hot cracking during cooling would need to be taken into account to determine properties.

Another design that can be used to reduce required rotor forging size is to make a built-up rotor using disk-type construction. A rotor of such design was actually designed and constructed as a backup for the Eddystone turbine (Reference 3.56). A DISCALLOY shaft was made onto which DISCALLOY disks were shrunk. This design significantly reduces the size of a single forging required and would allow significantly larger elements than can be manufactured using an integral forging. Disks as large as 2.08 m (82 in) in diameter and above 0.35 m (~12 in) thick have been manufactured from alloys such as Incoloy 901. The disk-type construction

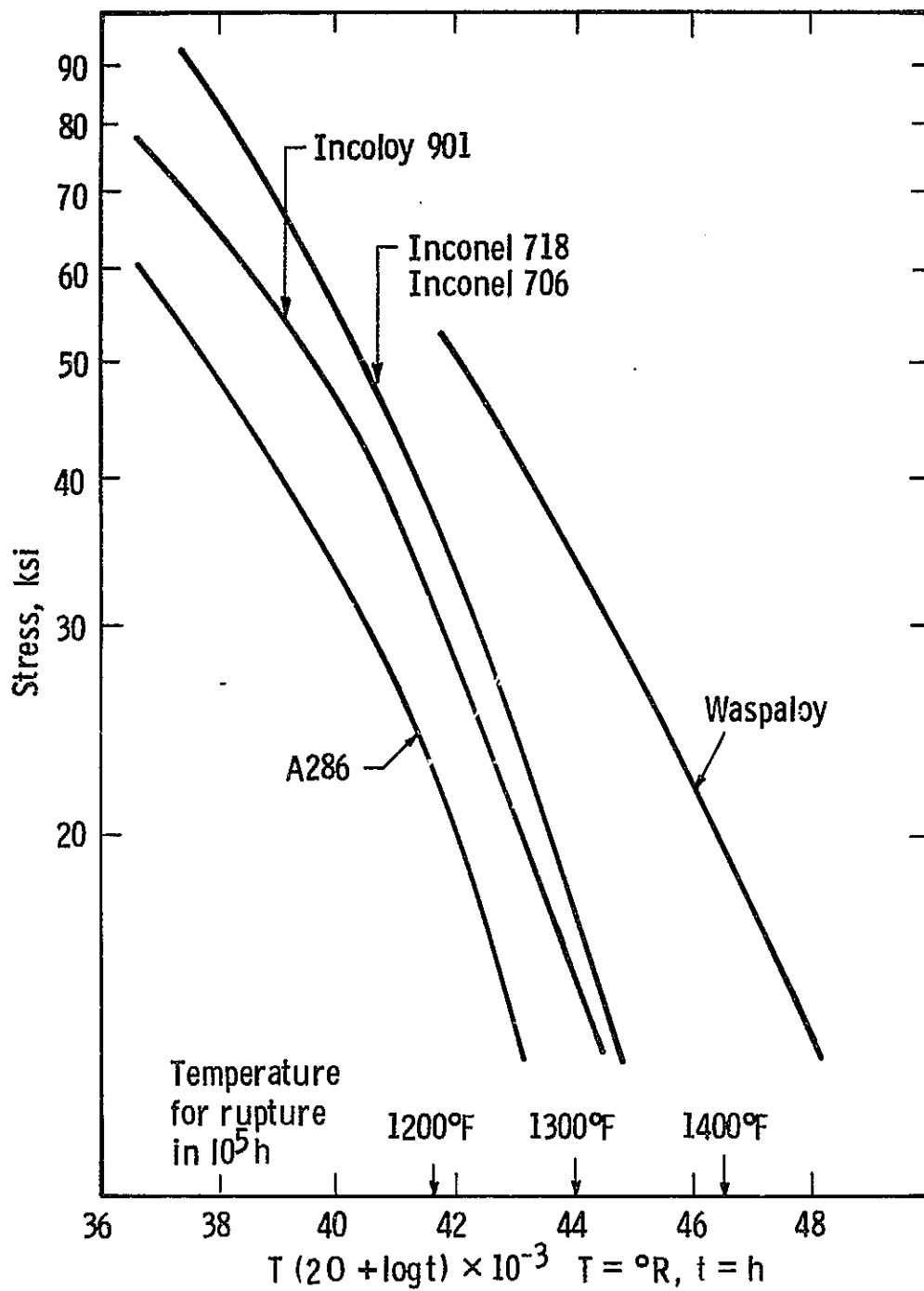


Fig. 3.20—Larson Miller parameter plot of steam turbine rotor alloys

would also permit a design that would limit the superalloys to only those sections of rotor which require them. This design would be of particular advantage in the higher temperature reheat turbines such as 1033°K (1400°F) where one could envision several disks of Waspalloy, followed by several of A286, and the remainder of the rotor of ferritic steel.

Through the use of separate high-temperature elements, the turbine configuration of the remainder of the turbine would be typical of a 24.2 MPa, 811°K (3500 psig/1000°F) plant in service today. Where a reheat temperature of 922°K (1200°F) or greater is used, however, additional intermediate pressure elements are required in order to prevent steam temperatures higher than 661°K (730°F) from entering the low-pressure element. This temperature limitation on low-pressure inlet steam results from the embrittlement of the nickel-chromium-molybdenum-vanadium steel which occurs with long-time exposure to higher temperatures (Reference 3.60). The cause of this embrittlement, referred to as temper embrittlement, has been shown to result from the diffusion of tramp elements such as phosphorus, tin, antimony, and sulfur to the prior austenite grain boundaries (Reference 3.60). These elements lower the fracture strength of these grain boundaries and result in an upward shift in the ductile-brittle transition temperature to near the temperature range encountered in service. The fracture toughness is decreased substantially as a result of temper embrittlement, and the critical flaw size required for brittle fracture is also reduced below the limit of detection. These materials should not be used under such conditions. Since temper embrittlement restricts low-pressure end steam temperatures to below 661°K (730°F), which necessitates the addition of an intermediate pressure element, alloy development to eliminate the problem is clearly required. The obvious solution would be to eliminate the occurrence of the tramp elements responsible; with current steelmaking practices, however, this is not an economical solution. Research aimed at understanding the reasons for impurity segregation and developing alloys to prevent it would have a large economic impact on high-temperature steam turbines.

#### 3.4.4 Blading

Steam turbine blading materials are selected to ensure a combination of high-temperature creep strength together with high fatigue strength under a mean stress loading. Although blading is designed so as not to undergo resonant vibrations, often during load transients, such as start-up, resonance conditions are realized. To prevent load buildup under these conditions, mid-span dampers or root sliding is usually designed into the blade.

Several years ago it was realized that, in addition to mechanical-type damping, the standard material used in nearly all turbines for blading -- 12% chromium steel -- possessed a high level of internal damping arising from magnetomechanical effects (Reference 3.61). In order to replace the ferritic steel, then, additional consideration has to be given to the influence this damping has on the resonant blade response.

The present 12% chromium steels are limited to temperatures below 839°K (1050°F) because of metallurgical instabilities and rapid fall-off in strength. For the 922°K (1200°F) service, K42B was successfully used in the Eddystone turbine. This alloy is no longer available, and either A286 or the stronger Refractaloy 26 could be used. For 1033°K (1400°F) service, the creep strength of an alloy such as Udimet 500 would be required. This alloy has many years of successful operation both in aviation and industrial gas turbines operating at comparable temperatures.

#### 3.4.5 Summary

Although not commercially available today in the sizes and configurations required, materials do exist that allow the construction of the steam turbines covered in this study. In most cases the materials selected have not been optimized for high-temperature steam conditions nor does there exist much relevant data on their behavior in this environment. In addition, there has been little experience on fabricating and



welding the heavy sections required in many of these applications. Taking these reservations into account, materials are recommended for the parametric points being studied, as shown in Table 3.16.

### 3.5 Material Considerations in Open-Cycle Gas Turbines/Recuperated or Combined-Cycle Systems

#### 3.5.1 Introduction

The efficiency of open-cycle gas turbines depends, to a large extent, on the temperature of the hot gas entering the turbines. The turbine must then be designed to maximize the turbine inlet temperature. The major material restraints in the design of a turbine are often the first-row guide vanes and rotating blades, since these components are subjected to the highest temperature gas and thus are limited by a combination of creep rupture and corrosion considerations. Since the limitations placed on materials by creep and corrosion are exponential functions of temperature, numerous techniques have been used to reduce the average metal temperature while increasing the gas turbine inlet temperature. Among these techniques, convection cooling, transpiration cooling, impingement cooling, and film cooling are most frequently employed to cool blades and vanes.

As a result of these considerations, designing turbines to operate at a specific turbine inlet temperature requires the complicated interaction of cooling technology and materials selection. Since extensive cooling impairs efficiency, there has been continuing interest in developing better high-temperature materials. This section will consider the application of these developments as current and future materials in the critical components in large industrial gas turbines.

#### 3.5.2 Turbine Blade Materials

Due to their excellent combination of high-temperature strength and corrosion resistance, nickel-based superalloys have been widely used as turbine blading in industrial gas turbines. One of the major problems

Table 3.16 — Material for Advanced Steam Turbines

Inlet Steam Conditions Pressure(psi)/Temp.(°F)	Inlet Piping and Inner Cylinder	High-Temperature Rotor	High Temperature Turbine Blade
2400/1000	2-1/4 Cr-1 Mo (A)	Cr-Mo-V (A)	403/422 (A)
3500/1000	2-1/4 Cr-1 Mo (A)	Cr-Mo-V (A)	403/422 (A)
5000/1000	2-1/4 Cr-1 Mo (A)	Cr-Mo-V (A)	403/422 (A)
2400/1200	316 (A)	A286 (A)	Refractaloy 26 (B) A286 (B)
3500/1200	316 (A)	A286 (A)	Refractaloy 26 (B) A286 (B)
5000/1200	316 (A) Kromarc 58 (B)	A286 (A)	Refractaloy 26 (B) A286 (B)
3500/1400	IN617 (B) HA188 (B)	WASPALLOY (C)	Udimet 500 (A) WASPALLOY (A)
5000/1400	S816 (C) HA188 (C) IN617 (C)	WASPALLOY (C)	Udimet 500 (A) WASPALLOY (A)

Note: Refer to Table 3.14 for boiler materials and materials application ratings for the above systems.

encountered in designing against creep in these alloys is their phase instability in the temperature range of interest. At temperatures above 1033°K (1400°F), the precipitation hardening phase,  $\gamma'$ , is continually growing and carbide phases are decomposing and reprecipitating. These phase changes make extrapolation of stress rupture properties to the long life anticipated in industrial gas turbines difficult. Although there has been extensive work on extrapolation procedures, none has been found to be universally adequate. For the purpose of this review, the Larson-Miller approach has been adopted to extrapolate the data on materials where only limited data are available. To arrive at a design allowable stress or temperature, the temperature corresponding to 360 Ms (100,000 hr) rupture life obtained from the data in Section 3.12, has been reduced by 27.8°K (50°F), which represents approximately a 75% reduction in strength.

In order to determine the relationship between these material design stress/temperature allowables and inlet gas temperature, once a metal temperature profile has been determined from cooling considerations, it is necessary also to consider the stress distribution in the turbine blade. The centrifugal stress is greater at the base of the airfoil and typically decreases on going to the blade tip, as shown in Figure 3.21. A typical temperature distribution profile along the blade has been superimposed on the stress distribution and included in this figure. The maximum temperature is seen at approximately the mid-section of the airfoil. The design life can be calculated by taking the temperature and stress corresponding to a given location on the blade. The life-limiting area of the blade corresponds to the mid-blade height area and not to the location of either the highest temperature or the highest stress.

At stresses typical of this design-limited location of the blades, superalloys typical of current production (U710) are limited to metal temperatures of 1061 to 1116°K (1450 to 1550°F), Table 3.17. Based on current development under way on alloys such as IN 792, it is anticipated that in the next several years a 42 to 55°K (75 to 100°F)

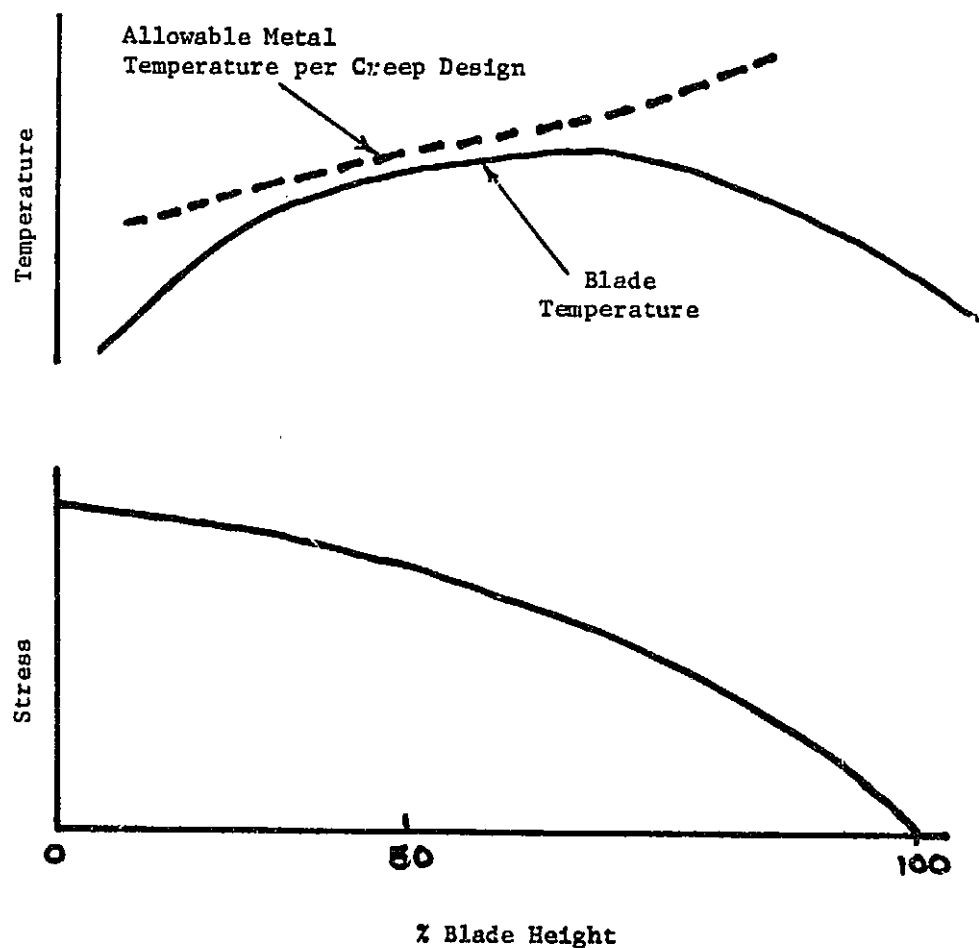


Figure 3.21 — Allowable metal temperatures for various locations on airfoil of a blade based on indicated temperature and stress profiles.

Table 3.17 — Design Allowable Temperatures for  
Current and Future Turbine Blade  
Materials

Status	Material	Temperature (°F) allowable for indicated stress (ksi)			Ref.
		20	15	10	
	Udimet 710	1450	1525	1575	3.62
	IN792	1525	1600	1675	3.63
	TRW-NASA VIA	1575	1650	1725	3.65
	AVCO Lycoming Development Alloy E2	1525	1650	1900	3.67
	Ni <sub>3</sub> Al-Ni <sub>3</sub> Cb ( $\gamma$ - $\delta$ )	1680	1730	1800	3.68
	W-Re-Hf-C Composite	2150	2150	2150	3.72
	Cr-7Mo-1Cb-0.1Y- .08B	1790	1850	1950	3.73

improvement in temperature capability will be realized without significantly sacrificing hot corrosion resistance, Table 3.17. Although IN792 is beginning to be applied in aerospace turbines, a several-year delay before its application in industrial gas turbines is anticipated because of the production difficulties usually encountered in introducing a new alloy. These difficulties in the past have usually been associated with obtaining a casting with the required low level of microporosity. The significant difference in the size of the casting for aerospace and industrial use is another area of concern. The introduction of hot isostatic pressing (HIP) as a production procedure to reduce casting microporosity may reduce the time lag for this source in the future; the results to date are very encouraging (Reference 3.64).

Another 28 to 42°K (50 to 75°F) improvement in temperature capability is obtained by introducing an alloy such as TRW-NASA VIA, Table 3.17 (Reference 3.64) and relaxing the requirement for base-metal corrosion resistance, relying instead on a coating for protection. This alloy probably represents the highest temperature capability it is possible to obtain by conventional investment-casting of nickel-based superalloys. Recognizing this, the industry has all but ceased development of next-generation nickel-based superalloys. It is clear that further increases in the temperature capability will require the application of a new alloy system and/or processing.

A new technique which promises to extend the temperature range of "near" conventional superalloys is mechanical alloying. Early attempts to utilize the process involved base alloys with limited intermediate temperature strength and produced alloys of insufficient strength for blade application (Reference 3.66). Using mechanical alloying to produce a yttria dispersion-hardened alloy with a base composition derived from IN792, a much stronger and corrosion-resistant material resulted (Reference 3.67). This technique is just beginning to be fully exploited, and in the next five years a temperature capability of 1366°K (2000°F) should be developed. As a powder process, mechanical alloying has the major drawback of requiring some secondary working after sintering. This makes the application of cooling technology difficult except for simple schemes involving electrochemical machining (ECM) holes. One possible technique to introduce more advanced cooling would be to extrude a hollow airfoil shape which could then be joined to a solid blade root by diffusion bonding.

Eutectic superalloys have met with considerable interest in the aerospace industry. By eutectic growth an in-situ composite is produced, consisting of a superalloy-type matrix reinforced by a high-temperature intermetallic such as  $\text{Ni}_3\text{Nb}$  or  $\text{TaC}$ . Currently, the strongest material of this class is the  $\gamma'-\delta$  ( $\text{Ni}_3\text{Al}-\text{Ni}_3\text{Nb}$ ) composite which provides strength in the 1189 to 1255°K (1680 to 1800°F) temperature range, Table 3.17. While the  $\gamma'-\delta$  system has relatively poor corrosion

C-2

resistance and will need to be coated, other eutectic superalloys such as  $(\text{Co-Cr})\text{Cr}_7\text{C}_3$  and  $(\text{Co,Cr})\text{TaC}$  have been developed with better corrosion resistance than conventional superalloys such as IN738 (References 3.69 and 3.70). The development of corrosion resistant alloys does demonstrate that although the development of eutectic alloys is restricted by phase diagrams, they can be developed to produce the desired compromise in strength and corrosion resistance.

Perhaps an even greater degree of control on properties can be obtained with artificially fiber-reinforced superalloys. In these systems a composite is made out of a wire processed to the desired strength and then placed in a matrix that can be optimized for corrosion resistance. This flexibility allows one to select the optimum combination of properties, and since the composite is man made, the distribution of the fibers can be selected to have maximum reinforcement where required, such as at mid-blade height. The short time rupture creep behavior of both eutectic and composite materials has been demonstrated to obey the rules of mixtures, so that strengths can be conveniently calculated from fiber and matrix properties for any volume fraction reinforcement.

The long-time rupture properties of man-made fiber-reinforced composites are influenced by the chemical reaction between the matrix (typically superalloy) and reinforcing material (Reference 3.71). This diffusion-controlled interaction results in a serious loss of properties, causing either intermetallic precipitation or, in the superalloy-tungsten wire case, recrystallization of the cold work-strengthened tungsten. Since the reason for the loss in strength is well understood, work on diffusion barriers has proceeded and it is anticipated that rule-of-mixture properties will result at least to around 1422 to 1478°K (≈2100 to 2200°F) temperature range (Reference 3.72).

Based on rule of mixture properties the W-Re Hf-C composite can be seen to have the highest strength and temperature capability of any metal system, Figure 3.22. These materials, along with the eutectic

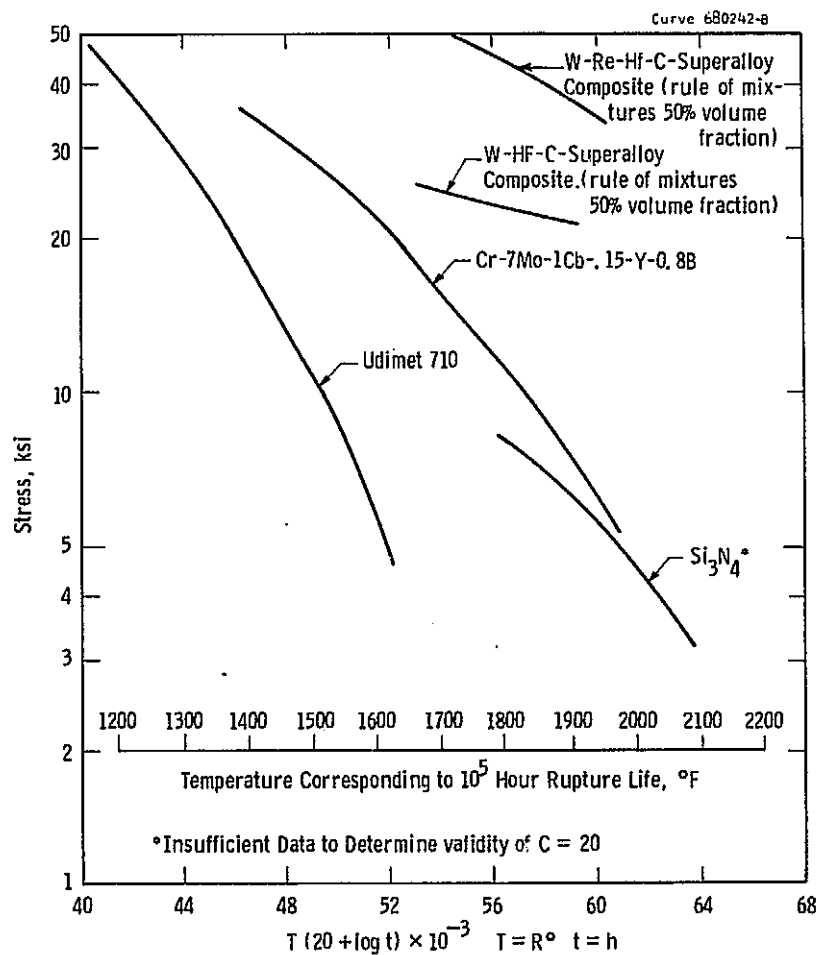


Fig. 3. 22-Larson Miller parameter plot of stress rupture strength of various gas turbine blading materials

REPRODUCIBILITY OF THE  
ORIGINAL PAGE IS POOR



composites, raise some new design problems, not normally encountered with conventional superalloy technology, which will have to be seriously addressed. The mismatch of the thermal expansion coefficients between the fiber and the matrix makes thermal fatigue properties an area of major concern. Off axis, anisotropic properties, shear strength, and fatigue would also have to be investigated in more detail to generate better design data than are presently available.

Since the end of World War II, a considerable research and development effort on chromium alloys for aircraft gas turbine service has been sponsored by governments of several Free World nations, notably Australia, the United Kingdom, and the United States. The sustained interest in chromium as a base for high-temperature structural components is founded on a number of factors. Chromium has a melting point advantage of 533 to 644°K (500 to 700°F) over such more commonly used metals as iron, cobalt, and nickel, and its density is significantly lower than that of the latter two. The oxidation resistance of chromium is vastly superior to that of the heavier, more refractory metals such as niobium, tantalum, molybdenum, and tungsten. Hot corrosion by environments which contain sulfur or alkali salts is greatly retarded in superalloys with only moderate additions of chromium, and chromium-based alloys have shown attractive behavior in limited hot corrosion testing. The elastic modulus of chromium is higher by about 30% than that of most superalloys, the coefficient of thermal expansion is considerably lower, and the thermal conductivity is higher by factors of two to five. These properties combine to offer much greater resistance to thermal shock or thermal fatigue than that exhibited by superalloys. The identified world resources of chromium are estimated at about 907.2 Mg ( $10^9$  tons). Thus, chromium is more abundant than nickel, for example, by an order of magnitude.

Unfortunately, the use of chromium alloys as structural components in such applications as advanced air-breathing turbine systems had been deterred by the lack of ductility at low temperatures, except in the purest forms of the unalloyed metal in the optimum microstructural

condition, and by the further embrittlement due primarily to reaction with nitrogen during extended exposure to air at elevated temperatures. There were also some early indications that the potential strength advantage over superalloys, suggested by the increased melting point, could not be realized by conventional alloying approaches.

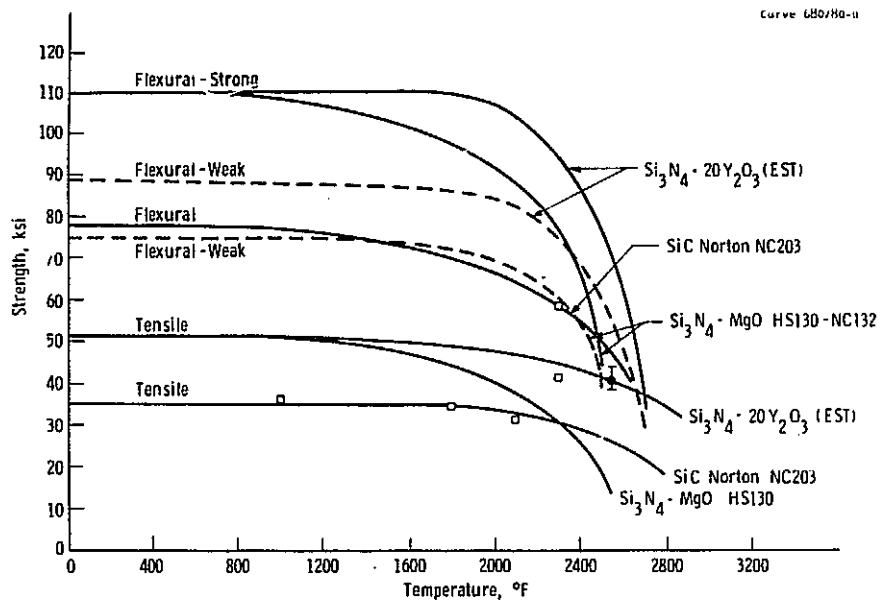
Several studies of chromium alloys over the past decade have identified alloy systems which not only have, in fact, achieved significant strength increases over the best currently available superalloys at temperatures above 1255°K (1800°F), but which also have given indications that the severity of the ductility and nitrogen-embrittlement problems could be greatly reduced. The alloying approach that has shown the most promise to date is based on dispersion of carbides or borides formed by the reactive metals of Groups IV-A and V-A in Cr-Mo or Cr-W matrices. On the basis of creep rupture characteristics, some alloys of the latter type offer a temperature capability of 1339°K (1950°F) (References 3.73 and 3.74). Other carbide-strengthened alloys (which contain no major substitutional solutes for solution strengthening) have shown considerable tensile ductility at subzero temperatures in both the wrought and recrystallized conditions, even when produced from chromium grades of only moderate purity. In all chromium alloys toughness at operating temperatures above their ductile-brittle transition (DBTT) is superior to that of any current superalloys.

Successful application of chromium alloys in structural components must (1) await the development of surface coatings for protection against nitridation (a field in which promising progress was made in 1969-1971 with monovalent solute additions) and (2) the emergence of an application in which design concessions can be made to the lack of toughness at temperatures below several hundred degrees, through expedients such as prewarming. A high-temperature utility turbine is one such application that justifies consideration of chromium. Since properties of chromium alloys at intermediate and elevated temperatures are rather attractive, it is possible that prewarmed designs could evolve. Since allowable metal temperatures are 394°K (250°F) higher than the limit

for superalloys, significant increases in the thermal efficiency of combined-cycle power generation could be attained.

Because of their high-temperature strength above 1366°K (2000°F), good corrosion resistance, and good thermal shock resistance, silicon carbide, and silicon nitride ceramics are being seriously considered as advanced turbine materials that can be used uncooled. Due to several stresses imposed in turbine design, it is thought that only fully dense forms of silicon nitride and silicon carbide are going to find application. Presently the application of ceramics for industrial turbine vane application is being explored by Westinghouse under ARPA sponsorship. The tensile properties and stress rupture strength are plotted in Figure 3.23. Currently the commercially available silicon nitride appears to be creep limited when uncooled to service temperature in the range of 1478°K (2200°F) (Reference 3.75). It is clear, however, that these properties do not represent the ultimate strength obtainable with these materials. Silicon nitride and to a lesser extent silicon carbide are currently creep controlled by the impurities present in the raw materials (Reference 3.76). Since relatively pure silicon carbide powder is already used in the manufacture of hot-pressed silicon carbide, it is not likely that its already very high creep strength will be significantly improved. In the case of silicon nitride, however, it is anticipated that substantial improvements in creep strength can result from slightly improved processing procedures (i.e., elimination of the glass phase at grain boundaries). Good progress is being made in this area.

Introduction of ceramics, chromium alloys, and to a lesser extent eutectic alloys will require a significant change in the design philosophy of blade and vane materials. The high "notch sensitivity" of most of these materials requires that critical stresses in elements of the component be analyzed exactly and material testing be conducted from a statistical probability of failure criterion. A three-dimensional finite element routine is required to analyze such components as interface contact stresses and rotor blade stresses. These tools are available.



Tensile strength of hot pressed  $\text{Si}_3\text{N}_4$  and SiC

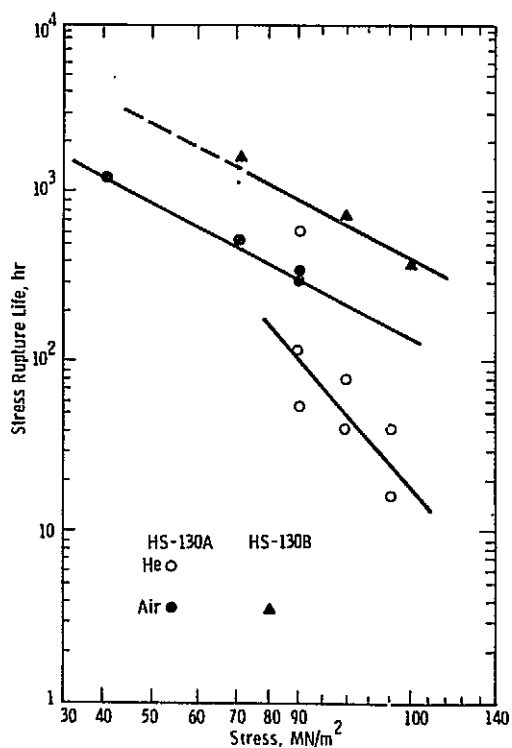


Fig. 3. 23 — Stress rupture, hot pressed  $\text{Si}_3\text{N}_4$  at 2300°F

In addition to the first-row blade material problem, the last-row turbine blade also represents a material-limited application. The thin cross-sectional area, combined with the twist and the long length, results in much higher stresses than those present in the first-row blade. Typical mid-height stresses of 344.7 MPa (50 ksi) operating at 922 to 1033°K (1200 to 1400°F) requires at least the strength of an alloy such as Udimet 710. The high strength of this alloy, together with the size of the blade [29.48 kg (65 lb)] presents difficulties in obtaining a precision-forged part with the required dimensions. Instead, a rather costly process of open-die forging followed by machining would be required. One material development which has the potential to meet this need is a superalloy-refractory metal composite described previously. At the lower temperature of this application, the interface reaction and the deterioration of wire properties are no longer problems. The low temperature also allows substitution of less dense molybdenum alloys for the tungsten alloys required in the first-row blade. Another technique which might also be evaluated is powder metallurgy. By using a hot isostatically pressed preform of a high-strength alloy such as IN792, the final hot-die forging pressure could be substantially reduced because of the superplastic behavior of the preform at high temperatures. At the same time, a fine-grained product having superior high-cycle fatigue strength would result. Since this application is at relatively low temperatures [922 to 1033°K (1200 to 1400°F)] grain growth treatments which have plagued powder metallurgical developments for high-temperature strength do not arise.

### 3.5.3 Turbine Vane Alloys

Cobalt-based superalloys have been the standard turbine guide vane alloy systems since the early development of gas turbines for many reasons. Although they are relatively weak at moderate temperature because of relatively coarse carbide precipitation and solid solution hardening, they have superior microstructural stability and retain their strength at much higher temperatures than  $\gamma'$  strengthened

nickel-based superalloys. In the relatively low stress [34.47 MPa (~5 ksi)] static vane application they possess a higher temperature capability. The cobalt-based alloys also are inherently more castable than are nickel-based superalloys; and this feature, together with their superior weldability, allows complex-cored, multiple-vane segments to be produced economically. In addition, cobalt-based alloys have demonstrated advantages in hot corrosion resistance. They possess higher thermal conductivity and slightly lower thermal expansion properties and thus should have better thermal fatigue resistance than Ni-base superalloys.

The standard alloys in current production for vanes are X-45 and Mar M-509. (See Section 3.12 for typical strength.) These alloys allow vane metal temperatures in the range of 1200°K (1700 F) to be reached. Higher temperature capability in the cobalt-based alloy system can be obtained by use of in-situ eutectic composite alloys such as (Co,Cr)-(Cr,Co)<sub>7</sub>C<sub>3</sub> containing a carbide phase reinforcement (References 3.77 and 3.78). These alloys represent a 56 to 111°K (100 to 200°F) temperature advantage over conventional alloys and, in addition, possess some degree of hot corrosion resistance. The processing of such materials to large complex-cored multivane segments would appear to require an extensive development effort. In addition, poor weldability of such materials could be anticipated.

More likely candidates for high-temperature vane applications appear to be the ceramic materials silicon nitride and silicon carbide discussed in the blade section. Their lower stresses in vane application, their excellent hot corrosion resistance, and their good thermal shock properties give them a considerable advantage in this application and the only direct approach to uncooled components. The relatively large space provided for the first stator vane in industrial gas turbines and the lack of concern for system weight makes the ceramic vane design required to reduce tensile stresses feasible. Rig testing of a silicon nitride vane design has proved very successful, and work on it will be continued (Reference 3.79).

#### 3.5.4 Summary

Based on the above discussion of high-temperature strength and the corrosion considerations given in Section 3.2, material selections were made for the recuperated open-cycle and combined-cycle gas turbines and are presented in Tables 3.18 and 3.19. It is assumed in this study that cooling will be used to limit blade and vane temperatures to within the limits specified by Table 3.17 for the alloys chosen. Basically, the metallic alloy selections represent the current materials being used for industrial gas turbines. For the hot corrosion environment produced by the low-Btu gas, MCrAlY overlay coatings are specified. Also included in this table is a listing of the developmental materials which, while not presently available for this application, appear to represent the best candidates for future development work to reduce the cooling required.

### 3.6 Materials for Closed-Cycle Gas Turbine System

#### 3.6.1 Corrosion Behavior of High-Temperature Materials in Impure Helium

##### 3.6.1.1 Introduction

There has been much research (References 3.80 to 3.94) over the past two decades on the corrosion behavior of materials in impure helium environments as part of the development of gas-cooled nuclear reactors. The materials that have been evaluated include low-alloy steels, ferritic and austenitic stainless steels, medium strength cobalt- and nickel-based alloys, superalloys, and refractory metals. The impurities in the helium atmospheres have included all the common carbon-, oxygen-, and hydrogen-bearing gases, such as carbon monoxide, carbon dioxide, water vapor, methane, and nitrogen.

The more recent and extensive materials investigations that have been carried out as part of the Dragon Project (References 3.93 and 3.94) have shown that there is a direct relationship between the concentration of impurities and the magnitude of corrosion.\* Unfortunately,

---

\*There is some disagreement on this effect, as discussed in Section 3.6.1.5.

Table 3.18 — Material Selection for Recuperated Open-Cycle Turbines

Parametric Points	Turbine Inlet Temp., °F	Cooling	Fuel	First-Row Vane	First-Row Blade	Last-Row Blade
1-5, 15-18, 34-38	2200	Air-cooled blade and vane	Dist. from coal	Mar M-509 (A) X-45 (A)	U500 cast (A) IN738 cast (B) W-reinforced superalloy composite (C) Cr alloys (C)	U710 forged (A) IN792 powder (B) Mo-reinforced superalloy composite (C)
19-23 39-43	2500	Air-cooled blade and vane	Dist. from coal	Mar M-509 (A) X-45 (A)	U500 cast (A) IN738 cast (B) W-reinforced superalloy composite (C) Cr alloys (C)	U710 forged (A) IN792 powder (B) Mo-reinforced superalloy composite (C)
24-28	1800	Air-cooled blade and vane	Dist. from coal	Mar M-509 (A) X-45 (A)	U500 cast (A) IN738 cast (B) W-reinforced superalloy composite (C) Cr alloys (C)	U710 forged (A) IN792 powder (B) Mo-reinforced superalloy composite (C)
44-48	2200	Air-cooled blade	Dist. from coal	Si <sub>3</sub> N <sub>4</sub> (B) SiC (B)	U500 cast (A) IN738 cast (B) W-reinforced superalloy composite (C) Cr alloys (C)	U710 forged (A) IN792 powder (B) Mo-reinforced superalloy composite (C)
49-53	2200	None	Dist. from coal	Si <sub>3</sub> N <sub>4</sub> (B) SiC (B)	Si <sub>3</sub> N <sub>4</sub> (C) SiC (C)	U710 forged (A) IN792 powder (B) Mo-reinforced superalloy composite (C)
54-58	2500	Air-cooled blade	Dist. from coal	Si <sub>3</sub> N <sub>4</sub> (B) SiC (B)	U500 cast (A) IN738 cast (B) W-composite (C) Cr alloys (C)	U710 forged (A) IN792 powder (B) Mo-reinforced superalloy composite (C)
59-63	2500	None	Dist. from coal	Si <sub>3</sub> N <sub>4</sub> (B) SiC (C)	Si <sub>3</sub> N <sub>4</sub> (C) SiC (C)	U710 forged (A) IN792 powder (B) Mo-reinforced superalloy composite (C)

3-96



Table 3.19 — Material Selection for Combined-Cycle Gas Turbines

Parametric Points	Turbine Inlet Temp., °F	Cooling	Fuel	First-Row Blade	First-Row Vane	Last-Row Blade
1, 87, 88	2200	Air-cooled blade and vane	Low-Btu Gas	CoCrAlY Coated: U500 cast (A) IN738 cast (B) W-reinforced superalloy composite (C) Cr alloys (C)	CoCrAlY Coated: Mar M-509 (A)	U710 forged (A) IN792 powder (B) Mo-reinforced (C) superalloy composite
2-71	1800 - 2600	Air-cooled blade and vane	Dist. from coal	U500 cast (A) IN738 cast (B) W-composite (C) Cr alloys (C)	Mar M-509 (A) X-45 (A)	U710 forged (A) IN792 powder (B) Mo-reinforced (C) superalloy composite
72-75	2200	Air-cooled blades	Dist. from coal	U500 cast (A) IN738 cast (B) W-composite (C) Cr alloys (C)	Si <sub>3</sub> N <sub>4</sub> (B) SiC (B)	U710 forged (A) IN792 powder (B) Mo-reinforced (C) superalloy composite
76-79	2200	None	Dist. from coal	Si <sub>3</sub> N <sub>4</sub> (C) SiC (C)	Si <sub>3</sub> N <sub>4</sub> (B) SiC (B)	U710 forged (A) IN792 powder (B) Mo-reinforced (C) superalloy composite
80-83	2200	Blade water cooled	Dist. from coal	U500 cast (A)	Si <sub>3</sub> N <sub>4</sub> (B) SiC (B)	U710 forged (A) IN792 powder (B) Mo-reinforced (C) superalloy composite
84	2200	Air-cooled blade and vane	High-Btu gas	U500 cast (A) IN738 cast (B) W-composite (C) Cr alloys (C)	Mar M-509 (A) X-45 (A)	U710 forged (A) IN792 powder (B) Mo-reinforced (C) superalloy composite

the gas composition in many of the previous investigations may not be relevant to real systems, and the results are of doubtful value. In addition, several of the previous studies were carried out under conditions permitting the composition of the gas to change in an undefined manner either during the course of the experiments or as a function of position in the furnace. The results of such experiments are of very little use in attempting to determine the effect of the environments on materials behavior.

The other significant factor to emerge from the Dragon studies (References 3.93 and 3.94), as well as from other recent investigations (References 3.91 and 3.92), is a deleterious creep stress corrosion effect in nickel-based alloys and austenitic stainless steels in impure helium environments. These various investigations have demonstrated that the environmental-mechanical property interaction involves intergranular oxidation of the minor, stable, alloying element (such as aluminum and titanium) resulting in both an increase in creep rate and a decrease in rupture strength and life.

In light of the previous discussion, the present review will be concerned with those investigations carried out in well-characterized gas phases. A general list of the studies that have been reported in the literature is given in Table 3.20, including the type and level of impurities, the temperature range, and the alloys investigated.

#### 3.6.1.2 Thermodynamic Considerations

The metal oxide equilibrium for the elements commonly used in high-temperature alloys in form of a  $\log P_{H_2O}/P_{H_2}$  versus temperature plot is shown in Figure 3.24. The implication of these data is that the oxidation reactions occurring will be selective and will involve the major alloying elements chromium, manganese, silicon, titanium, and aluminum. Since scales containing mainly chromium oxide tend to be brittle, nonprotective oxide scales are a distinct possibility.

Table 3.20 — Summary of Studies in Impure Helium Environments

Reference	Alloys	Temperature Range °F	Atmosphere
3.80	Nb; Nb - 1, 5% Zr; Nb + 5, 8, 10% Ti; 430 SS; 316 SS, Inconel 600, Inconel X 750	1500-1700	He with 200 & 10,000 ppm CO + 2 CO <sub>2</sub> (exact values unspecified) at 1 atm
3.80	Nb-1 Zr; Nb-20 Ti; 316 SS, 430 SS, C-1/2 Mo St; 1-1/4 Cr-1/2 Mo St; Inconel 702; Inconel X 750; Molybdenum	100 -1700	He with 5000 ppm H <sub>2</sub> + 5000 ppm CO at 1 atm
3.81	Rene 41, 430 SS, 304 SS Hastelloy X, Incoloy 800 Inconel X750	1650-1800	He with 3000 ppm H <sub>2</sub> + 3000 ppm CO at 1 atm (H <sub>2</sub> O and CO <sub>2</sub> unspecified; levels changed with time)
3.82	321H SS, 347 SS, 304 SS, 430 SS, Inconel 600	1200-1400	He with 200-300 ppm H <sub>2</sub> and CO or 2000-3000 ppm H <sub>2</sub> + CO at 2 atm (H <sub>2</sub> O and CO <sub>2</sub> content unspecified)
3.83	Inconel 600, 625, 702, 718; Incoloy 800; Hastelloy C, N, R-235 X-280, Haynes 25	1500-1900	He with 1.97% H <sub>2</sub> O at 1 atm
3.84	Hastelloy X-280 Haynes 25	2150-2200	Pure H <sub>2</sub> O at ~ .033 atm Pure CO <sub>2</sub> at ~ .11 atm Pure CO at ~ .033 atm (impurities conc. changed with time in some experiments)
3.85	406 SS; 304 SS; 316 SS; Hastelloy X-280; R-235, N; Inconel 600; Fe-30 Cr-1Y; PDRL-102	1940	He passed through graphite at 840-940°F (impurity levels unspecified)

Table 3.20 — Summary of Studies in Impure Helium Environments (Cont'd) - 2

Reference	Alloys	Temperature Range °F	Atmospheres
3.86	Incoloy 800, 901; LCN 155; HK 40, Supertherm; Inconel 600, 750 X, Hastelloy X, Nimonic 80A, 90, 100, 115, Udimet 700, Rene 41, 62, TAZ8 Astroloy	1832	99.99% pure He with unspecified impurity levels
3.87	Nimonic 75	1382-1832	Pure CO <sub>2</sub> , CO, H <sub>2</sub> O, CH <sub>4</sub> , H <sub>2</sub> , N <sub>2</sub> at $1.3 \times 10^{-5}$ to $1.3 \times 10^{-2}$ atm
3.87	Nimonic 75, C-MnSt, 2-1/4 Cr-1 MoSt; 9 Cr-1 Mo St; 12 Cr-1 Mo-V St; 304 SS, 321 SS, 347 SS, 316 SS, 316L SS	932-1650	A gas mixture of N <sub>2</sub> + CO + CO <sub>2</sub> + H <sub>2</sub> O + CH <sub>4</sub> (1:3:3:0.5: 0.5) at $1.3 \times 10^{-4}$ to $1.3 \times 10^{-2}$ atm
3.88	304 SS	750-1832	He containing CO <sub>2</sub> or CO <sub>2</sub> + CO (impurity levels well defined) at 0.13 atm total pressure
3.89	Esshete 1250; 316 SS; 310 SS; Incoloy 800; Inconel 600; Hastelloy X, C	1290	12.5 ppm CO, 12.5 ppm H <sub>2</sub> , 2.5 ppm in He at 40 atm total pressure
3.90	Nimonic 75, P.E. 16; Incoloy 800, Corronel 230, M313	1382-1922	Dragon Reactor: PN <sub>2</sub> = $3 \times 10^{-6}$ atm; PH <sub>2</sub> = $16 \times 10^{-6}$ ; PCO = $10 \times 10^{-6}$ ; PH <sub>2</sub> O = $1.6 \times 10^{-6}$ ; PCH <sub>4</sub> = $2 \times 10^{-6}$ ; PCO <sub>2</sub> < $0.4 \times 10^{-6}$
3.91	316 SS, Incoloy 800	1200-1470	1000 ppm H <sub>2</sub> , 1000 ppm CO, 100 ppm H <sub>2</sub> O in He at 1 atm pressure; "pure" He with measured impurity levels (Environmental Creep Studies)

Table 3.20. — Summary of Studies in Impure Helium Environments (Cont'd) - 3

Reference	Alloys	Temperature Range °F	Atmospheres
3.92	Mild St., 1% Cr-.5% Mo St; 2-1/4 Cr-1% Mo St, 316 SS; 20 Cr-35 Ni SS; 15 Cr-15 Ni SS	750-1382	500 ppm H <sub>2</sub> ; 500 ppm CO, 50 ppm H <sub>2</sub> O, 50 ppm CH <sub>4</sub> in He at 1 atm pressure (Environmental Creep Studies)
3.93, 3.94	Nimonic 75, 80A, 105; Inconel 625; Incoloy 800; IN-102; 321 SS; 347 SS; HDA 22,30 and 45; Nimocast 713 LC and PD 16; Mo; TZM; TZC; Nb Alloys	1382-1562	250 ppm H <sub>2</sub> ; 250 ppm CO; 50 ppm H <sub>2</sub> O in He at 1.8 atm total pressure; 30 ppm H <sub>2</sub> ; 20 ppm CO; 5 ppm H <sub>2</sub> O in He at 1.8 atm total pressure (Environmental Creep Studies)

$$1 \text{ atm} = 1.013 \times 10^5 \text{ Pa}$$

$$(^{\circ}\text{F}) = 1.8 \times (^{\circ}\text{C}) + 32$$

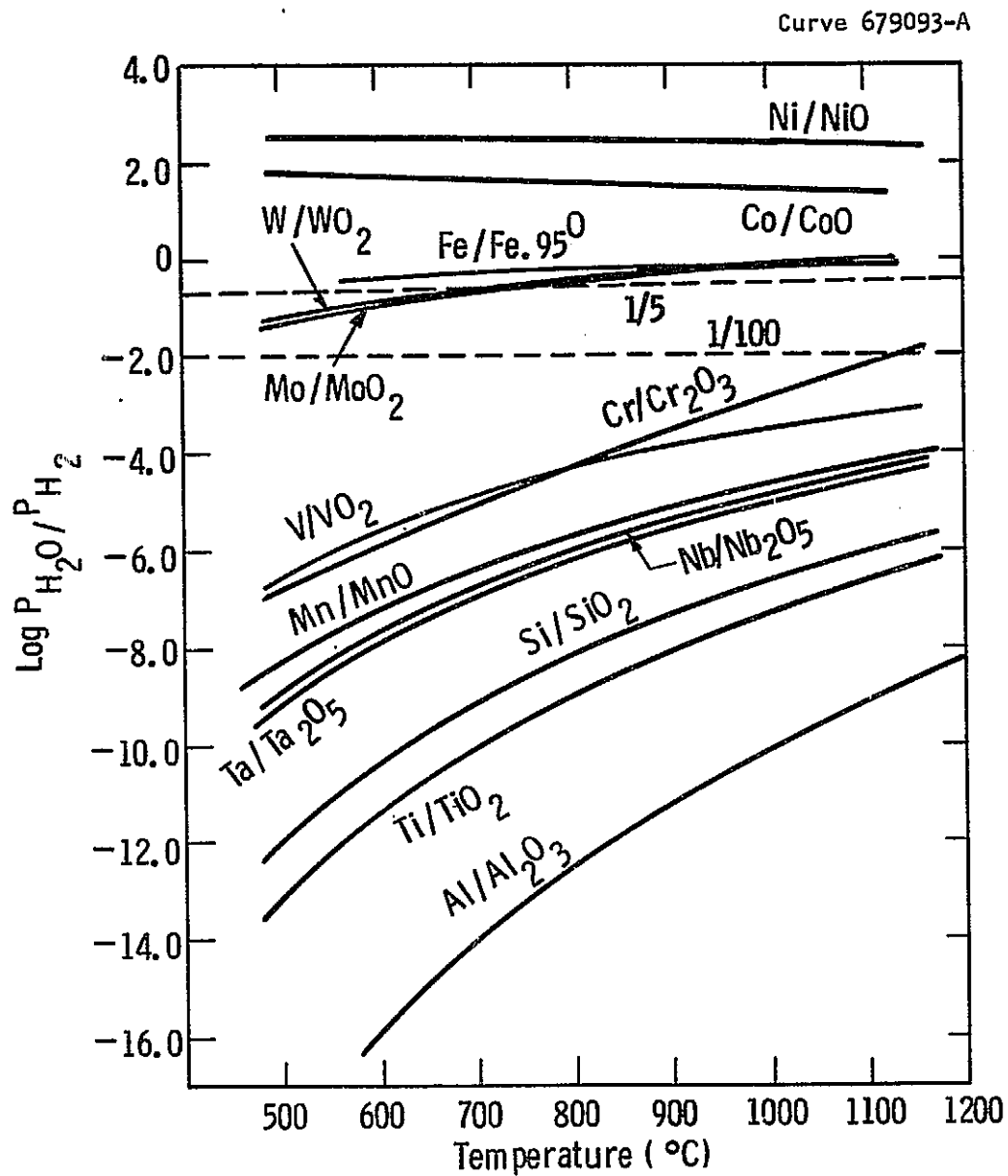


Fig. 3. 24—Equilibrium  $P_{\text{H}_2\text{O}}/P_{\text{H}_2}$  ratios for metal-oxide systems

Volatilization of metals and oxides is another important class of reactions that might occur. Thermochemical calculations show that the partial pressures of species such as molybdenum, chromium, and tungsten oxide vapors, and so forth [ $\text{MoO}_3(\text{g})$ ,  $\text{CrO}_3(\text{g})$ ,  $\text{WO}_3(\text{g})$ ], are low in the temperature and oxygen potential ranges being considered in this study.

### 3.6.1.3 Gas-Solid Reactions in Dragon Reactor Coolant

The nature of the interaction between impure helium and a number of nickel-based alloys has been extensively studied as part of the Dragon Project. Recently, Pearce and Sperry (Reference 3.90) have reported the results of an electron probe microanalytical examination on specimens exposed in the Dragon reactor at temperatures above 1023°K (1382°F) for periods of either 22.11 or 42.6 Ms (256 or 493 days). The materials investigated include Nimonic 75, Nimonic P.E. 16, Incoloy 800, Corronel 230, M313. The composition of these alloys is listed in Table 3.21, and the results are summarized in Table 3.22. The significant conclusions of this study were that: (1) oxidation of all alloys tested resulted in a surface oxide scale consisting in every instance of a chromium-rich layer with some enrichment of titanium and manganese;\* (2) internal oxidation occurred in all alloys with the formation of aluminum oxide concentrated at the grain boundaries (even with aluminum contents as low as ~0.1 wt%); (3) there was a tendency to form an apparently continuous surface layer of aluminum oxide underneath the main oxide layer in M313 and Nimonic P.E. 16. It follows from these results that the oxide film formed on these representative nickel-based alloys is not protective, resulting in internal oxidation. This type of environmental interaction is the precursor to a potentially serious stress-creep corrosion effect.

\*Enrichment of nickel or iron in the oxide layer was not observed except in the case of Corronel 230 where a nickel-rich oxide scale was observed.

Table 3.21 — Composition of Alloys Evaluated in the Pearce and Sparry (Reference 3.90) Study

Alloy	Weight %												Others
	Cr	Ni	Fe	Ti	Al	Mo	Mn	Co	Si	Zr	Cu	C	
Nimonic 75	19.45	Bal	3.61	0.43	0.22	< 0.2	0.4	0.18	0.2	0.025	0.11	0.11	Mg 0.03
Nimonic PE16	16.15	43.3	Bal	1.1	1.21	3.3	0.06	< 0.2	0.17	0.035	0.03	0.08	
Incoloy 800	20.4	31.7	Bal	0.4	0.32	< 0.2	0.68	0.08	0.43	--	0.05	0.04	
Corronel 230	34.65	Bal	2.2	0.2	0.2	--	0.32	--	0.3	--	--	0.015	
M313	30.8	Bal	--	1.55	0.92	--	< 0.05	--	0.15	0.04	--	0.04	B 0.004



Table 3.22 — Results of Electron-Probe Examination of Alloys Exposed in the Dragon Reactor\*

Alloy	Temperature Range °F	Time (hours)	Results
Nimonic 75	1382-1526	11,800	10 $\mu\text{m}$ surface scale composed of $\text{Cr}_2\text{O}_3$ with Ti and Mn enrichment; 30-40 $\mu$ granular penetration ( $\text{Al}_2\text{O}_3$ )
Nimonic P.E. 16	1382-1526	6,150	8 $\mu\text{m}$ surface scale - $\text{Cr}_2\text{O}_3$ with Ti; 35 $\mu\text{m}$ intergranular penetration ( $\text{Al}_2\text{O}_3$ ); thin, nearly continuous $\text{Al}_2\text{O}_3$ layer beneath $\text{Cr}_2\text{O}_3$ ; possible Cr carbide formation at 75 $\mu$
Incoloy 800	1742-1922	11,800	5 $\mu\text{m}$ surface scale - $\text{Cr}_2\text{O}_3$ with Ti, Si and Mn; 20 $\mu\text{m}$ intergranular penetration ( $\text{Al}_2\text{O}_3$ )
Corronel 230	1742-1922	6,150	2 $\mu\text{m}$ inner surface scale - $\text{Cr}_2\text{O}_3$ with Ti; 8 $\mu\text{m}$ outer porous surface scale with thin layer of $\text{NiO}$ , Cr and Fe enrichment, Ni inclusions; 45 $\mu\text{m}$ intergranular penetration ( $\text{Al}_2\text{O}_3$ )
M313	1742-1922	6,150	2 $\mu\text{m}$ surface scale - $\text{Cr}_2\text{O}_3$ ; 20 $\mu\text{m}$ intergranular penetration ( $\text{Al}_2\text{O}_3$ )

\* Coolant Composition:  $\text{PN}_2 = 3 \times 10^{-6}$  atm;  $\text{PH}_2 = 16 \times 10^{-6}$  atm;  $\text{PCO} = 10 \times 10^{-6}$  atm;  $\text{PH}_2\text{O} = 1.6 \times 10^{-6}$  atm;  $\text{PCO}_2 < .4 \times 10^{-6}$  atm

1 atm =  $1.013 \times 10^5$  Pa

(°F) = 1.8 x (°C) + 32

1 hr = 3600 s

Table 3.23 — Chemical Compositions of Alloys in the Environmental Creep Study by Woods et al. (Reference 3.92)

Material	wt %									
	C	Mn	Si	S	P	Ni	Cr	Mo	Ti	Al
Mild Steel	0.24	0.75	0.18	0.022	0.026	0.09	0.07	0.03	--	--
1 Cr-Mo	0.09	0.50	0.25	0.031	0.024	--	0.93	0.47	--	--
2-1/4 Cr-Mo	0.08	0.41	0.29	0.019	0.024	--	2.10	0.91	--	--
Type 316 SS	0.04	1.70	0.34	0.012	0.018	12.1	17.1	2.81	--	--
20 Cr-35 Ni SS	0.05	0.72	0.57	0.003	--	31.0	20.1	--	0.55	0.34
15 Cr-15 Ni SS	0.10	1.80	0.51	0.012	0.006	14.8	14.9	1.28	0.50	--

Table 3.24 — Gas Analysis Results of the Environmental Creep Studies by Woods et al. (Reference 3.91)

Gas	Nominally pure He			Nominally impure He*		
	Range (all tests) ppm	Average (all tests) ppm	Average (long-term tests) ppm	Range (all tests) ppm	Average (all tests) ppm	Average (long-term tests) ppm
Hydrogen	5-680	336	26	1000-1600	1220	1200
Carbon Monoxide	10-100	70	< 5	10-1100	815	960
Water	4-160	105	27	200-700	475	147
Methane	5-20	10	< 5	5-20	9	< 5
Oxygen	1-20	8	10	10-50	21	20
Nitrogen	40-200	132	29	70-200	132	88

\*Nominal composition: 1000 ppm H<sub>2</sub>, 1000 ppm CO, 100 ppm H<sub>2</sub>O

#### 3.6.1.4 Mechanical Property Interaction

Environmental creep and stress rupture studies have been carried out by Wood et al. (References 3.91 and 3.92), and by Huddle (References 3.93 and 3.94). In one of the former studies (Reference 3.92), long-term tests [up to 36 Ms (1000 hr)] were carried out on three ferritic and three austenitic steels (see Table 3.23) in air and helium containing nominally 500 ppm hydrogen, 500 ppm carbon monoxide, 50 ppm water vapor, and 50 ppm methane in the temperature range from 672 to 1024°K (750 to 1383°F). Preliminary tests (Reference 3.91) were also carried out on 316 SS at 1073°K (1472°F) and Incoloy 800 at 923°K (1202°F) for 1.8 Ms (500 hr) in two impure helium environments (see Table 3.24). Unfortunately, there is considerable variation in these gas mixtures, with significant oxygen contamination. Some of their results are shown in Figure 3.25. The helium environment reduces the creep and rupture strengths of 316 SS by 5 to 10% and creep life by 40 to 50% relative to air in the temperature range of from 923 to 1023°K (1202 to 1382°F). Similar results were found for the 15 Cr-15 Ni alloy and the 20 Cr-35 Ni alloy with the latter steel showing a 60 to 70% reduction in creep life. No effect was found in the mild steel at 672°K (750°F). The tests on the 1% chromium steel at 773°K (932°F) and on the 2-1/4 Cr-1 Mo steel at 823°K (1022°F) were still in progress, but limited results suggest that these steels are adversely effected by the helium environment.

Supplemental metallographic examinations on the austenitic steels showed that specimens tested in helium contained considerably deeper surface cracks than those tested in air. In addition, a non-continuous oxide scale was formed on those specimens tested in helium, with chromium depletion below the surface and considerable grain boundary oxidation. The intergranular cracking was associated with the grain boundary oxidation. The authors concluded that grain boundary weakening associated with the intergranular oxidation results in an increase in the creep rate and that this process with or without superposition of surface cracking causes a reduction in rupture strength.

Curve 679092-A

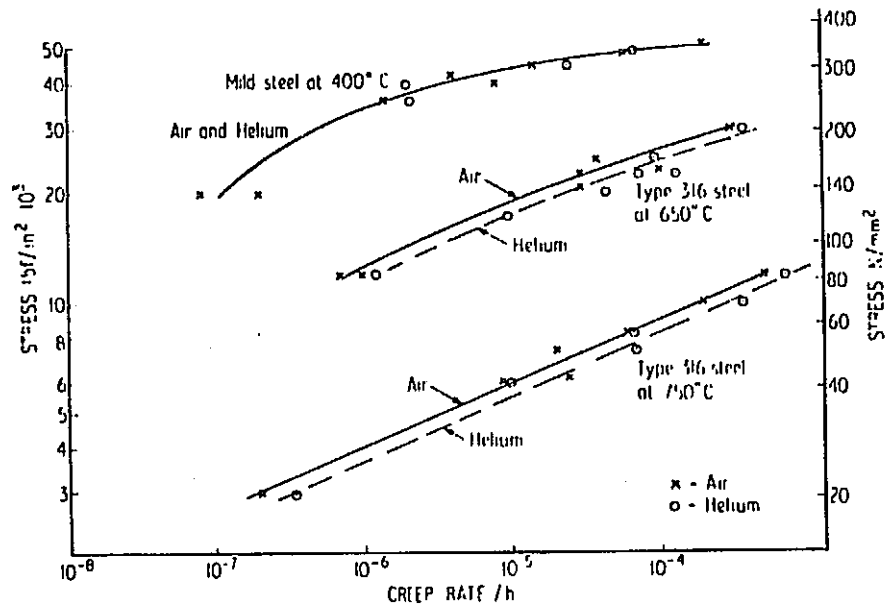


Fig. 3. 6. 2a—Effect of environment on the creep rates of mild steel and type 316 steel

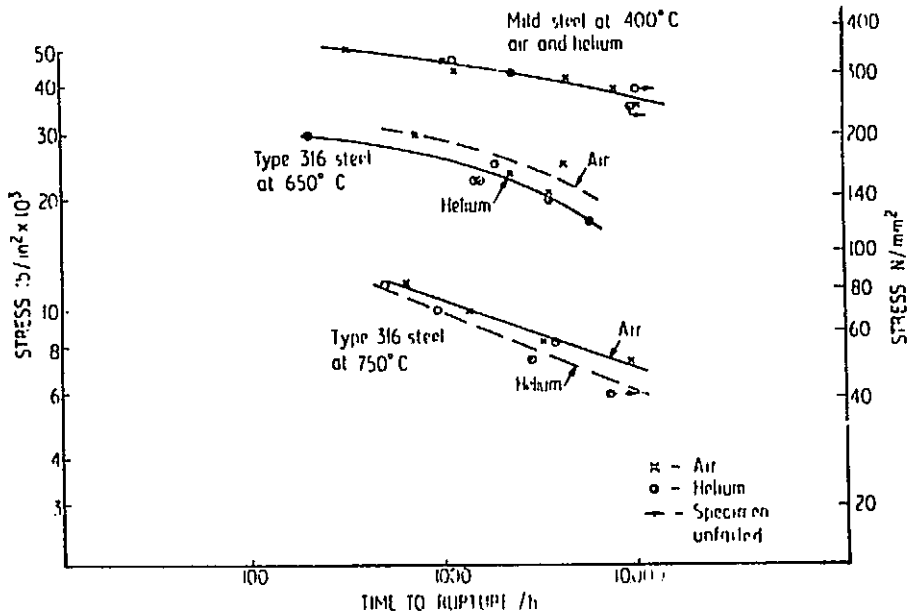


Fig. 3. 25—Effect of environment on the times to rupture of mild steel and type 316 steel

Huddle (References 3.93 and 3.94) has reported results of environmental creep studies carried out in impure helium in the temperature range of between 1023 and 1123°K (1382 and 1562°F). Two levels of impurities have been used in the helium: (1) 250 ppm hydrogen; 250 ppm carbon monoxide; 50 ppm water vapor at 182 Pa (1.82 atm) total pressure, and (2) 30 ppm hydrogen, 20 ppm carbon monoxide and 5 ppm water vapor at 182 kPa (1.82 atm) total pressure. The materials that have been investigated include 307 and 347 SS, the Nimonic alloys 75 and 80A, IN102, Inconel 625, HDA22, 30 and 45, Nimocast 713LC, and PD16, unalloyed molybdenum, the molybdenum alloys TZC and TZM, and the niobium alloy SU16. The results of these studies, which have only been reported in a qualitative manner, show that the alloys containing aluminum and titanium such as 321 SS, Nimonic 75, Incoloy 800, and the  $\gamma'$ -strengthened superalloys, suffer significant surface deterioration (i.e., intergranular oxidation leading to surface cracking), particularly in highly contaminated gases, whereas those containing niobium and tungsten, such as 347 SS, Incoloy 807, Inconel 625 IN102, are virtually unattacked. All the wrought superalloys tested were attacked whereas certain cast materials containing tungsten (713LC and PD16) were completely resistant. Molybdenum and its alloys exhibited excellent corrosion resistance, with no weight loss and no effect on the high-temperature mechanical properties. On the other hand, the niobium alloys embrittled to the point of disintegration.

#### 3.6.1.5 Effect of Concentration of Impurities

Huddle (Reference 3.94) concluded that "by far the most significant factor to emerge from the (Dragon) Project's work is the relationship between the concentration of the impurities and the magnitude of the corrosion." Photomicrographs of Nimonic 75 exposed in the unstressed condition for 10.8 Ms (3000 hr) in a test loop containing 250 ppm hydrogen, 250 ppm carbon monoxide, and 50 ppm water vapor, a water vapor-hydrogen ratio of 0:1 show considerably more internal attack than do those of specimens exposed in the Dragon Reactor for 75.6 Ms (21,000 hr) which also have a water vapor-to-hydrogen ratio of ~0:1 but considerably lower impurity levels (see Table 3.22). On the

Table 3.25 — Chemical Composition of Alloys Evaluated in the Study by  
Claudson and Westerman (Reference 3.83)

Alloy	Composition, wt %												
	Cr	Fe	C	Si	Co	Ni	Mn	Mo	Al	Ti	W	Cb	V
Inconel 600	15.46	6.72	0.05	0.28	0.07	Bal	0.32		0.18				
Inconel 625	22.0	3.0	0.03	0.30		61.0	0.15	9.0	0.2	0.2		4.0	
Inconel 702	15.47	0.50	0.04	0.18		79.73	0.02		3.29	0.69			
Inconel 718	20.0	Bal	0.10	0.75		52.0	0.5	3.0	1.0	1.3		5.0	
Incoloy 80C	20.36	47.55	0.04	0.24		30.45	0.20		0.34	0.4			
Hastelloy C	15.52	5.84	0.07	0.06	2.10	Bal	0.63	15.66			3.54		0.24
Hastelloy N	6.42	3.93	0.07	0.56	0.12	Bal	0.52	16.22			0.06		1.23
Hastelloy R-235	15.47	9.97	0.14	0.08	0.18	Bal	0.04	5.46	2.10	2.59			
Hastelloy X-280	21.73	18.68		0.53	0.11	Bal	0.75	8.65			0.38		
Haynes Alloy 25	19.93	2.47	0.07	0.52	Bal	10.42	1.44				14.91		

other hand, Woods et al. (Reference 3.91), reported that there is no apparent difference in creep behavior or metallographic observations of specimens tested in nominally pure helium and impure helium (see Table 3.24). Since the oxygen potential of these two environments as determined by the water vapor-to-hydrogen ratio was similar for both environments (i.e., ~1:3) and the absolute level of impurities were vastly different, these authors suggest that only the oxygen potential, not the level of impurities, is important.

These two results apparently disagree. Since the gas compositions in the studies by Woods et al., (see Table 3.24) showed considerable variation in impurity level and significant oxygen contamination, the conclusions of this study must be considered invalid. Thus, the impurity concentration dependency must be accepted as a real effect at the present time, and many of the previous studies on corrosion in impure helium must be considered to be of doubtful value.

#### 3.6.1.6 Gas Solid Reactions in Water Vapor-Helium Atmospheres

An investigation of the corrosion behavior of several high-temperature alloys in water vapor-helium atmospheres containing ~2% water vapor have been carried out by Claudson and Westerman (Reference 3.83). The alloys that were investigated are shown in Table 3.25, and the results are summarized in Table 3.26. The major conclusions of this study were that: (1) Hastelloy N, Hastelloy X-280, Inconel 600, Inconel 625, and Haynes 25 have a corrosion resistance superior to that of Hastelloy R-235, the least corrosion resistant of all alloys tested; (2) at 1200°K (1700°F) the same relative grouping was found as in the 1089°K (1500°F) tests, with more definitive evidence of intergranular attack in Haynes 25, Inconel 718, and Inconel 600 at 1203°K (1706°F) than at 1088°K (1499°F); (3) Hastelloy X-280, Hastelloy C, and Hastelloy N exhibited good oxidation resistance at 1311°K (1900°F), apparently forming a tight, adherent oxide film with little or no grain boundary or internal penetration; all other alloys show significant amounts of internal attack except Haynes 25, in which relatively minor internal

Table 3.26 — Corrosion Behavior of Several High-Temperature Alloys in Helium with 1.97% H<sub>2</sub>O for 300 Hours

Alloy	Temperature (°F)	Weight Change (mg/cm <sup>2</sup> )	Intergranular Attack
Hastelloy C	1500	+0.138	None
	1700	+0.459	None
	1900	+0.701	Little or none
Hastelloy N	1500	+0.109	None
	1700	+0.316	None
	1900	+0.765	Little or none
Hastelloy X-280	1500	+0.099	None
	1700	+0.432	None
	1900	+0.908	Little or none
Haynes 25	1500	+0.246	None
	1700	+0.750	Slight
	1900	+1.047	Slight
Inconel 625	1500	+0.226	None
	1700	+1.1	None
	1900	+4.2	Significant
Inconel 600	1500	+0.178	None
	1700	+0.555	Slight
	1900	+1.46	Significant
Inconel 702	1500	+0.490	Slight
	1700	+1.82	Slight
	1900	+1.79	Significant
Inconel 718	1500	+0.40	Slight
	1700	+1.62	Slight
	1900	-13.8	Significant
Incoloy 800	1500	+0.53	Slight
	1700	+1.46	Slight
	1900	+2.37	Significant
Hastelloy R-235	1500	+0.964	Significant
	1700	+3.56	Significant
	1900	+6.92	Gross

1 atmosphere total pressure; °F = 1.8 x (°C) + 32; 1 hr = 3600 Sec



oxidation occurred. There is a more or less direct correlation between intergranular attack and the aluminum and titanium content with Hastelloy R-235 showing the worst attack and having the highest aluminum and titanium content. These results are in qualitative agreement with the Dragon Reactor studies.

#### 3.6.1.7 Summary of Corrosion Behavior in Impure Helium

A great deal of information on the behavior of material in impure helium environments has been generated in support of the closed-cycle gas turbine for gas-cooled reactors. This work has demonstrated that due to the very low oxidizing potential of this environment, selective internal oxidation of aluminum and titanium can occur in nickel- and cobalt-based alloys and in austenitic stainless steels. This intergranular attack, decreasing the important strengthening benefits of these elements, produces a stress-creep corrosion effect resulting in an increase in the creep rate (relative to air) and a decrease in the rupture life. The addition of niobium and tungsten to these alloys, however, has been found to decrease the extent of the attack.

Molybdenum and its alloys TZM and TZC have been shown to exhibit excellent corrosion behavior, while niobium alloys such as SU16 are embrittled to the point of disintegration.

The translation of these results to the coal-fired furnace systems of the present study is hindered by the fact that the degree of deterioration in impure helium environments appears to be dependent on the concentration of impurities. At present, there are insufficient data to determine what the specific levels of impurities will be in the coal-fired furnace system under consideration and what effect the expected higher oxidizing potential of these systems will have on the extent of impurity-corrosion problems.

If, however, the oxidizing potential is sufficient to form a protective scale typical of that formed in air, then the severity of the problem will be reduced. One technique to ensure freedom from

selective internal oxidation would be intentionally to dope the helium with sufficient oxygen. While this technique can be used for the 922 and 1089°K (1200 and 1500°F) helium turbine inlet temperature cases, it cannot be employed at 1255°K (1800°F) because at 1255°K (1800°F) the superalloys do not have sufficient strength (see Section 3.6.2), and molybdenum alloys will be required for gas turbine blading. The very low oxidation resistance of molybdenum will make doping ineffective in preventing internal oxidation of the superalloys.

In the following sections, materials have been selected on the assumption that selective oxidation of aluminum, titanium, and silicon will occur and that alloys free of these elements should be preferred.

#### 3.6.2 Selection of Heat Transfer Materials for Closed-Cycle Gas Turbine Systems

In all of the closed-cycle gas turbine systems being considered in the present study, the helium is heated in either a pressurized or atmospheric fluidized bed furnace. The selection of heat transfer materials for this application must consider not only the effects of impure helium corrosion, as outlined in the previous paragraphs, but also the fire-side corrosion problem discussed in Section 3.2. In addition, since the furnace tube contains pressurized helium from the exhaust of the gas turbine compressor, its material selection and design must take into account the creep strength required to prevent mechanical failure.

As was discussed in Section 3.2, the fire-side corrosion data presently available are not detailed enough to allow specific selection of materials to be made based on the different types of coals being used. It has been assumed, therefore, that the environments present will be severe enough to result in coal-ash corrosion problems, and the materials have been selected to resist this attack.

In order to prevent mechanical failure of the pressurized furnace tube the design stress allowables have been obtained from the

ASME Boiler and Pressure Vessel Code (Reference 3.95) and the tube wall thickness required derived from equations similar to those discussed in Section 3.3.5.

Although the helium furnace tube operates at a much lower pressure[6.895 MPa (1000 psi)]than the steam boiler tubes considered in Section 3.3, the very high metal temperature[ $>1255^{\circ}\text{K}$  ( $>1800^{\circ}\text{F}$ )] encountered requires high-temperature materials not presently contained in the ASME Code.

To determine the maximum allowable working stress for candidate materials not contained in the ASME code, a value equal to 67% of the rupture stress at 360 Ms (100,000 hr) at the specified temperature was used. Where long-time creep rupture data were not available, the Larson-Miller parametric extrapolation procedure was used to obtain 360 Ms (100,000 hr) data.

Design stress allowable curves versus temperature for candidate furnace tubing were previously generated and presented in Section 3.3, Figure 3.19. Based on these curves the tube wall thickness required to contain 6.895 MPa at  $1089^{\circ}\text{K}$  (1000 psi at  $1500^{\circ}\text{F}$ ) has been calculated and is presented in Table 3.27.

Table 3.27 — Tube Wall Thickness Required for a 3 in id Tube at  $1500^{\circ}\text{F}$  Metal Temperature

Material	Wall Thickness, in
S816	0.21
HA188 } L605 } IN617 }	0.36
Hastelloy-X	0.43
17-14 CuMo } Incoloy 802 }	0.43
316 } 347 }	0.88

This table serves to illustrate that although the helium pressure is relatively low, advanced material with higher temperature strength than the austenitic stainless steels are required.

In order to reduce the potential for internal oxidation and environment stress interactions consideration was given to decreasing the titanium and/or aluminum content of the alloys selected as well as increasing the refractory elements tungsten, tantalum, and niobium. In Table 3.28 the amount of these elements in candidate materials are indicated.

Table 3.28 — Partial Chemistry of Candidate Heat Transfer Materials

Material	Composition, %				
	Cr	W	Ta + Nb	Ti	Al
S816	20	4	4	--	--
HA188	22	14	--	--	--
L605/HS25	20	15	--	--	--
IN617	22	--	--	0.35	1.0
Hastelloy	22	0.6	--	--	--
17-14 CuMo	16	--	0.55	0.26	--
Incoloy 802	21	--	--	0.75	0.58

In addition to having the highest temperature capability of the tubing alloys, S816 is free of titanium or aluminum and contains high levels of the refractory elements, making it an attractive candidate for the highest temperature service. On this same bases, IN617 and IN802 containing modest amounts of titanium and aluminum and no refractory elements, and although having creep strength similar to that of L605, HA188, and 17-14 Mo, respectively, do not appear to be as well suited for impure helium service.

Based on these considerations together with the fire-side corrosion recommendations presented in Section 3.2, the materials recommended for heat transfer applications in impure helium are given in Table 3.29.

Table 3.29 — Recommendations for Heat Transfer Materials to Operate in Impure Helium

Closed-Cycle Recuperated Parametric Points	Closed Combined Cycle Parametric Points	Helium Turbine Inlet Temperature	Recommended Materials for Highest Temperature Tube
1-4	1-3	1200	304 (A) 316 (A) 17-14 CuMo (B)
5-8 13-48	4-6 10-48	1500	HA188 (B) L605 (B) Inco Clad 671 on HA188 (B)
9-12	7-9	1800	Inco Clad 671 on HA188 (C) Inco Clad 671 on S816 (C)

### 3.6.3 Material Selection for Closed-Cycle Helium Gas Turbines

As discussed in Section 3.5, the major problem to be considered in selecting materials for gas turbine applications is adequate creep strength and compatibility with the environment. In open-cycle gas turbine nickel-based superalloys have been developed by utilizing the unique, high-temperature strength of the intermetallic precipitation hardening phase  $\gamma'$  (nickel aluminide, titanium) to obtain creep resistance, and a combination of chromium, aluminum, and other elements to form protective oxides scales. In helium closed-cycle turbines, although high-temperature creep resistance is still required, the low oxidizing potential is such that protective scales may not form on nickel-based alloys, and they may suffer a deterioration in strength because of selective internal oxidation of the strengthening elements, aluminum and titanium. Another problem encountered in

selection of superalloys for the present study is their rather limited temperature capability. In Table 3.17 the most advanced conventional superalloy (NASA-TRW VIA) is seen to be limited to temperatures of approximately 1172°K (1650°F) for 360 Ms (100,000 hr) service. The application of the cooling technology to limit the blade metal temperature to several hundred degrees below the turbine inlet gas temperature as practiced in open-cycle gas turbines presents additional problems in helium turbines. The high thermal conductivity of helium results in very steep temperature gradients through the blade, which in turn generates high thermal stresses. While limited application of compressor bleed-off type cooling is possible in a closed-cycle system, the potential for large-scale cooling to drastically reduce metal temperatures is not available.

In order to design helium turbines to operate with a 1255°K (1800°F) inlet temperature, consideration must be given to alloy systems, other than nickel-based superalloys. The high inlet temperature problem is further complicated by the higher speeds desired in the compressor drive section of the split-shaft turbine. Since the centrifugal stresses increase with the square of the rotational speed, stresses significantly higher than conventional turbines result. For the base case parametric Point 5, a speed of 106.5 rps (6388 rpm) is used, which increases the stress by a factor of 3.14 compared to a conventional 60 rps (3600 rpm) turbine operation.

The options considered previously for open-cycle systems are potential candidates also for higher temperature alloy systems. Tungsten reinforced superalloy composites, eutectics, oxide dispersion strengthening alloys, and so on all may be developed for this application. The freedom from oxidation concerns, however, allows consideration of the much higher strength refractory metal alloys previously discounted for lack of protective scales. As discussed in Section 3.6.2; the niobium alloys, while having the required creep strength, suffer internal oxidation and deteriorate in impure helium environments.

The refractory system that shows the greatest potential for blading and vane application is that using molybdenum. The only molybdenum alloy which is commercially available and for which there is long-time creep data in a helium environment is Mo-TZM (References 3.96 and 3.97). The alloy Mo-TZM also has demonstrated the excellent forgeability required to produce the air-foil shapes desired (Reference 3.98). The forging can be carried out in air after the blank has been heated in conventional furnaces having a neutral or slightly reducing atmosphere.

Based on the long-time creep properties of Jackobeit (References 3.96 and 3.97), a design allowable curve for Mo-TZM has been constructed as a function of temperature (Figure 3.26). Again, as in previous cases, the design allowable stress has been assumed to be 67% of the stress to cause rupture in 360 Ms (100,000 hr). A Larson-Miller parametric extrapolation was used to obtain values at temperatures and times where data did not exist. Also included in Figure 3.26 are the conventional nickel- and cobalt-based superalloys. The higher density of Mo-TZM results in proportionately higher centrifugal stresses, so the stress allowable for Mo-TZM has been reduced to allow direct comparison of the alloys high-temperature strength.

With a 1255°K (1800°F) turbine temperature, only Mo-TZM has the required stress allowable for first-row blading. The reduced stress on the vane, however, permits an advanced superalloy, such as TRW-NASA VIA with marginal cooling, to be considered, or uncooled Mo-TZM. On passing through the compressor drive turbine, the helium cools, reaching a temperature of 1066°K (1460°F) at the transition from the compressor drive to the power turbine. At this temperature the Mo-TZM no longer has a significant strength advantage over superalloys, so near-conventional materials can be used in the last stage of the power turbine. In the power turbine, the stresses are reduced by a factor of 3 because slower rotational speed obviates the need for Mo-TZM, and lower strength superalloys can be used.

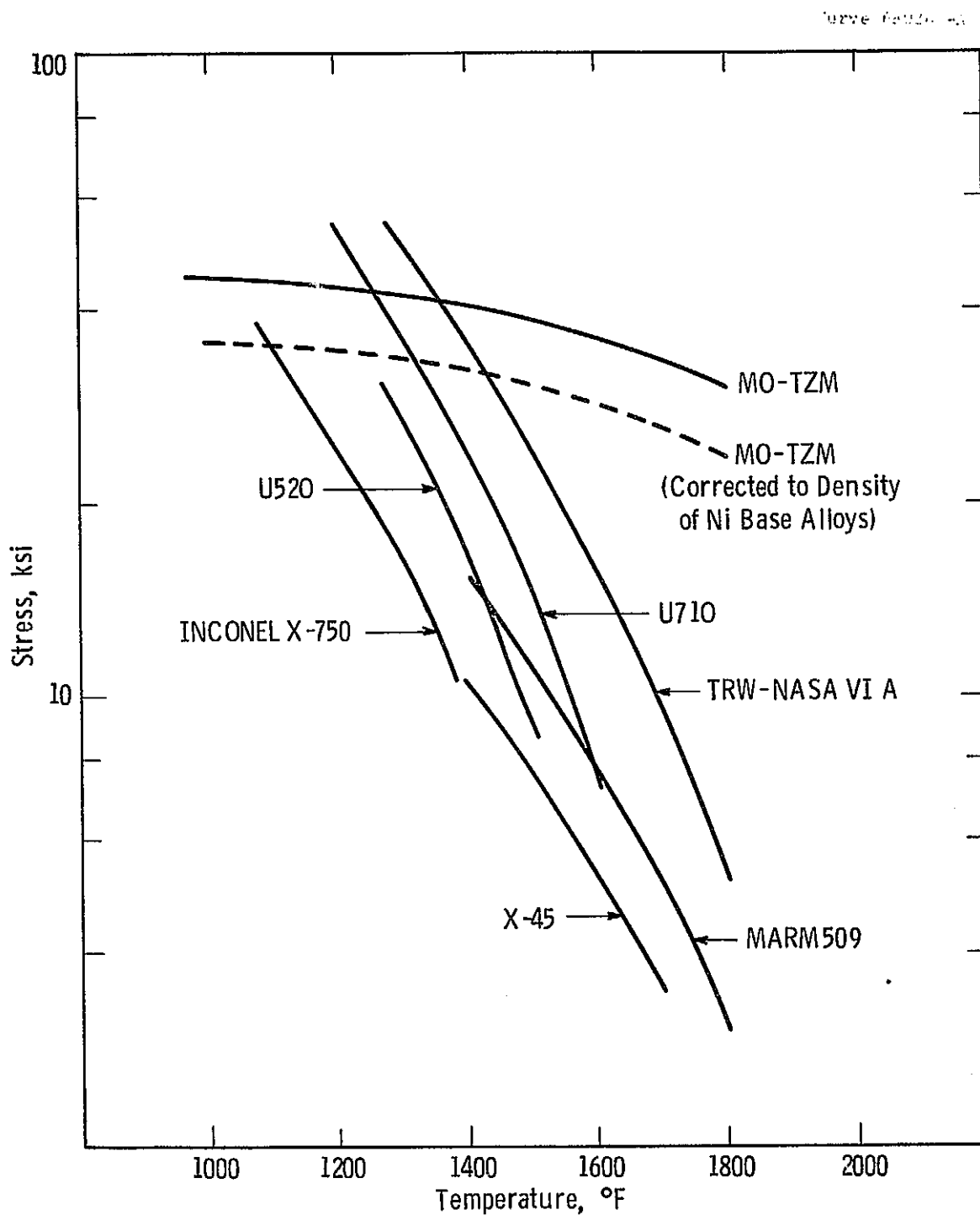


Fig. 3. 26 —Design allowable stress for closed-cycle helium gas turbine materials



For the turbine inlet temperatures of 1089 and 922°K (1500 and 1200°F) nickel- and cobalt-based superalloys have sufficient strength to design the entire turbine from these materials. It has been assumed (in the absence of sufficient data) that the temperature will be sufficiently low that the kinetics of the internal oxidation will be slow enough to present no problem. Since these systems are free of Mo-TZM, it will be possible, in addition, partially to control the internal oxidation by doping with oxygen raising the oxidizing potential.

Table 3.30 contains a summary of the material recommendations for the helium closed-cycle gas turbine.

Table 3.30 — Materials Selection for Closed-Cycle  
Helium Gas Turbine

Parametric Point	Turbine Inlet Temperature, °F	First-Row Blade Compressor Turbine	Last-Row Blade Compressor Turbine	First-Row Blade Power Turbine	Last-Row Blade Power Turbine	First-Row Vane Compressor Turbine
1-4	1200	Inconel X-750 (A)	Inconel X-750 (A)	Inconel X-750 (A)	Inconel X-750 (A)	X-45 (A)
5-8, 13-48	1500	Mar M200 (B) TRW-NASA VIA (B)	Inconel X-750 Udimet 520 (A)	Inconel X-750 (A)	Inconel X-750 (A)	Mar M509 (A) X-45 (A)
9-12	1800	Mo-TZM (B)	Mar M200 (B) TRW-NASA VIA (B)	Udimet 520 (A)	Inconel X-750 (A)	Mo-TZM (B) TRW-NASA VIA (B)

3-122

REPRODUCIBILITY OF THE  
ORIGINAL PAGE IS POOR

### 3.7 Materials for Potassium and Cesium Vapor Rankine Cycle Components

The metal vapor Rankine topping cycle system, described in Section 8, proposes to employ potassium or cesium as the working fluid. These alkali liquid metals possess compatibility and chemistry problems totally unlike those experienced with steam systems and, thus, require special consideration with respect to subsystem materials selections and interactions. In review, the proposed system will include a coal gas fired boiler (either a pressurized, fluidized bed, or a pressurized furnace) to create potassium or cesium vapor; a metal vapor turbine; a liquid metal loop to pump condensate back to the boiler; a metal vapor condenser-steam generator; an inert cover gas system to prevent alkali-metal reactions with air or moisture and to protect possible refractory metal turbine components; special shaft seal and bearing systems that operate in alkali-metal or dry inert gas environments, at low or elevated temperatures; and a special instrument system with monitoring devices pertinent to alkali-metal and inert cover gas operations.

Base case reference materials must be compatible with the following temperatures and pressures:

- (A) Potassium boiler 1033°K (1400°F), potassium side 1.38 to 2.07 MPa (200 to 300 psi), fire-side pressure 103.4 kPa (15 psia).
- (B) Potassium turbine 1033°K (1400°F), inlet 866°K (1100°F), outlet 20.68 kPa (3 psia).
- (C) Potassium loop 866°K (1100°F) (condenser to 1033°K (1400°F) (boiler), small pressure head, flowrate within Liquid Metal Fast Breeder Reactor technology limits.
- (D) Condenser-Steam Generator 866°K (1100°F), 20.68 kPa (3 psia), 811°K (1000°F) steam 24.13 MPa (3500 psia) steam.

Variations from these base case conditions are described in Section 8, and will also be treated in this section.

The materials required to fabricate the subsystems described must be selected with respect to temperature of operation, stress, pressures, material compatibility (alkali metal, oxygen, moisture, nitrogen, etc.) fabricability, joining, material strength (particularly creep strength), and potential system operating practices. Materials selections for the subsystem components were evaluated on the basis that the materials in relation to the specific application were established, near term, developmental, or speculative, in accordance with the rating criteria described in Subsection 3.1, and materials described here are followed by the appropriate rating letter in parentheses.

Alkali-metal practice, material compatibility, and operational experience have been established; and several considerations are worth noting prior to analyzing subsystems. Potassium and cesium are reactive with air or moisture, and sealed hermetic systems, with dry, inert cover gas environments are necessary to the maintenance of clean liquid metal systems. Oxygen in the high ppm range is detrimental to alkali liquid metal loop operation in that the oxygen enhances corrosion and mass transport. Such loops will generally employ cold traps (precipitation process) or hot traps (reactive gettering) to control oxygen levels to acceptable levels (1 to 2 ppm). Also, bimetallic loop systems incur corrosion effects due to dissimilar metal coupling. Two problems unusual to historical practice in forced loop systems result because the proposed potassium (cesium) loop will operate with two phases. First, the pure distillate which condenses in the turbine and condenser-steam generator will have a high solubility for containment materials, and will subject these areas to a high corrosion potential. Oppositely, the saturated fluid (i.e., having a solubility level of dissolved solutes) evaporating in the boiler will leave a residue of nonvaporized solute materials. Both of these problems may be alleviated by bypassing some saturated boiler fluids to the condenser.

Alkali liquid metals are now handled in large quantities, at elevated temperatures, in a routine fashion with proper control, monitoring, and safety equipment.

### 3.7.1 Liquid-Metal Boiler

The potassium (cesium) boiler design is described in Section 8. Two heat sources are described: (1) A pressurized, fluidized bed using Illinois No. 6 bituminous, Montana subbituminous, and North Dakota lignite fuels; (2) a pressurized furnace using clean gas. Potassium exit temperatures from the boiler will be 1033°K (base case) 1089, and 1144°K (1400, 1500, and 1600°F). Fire-side pressures will be 1.37 to 2.09 MPa (200 to 300 psi), while potassium pressures will be 0.103 to 0.344 (15 to 50 psia). For the base case conditions, most of the potassium system may be subatmospheric in pressure. The pressurized, fluidized bed (PFB) will present serious fire-side corrosion problems due to the presence of coal impurities such as vanadium, chlorine, fluoride, sodium, and potassium salts, and so on, which lead to rapid corrosion and oxide scaling. The pressurized furnace (PF) will operate with a clean gas as fuel and is not expected to present a serious fire-side problem to materials selection and corrosion.

The potassium PFB boiler can present serious problems. The most corrosion resistant materials for the fire-side of the boiler tubes will be high nickel-chromium content alloys (see Subsection 3.2). These materials, however, are not compatible with potassium. Solutions to this problem of dual-side incompatibility may require resolution through:

- (1) A duplex tube: A gas/fire resistant alloy fabricated over a potassium-compatible alloy
- (2) One-alloy tube: A single-metal tube whose alloy may be compatible both with coal gas fuels and potassium (possibly HA-188(C) or Incoloy 800 (C).
- (3) Coatings: A high nickel-chromium alloy or MCrAlY coating may be deposited on the outside of a potassium-compatible substrate tube, or a potassium-compatible material such as molybdenum may be deposited on the inner diameter of fire-side compatible materials.

Resolutions (1) and (3) may require complex fabrication and joining schemes. They may also result in the formation of brittle inter-metallics (interdiffusion) and/or coating spallation. The primary cause of failure of previous clean gas-fired potassium boilers has been thermal fatigue (References 3.99 and 3.100).

Excellent potassium corrosion resistance has been reported for a clean gas-fired 316 SS boiler with a fire-side temperature of 1155°K (1620°F) after 43.2 Ms (12,000 hr) of operation (Reference 3.99). Studies of boiling potassium contained in nickel, iron, and cobalt alloy vessels have been made at liquid-vapor temperatures ranging up to 1144°K (1600°F) (Reference 3.101). Tests for 5.4 to 10.8 Ms (1500 to 3000 hr) in boiling potassium show that type 316 SS and Haynes 25 (L-605) are equally resistant to attack. In contrast to all-liquid potassium tests (single phase), corroded areas in boiling loops are less likely to be preferentially leached of any metallic constituent (Reference 3.101. These and similar results in other studies (Reference 3.102) indicate that single-phase loop data cannot be extrapolated to boiling and condensing loop situations.

Indications are that 316 SS and Haynes 25 (L-605) will be compatible with clean, boiling, and condensing potassium to 1144°K (1600°F) (Reference 3.102). Similar tests with Inconel (78Ni-15Cr-7Fe) and Hastelloy X(45Ni-24Fe-22Cr-9Mo) showed intergranular cracking[0.51 mm (0.02 in)] deep and decarburization and grain growth in the first case, and severe mass transfer problems in the second case. Thus, nickel-based alloys should be avoided in these systems. The average measured corrosion rates of 316 SS and Haynes 25 were <80 pm/s (<1 mil/year) in the condenser zones, and wall surface roughening (i.e., deposits) in the boiler zones (Reference 3.102). Cracks appearing in both systems were attributed to thermal fatigue due to unstable boiling. It has been reported that loops without boiling instabilities, and with Nb-1 Zr or zirconium chip getter inserts, did not develop fatigue cracks (Reference 3.102).

Niobium and tantalum alloys are considerably more resistant than conventional alloys to attack by potassium above 1172°K (1650°F). The corrosion resistance of Nb-1 Zr has been evaluated in refluxing capsules containing potassium at 1172 to 1477°K (1650 to 2200°F) for periods up to 18 Ma (5000 hr) (References 3.101 and 3.102). Capsules and tab inserts have generally been negligibly corroded. Niobium and its alloys are getters which tend to combine with both nitrogen and carbon from austenitic stainless steels or cobalt-based alloys, lowering their ductility, whereas TZM tabs in Haynes 25 loops remove only carbon in the presence of zirconium tabs (Reference 3.101).

For potassium-side compatibility of the PF boiler (i.e., clean gas fuel), the material selections given in Table 3.31 are recommended (with the order of preference noted).

Table 3.31 — Materials Recommended for Pressurized Potassium Boilers

Temperature	Material
to 1400°F	1. 316 SS (A)
	2. Incoloy 800 (C)
to 1500°F	1. 316 SS (A)
	2. Incoloy 800 (C)
to 1600°F	1. Incoloy 800 (C)
	2. Haynes 25 (B)
	3. HA-188 (C)

Fire-side material protection would not be considered necessary as estimated by previous experience with clean-fired potassium boiler materials such as 316 SS (Reference 3.99). Secondary selections (Incoloy 800, HA-188) were made on the basis of supplying some fire-side protection.

For potassium compatibility of the PFB boiler (i.e., coal gas with vanadium, sulfur, sodium, chlorine, etc.), the material candidates shown in Table 3.32 are recommended (with the order of preference noted).

Table 3.32 — Candidate Materials for PFB Potassium Boilers

Temperature	Material
to 1400°F	1. Incoloy 800 (C) 2. Inco Clad 671 od on Incoloy 800 id (C)
to 1500°F	1. Incoloy 800 (C) 2. Inco Clad od on Incoloy 800 id (C)
to 1600°F	3. HA-188 (C) 1. HA-188 (C) 2. Inco Clad 671 od on Incoloy 800 id (C) 3. Inco Clad 671 od on HA-188 id (D) 4. Nb-1Zr potassium side with fire-side cladding (D)

Fire-side material selections will dictate the dual-side approaches discussed earlier. Although Haynes 25 may be subject to thermal embrittlement, HA-188 has supposedly eliminated this problem. The Nb-1Zr would require an extra cladding on the fire side and is a speculative consideration. Newer materials such as HA-188, which must still be evaluated with potassium, may play a more prominent role, depending on their fire-side corrosion resistance and as yet unconfirmed compatibility with potassium. Finally, FeCrAlY and CoCrAlY-type coatings may be employed (C,D) for iron- and cobalt-based alloys which have compatibility problems on the fire side, but would only provide short-term protection.



Although coatings for fire-side protection are mentioned here, a detailed analysis of their application and requirements is presented in Subsection 3.2. It should be noted that 316 SS and Haynes 25 have been shown to possess excellent potassium-side compatibility. Although HA-188 has not been tested for potassium compatibility (the alloy is similar to Haynes 25 but has increased nickel and lanthanum additions), it is reasonable to expect the lanthanum to act as a getter (i.e., as zirconium to Nb-1Zr; as hafnium to T-111) and thus to improve the compatibility (corrosion resistance) with potassium over that of Haynes 25.

Compatibility work for cesium has not been as extensive as that for potassium. Indications are that 304 SS and 316 SS would be relatively immune to cesium attack up to 1144°K (1600°F), although a slight reduction in strength and small amounts of carbon transfer would occur (Reference 3.102). Generally, cesium will be more compatible with structural materials than potassium or sodium. Some nickel alloys may also be more acceptable in a cesium environment than in a potassium environment (i.e., Rene' 41, Inconel X) (Reference 3.102).

Refractory metals show excellent compatibility with cesium liquid and vapor (when the oxygen content is low), particularly gettered alloys such as Nb-1 Zr, D-43, B-66, Mo, TZM, Mo-50 Re, T-111, etc. Compatibilities are excellent to 1644°K (2500°F) and above (Reference 3.102). Thus, more material freedom would exist in selecting components for a cesium vapor Rankine topping cycle than in those for potassium. Table 3.33 lists possible materials selections for a pressurized furnace (PF) cesium boiler system (cesium-side materials) (selection preference noted). Table 3.34 lists materials candidates for pressurized fluidized bed (PFB) cesium boiler systems. The cesium-side compatible materials could require a gas fire-side compatibility coating.

Table 3.33 — Candidate Materials for PF Cesium Boilers

Temperature	Material
to 1400°F	1. 316 SS (A) 2. Inconel (C)
to 1500°F	1. 316 SS (A) 2. Incoloy 800 (C)
to 1600°F	1. Incoloy 800 (C) 2. Haynes 25 (C) 3. HA-188 (C)

Table 3.34 — Candidate Materials for PFB Cesium Boilers

Temperature	Material
to 1400°F	1. Inconel (C) 2. Incoloy 800 (C) 3. Inco Clad 671 od on Incoloy 800 id (C)
to 1500°F	1. Incoloy 800 (C) 2. Inco Clad 671 od on Incoloy 800 id (C) 3. HA-188 (C)
to 1600°F	1. HA-188 (C) 2. Inco Clad 671 od on Incoloy 800 id (C) 3. Inco Clad 671 od on HA-188 id (C)

The increased compatibility of cesium with high nickel-content alloys could permit more flexibility in handling fire-side problems. For instance, Incoloy 800 is also recommended as a fire-side material for the alkali-metal boiler. Cesium, with its higher mass and resulting smaller turbine requirements, and probably better (than potassium)

material compatibility with structural components, is an attractive working fluid.

For both potassium and cesium systems with the prime selection alkali-metal side materials described, general corrosion rates of (1 to 2 mils/year) can be expected if oxygen levels are kept below 1 to 2 ppm. These are typical corrosion rates for these conditions and can be projected as wastage factors when long life strength and integrity are forecast.

### 3.7.2 Metal Vapor Turbine

The potassium metal vapor turbine, for the base case condition, will operate with an inlet temperature of 1033°K (1400°F) and pressure of 103.4 kPa (~15 psi) abs. Condensate removal may be provided. Turbine condensate exit temperature will be 866°K (1100°F). Potassium inlet ducts will be about 1.22 m (48 in) in diameter (4 ducts), and exit duct work will be larger. Tip diameters could extend to 4.57 m (15 ft) in the last stage if a low velocity of about (900 rpm) is selected to minimize stress and creep requirements. For material fabrication constraints (discussed later in this section), a turbine disk of 1.83 (6 ft) diameter was selected as a maximum permissible dimension for this study. Inlet stages will operate at 1033°K (1400°F) (base case) while exit (last) stages should operate at about 866°K (1100°F). Thus, materials selections may vary from stage to stage as a function of temperature and stress.

The potassium boiling and condensing tests discussed in the previous section demonstrate that for 922 to 1144°K (1200 to 1600°F) temperatures with high purity potassium, cobalt- and iron-based alloys are more compatible than are nickel-based alloys. Typical low-pressure turbine materials such as Astroloy, A-286, U-700, and so on, have not been extensively tested in potassium. Consideration of alloy composition, however, and comparative performance of similar alloys indicates that the materials listed in Table 3.35 may be acceptable

turbine components for low-pressure turbine application (uncooled blades). Selections were made with the assumption that the shaft, disk, and blades would not be cooled.

Table 3.35 — Low-Pressure Turbine Components

Component	Use to 1400°F Inlet T
Inlet Casing	304 SS (B)
Disk (uncooled)	Incoloy 901 (C), Refractaloy 26 (D)
Blades	U1700 (C)
Turbine Casing	304 SS (B)
Shaft	Incoloy 901 (C), Incoloy 717 (D) Waspalloy
Tie Bolts	U-700 (C)
Exhaust Scroll	304 SS (B)
(Potassium system at 1 to 2 ppm oxygen contamination level)	

Materials selections for rotating components were based primarily on 360 Ms (100,000 hr) rupture life strength from Larsen-Miller plots. For instance, A286, a typical shaft material, has a 360 Ms (100,000 hr) rupture life stress of less than 68.95 MPa (10 ksi) at 1033°K (1400°F), whereas the equivalent conditions for Incoloy 901, Refractaloy 26, and Waspalloy are 68.95, 103.42, and 137.90 MPa (10, 15, and 20 ksi) respectively. These properties are presented in Subsection 3.12.

High-temperature, high-strength turbine materials have been extensively tested in boiling and refluxing potassium. These are primarily refractory metal alloys. Capsule tests investigating the compatibility of turbine materials with potassium have been performed. Hoffman (Reference 3.103) reports the testing of TZM inserts in two Nb-1 Zr refluxing capsules in potassium at 866°K (1100°F) for 9 and 18 Ms (2500 and 5000 hr). Although the TZM was slightly decarburized, there was no evidence of corrosion or activity gradient mass transfer between the Nb-1 Zr and the TZM. Simons and Lagedrost (Reference 3.104) refluxed boiling potassium in TZM capsules from 708 to 955°K

(1499 to 2300°F) for 18 Ms (5000 hr). The oxygen content of the potassium varied from 20 to 500 ppm. There was no attack of the TZM with low-oxygen potassium. Mass transfer of molybdenum and titanium occurred at the liquid-vapor interface as the oxygen content of the potassium was increased.

Scheuerman and Barrett (Reference 3.105) investigated the compatibility of Nb-1 Zr, T-111, and T-222 capsules from 1173 to 1573°K (1652 to 2372°F) for 14.4 to 36 Ms (4000 to 10,000 hr) with refluxing potassium. No corrosive attack was noted in any of the refractory alloys investigated. Ta-10W capsules tested from 1253 to 1473°K (1796 to 2192°F) (with the same 20 ppm or less oxygen liquid potassium) showed intergranular attack to 0.406 mm (16 mils). Alloys with oxygen getters (titanium, zirconium, hafnium) were concluded to be more resistant to attack by potassium because of their ability to tie up the oxygen and prevent it from entering the corrosion reactions. Concurrence with these observations has also been expressed by other investigators (References 3.106 to 3.108).

Chandler (Reference 3.109) has shown pure niobium to be extremely compatible with boiling potassium to 1589°K (2400°F). Pure tantalum, however, was found to lose weight in liquid potassium in direct proportion to the amount of oxygen present in the potassium (50 to 3000 ppm) (Reference 3.110). At temperatures above 873°K (1112°F) and with oxygen levels greater than 20 ppm, tantalum was found to suffer intergranular attack.

In general, capsule tests show that TZM, Nb-1 Zr, and T-111 are acceptably compatible with refluxing and boiling potassium for the temperature conditions that will be present in the turbine. Again, this is with the reservation that the oxygen contamination of the potassium be confined to amounts of 1 to 2 ppm. Ungettered refractory metals and alloys (such as pure tantalum, or Ta-10W) should be avoided.

Natural convection and pumped two-phase loops simulate actual applications for refractory metal-alkali liquid metal systems to a greater extent than do capsule tests. Materials that exhibit good liquid-metal compatibility in the capsule tests are used for loop studies.

A Nb-1 Zr loop with Nb-1 Zr simulated turbine blades was operated at ORNL (Reference 3.111) for 10.8 Ms (3000 hr). The potassium vapor varied from 83 to 96% quality and flowed at 4.16 g/s (33 lb/hr), producing a velocity of 944 to 396 m/s (3100 to 1300 ft/s) in the loop. The liquid temperature varied from 1348 to 628°K (1966 to 671°F) and vapor temperature from 1373 to 963°K (2012 to 1274°F). No corrosion or erosion was detected in the system, except for a 25.4  $\mu$ m (1 mil) deep roughening found in a second-stage blade specimen. This erosion was believed to be the result of low-quality potassium vapor impinging on the blade leading edge.

A Nb-1 Zr two-phase forced circulation loop with TZM simulated turbine blades was operated for 18 Ms (5000 hr) at a flow rate of 2.52 to 5.04 g/s (20 to 40 lb/hr), producing local velocities of 253 to 411 m/s (830 to 1350 ft/s). This 1373°K (2012°F) potassium flow through a TZM nozzle and blades had a quality of 88%.

The effect of high-velocity flow rates on TZM simulated turbine blades was studied in potassium vapor at 1025°K (1385°F) at 163 m/s (535 ft/s) in a 10.8 Ms (3000 hr) test (Reference 3.112). The maximum corrosion/erosion found was less than 25.4  $\mu$ m (1 mil). It is assumed that corrosion by potassium vapor would be negligible in such systems if the vapor quality could be kept higher than 90%. This finding, together with Jansen and DeVan's (Reference 3.111) observations for low-quality potassium vapor in the Nb-1 Zr turbine simulator, recommends interspool moisture removal and/or an interspool reheating to prevent turbine blade erosion due to low-quality vapor.

These studies plus others (Reference 3.113) indicate that TZM, Nb-1 Zr, and T-111 (Reference 3.114) will exhibit no serious incompatibility with potassium liquid or vapor under the operating conditions

proposed for the potassium turbine. Serious dissolution corrosion or dissimilar metal coupling should not be expected if oxygen levels in the system are kept low (less than 1 to 2 ppm) in the potassium. The only notable metal removal found in potassium vapor turbine simulation studies has been when low-quality vapor was used. Although TZM-316 SS systems have exhibited mass transport of zirconium, nitrogen, oxygen, and carbon (Reference 3.110) above 1478°K (2200°F), no such effects have been noted for TZM in an all refractory metal system.

Extensive mechanical property analyses of stainless steels in liquid sodium have been performed (Reference 3.115). Unfortunately, little information is available on the mechanical properties of refractory metal alloys in liquid potassium. The yield strengths of TZM test pieces after 10.8 Ms (3000 hr) exposure in 1003 to 1343°K (1346 to 1957°F) boiling potassium were not much different from those of TZM pieces exposed to the same temperature in argon (Reference 3.116). Creep rupture tests of TZM in saturated potassium vapor for periods to 5.54 Ms (1539 hr) at 1373°K (2012°F) reveal no significant effects by the potassium vapor over nonpotassium conditions (Reference 3.117). Other investigators report the same findings (Reference 3.119). The fatigue properties of TZM have also been reported as being unaffected by potassium (Reference 3.119).

As a result of these findings, the material TZM is a prime selection for the high-pressure turbine disk, blades, disk tie bolts, center torque tube, and so forth. These and other materials are indicated in Table 3.36.

Since several refractory metals were specified for high-pressure (temperature) turbine application, further comment is required. TZM is an ideal material for the high-temperature rotating components of the turbine and has been employed in similar structures in aerospace programs. These turbines, however, were of smaller diameter, considerably

Table 3.36 — High-Pressure Turbine Components

<u>Component</u>	<u>Use to 1500°F Inlet T</u>	<u>Use to 1600°F Inlet T</u>
Inlet Casing	Incoloy 801 (C)	HA-188 (C)
Disk*	TZM (B), Waspalloy (D) Refractaloy 26 (D)	TZM (B), Waspalloy (D), Refractaloy 26 (D)
Blades	TZM (B)	TZM (B)
Turbine Casing	HA-188 (C)	HA-188 (C)
Shaft	Waspalloy (C)	Waspalloy (C)
Exhaust Scroll	HA-188 (C)	HA-188 (C)

(Potassium system at 1-2 ppm oxygen levels.)

\* Cooling required for superalloy selections.

easing fabrication problems. Large components of the dimensions required here present particular difficulty. The largest TZM ingots available today are 0.381 to 0.457 (15 to 18 in) in diameter and 1.524 to 1.829 m (5 to 6 ft) long. For instance, to prepare a TZM stub shaft or disk, the following might be necessary:

- Extrude ingot at 1505°K (2250°F)
- Recrystallize at 1811°K (2800°F)
- Forge at 2144°K (3400°F), finish at 1811°K (2800°F)
- Recrystallize at 1894°K (2950°F)
- Forge at 1811°K (2800°F); stress relieve at 1533°K (2300°F)

All operations must be performed with a protective cover. Considerable energy is required to forge TZM at these temperatures, even with small billets. A review of TZM suppliers and fabricators around the country has shown that: (1) Ingots of 0.61 m (2 ft) diameter by 1.524 to 1.829 m (5 to 6 ft) long would be very difficult to form; (2) forgings of cast TZM to disks 0.914 to 1.219 m (3 to 4 ft) in diameter and 0.152 to 0.305 m (1/2 to 1 ft) thick are not considered possible; (3) cast TZM disks would not have the strength; (4) powder metallurgical TZM would not have the strength, even if presses of sufficient size could be found to form them. The consensus appears to be that forged TZM components over 0.61 to 0.914 m (2 to 3 ft) in diameter would



exceed the present manufacturing capability in this country. The investment of considerable time and money might result in greater capability. Since TZM cannot be welded, a piece-assembled disk cannot be considered. An interlocked TZM mosaic structure would be possible, but not desirable. The forging of TZM turbine blades was not viewed as a problem.

Alternatively, high-strength, gettered niobium- or tantalum-based alloys such as D-43, FS-85, or T-111 could be considered for this application. Even with this substitution, a considerable developmental effort would still be required to arrive at a solution for fabricating large components.

One alternative would be to cool the disk and shaft. Then superalloys such as Incoloy 901 or Refractaloy 26 could be employed for the disk. The largest disk made for gas turbine application is a 2.08 m (82 in) diameter Incoloy 901 unit. Cooling such a unit would permit the employment of superalloys and would also reduce their (potential) compatibility problem (nickel-based) with potassium.

### 3.7.3 Liquid-Metal Loop

A pumped potassium loop will be required in the base case, to transport potassium condensate from the condenser/steam generator to the boiler. The pumping head will be 1034 kPa (15 psi) abs (boiler) minus 6.9 to 13.8 kPa (1 to 2 psi) abs (condenser) plus gravity and fluid-flow losses. A zirconium chip hot trap should be provided for oxygen maintenance, and the necessary instrumentation to monitor loop conditions should be present (see Section 3.7.7). The loop should be of all welded construction, with properly isolated valve stems, and so on. The electromagnetic (EM) pump would be desirable to avoid material (cavitation) and seal (leakage) problems.

Considerable loop experience with sodium exists; and instrumentation, control, fabrication, and operational devices have been developed and improved. Most of the components and concepts can be extrapolated to potassium application. For these temperature ranges and

pressures the loop portion of the potassium cycle should not present problems in materials selection or performance. Again, nickel alloys should be avoided. A 316 and 304 SS loop structure should be more than adequate in performance and capability. Note that since the condensate entering the loop will be a pure distillate, a means of reducing dissolutive corrosion by introducing some saturated (solute) potassium from the boiler region into the condenser should be provided. A small amount of solute-saturated potassium, experiencing a logarithmic drop in solute solubility with temperature reduction, should supply adequate solute to saturate the condensate. For instance, at a temperature of 1033°K (1400°F) some of the potassium flow leaves as vapor ( $F_V$ ) and some leaves to be recycled to the condenser ( $F_{RC}$ ). The net flow is  $F_N$ . The amount that is recycled must be saturated, with its solubility limit of solutes at 1033°K (1400°F) ( $S_{1400}$ ) such that upon entering the condenser, the solute carry-over will saturate the condensate from the turbine at 866°K (1100°F) ( $S_{1100}$ ). The relation to be satisfied is,

$$(S_{1400}) F_{RC} = (S_{1100}) F_N \quad (3.11)$$

where

$$F_N = F_{RC} + F_V \quad (3.12)$$

Using Equation 3.4

$$\frac{F_{RC}}{F_N} = \frac{S_{1100}}{S_{1400}} \quad (3.13)$$

and Equation 3.13 projects the amount of boiler fluid that must be recirculated to saturate the turbine condensate to minimize condenser and loop corrosion. Solubilities of some materials in potassium have been developed (Reference 3.102).

<u>Material</u>	<u>Temperature</u>	<u>Solubility in Potassium</u>
αFe	1400°F	180 ppm (w)
	1100°F	15
Ni	1400°F	10
	1100°F	2

Equation 3.13 projects that 8 to 20% of the boiler fluid should be recycled to the condenser to minimize dissolutive corrosion in the condenser and surface build-up in the potassium boiler. The recycle flowrate and the projected loop flowrates are low enough that high-velocity corrosion correlations can be ignored. The solute recirculation system will also provide a by-pass for the turbine. Thus, if a turbine is lost or down, the by-pass could be employed to provide heat energy for the steam generator, permitting the plant to continue operating at a reduced power level.

Selected materials for the potassium condenser to boiler loop base case 866°K (1100°F) and alternative cases are given below:

<u>Loop Temperature</u>	<u>Material Selected</u>
to 1100°F	2 1/4 Cr-1 Mo (B) 316 SS (A)
1200°F	316 SS (A)
1300°F	316 SS (A)

Materials for cesium fluid in the loop should be much the same.

#### 3.7.4 Metal Vapor Condenser/Steam Generator

Potassium condensate will enter the condenser/steam generator at 866°K and 6.89 to 13.80 kPa (1100°F and 1 to 2 psi) abs in the base case. Steam will leave the unit at 811°K and 24.13 MPa (1000°F and 3500 psia). Low-temperature potassium-compatible materials such as 2-1/4 Cr-1 Mo (Croloy) and 316 SS would be prime candidates for this system. For a condenser/steam generator tube size of 25.4 mm (1 in) od (with steam on the id), the minimum wall thickness as derived from material strength and boiler tube specifications is given in Table 3.37. Thus, at 866°K (1100°F), 2-1/2 Cr-1 Mo could be employed in the steam generator. At 922 to 978°K (1200 and 1300°F), 316 SS would be the selection.

Table 3.37 — Minimum Wall Thickness of Boiler Tube

<u>Material</u>	<u>Temperature (°F)</u>	<u>Maximum Allowable Tube Stress (psi)</u>	<u>Minimum Wall Thickness (in)</u>
2 1/4 Cr-1 Mo	1100	4000	~0.35
	1200	2000	~0.5
	1300	—	—
304/316 SS	1100	8000	~ .16
	1200	6000	~ .20
	1300	4000	~ .35

(Data from Subsection 3.12)

If higher strength materials are required, Haynes 25 or HA-188 could be employed. The selection of Incoloy 800, however, should remain as the prime alternative to 316 SS. Incoloy 800 does not appear susceptible to chloride stress corrosion cracking and for this reason, as well as for its higher strength, could be selected over 316 SS for the condenser/steam generator. Table 3.38 summarizes the material selected for the condenser/steam generator.

Table 3.38 — Summary of Materials Selected for the Condenser/Steam Generator

<u>Temperature</u>	<u>Material</u>
to 1100°F	2 1/4 Cr-1 Mo (B), (2) 316 SS (B)
to 1200°F	316 SS (B), Incoloy 800 (C)
to 1300°F	316 SS (B), Incoloy 800 (C)

### 3.7.5 Cover Gas System

Alkali liquid metals such as potassium and cesium are very reactive with oxygen and moisture. Oxides and hydrogen are evolved, and both can be detrimental to system performance. Since the alkali metals will also continually clean protective oxides, and so on, from the system and turbine material surfaces, these surfaces also will be subjected to potential oxidation and dissolution problems. Refractory metals and

alloys, of course, should not be exposed at elevated temperatures to oxygen or to moist atmospheres. Note also that for the base case [1033K (1400°F)], the entire Rankine system may be at subatmospheric conditions, ideal for in-leakage of contaminants. For these reasons an inert, dry, protective cover gas is required for system protection.

Since high-temperature nitriding could occur with a nitrogen cover gas system, argon or helium is recommended. Argon is the first choice since it is heavier than air and will stay in pits or sunken closures which may be assembled around the system. Leakage of argon or helium into the turbine through shaft seals and cracks may dictate the choice of helium (less mass and, therefore, less interference with turbine efficiency, performance, etc.). The cover gas should be recycled for purity maintenance (i.e., NaK bubbler, hot copper chips, molecular sieve, hot getters such as zirconium, titanium, etc.) to remove oxygen, water vapor, and nitrogen. Vapor traps should be provided at obvious gas interfaces with the potassium system to prevent potassium transfer into the gas purification system.

The basic cover gas purification train and components will operate at ambient temperatures and can be constructed of mild steel or 316 SS if necessary. A gas recirculation and purification system is better than stagnant pressure maintenance since system outgassing and contaminant in-leakage can be more readily handled.

Additional gas system components will be necessary. Main subsystem additions will be separate gas pumps and controls for gas buffer shaft seals and provision to remove lubricants, and so forth from outboard bearings of the gas system (which is recirculated). Seal gas which enters the turbine will be pumped to the condenser/steam generator and must be removed from this chamber before building up a back pressure to counteract turbine performance. The solubility of helium or argon in alkali metals is not greater than a few ppm, and the influence of these dissolved cover gases on the boiler operation will be negligible. Some small solubility may be beneficial in the prevention of boiling instability and concurrent system shocks.

Recommended practice before starting operation of the system is a vacuum bake-out of all internal surfaces for the removal of adsorbed gases and moisture. Strip heaters should be provided for this purpose, as well as for temperature maintenance to liquify potassium at start-up. One or two hot dumps (to the sump tank) of the liquid potassium parts of the system will also aid in removing adsorbed contaminants, and so on and transferring them to the sump (dump) tank.

Since some of the potassium lead-in ducts, exit ducts, and so forth are large, material strength requirements may make a vacuum degas cycle unacceptable. A second option for system cleanup would require a purge of high-purity helium or argon through the heated system until the purge gas exit purity indicates a cleanup of all internal surfaces. Subsequent operation and hot dumps with potassium should clean the system.

#### 3.7.6 Shaft Seal and Bearings

Several options exist with respect to shaft seals and bearings. High-temperature potassium lubricated bearings may be employed inside the turbine working area, with outboard potassium and gas seals. The gas seal would be employed to prevent contaminants from leaking into the potassium-bearing and turbine-working area. A second option would place the gas seal inboard; then an oil seal; then an organic-lubricated bearing outboard of the system where temperatures would be lower. The second arrangement would permit mechanical or maintenance activity on the bearing without complete machine strip-down and decontamination.

Several programs have investigated the effects of alkali liquid metal environments on bearings and seals (References 3.99, 3.120-3.122). The most exhaustive is one (References 3.99 and 3.124) in which the compatibility of several bearing materials with potassium is considered. The materials were (1) nonrefractory metals and alloys; (2) refractory metals and alloys; (3) iron-nickel-cobalt bonded carbides; (4) carbides; (5) oxides; (6) borides; and (7) refractory metal bonded carbides. Bearing materials may be expected to operate at temperatures up to 811°K (1000°F). In the work reported potassium compatibility test

temperatures to 1144°K (1600°F) were evaluated in order to further state-of-the-art experience.

Nb-1 Zr capsule potassium compatibility tests at 1144°K (1600°F) showed that the oxides (Lucalox, Zircoa 1027), the nonrefractory metals and alloys (Star J), and the iron-nickel-cobalt bonded carbides all incurred serious weight and dimensional changes. Oxygen in the potassium varied from 11 to 32 ppm; TiC (niobium binder) appeared to possess stability in liquid potassium to 1144°K (1600°F); WC (Grade 7178) was suspected to corrode in potassium at 922°K (1200°F) [but did not corrode at 811°K (1000°F) or less]; and a weight loss through carbon migration was noted.

Liquid potassium friction and wear tests were conducted (Reference 3.99) between the most promising high-temperature bearing material combinations at 478 and 700°K (400 and 800°F). The combinations were TZM-7178, 7178-7178, and TiC (10% Nb)-TiC(10% Nb). Results indicated that the TiC(10% Nb)-TiC(10% Nb) test incurred the lowest weight loss and wear rate and displayed the lowest friction of the three combinations.

Results indicated that the materials of the three tests mentioned above would serve well at a design-rated temperature of 811°K (1000°F). Mechanical compression tests conducted in this program indicated that the 7178 grade has a ductility advantage over the TiC (10% Nb) which is of considerable importance in designing the turbine bearings.

Inboard, potassium-lubricated bearings would be difficult to monitor, maintain, and repair. Outboard, organic-lubricated bearings would require inboard seals. Tandem gas circumferential seals have been evaluated for performance in alkali liquid-metal environments and have been successful in maintaining machine internals at more than 1 ppm oxygen, moisture contamination, in other words, minimal backstreaming (Reference 3.124). The seal materials were also required to operate in dry, inert atmospheres with minimal wear rates and met these requirements. In this situation, the gas seal would prevent contaminant (gaseous, organic) in-leakage, as well as prevent potassium vapor out-leakage. The gas would

Table 3.39 - Summary of Materials Selection for Liquid-Metal Rankine System Components.

Condition (1)	Column	(1) PFB	(2) PF	(3) PFB	(4) PFB	(5) PFB	(6) PFB
K-Turb inlet T (°F)		1400	1400	1500	1500	1600	1600
K-Condensate T (°F)		1100	1100	1200	1200	1300	1300
Steam Turbine inlet T (°F)		1000	1000	1000	1100	1000	1200
Base Case							
Components							
Boiler		Incoloy 800 (C)	316 SS (A)	Incoloy 800 (C)	Incoloy 800 (C)	HA-188 (C)	HA-188 (C)
Turbine							
Inlet casing		304 SS (B)	304 SS (B)	Incoloy 801 (C)	Incoloy 801 (C)	HA-188 (C)	HA-188 (C)
Disk		Incoloy 901 (C)	Incoloy 901 (C)	Waspalloy (D) (3)	Waspalloy (D) (3)	Waspalloy (D) (3)	Waspalloy (D) (3)
Blades (2)							
Stage 1		U-700 (C)	U-700 (C)	TZM (B)	TZM (B)	TZM (B)	TZM (B)
Stage 2		U-700 (C)	U-700 (C)	TZM (B)	TZM (B)	TZM (B)	TZM (B)
Stage 3		U-700 (C)	U-700 (C)	TZM (B)	TZM (B)	TZM (B)	TZM (B)
Stage 4		U-700 (C)	U-700 (C)	TZM (B)	TZM (B)	TZM (B)	TZM (B)
Turbine case		304 SS (B)	304 SS (B)	HA-188 (C)	HA-188 (C)	HA-188 (C)	HA-188 (C)
Shaft		Incoloy 901 (C)	Incoloy 901 (C)	Waspalloy (C)	Waspalloy (C)	Waspalloy (C)	Waspalloy (C)
Tie bolts		U-700 (C)	U-700 (C)	—	—	—	—
Exhaust scroll		304 SS (B)	304 SS (B)	HA-188 (C)	HA-188 (C)	HA-188 (C)	HA-188 (C)
Loop		2-1/4 Cr-1 Mo (B)	2-1/4 Cr-1 Mo (B)	316 SS (A)	316 SS (A)	316 SS (A)	316 SS (A)
Condenser/Steam Generator		2-1/4 Cr-1 Mo (B)	2-1/4 Cr-1 Mo (B)	316 SS (B)	316 SS (B)	316 SS (B)	316 SS (B)
Case (4)							
Potassium		1,2,3,7,8,11,13,15, 17,19,20,21,22	4,5,6,9,10,12,14,16, 18,43,44,45,46,47,48	23	25,28,31,34	24	26,27,29,30,32, 33,35,36,37,38,39
Cesium		40,41,42					

(1) PF = Pressurized furnace, CLEAN gas fired.

PFB = Pressurized fluidized bed, boiler in coal fuel.

(2) Variation of blade material with turbine stage to be evaluated in Phase 2 of this study.

(3) Selection of Waspalloy is for 6 foot diameter disks. For 2-3 feet in diameter or less, TZM (B) would be selected.

(4) Case numbers from cycle analysis, see Section 8.



have to be purified and organic contaminants (from adjacent outboard bearings) removed prior to its reinsertion into the seal.

### 3.7.7 Instrument Subsystems

Instrument subsystems necessary to guarantee material integrity and freedom from corrosion, strength loss, and so forth would include the following: (1) instruments for the alkali-metal loop; (2) instruments for the cover gas system; (3) instruments for the various interface situations.

Oxygen, moisture, carbon, and hydrogen meters are commercially available and can be employed to monitor liquid-metal loop conditions. A rise in loop oxygen would indicate a seal loss, the onset of advanced corrosion processes, and possible emergency conditions leading to system shutdown. Detection of moisture in the potassium system (water vapor or hydrogen) would indicate a leak (rupture) onset condition in the condenser/steam generator.

Cover gas impurities can be detected with a gas chromatograph (nitrogen, hydrogen, carbon monoxide, carbon dioxide, etc.), a solid electrolyte (oxygen), moisture monitors (water vapor), and so on, all with on-line read-out and alarm capability.

Alkali-metal leaks (potassium) may be detected with new instruments such as the sodium ionization detector (SID) currently being developed by Westinghouse, which would require modification for potassium or cesium application.

All these instruments are described in greater detail in Subsection 3.8. Their employment in an alkali liquid-metal vapor Rankine topping cycle system would be considered essential to system operation and maintenance.

### 3.7.8 Summary of Prime Materials Selected for Liquid-Metal Rankine Cycle Components

Table 3.39 represents the prime materials selection for the liquid metal vapor Rankine topping cycle system components, base case,

and parameter variation cases. Case description (reference) numbers relate to the case analyses and description in Section 8. The materials recommended are rated according to Subsection 3.1.

### 3.8 Materials for Sodium and Lithium MHD System Components

The evolution of laboratory size liquid-metal MHD generators to those of utility plant scale will require the optimum selection of construction materials and the utilization of advanced liquid-metal technology. At the present time a number of laboratories throughout the United States and Europe have intensive development programs designed to investigate the commercial feasibility of liquid-metal MHD generators (Reference 3.125).

The proper selection of liquid-metal MHD plant construction materials will play an important role in the overall plant feasibility and efficiency. For this particular program and from liquid-metal considerations, three basic MHD plant configurations are being considered: (1) the base case binary plant operating at a power level of 1000 MWe employing liquid-metal MHD topping with sodium/argon at 922°K (1200°F) as the two-phase working fluid, (2) a plant similar to the base case with the temperature of the sodium/argon two-phase fluid at 1089°K (1500°F), and (3) a plant, operating at a power level of 1000 MWe employing lithium/helium, at a temperature of 1089°K (1500°F), as the two-phase working fluid (Reference 3.126). For each of the cases identified, the materials study was carried out for all MHD plant components which may, of necessity, or potentially, through vapor transport contact the liquid/vapor alkali metal. These components, which comprise the total liquid-metal section of the MHD plant, may be briefly described as: (1) the heat source, (2) the MHD generator including mixer, duct, and nozzle, (3) the liquid-metal loop including separator and diffuser or pumps, and (4) the cover and/or accelerating gas system which also includes the regenerator and heat rejection system. A section detailing the required instrument subsystems necessary for liquid-metal leak detection, liquid-metal purity

monitoring and cover, and/or accelerating gas purity monitoring is presented. Finally, potential problem areas are discussed briefly.

### 3.8.1 Heat Source - Alkali Metal/Accelerating Gas Combustion System Heat Exchanger

The detailed design of the alkali-metal and accelerating gas heat exchanger is presented in Section 11; the combustion-side material requirements are discussed in Subsection 3.2. As detailed in the following discussion, the selection of materials for the sodium/argon base case 922°K (1200°F) may be based on current liquid-metal technology. Thus, austenitic stainless steels such as 304 and/or 316 may be employed. At higher sodium/argon temperatures 1089°K (1500°F) Haynes Alloy 188 or Haynes Alloy 25 may be a more suitable material, while the system employing lithium/helium as the two-phase working fluid may require refractory metal alloys. Such materials as B-88 (Nb-28W-2Hf-0.07C) or Nb-1Zr should be given prime consideration. These refractory metal alloys must be protected from oxidizing atmospheres. The recommended construction materials for the alkali-metal side of the heat source are tabulated in Table 3.40.

Table 3.40 — Heat Source Alkali-Metal Side Materials Selection

	<u>Sodium/Argon</u>	<u>Lithium/Helium</u>
1200°F	316 SS (A)*	--
(base case)	304 SS	--
1500°F	Haynes Alloy 188 (C)*	B-88 Nb-28W-2Hf-0.07C(C)*
	Haynes Alloy 25 (B)*	Nb-1Zr (C)

\*Materials application rating per Subsection 3.1.

If, because of final design considerations, a structural material must be selected which is primarily compatible with combustion products (high-nickel alloys), then two options may be considered:

- (1) employ a combustion-side compatible material and coat (internally) the alkali-metal side with a protective layer such as molybdenum; or
- (2) consider a duplex tube configuration whereby the sodium or lithium side employs alkali-metal compatible materials, and the combustion gas side employs combustion-product compatible materials.

#### 3.8.1.1 Potential Problem Area

From a design point of view, the use of single-wall heat exchanger tubes is preferred, and therefore structural materials must be compatible with both alkali metals and combustion gas products. For the base case design and for the case employing sodium/argon at 1089°K (1500°F), the selected sodium-side compatible materials may be employed. On the other hand, a refractory metal (molybdenum) coating may be necessary if combustion-product compatible materials are required. Problems associated with large-scale deposition techniques, such as chemical vapor deposition (CVD), must be investigated and long-term integrity of the coating must be evaluated. Alternatively, large thermal losses may limit the use of a concentric duplex-tube configuration.

#### 3.8.2 MHD Generator Including Mixer, Duct, and Nozzle

A description of the liquid-metal MHD generator is presented in Section 11. Basically, the MHD generator consists of: (1) a mixer designed to mix the accelerating gas with the alkali metal to form a two-phase system with a high void fraction, (2) the MHD generator duct consisting of the electrodes and insulators which are required to be compatible with the liquid alkali-metal/accelerating gas two-phase system at an operating temperature between 922 and 1089°K (1200 and 1500°F), and (3) the nozzle designed to feed the two-phase mixture into the liquid-metal/accelerating gas separator.

##### 3.8.2.1 Structural Materials

As previously described, the base case MHD generator is designed to operate with a sodium/argon two-phase mixture at 927°K and 8.27 MPa (1200°F and 1200 psia). For the base case design, based on current state-of-the-art LMFBR liquid-metal technology, the reference structural material would be 316 SS (Reference 3.127).

Alkali-metal compatibility studies and experience gained from both laboratory-scale experiments and plant-size liquid-metal loops have

shown that common austenitic steels such as 304 and 316 can be utilized up to 811°K (1000°F) in flowing sodium systems with virtually unlimited life, provided the oxygen and carburizing potential of the fluid are maintained at low ppm levels (Reference 3.127). Specifically for type 316 SS, a 108.6 Ms (30,000 hr) sodium exposure study at 866 and 922°K (1100 and 1200°F) has shown that the material weight loss may be expressed by Equation 3.14.

$$100R = V^{0.884} O^{1.156} \exp \left( 12.845 - \frac{23,827}{T + 460} - 0.00676 \frac{L}{D_i} + \frac{2.26}{t + 1} \right) \quad 3.14$$

where  $R$  = removal of hot-zone metal, mg/cm<sup>2</sup> month  
 $V$  = velocity, ft/s  
 $O$  = oxygen level, ppm  
 $T$  = temperature, °F  
 $\frac{L}{D_i}$  = distance ratio downstream from hot leg  
 $t$  = exposure time, months.

In addition, Type 316 SS was approximately neutral to carbon transfer in a monometallic system. It carburized to several mils, however, when combined with 2-1/4 Cr-1 Mo or 5 Cr-1/2 Mo-1-1/2 Ti steels (Reference 3.128). In general, for the 300 series stainless steels, if the purity of the sodium is controlled to very high levels (1 to 2 ppm) and the system temperature remains below 978°K (1300°F), the corrosion rates are less than 0.8 pm/s (1 mil/year) (References 3.129 and 3.130).

For this specific application, heavy wall stainless steel will be required because of the high [8.27 MPa (1200 psia)] ambient pressures involved. Thus, the small material losses as a result of liquid-metal corrosion are not limiting. On the other hand, the sodium corrosion process for stainless steel is somewhat selective for specific alloying elements (nickel and chromium), and if the compositional gradients are sufficiently large, phase changes can occur at the containment wall/sodium interface, thus changing the physical properties and the mechanical strength. If system design requirements are established

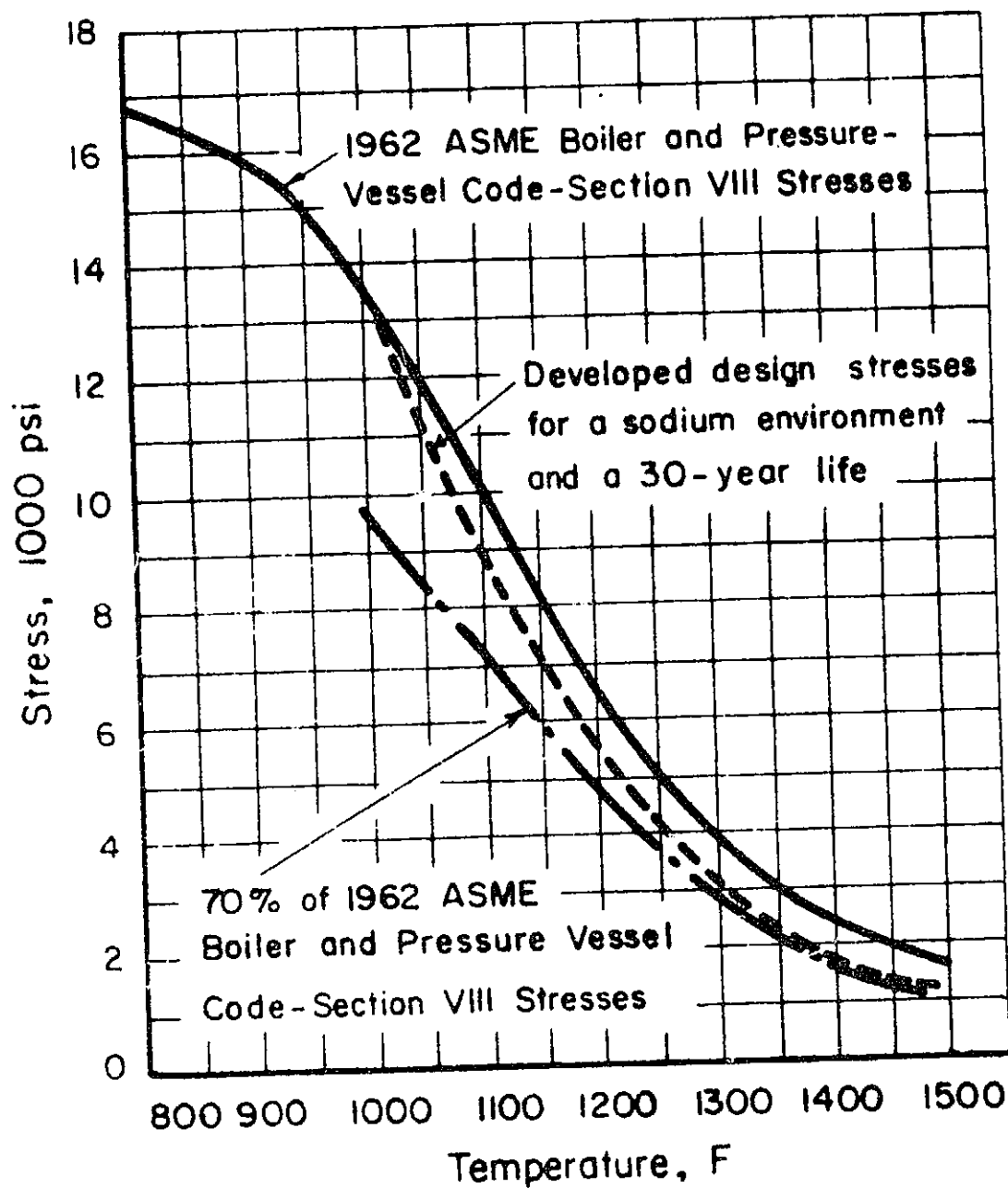


Figure 3.27 — Developed design stresses for Type 316 SS in a sodium environment and a 30-year life (Reference 3.127).

according to the developed design stresses for 316 SS as detailed in Figure 3.27, then 946 Ms (30 yr) plant lifetimes are fundamentally feasible, although other limiting parameters such as alkali-metal purity, the influence and interaction with other metallic and/or ceramic materials, and overall plant operation must be considered (Reference 3.127).

At temperatures above 922°K (1200°F), nickel- and cobalt-based alloys may be considered as structural materials for the sodium argon MHD generator because of their good high-temperature strength. It is in this temperature region, however, that the corrosion rate of nickel-based alloys accelerates as compared with that of stainless steel. For example, the corrosion rate for Incoloy 800, an iron-based superalloy with high nickel levels, in low oxygen (<10 ppm) sodium is approximately 0.12 pm/s at 922°K (0.15 mil/yr at 1200°F) and with a sodium velocity of 2.1 m/s (6.89 ft/s), and is 0.80 pm/s at 978°K (1 mil/yr at 1300°F) at 5.2 m/s (17.06 ft/s). The latter rate is about two to three times that of stainless steel under the same conditions. Although oxygen in sodium, however, in the range of 0 to 500 ppm, has little effect on the corrosion of high-nickel alloys, it is more sensitive to the flowing velocity of the sodium, thus suggesting that the controlling step in the corrosion reaction is diffusion across a boundary layer at the metal surface.

At higher temperatures 1033°K (1400°F), cobalt-based alloys are more resistant to sodium corrosion than are nickel-based alloys and may be superior to stainless steel. For example, a cobalt alloy containing 20 Cr-10 Ni-6.5 Mo is reported to corrode at about half the rate of Type 316 SS after 18 Ms (5000 hr) exposure to hot trapped sodium at 1033°K (1400°F) ( $-0.3 \text{ mg/cm}^2$  compared with  $-0.6 \text{ mg/cm}^2$ ) (Reference 3.138).

In general, molybdenum and TZM appear to be relatively resistant to sodium corrosion at temperatures to 1255°K (1800°F), but present-day, large-scale plant fabrication techniques have not been sufficiently developed to make their use economically and practically feasible.

Additionally, the refractory metals and alloys appear to be the most suitable structural materials for the lithium/helium closed-cycle MHD system which should be capable of operating at temperatures up to 1089°K (1500°F). For example, niobium, tantalum, and molybdenum show relatively good resistance to lithium at 1272°K (1830°F), whereas zirconium and titanium appear only fair (Reference 3.131). In addition, the gettered refractory metal alloys such as B-88 or Nb-1 Zr, exhibit good resistance to attack by high-purity lithium at temperatures up to 1478°K (2200°F). The corrosion resistance of the niobium-based alloys to lithium is reduced by the addition of oxygen to the lithium, the niobium itself, or the atmosphere (in this case, the helium accelerating gas). Alloying the niobium with a small amount of an oxygen getter such as zirconium decreases the sensitivity to oxygen contamination.

Only limited studies have been carried out on the corrosion behavior of tantalum and tantalum-based alloys. Since tantalum behaves in a manner similar to niobium, a stable oxide former such as hafnium is necessary to produce corrosion resistance. The corrosion resistance of molybdenum and molybdenum-based alloys such as TZM (Mo-0.5 Ti-0.08 Zr) and Mo-50 Re have been studied, and neither alloy showed evidence of attack in the temperature range of 1644 to 1922°K (2500 to 3000°F) for sodium exposures up to 3.6 Ms (1000 hr) (Reference 3.125).

In summary, the preferred structural material for the MHD generator (mixer, duct, and nozzle) appears to be the 300 series stainless steels (Type 316), provided that the purity of the sodium is controlled to a high degree and the material temperature remains below 978°K (1300°F). For higher temperature operation [978 to 1089°K (1300 to 1500°F)] the iron-based superalloy Incoloy 800 and cobalt-based alloys such as Co-20 Cr-10 Ni-6.5 Mo or Haynes Alloy 25 appear to be more suitable from a material strength point of view. The corrosion of the Incoloy 800 and the nickel-based alloys is more dependent on the velocity of the flowing liquid metal; only limited, short-term compatibility studies have been carried out on cobalt-based alloys. The refractory metals and alloys such as niobium, molybdenum, B-88 (Nb-28W-2Hf-0.07C),



Nb-1 Zr, and TZM would be required structural materials for lithium MHD generators operating at temperatures up to 1089°K (1500°F). A listing of recommended materials is given in Table 3.41.

Table 3.41 — MHD Generator (Mixer, Duct, and Nozzle)  
Materials Selection

	<u>Sodium/Argon</u>	<u>Lithium/Helium</u>
1200°F	316 SS (A)*	--
(base case)	Haynes Alloy 25 (B)*	B-88 or Nb-1Zr (C)*

\*Materials application rating per Subsection 3.1.

### 3.8.2.2 MHD Duct Electrodes and Insulators

As indicated previously, 316 series stainless steel may be utilized as an electrode material within the MHD duct employing the sodium/argon two-phase mixture. Since the electrodes will not have to be load-bearing members of the MHD generator (support will be provided by the external shell of the generator as described in Section 11), Type 316 SS may be utilized to temperatures up to 978°K (1300°F). For much higher temperatures up to 1089°K (1500°F), Haynes Alloy 25 may be considered. For use in the lithium/helium two-phase mixture, the refractory metals and alloys may be considered.

A more serious problem is the selection of the proper and suitable insulator materials. Only a limited amount of short-term [0.36 to 3.6 Ms (100 to 1000 hr)] test data are currently available indicating that ceramics (insulators) exposed to sodium resist attack according to their stability, as predicted from thermodynamic data, their purity, and density (porosity) (References 3.127 and 3.132). While present-day information is very limited as to the compatibility of ceramic materials with sodium at the required MHD operational parameters, high density (99 + % theoretical), high-purity 99.9%), aluminum oxide and magnesium oxide appear to be the best candidate materials, while high-density, high-purity magnesium oxide and beryllium oxide may be considered for the lithium/helium environment. High-density (97.8 to 99 + % theoretical) insulator materials are generally

commercially available in brick form 88.9 by 63.5 by 228 mm (3-1/2 by 2-1/2 by 9 in) or may be applied as a continuous sheet by flame-spraying techniques. A thickness of 0.12 to 0.25 mm (5 to 10 mils) is readily achieved by flame-spraying techniques, although low theoretical densities (80%) are usually obtained. Because of the toxicity associated with beryllium compounds, the flame-spraying of beryllium oxide will not be considered.

In conclusion, present-day information indicates that both material purity (grain boundary impurities) and porosity play an important role in the corrosion resistance of ceramics with alkali metals. Since the effects of a dynamic alkali-metal environment have not been fully investigated for insulator materials for MHD generators, long-term dynamic sodium compatibility studies must be carried out before a final materials selection is made. Table 3.42 summarizes potential candidate electrode and insulator materials for the three MHD cases.

Table 3.42 —MHD Generator Electrode and Potential Insulator Materials Selection

<u>Temperature</u>	<u>Sodium/Argon</u>	<u>Lithium/Helium</u>
1200°F	Electrodes - 316 SS (A)	--
(base case)	Insulators - $Al_2O_3$ or MgO (C)*	--
1500°F	Electrodes - Haynes Alloy 25 (B)*	Electrodes - B-88 or Nb-1Zr (B)*
	Insulators - $Al_2O_3$ or MgO (C)*	Insulators - MgO, BeO (C)*

\*Materials application rating per Subsection 3.1.

### 3.8.2.3 Potential Problem Areas

Although the selection of structural materials for the closed-cycle liquid-metal MHD generator is based on current state-of-the-art liquid-metal technology, no information is available about effects of high-pressure [8.27 MPa (1200 psi) abs] on the corrosion rate of the recommended metals and alloys. If the liquid-metal MHD generator is to be operated at temperatures and environments at which the use of

refractory metals and alloys will become necessary, then present-day fabrication techniques must be scaled up to handle large-size plant components. Finally, experimental studies will be necessary in order to select methods of application and alkali-metal compatible ceramic materials for use as insulators in the MHD duct.

### 3.8.3 Liquid-Metal Loop Including the Separator and Diffuser

A large liquid-metal loop, as described in Section 11, will be required to supply high-purity alkali metal to the MHD generator. This section addresses the problems associated with the maintenance of high-purity liquid metal in order that the corrosion rate of the recommended structural materials will be minimized. As indicated in Subsection 3.8.2, the recommended loop construction materials will consist primarily of 316 SS [sodium/argon at 922°K (1200°F)]; but depending upon the selected operating temperature and alkali metal (sodium or lithium), the recommended alternative materials may be utilized. The same materials employed for the construction of the liquid-metal loop may also be employed for the separator and diffuser components of the MHD generator loop. Table 3.43 lists candidate materials for each MHD plant configuration.

Table 3.43 — Liquid-Metal Loop and Associated Components  
Materials Selection

<u>Temperature</u>	<u>Sodium/Argon</u>	<u>Lithium/Helium</u>
1200°F (base case)	316 SS (A)*	--
1500°F	Haynes Alloy 25 (B)*	B-88 or Nb-1Zr (C)

\*Materials application rating per Subsection 3.1.

In general, large liquid-metal loops employ either mechanical or electromagnetic pumps as a means of establishing a dynamic flow of liquid metal. Because of the high pressure of operation [2.27 MPa (1200 psi)], a number of pumps may be required to be series/parallel connected in order that the required operational pressures may be maintained; this aspect is discussed in detail in Section 11. As noted,

appropriate liquid-metal charge and dump tanks are also an integral part of the liquid-metal loop and are usually situated at the lowest portion of the system to permit gravity drainage.

From a materials corrosion point of view, the most crucial aspect of a liquid-metal loop system is the impurity trapping mechanism which is utilized to maintain the alkali metal at a high degree of purity, usually on the order of 1 to 5 ppm. A circulating cold trap is generally employed for large liquid-metal systems, whereby temperature-dependent impurities are precipitated from the alkali metal. Cold traps reduce the temperature of sodium as it circulates through a wire mesh packed tank where dissolved impurities precipitate and/or crystallize on the packing. Traps of the types described are able to reduce oxygen impurity levels in sodium to 0.5 to 1.5 ppm (References 3.133 and 3.134). The solubility of oxygen in sodium may be described by Equation 3.15.

$$\log S = 6.239 - \frac{2447}{T} \quad 3.15$$

where S is the ppm  $O_2$  by weight and T is the fluid temperature in °K. Thus, in order to maintain the oxygen level in a large sodium loop at the 2 ppm level, a cold-trap temperature of 413°K (284°F) must be maintained (Reference 3.135).

A liquid-metal cold trap should be designed in such a manner as to provide a volume which will retain the liquid metal for at least 300 s (5 min). Basically, the time required for alkali-metal purification by this technique will depend upon (1) the nature of the impurities, (2) the alkali-metal temperature-dependent solubility, (3) the starting and ending concentration level, (4) the comparative sizes of the system and trap, and (5) the cold-trap circulation rate. If one assumes that there are no additional cold traps in a given liquid-metal system, then the performance of a circulating cold trap may be described by Equation 3.16.

$$\frac{x - x_c}{x_o - x_c} = e^{-(w/W)\theta} \quad 3.16$$

where  $x_o$  = original oxygen content  
 $x_c$  = saturation oxygen content at cold-trap temperature  
 $x$  = oxygen content of system at any time  
 $\theta$  = elapsed time  
 $w$  = cold-trap flow rate, lb/hr  
 $W$  = total alkali metal charge, lb

The flexibility attainable by this technique permits the control of many alkali-metal impurities at defined concentrations. The primary requirement for the effective use of cold traps is the knowledge of the solubility of the impurities anticipated in the alkali metal (Reference 3.133).

#### 3.8.3.1 Potential Problem Areas

Since the useful life time of an alkali-metal cold trap will be directly related to the total influx of impurities into the alkali metal as a function of time and to the nature of the contaminants, the potential sources of impurities within the MHD plant must be established. In the design, construction, and eventual operation of a plant-size liquid-metal MHD generator the following aspects must, therefore, be considered: (1) the impurity level in the loop cover gas and MHD generator accelerating gas; (2) the influx of impurities as a result of air leakage through seals and gaskets throughout the entire MHD plant; (3) plant start-up requirements - a bake and gas purge cycle is considered essential; and (4) plant shutdown, alkali-metal decontamination, and cleanup requirements.

#### 3.8.4 Gas System Including the Steam Generator

The closed-cycle liquid-metal MHD generator will require a gas system to supply both cover gas for the alkali-metal loops and also serve as the supply for the accelerating gas for the MHD generator. A detailed discussion of the gas supply system, including the compressor requirements, is presented in Section 11.

The total amount of normal impurities generally encountered in as received high-purity gases such as argon is less than 50 ppm (v)\*. Specifically, 8 to 10 ppm (v) oxygen, 1 to 2 ppm (v) carbon dioxide, 8 ppm (v) water, and 20 ppm (v) nitrogen. Purification of the as received gas will serve to protect the alkali metal and containment materials from contamination. For most alkali-metal applications, the cover gas should contain less than 5 ppm (v) oxygen and less than 5 ppm (v) water vapor. Because refractory metals are susceptible to oxidation and nitriding, oxygen and nitrogen must be removed from systems utilizing these metals and alloys.

A number of purification techniques exist for removing contaminants from inert gases (Reference 3.136). These include (1) NaK bubblers; (2) hot copper chips to remove oxygen, hydrocarbons, and carbon monoxide; (3) activated alumina and molecular sieve to remove water vapor, and (4) hot gettering materials such as zirconium, titanium, and uranium to remove oxygen, water, and nitrogen.

Since the potential exists for alkali-metal vapor carry-over into the steam generator and regenerator-economizer portion of the MHD loop, some consideration must be given to the compatibility of the structural materials with alkali-metal vapor and condensates. In addition, since the steam generator will be interfaced with a standard steam bottoming plant, the selected structural materials must be compatible both with the alkali-metal accelerating gas on one side of the steam generator tube bundle and with the water (steam) on the other. For the base case sodium/argon MHD system the steam generator construction material may be Croloy (2-1/4 Cr-1 Mo), which has previously been demonstrated to be compatible with both the steam side and sodium side of LMFBR plants if the  $T_{\text{mean}}$  of the heat exchanger tube is less than 839°K (1050°F) (Reference 3.137). If the  $T_{\text{mean}}$  is greater than 839°K (1050°F), then 304 SS will be required. Haynes 188 is recommended for the sodium/argon system at 1089°K (1500°F). A much more complex situation becomes apparent when the potential of lithium vapor transport into the steam generator is considered. The solubility of refractory metals and alloys in lithium is rather low, that of iron and chromium is intermediate, and

---

\*(v) = volume basis

that of nickel is high. In general, the base-metal alloys do not exhibit promising corrosion resistance, and most attention has been directed toward the refractory metals. For this particular steam generator application a duplex tube configuration may be necessary in which the helium/lithium side of the generator will be a refractory metal alloy such as B-88 or Nb-1 Zr.

#### 3.8.4.1 Potential Problem Areas

The possibility of alkali-metal vapor transport into the steam generator and regenerator economizer of the liquid-metal MHD system exists, although the actual fate of the alkali metal remains questionable. One potential problem exists with the steam generator, since there is a temperature difference between the inlet and outlet sides of the unit. This may cause the liquid-metal vapor to plate out on the steam generator tubing bundles. Also, because of this condensation problem, impurities present within the liquid metal may also be removed. Thus, the steam generator may actually serve as an alkali-metal vapor trap; if the vapors are saturated with impurities they may also be removed at the steam generator site.

The steam generator construction material for the base case sodium/argon MHD system may be Croloy (2-1/4 Cr-1 Mo) or 304 SS, but because of the corrosion problems that exist with the lithium/helium system a more complex materials problem is encountered. The refractory metal alloys, such as B-88 or Nb-1 Zr, are compatible with lithium at steam generator inlet temperatures of 894°K (1150°F), but the problems associated with utilizing these alloys (such as fabrication, oxidation, nitriding, etc.), must be carefully considered and solved.

#### 3.8.5 Closed-Cycle Liquid-Metal MHD Materials Selection Summary

A summary of the materials selection for the closed-cycle liquid-metal MHD system is presented in Table 3.44. The materials rating criteria, as discussed in Section 3.1, have been used to categorize the selected materials in terms of the additional research effort

Table 3.44 — Materials for Sodium and Lithium MHD System Components

<u>System Component</u>	<u>Sodium/Argon 1200°F (base case)</u>	<u>Sodium/Argon 1500°F</u>	<u>Lithium/Helium 1500°F</u>
Heat Source	316 SS (A)*	Haynes Alloy 188 (C)* Haynes Alloy 25 (B)*	B-88 or Nb-1 Zr (C)*
MHD Generator - mixer, duct, nozzle	316 SS (A)*	Haynes Alloy 25 (B)*	B-88 or Nb-1 Zr (C)*
MHD Generator electrodes	316 SS (A)*	Haynes Alloy 25 (B)*	B-88 or Nb-1 Zr (C)*
MHD Generator insulators	Al <sub>2</sub> O <sub>3</sub> or MgO (C)*	Al <sub>2</sub> O <sub>3</sub> or MgO (C)*	MgO or BeO (C)*
Liquid-Metal Loop including separator and diffuser	316 SS (A)*	Haynes Alloy 25 (B)*	B-88 or Nb-1 Zr (C)*
Cover Gas/Accelerating Gas System	316 SS (A)*	316 SS (A)*	316 SS (A)*
Steam Generator	2-1/4 Cr-1 Mo (<1050°F) (A)* 304 SS (>1050°F) (A)*	Haynes Alloy 188 (C)*	B-88 or Nb-1 Zr . (duplex tube con- figuration - Li side) (C)*

\*Materials application rating per Subsection 3.1.



required. Note that structural and electrode materials required for the base case liquid-metal MHD system, utilizing sodium/argon as the two-phase fluid mixture, may be specified from present-day state-of-the-art liquid-metal technology. On the other hand, the selection of insulator materials requires considerable developmental effort. Similarly, the selection of all materials for the lithium/helium parametric case remains somewhat speculative at this time.

### 3.8.6 Instrument Subsystems

The closed-cycle liquid-metal MHD generator will require specific on-line instrumentation to monitor potential fault conditions in four separate areas (1) cover gas/accelerating gas impurity monitors, (2) liquid-metal impurity monitors, (3) alkali-metal vapor detectors for liquid-metal leaks, and (4) leak detection/leak location devices specifically for steam generator applications.

#### 3.8.6.1 Cover Gas/Accelerating Gas Impurity Monitors

Commercial instrumentation is currently available to monitor all the specific impurities in inert gas systems such as argon and helium. For example, oxygen may be continuously monitored with solid-state electrolyte devices which are capable of detecting levels below 0.5 ppm (v). Standard gas chromatographic techniques may be employed to measure such impurities as nitrogen, hydrogen, oxides of carbon (carbon monoxide, carbon dioxide), and hydrocarbons; detection sensitivities in the range of 0.5 to 1 ppm (v) are considered standard. Water vapor to 1 ppm (v) may be measured by a number of moisture monitors currently being employed in large industry (Reference 3.133). Thus, the currently available commercial inert gas impurity monitors are capable of measuring the important impurities in the gaseous environments for this application.

#### 3.8.6.2 Liquid-Metal Impurity Monitors

Two of the most important impurities which must be continuously monitored in liquid sodium systems are oxygen and hydrogen. For the liquid sodium system, commercial on-line instrumentation is presently available; oxygen may be monitored in liquid metals at the low ppm level with solid electrolyte oxygen meters, and hydrogen may be monitored to fractional ppm levels with diffusion-type hydrogen meters (References 3.138, 3.139, and 3.140). In addition to oxygen, nitrogen and carbon impurity levels must be monitored in liquid lithium systems.

#### 3.8.6.3 Alkali-Metal Vapor Detectors

Leak detection devices are essential throughout a plant utilizing liquid alkali metals to monitor the onset of leaking alkali metal into the surrounding plant environment. Although many devices have been constructed and tested, one of the most promising to date is the Sodium Ionization Detector mentioned in Section 3.7.7. This device has the capability of detecting sodium vapor in the parts-per-billion range in both inert atmospheres and those containing 1 to 2% oxygen and water vapor. At the present time the selectivity of the detector for sodium, its speed of response, and potential low cost make it a prime candidate for sodium vapor detectors which must be located in critical areas throughout an MHD plant (Reference 3.141).

#### 3.8.6.4 Steam Generator Leak Detection/Leak Location Devices

Since a standard steam bottoming plant will be an integral part of the liquid-metal MHD cycle, steam generators will be interfaced with the argon exiting from the MHD generator [894°K (1150°F) for the base case] and steam turbine loops [811°K (1000°F) steam at 24.13 MPa (3500 psi) abs for the base case]. Because of the pressure differential across the steam generator tube bundles, 2.07 to 2.76 MPa (300 to 400 psi) abs argon versus 24.13 MPa (3500 psi) abs steam, the onset of a leak will be immediately indicated by an increase in water vapor level in the argon at the downstream side of the steam generator. Thus,

standard moisture monitors, as described in Section 3.8.6.1 may be employed as leak detection devices.

Alternatively, if alkali metal (sodium or lithium) is also vapor transported into the steam generator, then during a leak situation the potential exists for the reaction of alkali metal with steam, with the subsequent evolution of hydrogen gas. A hydrogen detector, therefore, may also be required for the leak detection system employed in the steam bottoming plant of liquid-metal MHD generators.

It is also possible, but less likely, that argon gas may enter the high-pressure steam loop during the onset of a leak within a steam generator through crack diffusion processes. In this case, leaks may be monitored by noting the increase of argon in the steam loop by standard mass spectrometric techniques (Reference 3.142). This method is not an on-line, continuous technique, and therefore real time monitoring is not feasible. This method should thus be considered only as a redundant or alternative leak detection technique.

Once a leaking tube bundle within a steam generator has been detected, it must be decided whether or not the plant must be shut down for repairs. Since the rupture of a heat exchanger tube within the steam generator of the liquid-metal MHD plant could lead to alkali metal-water (steam) reactions, a more crucial situation exists in this plant than in standard, present-day power generation facilities. If plant shutdown is required, then currently available leak location methods such as eddy current testing and/or helium-mass spectrometric techniques may be employed to locate the suspect tube(s).

#### 3.8.6.5 Potential Problem Areas

At the present time, commercial on-line liquid-metal impurity monitors for oxygen and hydrogen in sodium are available. Although theoretically feasible, these devices have not been tested in lithium systems. Also, the need for an on-line alkali-metal nitrogen and carbon meter will be necessary for the lithium MHD system, but these devices are

Table 3.45 - Closed-Cycle Liquid-Metal MHD Instrument Subsystem Requirements

Subsystem	Sodium/Argon System	Lithium/Helium System
Cover Gas/Accelerating Gas Loop - impurity monitoring	O <sub>2</sub> - solid state electrolyte N <sub>2</sub> , H <sub>2</sub> , CO, CO <sub>2</sub> , C <sub>x</sub> H <sub>x+2</sub> - gas chromatography H <sub>2</sub> O - capacitance type moisture monitor	O <sub>2</sub> - solid state-electrolyte N <sub>2</sub> , H <sub>2</sub> , CO, CO <sub>2</sub> , C <sub>x</sub> H <sub>x+2</sub> - gas chromatography H <sub>2</sub> O - capacitance type moisture monitor
Liquid Metal Loop - impurity monitoring	O <sub>2</sub> - solid electrolyte oxygen meter H <sub>2</sub> - diffusion-type hydrogen meter N <sub>2</sub> - not currently commercially available	O <sub>2</sub> , H <sub>2</sub> , N <sub>2</sub> , C - technologically feasible but not currently available commercially
Ambient Environment - alkali-metal vapor detection	Na - sodium ionization detector (SID), technically proved, not commercially available	Li - lithium ionization detector, technically feasible not commercially available
Steam Generator - leak detection	H <sub>2</sub> O in argon - capacitance type moisture monitor Argon in H <sub>2</sub> O (steam) - mass spectrometric technique	H <sub>2</sub> O in helium - capacitance type moisture monitor Helium in H <sub>2</sub> O (steam) - mass spectrometric technique
Steam Generator - leak location	Eddy current testing and/or helium - mass spectrometric techniques	Eddy current testing and/or helium - mass spectrometric techniques

REPRODUCIBILITY OF THE  
ORIGINAL PAGE IS POOR

not currently available (Reference 3.143). Alkali-metal vapor detectors of the ionization type have not been tested in lithium systems; theoretically, these detectors should be applicable, but experimental verification is necessary.

#### 3.8.6.6 Instrument Subsystem Summary

A summary of the instrumentation subsystem requirements for monitoring impurities within the components of the liquid-metal MHD two-phase fluid is presented in Table 3.45. As noted, for the base case configuration utilizing sodium/argon as the two-phase fluid mixture, the required instrumentation is either currently commercially available or in the latter stages of development. The alkali-metal instrumentation requirements for the lithium/helium system are technologically feasible, but a strong developmental effort is required.

### 3.9 Materials for Open-Cycle MHD Systems

#### 3.9.1 Background

Open-cycle MHD power generation is a high-temperature process that has the theoretical potential to convert fossil fuels directly into electrical energy at high efficiencies. It is also the only advanced energy conversion technique that could directly use coal as a fuel. The combination of high temperatures, however, and the large quantities of coal ash constituents presents serious materials problems throughout the entire system. Some of these problems may be avoided, or their magnitude may be diminished (by use of separately fired air preheaters, cold generator walls, gasified or liquified coal as a fuel, etc.). In doing so, however, serious penalties are paid in reduced system efficiencies and/or in additional capital/operating costs. These material problems -- primarily questions on long-term materials durability -- are major obstacles to the commercial realization of coal-fired, open-cycle MHD power generation.

Not only are these material problems serious -- they are also poorly defined, mainly because the charged emphasis on the use of coal as a fuel is so recent. As a result, there are few facilities that either burn coal or simulate its burning. The tests conducted in these facilities are of short duration and are limited in scope. Finally, materials evaluation under these coal-fired MHD conditions is virtually nonexistent. Many programs are planned or have been initiated to provide the information and understanding necessary to select and apply materials to various components of the coal-fired MHD system. At this time, however, evaluation of the nature and magnitude of the materials problems in the coal-fired system is difficult and subject to speculation. The conditions in this system need to be qualitatively described.

The combustion of coal will introduce significant quantities of inorganic ash (up to 20% by weight of the coal) into the open-cycle MHD system. The composition and quantity of this ash will vary from coal to coal (as can be seen in the three coals considered in this study). During combustion, the inorganic ash constituents and the sulfur in the coal react with the alkali seed to produce a very complex and corrosive environment. While the gaseous seed products are allowed to pass downstream, the ash constituents can either be directed toward the cooler walls of the combustor where condensation occurs as a molten slag or be directed downstream (100% ash carry-over). In the former case, 80 to 95% of the ash products are removed from the system in the combustor, with the more volatile constituents being carried downstream. This variation in combustion conditions creates a difference in the quantity, by a factor of 5 to 20, and in the composition of the ash downstream. These two conditions, in turn, will effect the nature and magnitude of slag-seed corrosion throughout the system.

As the hot combustion gases pass from the combustor toward downstream components, their temperature begins to fall. As the gas temperature falls, and as these combustion products move into cooler

downstream components, various slag constituents begin to condense and deposit. This process occurs first on the walls of the generator itself. It continues downstream so that the chemistry of the slag layer varies in the axial direction of the system. At some point the seed also begins to condense. Upstream from this point, the slag will essentially be free of seed; downstream, as the temperature progressively decreases, the liquid and solid slag will contain increasing amounts of seed.

In the cooler parts of the MHD system, such as the heat recuperator and steam generator components, the deposits will contain liquid seed compounds, particularly potassium sulfate, which are corrosive to both metals and ceramics. In order that seed recovery be economical the condensation of ash and seed constituents must also occur in such a manner that very little seed (<5%) is trapped in the slag condensates.

While the corrosive problems associated with the presence of large quantities of ash have been regarded as very deleterious to long-term component life, the presence of a slag layer that lines the walls of components such as the combustor and generator may provide some beneficial effects. For example, there is generator experience (References 3.144 and 3.145), theoretical modeling studies of generator performance (Reference 3.146), and materials considerations (References 3.147 and 3.148) that indicate that generator durability and performance is improved by the formation of a continuous slag layer on the generator walls. While this is based only on short term tests (tens of hours), many MHD systems designers and materials specialists feel that full-scale, long-term operation of MHD generators must be approached on the basis of the presence of a protective slag layer on generator walls: and that considerable attention must be placed on the understanding of this layer's properties, its interaction with wall materials, its effect on generator performance, and so on. This concept will be discussed in more detail in the section on generator materials.

Therefore, the primary consideration for materials throughout the coal-fired open-cycle MHD system is their resistance to the corrosion and erosion by the ash- and seed-containing MHD environment. Although

there are other serious requirements such as electrical properties, thermal stress damage resistance, thermal fatigue, and so on, they must be regarded as secondary at this point.

Experiments are needed to demonstrate the durability of materials in various subsystems, and information is needed on the conditions found in the MHD environment, the nature of slag and seed condensates at various locations in the system, the properties of these deposits, and their interaction with various component materials. Little is known about many factors; programs are under way, however, at the National Bureau of Standards (Reference 3.149) and at Battelle's Pacific Northwest Laboratories (Reference 3.150) to characterize MHD slags and to measure their properties. Properties of interest are slag viscosity, surface tension, wettability, electrical conductivity, vaporization, and thermal conductivity. Knowledge about the corrosion resistance of various high-temperature materials to these slag/seed mixtures is also needed. There are virtually no such data available to make engineering estimates of lifetimes or maximum use temperatures of materials. Studies of this type are now under way at the University of Utah (Reference 3.151), Westinghouse (Reference 3.152), and the University of Tennessee Space Institute (Reference 3.153).

With this overview of the state-of-understanding of materials problems in coal-fired, open-cycle MHD systems, the following sections will discuss the state-of-the-art and the selection of materials for the major subsystems. The discussion in each section will first consider the selection of materials where a relatively clean (ash-free) fuel is used and, second, discuss the selection of materials in a system where large quantities of ash are present (i.e., where coal is burned). Selection of materials under clean conditions will center on considerations other than corrosion or erosion resistance, and selection under ash-containing conditions will focus on corrosion-erosion problems.



### 3.9.2 Combustor Materials

MHD combustors are judged primarily on the basis of the conductivity of the plasma that they generate. A value of conductivity between 5 and 10 mho  $m^{-1}$  is generally considered to be required for efficient MHD power generation. The conductivity is dependent upon plasma temperature; the minimum acceptable outlet temperature for an open cycle MHD combustor is 2600°K (4220°F) (Reference 3.154). A second requirement is one of high thermal efficiency or high fuel efficiency. A very large portion of the heat input in the fuel must appear as heat in the MHD plasma in order to benefit from high conversion efficiencies in the MHD power plant.

The role of refractory ceramic combustor linings is to aid in the achievement of the necessary plasma temperatures by reducing the heat losses through the combustor walls. In clean fuel systems several materials have been used with varying degrees of success -- for example, zirconia stabilized with magnesia, calcia or yttria, alumina, and magnesia. These materials have been used in various forms -- as concretes, castables, and as bricks. They should be fabricated to resist erosion and corrosion by the alkali-seeded gas stream and to resist thermal stress damage during operation. The selection of compositions is dependent on combustor design and operation. Stabilized zirconia is the most refractory, least volatile composition, but it suffers from poor thermal shock resistance and high cost, particularly if it is stabilized with yttria. Under clean fuel conditions, therefore, either established (A) or near-term (B) materials will be adequate for combustor linings.

While the combustors used in burning clean fuels are usually single-stage units, the combustors for burning coal or other ash-containing fuels can be more complex, containing two or three stages for complete combustion. This increased complexity is aimed at the removal of most (> 80%) of the ash in the combustor in order to reduce the corrosion problems in downstream components. The ash is removed by introducing a swirling action in the combustor, which causes the ash constituents in the gas stream to impinge on the cooler walls of the combustor. These

constituents condense as a molten slag which is drained from the combustor. If the combustor walls are water cooled, a slag layer several millimeters in thickness will build up. This slag layer can act as a refractory liner which both protects the outer metal wall and reduces heat losses (References 3.155 to 3.157). Tager and his co-workers (Reference 3.158) at the Krzizanovski Power Institute in Moscow have even intentionally added oxides such as calcia to produce a more viscous and thicker slag layer in order to further reduce heat losses.

The results of tests on a number of coal-burning combustors indicate that the combination of high temperature and the large quantities of molten slag presents serious corrosion (and erosion) problems to the use of any refractory ceramic liner. For example, Dicks (Reference 3.159) reported the severe degradation of zirconia brick after only 3.6 ks (1 hr) of operation in his axial plug flow cylindrical coal combustor. Both the British (Reference 3.155) and the Russians (Reference 3.157) indicate their feelings that the successful use of such linings is unlikely. Use of a low thermal conductivity refractory liner between the metal outer wall and the slag layer would be beneficial in terms of reducing thermal losses. The refractory-slag interface, however, must be maintained below the freezing point of the slag at all times, and the slag layer must adhere to the refractory. A possible approach in this direction that has not been tried would be to plasma- or flame-spray a dense slag coating on this liner before start-up.

Although designers have found the use of refractory liners to be beneficial in reducing thermal losses and in achieving desired plasma temperatures in systems burning clean fuels, their experience to date on coal-burning combustors, where these materials are used in the same manner, has resulted in severe corrosion by the coal slag. The incentive to pursue new materials, novel operating procedures, modified designs, and so on, to circumvent these problems is diluted by the fact that the slag layer itself can provide some of the desired benefits offered by refractory liners. The exception to this trend is the three-stage coal combustor designed by and under construction at the U.S. Bureau of Mines (Reference

3.156). This facility is specifically designed to use state-of-the-art materials (A, B, possibly C) while possessing high thermal efficiency and very high (>95%) slag rejection.

### 3.9.3 Generator Materials

#### 3.9.3.1 Electrodes

The development of suitable electrode and insulator materials has presented the greatest challenge to the materials technologist in the development of clean, fuel-fired, open-cycle MHD. These materials must possess certain electrical properties in addition to resistance to the severe environment. Specifically, the electrode materials in the MHD generator should meet the following requirements:

- 1) Adequate electrical conductivity ( $>10^{-1} \text{ ohm}^{-1} \text{ cm}^{-1}$ ) at current densities of more than  $1 \text{ A/cm}^2$ . This conduction should be primarily by electrons.
- 2) Good thermionic (electron) emission. Since electrons are being exchanged from the ionized gas, the anode and cathode should be good electron acceptors and emitters.
- 3) Corrosion resistance (to potassium seed).
- 4) Erosion resistance (to the high-velocity gases, to liquid droplets, and to particulates in the gas stream).
- 5) Good thermal conductivity (to provide for an adequate heat flux from the hot plasma to sufficiently cool the hot face of the electrode and to reduce thermal gradients and thermal stresses).
- 6) Oxidation (or reduction) resistance (stability in the MHD at oxygen partial pressures of 10.1 to 1013 Pa ( $10^{-4}$  to  $10^{-2}$  atm)).
- 7) Thermal stress damage resistance (resistance to crack and propagation in start-up and cool-down and at temperatures with high heat fluxes and temperature gradients).
- 8) Compatibility [to insulators, metal or ceramic current leads (with passage of dc current), cements, etc.].
- 9) Mechanical stability (creep resistance, thermal fatigue resistance).

10) Ease and cost of fabrication (must be realistic in face of the need to construct a full-scale MHD plant).

The development and evaluation of electrodes has involved three classes of materials: metals, oxide ceramics, and nonoxide ceramics. This work is reviewed in some detail in the literature (References 3.154 and 3.159 to 3.162) and will only be summarized in this discussion.

Water-cooled metal electrodes are attractive on the basis of ease of fabrication, electrical properties, mechanical properties, thermal conductivity, and so on; the cold surfaces, however, promote high thermal and electrical losses and permit seed condensation, which is believed to cause erratic and degenerative electrical performance. The most deleterious effects, however, arise from nonuniform current transfer (arcing) from the plasma across the cool boundary layer to the cold electrode surface. This arcing is localized and produces enhanced erosion because of the extreme localized heating. The combination of arcing and seed condensation leads to electrochemical erosion of the material and subsequent power losses. Seed condensation can be avoided by use of wall temperatures in excess of 1473°K (2192°F) (Reference 3.164). At these temperatures, however, most metals encounter severe oxidation. The only metallic compositions that have demonstrated promise at temperatures above 1273°K (1832°F) are cobalt-based superalloys tested by Bone (Reference 3.165) in the VEGAS generator, the unspecified oxidation resistant tungsten alloys used by the Soviets (Reference 3.166) in their U-25 generator, and a chromium-based cermet developed by Reynolds Aluminum (Reference 3.167). Bone estimates the maximum use temperature of the cobalt alloys as 1493°K (2227°F), and the Soviets indicate that the tungsten-chromium alloys have been used in the 1273 to 1773°K (1831 to 2731°F) temperature regime. The chromium electrode patented by Reynolds Aluminum has additions of thorium dioxide dispersed through it to enhance thermionic emission. It is claimed to have good slag resistance, and the volatility of chromium offers no difficulties if it is covered with slag.

A number of nonoxide ceramics have been developed and evaluated as electrodes in clean fuel-fired systems. These materials

are attractive in that they possess excellent electrical and thermal properties; they are limited, however, by their poor oxidation resistance above 1273°K (1831°F). The most promising compositions of this class ( $\text{SiC}$ ,  $\text{Mo}_2\text{Si}$ ,  $\text{ZrB}_2\text{-SiC}$ ) rely on the formation of a silica or a silicate protection layer for oxidation resistance. The reaction of this silica-based layer with potassium forms a fluid potassium oxide-silicon dioxide glass which limits the use of these materials to temperatures less than 1673°K (2551°F) (Reference 3.162). The thermionic emission of silicon carbide is also inadequate, and additions of such materials as molybdenum, titanium, and chromium have been used to improve this property (Reference 3.168).

Therefore, while metals are the most promising electrode materials in cold [ $<1273^\circ\text{K}$  ( $1831^\circ\text{F}$ )] wall channels, and oxidation resistant refractory alloys and nonoxide ceramics show promise in moderately hot [ $1273$  to  $1773^\circ\text{K}$  ( $1831$  to  $2731^\circ\text{F}$ )] channels, the only class of materials that show any promise in hot [ $>1773^\circ\text{K}$  ( $2731^\circ\text{F}$ )] channels are the refractory oxides. At these high temperatures both the problems of destructive arc erosion and seed condensation are avoided. Generator thermal and electrical losses are also reduced by operating the walls at these temperatures. Much effort has been directed toward developing refractory oxides with electronic conduction. The refractory oxides typically have very large band gaps, resulting in high resistivities. Two compositions have been identified that have both high-temperature stability and adequate electrical conductivities to serve as hot MHD electrodes. These compositions are based either on zirconium oxide or on the rare earth perovskite-structured chromites. The development and properties of each are reviewed in detail elsewhere (References 3.159, 3.161, and 3.169 to 3.171). This discussion will briefly summarize the experience with these oxides, including that of the Soviets with both materials.

Compositions based on zirconia received early attention as potential MHD electrode materials. Additions of calcium oxide or yttrium oxide were found not only to stabilize zirconium oxide but also to provide for conductivities that are adequate to meet electrode requirements

above 1373°K (2011°F). Because this conduction is almost entirely ionic there is degradation of these compositions with time by electrolysis at even moderate ( $\sim 1 \text{ A/cm}^2$ ) current densities (References 3.159, 3.172, and 3.173). This deficiency can be avoided, in part, by the use of electrode designs incorporating metallic fibers, pins, or screens which will reduce the local zirconium oxide current density with the metal carrying the major portion of the current (References 3.174 and 3.175). Although calcia- or yttria-stabilized zirconia electrodes can function satisfactorily for tens or even hundreds of hours, they are not the solution for hot electrodes for long-duration MHD plants. The conduction of these materials must be predominantly electronic in nature to prevent electrolysis and electrode degradation.

Additions of rare earth oxides such as cerium oxide, praseodymium oxide, neodymium oxide, and lanthanum oxide produce varying degrees of electronic conductivity in zirconia compositions. The Soviets have spent considerable effort in developing an electronically conducting zirconia, based on ternary compositions of zirconia and rare earth oxides. Although they have revealed no information as to the composition of these electrodes, it has been claimed that they have operated successfully for hundreds of hours at temperatures close to 2273°K (3631°F) at current densities of more than  $2 \text{ A/cm}^2$  (Reference 3.176). It appears that the major obstacle to the full development of zirconia-based compositions as suitable electrode materials is the identification of a suitable current lead material. Since the conductivity of these rare earth zirconias is very temperature dependent, they become resistive and subject to large voltage drops and joule heating at temperatures below 1273°K (1831°F). Proper selection of suitable materials to carry the current ultimately to copper wire becomes important. Selection of these materials must be made on the basis of compatibility with the passing of direct current at moderately high current densities. One possible solution (Reference 3.177) is a composite electrode consisting of an electronically conducting zirconia bonded to a ceramic ( $\text{Nb}_2\text{O}_5$  doped  $\text{CeO}_2$ ) current lead material that has high conductivity at

moderate [873 to 1472°K (1614 to 2691°F)] temperatures. The ceramic current lead material is, in turn, bonded to an oxidation resistant alloy (similar to the Inconel series).

The rare earth chromites when doped with alkaline earth oxides are unique as oxides in that they possess both high electronic conduction, even to room temperature (see Figure 3.28), and very high melting points.

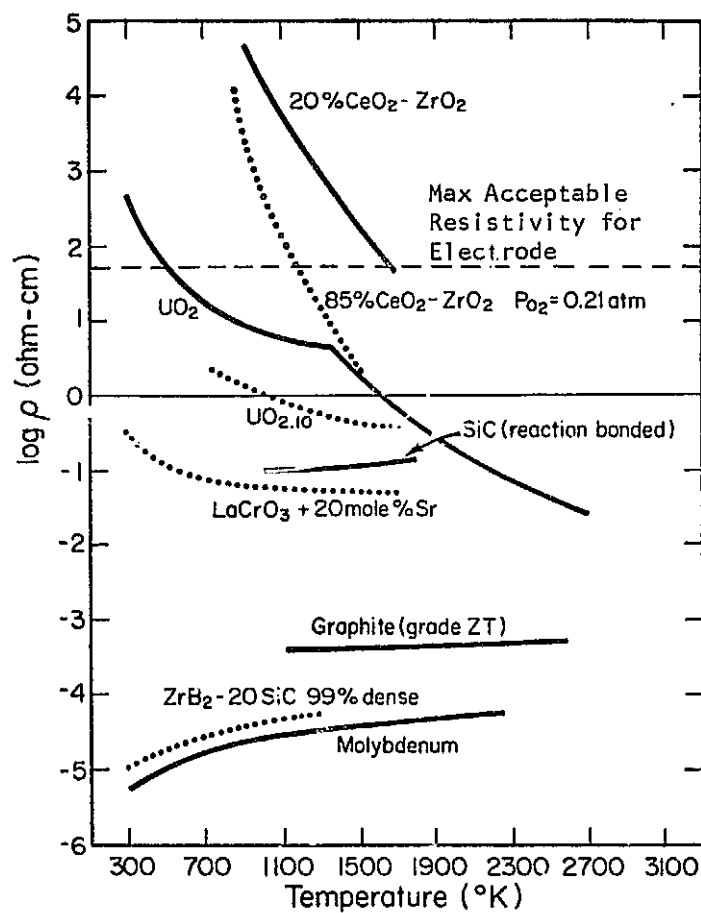


Figure 3.28 — Resistivity of electrode materials (Reference 3.147).

While these materials possess other very desirable features, such as a small resistivity variation with temperature and the possibility of making the current lead contact at low temperatures, they are limited in maximum use temperature by the preferential volatilization of chromium (Reference 3.178). The extrapolation of vaporization data for  $\text{La}_{.8}\text{Sr}_{.2}\text{CrO}_3$  to higher temperatures predicts that vaporization losses would limit this material's use to approximately 2023°K (3181°F) (where recession rate 317 pm/s (1 cm/yr).

Meadowcraft and Wimmer (Reference 3.179) also reported data on a few other compositions that suggested that either substitution of magnesium or calcium for the strontium and of aluminum for part of the chromium would further reduce vaporization rates. In fact, one composition ( $\text{La}_{.2}\text{Ca}_{.8}\text{Cr}_{.75}\text{Al}_{.25}\text{O}_3$ ) had a vaporization rate seven times lower than  $\text{La}_{.8}\text{Sr}_{.2}\text{CrO}_3$  at 1873°K (2911°F) under the same conditions. These results would suggest a possible increase in use temperature of 200°K (360°F). It should be noted that these compositions were not measured for electrical resistivity and that some caution must also be applied in the extrapolation of these data.

Recent work (Reference 3.180) by the Indian Atomic Energy Commission on  $\text{LaCrO}_3$  demonstrated an increase of approximately 200°K (360°F) in maximum operating temperature by substitution for strontium by other (unidentified) dopants. Electrodes of these compositions were operated in an oxygen-gas flame for tens of hours at 2273°K (3631°F) without significant loss of material. The high melting point, plus reasonable vaporization rates at very high temperatures, puts  $\text{LaCrO}_3$  and possibly other rare earth chromites in the unique position of having a very low resistivity at room temperature coupled with high-temperature use capabilities. This is shown graphically in Figure 3.29 which depicts the useful temperature range of several possible electrode materials. The maximum use temperature is defined by the melting point or temperature where vaporization losses become appreciable; the minimum use temperature is defined by the temperature at which the resistivity is equal to 50 ohm-cm. The ideal electrode material would be one that



is stable at very high temperatures and yet has adequate low-temperature conductivity for coupling to metal current leads at temperatures approaching room temperature.  $\text{LaCrO}_3$ -based compositions are unique as oxides in meeting both of these requirements. Therefore, although both zirconia and rare earth chromite compositions show promise as electrodes, both require further development for long duration 36 Ms ( $\sim 10,000$  hr) use at temperatures approaching  $2273^\circ\text{K}$  ( $3631^\circ\text{F}$ ).

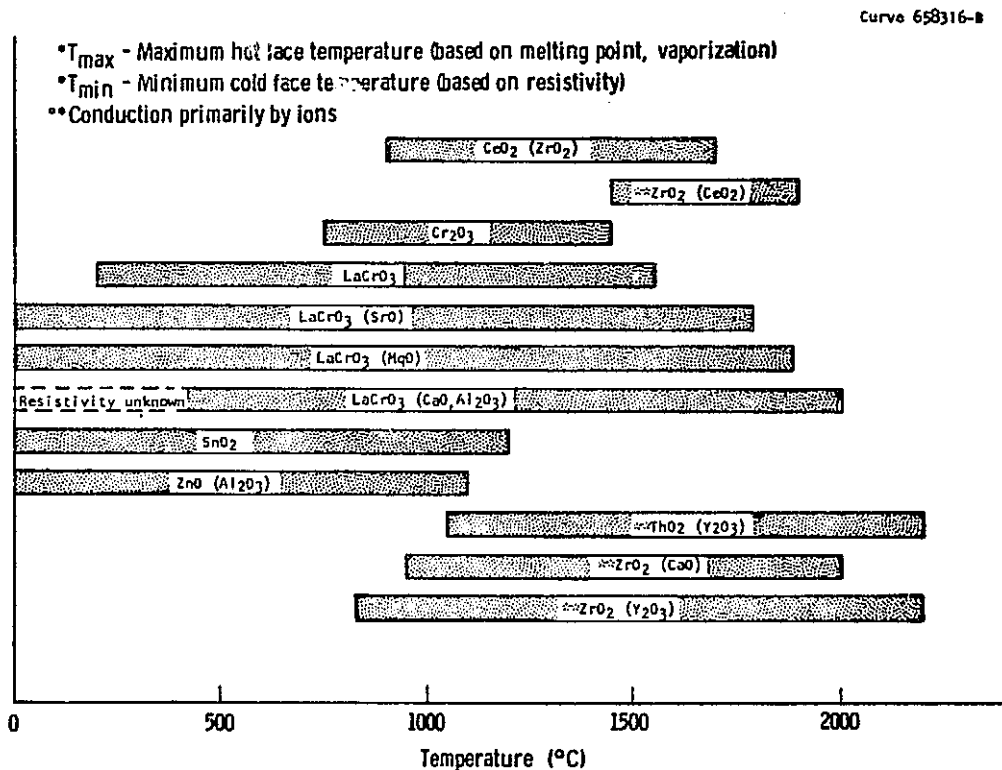


Fig. 3.29—Useful temperature range of several possible electrode materials

In summary, in the past fifteen years much experience has been accumulated with the use of electrodes whose surface temperatures vary from a few hundred to 2273°K (3631°F). Although substantial progress has been made, a workable electrode for long-duration use in clean fuel-fired generators does not exist today. Some of the most serious problems are located not at the hot surface but rather at the cold surface of the electrode. Serious attention must be given to the current lead problem. When the 36 Ms (10,000 hr) electrode is developed, it will be the result of a coupling between materials development and electrode design.

### 3.9.3.2 Insulators

High-temperature electrical insulation materials, either the insulating sidewalls or the interelectrode insulators, must meet requirements 3 through 10 outlined for electrodes in the previous discussion (Section 3.9.2). Insulators must provide the necessary electrical insulation by having resistivities greater than 100 ohm-cm and dielectric breakdowns greater than 4 kV/m (1.22 kV/ft) at temperature. Insulation materials have not been the subject of studies as extensive as those of electrode materials. Reviews of the literature (References 3.154, 3.159, 3.161, and 3.162) also indicate that insulator development has been limited to the following oxides: alumina, magnesia, and the zirconates of calcium and strontium. Beryllium oxide has been used in at least one study (Reference 3.181), but it generally has been discounted due to its toxicity. Aluminum oxide has excellent high-temperature insulation properties but reacts with potassium at temperatures above 1573°K (2371°F) to form  $K_2O \cdot 11Al_2O_3$  (potassium  $\beta$ - $Al_2O_3$ ) (References 3.182 and 3.183). Strontium and calcium zirconates are very refractory [melting points >2573°K (4171°F)], possess good seed resistance, but suffer from poor thermal shock resistance due to a very low thermal conductivity. Magnesia has, thus, been generally used as the insulating material in hot- or moderately hot-wall channels, and alumina has been used in cold-wall channels.

A major problem encountered with insulation materials is the penetration of seed compounds into the pore structure of insulator ceramics. Seed penetration produces two deleterious effects: the degradation of insulator resistance at temperature (Reference 3.184), as shown in Figure 3.30, and the catastrophic failure of the insulator due to the reaction of these compounds, primarily potassium carbonate, with water vapor in the atmosphere after cool-down (Reference 3.185). These reactions result in a 40 to 60% volume increase and the generation of large stresses which lead to disintegration of material. The critical temperature range occurs where potassium carbonate is a liquid, in other words, 1073 to 1473°K (1972 to 2692°F). The Soviets (Reference 3.186) have given serious attention to this problem in terms of developing microstructures that minimize this penetration yet are thermal-shock resistant by using special insulator designs and by controlling start-up and shutdown procedures to minimize seed penetration.

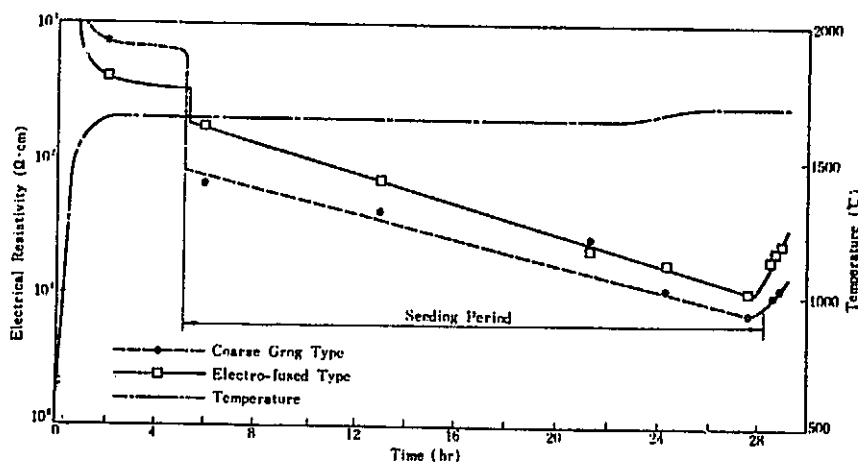


Figure 3.30 — Time dependence of resistivity of MgO refractories under a MHD condition (Reference 3.184).

Attempts to reduce or eliminate the condensation and penetration of seed compounds into the generator walls by blowing gas into the generator

through cracks or through porous ceramic bodies have been reported by several investigators (References 3.184, 3.187, and 3.188). While success has been claimed both in reducing material recession rates (by two orders of magnitude with  $ZrB_2$ ) (Reference 3.187) and in reducing thermal stresses (Reference 3.181), this technique has not been demonstrated on a large scale over long time periods. Two problem areas are apparent with this technique: fine control is required in the gas blowing process, and the boundary layer can become resistive with the injection of cool, potassium-deficient gases. The Soviets are currently applying this technique to their magnesium oxide insulating walls. A porous (18 to 24%) magnesia with pore size of 30 to 50  $\mu m$  has been developed that satisfactorily allows for the injection of a gas in laboratory test rigs (Reference 3.172).

A second technique that has been used to maintain generator walls is the so-called replenishment technique (Reference 3.189). Replenishment of the generator walls is made either intermittently or continuously by injecting mixtures of various oxides into the gas stream in the combustor. These oxides then condense out on the generator walls, replacing material that has been removed by erosion, corrosion, and so on. Again, this technique has not been proved for long-duration tests.

The use of ceramics as electrodes or insulators in the generator duct also poses serious problems with respect to the thermal stress damage of these materials. Studies on a number of materials indicate that, given the range of thermal conductivities of most oxide ceramics, the thickness of electrodes and the insulators would be relatively small, ranging from a few to 25 mm (0.04 to 1 in) in thickness. The temperature gradient imposed on these thin sections is severe, of the order of 100°K/mm (4572°F/in) or more. These gradients will impose high thermal stresses on these materials which can lead to failure in use at temperature. In addition, there is a danger of failure due to thermal shock during start-up and shutdown.

Thermal stress damage resistance can be built into a given ceramic composition by development of suitable microstructures. These microstructures are based on criteria developed for crack propagation (Reference 3.190). Materials with low strength combined with high values of elastic modulus and high ratios of the energy to propagate a crack to the energy required to initiate a crack (Reference 3.191) are resistant to thermal stress damage. Microstructural features that are desired include 15 to 25% porosity, a wide variation in grain sizes (Reference 3.192), and the presence of second phases and microcracks (Reference 3.193). These microstructures are in conflict with those required for both corrosion and erosion resistance, where high density, in particular, is required; while recognizing these trade-offs, optimum microstructures must be developed.

Some of the thermal stress requirements can also be reduced by good design. For example, the Soviets have found that the sizes of various ceramics must be kept to below certain critical dimensions. For magnesium oxide, this is approximately 38.1 mm (1.5 in).

The requirements of minimum seed penetration, thermal stress damage resistance, and erosion resistance require significant efforts in ceramic processing. The Soviets are devoting much effort on ceramic processing to produce the ceramics needed for their U-02 and U-25 test facilities. Not only have monolithic bricks been developed, but also high-temperature cements, concretes, and coatings. The need for ceramics whose properties are tailored for various MHD applications has not been fully appreciated in this country, and the failure of materials in many cases can be laid to the use of off-the-shelf materials.

In summary, while the materials problems in the clean fuel-fired MHD generator are far from the solutions required for a base-load plant, there have been significant advances in the past decade, particularly due to the large materials effort at the High-Temperature Institute in Moscow. There exists a wide selection of materials for use over a range of generator wall temperatures. These electrode and insulator materials are shown in Table 3.46, with maximum use temperatures, their limitations, and their material application ranking (see Section 3.1).

Table 3.46 — Recommended Generator Materials for Use  
with Clean Fuels

<u>ELECTRODES</u>			
<u>Maximum Use Temperature °C</u>	<u>Material</u>	<u>Limitations</u>	<u>Material Application Rating</u>
500	Copper	<u>a</u> , o	C
700	Stainless steel	<u>a</u> , o	C
900	Inconel	<u>a</u> , 0	C
1200	Co-based alloys	o	D
1200(?)	W-Cr alloys	o	D
<1500	Cr-ThO <sub>2</sub> alloys	v	D
1350	Mo <sub>2</sub> Si	o plus k	D
1350	SiC	o plus k, <u>+</u>	C
1350	ZrB <sub>2</sub> -20 w/o SiC	o plus k	C
1600	CeO <sub>2</sub> -2 w/o Ta <sub>2</sub> O <sub>5</sub>	v	D
1800	ZrO <sub>2</sub> -18 m/o CeO <sub>2</sub>	<u>i</u> , v	D
1900+	ZrO <sub>2</sub> -RE <sub>2</sub> O <sub>3</sub>	v	C
1700	La <sub>.8</sub> Sr <sub>.2</sub> CrO <sub>3</sub>	v	C
1950	La <sub>.8</sub> Ca <sub>.2</sub> Cr <sub>.75</sub> Al <sub>.25</sub> O <sub>3</sub>	v	D
2000	ZrO <sub>2</sub> -10 m/o Y <sub>2</sub> O <sub>3</sub>	<u>i</u> , <u>ts</u>	C

<u>INSULATORS</u>			
<u>Maximum Use</u>	<u>Material</u>	<u>Limitations</u>	<u>Material Application Rating</u>
1300	Si <sub>3</sub> N <sub>4</sub>	o plus k	C
1300	Al <sub>2</sub> O <sub>3</sub>	k	B
1700	SrZrO <sub>3</sub>	<u>ρ</u> , <u>ts</u>	C
1700	CaZrO <sub>3</sub>	<u>ρ</u> , <u>ts</u>	C
1800	MgO	v, <u>ρ</u>	B-C

Legend: i - ionic conduction      e - electrochemical reactions  
 o - oxidation                      t - thermionic emission  
 v - vaporization                  a - arc erosion  
 k - seed reactions                ρ - resistivity  
 - designates a limitation      ts - poor thermal shock resistance  
     at all temperatures

### 3.9.3.3 Coal-Fired MHD Generator Materials

The direct use of coal as the fuel in the MHD system requires a reevaluation of materials for the generator channel. The ash constituents introduced into the system by the combustion of coal will condense in various parts of the system as a corrosive liquid slag. The corrosion of refractory duct materials is shown schematically in Figure 3.31 where the recession rate of a given material is plotted against temperature. When only the alkali seed is present, there is loss of material in the temperature range where the seed is present as a liquid. The Soviet MHD specialists term this the forbidden region, or a temperature regime to be avoided during operation, not only because of corrosion but also because of the interelectrode shorting caused by the conductive potassium compounds.

When both seed and slag are present, the temperature region for liquid formation and vigorous corrosion extends several hundred degrees higher, due to the lower volatility of slag components. The composition of this liquid slag also varies with temperature. Below 1673°K (2551°F), it will contain large amounts of potassium sulfate which will act as the primary corrosion agent; while at higher temperatures potassium sulfate will vaporize into the gas stream, and corrosion will be due to the alumino-silicate slag. This situation is complicated by thermal gradients across the slag layer, by variations in slag chemistry and temperature in the axial direction of the duct, by chemical segregation due to electric current, and so on.

A slag layer that coats the generator walls will affect both material (generator) durability and generator performance. Since both of these factors are requirements of base-load, open-cycle plants, several questions must be addressed. Can both requirements be met? What are the trade-offs? What is the optimum wall temperature? What effect will operating conditions such as gas velocity, gas temperature, combustor slagging conditions, and so forth, have on generator durability and performance? Currently both MHD generator and materials specialists are

C-3

putting considerable effort into experimental and theoretical studies to answer these questions, which are crucial to the success of coal-fired MHD power generation.

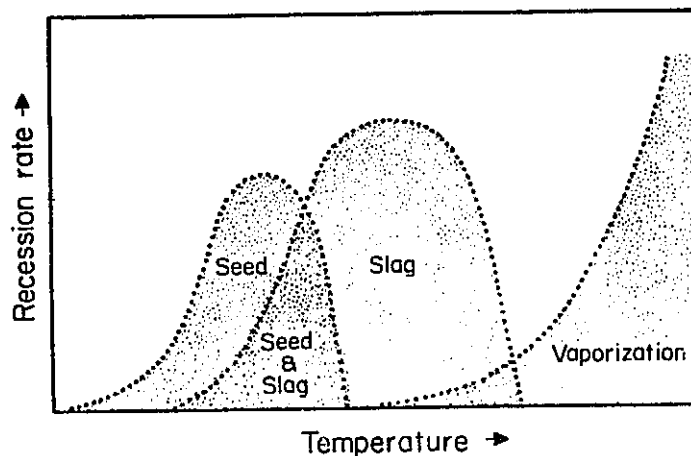


Figure 3.31 — Schematic recession rates as a function of temperature (Reference 3.147).

Presently, there are two general approaches taken in dealing with coal-fired generator problems: the protective slag layer approach and the high slag rejection-hot wall approach. The former approach is advocated by a majority of both MHD generator and materials specialists. In part this is because this approach may be viewed as an extension of the electrode replenishment scheme developed several years ago (Reference 3.189). This concept allows for the formation of a continuous slag layer which coats the generator walls. To be successful this layer must be controlled by the use of suitable modifiers. Extensive information on slag chemistry, slag properties, and slag reactions with other materials will be required. Properties such as electrical and thermal conductivity, viscosity, surface tension, wettability, vaporization, phase equilibrium, and so on, are particularly important in determining the effect that a slag layer will have on generator performance.



A schematic diagram of a slag-coated generator wall is shown in Figure 3.32. Also included are representations of the variation in temperature, electrical conductivity, composition, potassium concentration, viscosity, and the activity of oxygen and sulfur from the base electrode to the plasma.

The thickness of this slag layer has been both calculated (Reference 3.146) and measured (References 3.144 and 3.145) to be of the order of 1 mm. The temperature at the slag-plasma interface is primarily dependent upon slag viscosity and channel aerodynamic conditions and is somewhere near 2000°K (3140°F) (Reference 3.199). The temperature at the electrode-slag interface is controlled by the thermal flux through the electrode wall. Channels with significant amounts of water cooling, such as at U.T.S.I. (Reference 3.144), operate where this temperature is only a few hundred degrees centigrade. In this case, the slag at the electrode surface is frozen, and corrosion would be expected to be minimal. At these temperatures, however, a penalty is paid in terms of voltage drops through the resistive slag layer.

Rosa (Reference 3.194) has calculated acceptable values of resistivity for channel coatings (approximately 1 mm (40 mils) thick) as a function of temperature (see Figure 3.33). The upper limits are based upon voltage considerations, and the lower limits are based on interelectrode current leakage considerations. Electrical resistivity data reported by the National Bureau of Standards (Reference 3.148) indicate that MHD slags fall into the allowable regions. Maxwell (Reference 3.146) has also considered the effect of resistive coatings on generator performance on both a theoretical and experimental basis. This work indicates that resistive layers even out the current concentrations on electrode surfaces that lead to destructive arcing. Maxwell's calculations also indicate that the joule heating of resistive layers will become significant if resistivities become too high. This analysis appears to explain the performance of cold-wall (Reference 3.144) and moderately hot-wall (Reference 3.170) generators with resistive wall coatings.

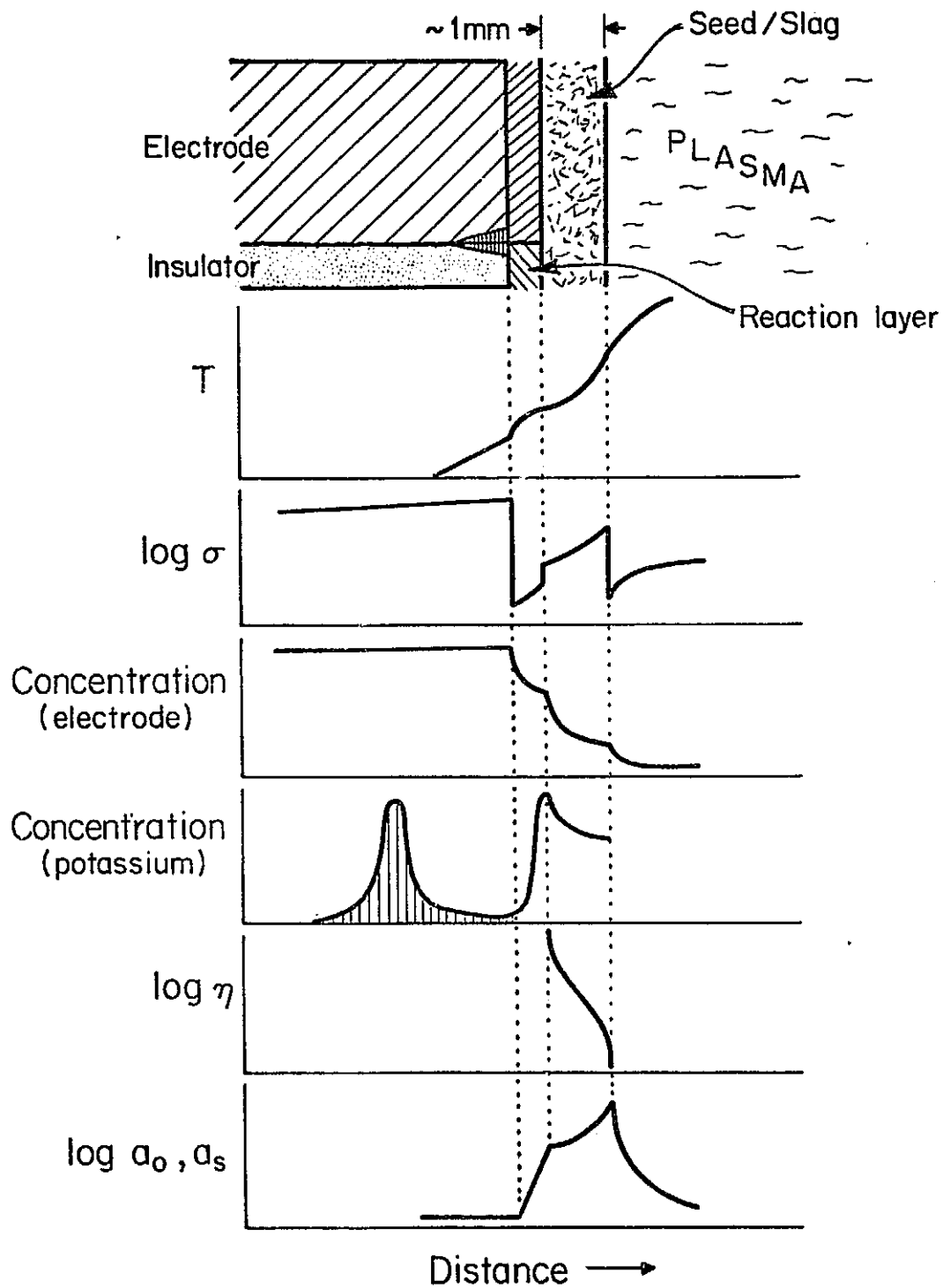


Figure 3.32 — Schematic of property profiles  
(Reference 3.147).

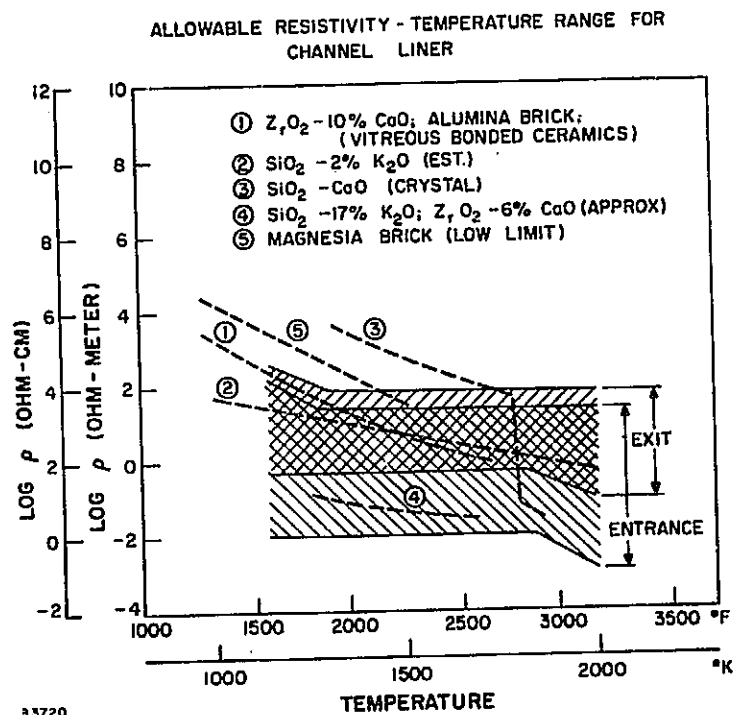


Figure 3.33 —Envelope of allowed values of resistivity vs temperature (Reference 3.194).

Generator experience with slag-coated walls is very limited at present; clearly, more information of a longer term nature is needed to demonstrate the effect of the slag layer on generator performance and durability. The question of the optimum electrode surface temperature appears to be crucial. If adequate generator performance over a long duration can be demonstrated at temperatures below 1273°K (1831°F), metal electrodes may be used satisfactorily. If temperatures above 1273 to 1473°K (1831 to 2191°F) are required, however, ceramic electrodes will be preferred, and the problem of corrosion by seed and slag compositions must be seriously addressed.

Corrosion of refractory oxides by alumino-silicate slags is a serious problem. For example, if a simple two component  $\text{Al}_2\text{O}_3$ - $\text{SiO}_2$  slag is considered, liquid formation due to the reaction of the oxide insulators in Table 3.46 will occur at 1703 to 1873°K (2605 to 2911°F) (Reference 3.195). Presence of other oxide components in the slag would further lower these temperatures. Corrosion studies at the University of Utah (Reference 3.171) have shown an exponential increase in corrosion rates with temperature. Alumina, the most corrosion resistant material tested, loses 1 mm (0.040 in) of material at 1723°K (2941°F) and 400 mm (15.75 in) at 1823°K (2821°F) in a 3.6 Ms (1000 hr) test.

The corrosion rate is governed by several factors: slag composition, equilibrium solubility of the refractory in the slag, temperature gradient, grain size, porosity, grain boundary phases, and so forth. Although corrosion can be controlled by either the interface reaction or by diffusion through the slag layer, in the case of corrosion of refractories by slags, the latter is the rate-controlling step. The dissolution is governed by the flux of material,  $J$ , according to Fick's Law

$$J = -D \frac{\Delta C}{\Delta X}$$

where  $D$  is the diffusivity of the slowest species through the effective boundary layer thickness  $\Delta X$ . The concentration gradient,  $\Delta C = C_e - C_s$ , is the difference between the equilibrium saturation concentration (electrode components in the slag),  $C_e$ , and the steady-state composition of that component in the slag beyond the boundary layer,  $C_s$ . Since diffusivity and viscosity (or fluidity) are intimately related in slags, corrosion rates are usually found to be particularly sensitive to slag fluidity (or viscosity (Reference 3.196), as shown in Figure 3.34.

In order to achieve long-term generator operation under slagging wall conditions, the following measures have been proposed (References 3.147 and 3.148) to reduce the corrosion rates of generator materials: 1) control of gas-phase and slag-seed layer compositions and 2) control of electrode composition, surface temperature, and microstructure. The

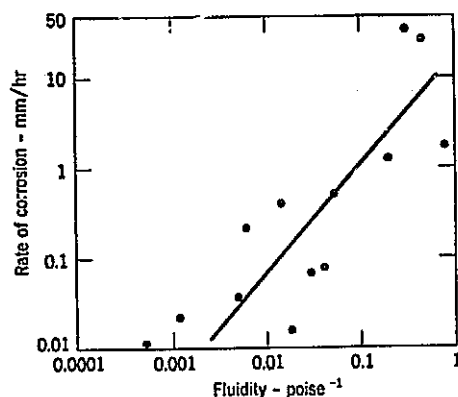


Figure 3.34 — Relation between slag attack and fluidity (Reference 3.196).

effect of these factors has been reviewed by Bowen (References 3.147 and 3.197). In effect, these measures all reduce  $J$ , the flux of material being transported by either increasing  $\Delta X$  or decreasing  $D$  and  $\Delta C$ . The most significant changes in the corrosion rate can be obtained by reducing  $\Delta C$  to zero. This is accomplished by adding additives such as zirconium oxide to the slag or gas phase when zirconia electrodes are used or chromium oxide when chromite electrodes are used. It also suggested that compatible insulator materials such as zirconate insulators with zirconium oxide electrodes and silicon nitride or Sialon insulators with silicon carbide electrodes (Reference 3.197) be used.

This line of reasoning leads to the concept of electrode (and insulator) compositions in equilibrium with the slag. Bowen and his co-workers (Reference 3.197) have identified hercynite ( $\text{FeAl}_2\text{O}_4$ ) as such a compound. Hercynite appears to have adequate high-temperature electronic conductivity and has been identified in one partially crystallized MHD slag (Reference 3.198) where eastern coal has been burned. To provide for good, low-temperature conductivity it is proposed that hercynite be graded with hematite ( $\text{Fe}_3\text{O}_4$ ) which has a resistivity of  $10^{-2}$  ohm-cm at room temperature. Hematite, in turn, is in equilibrium with iron at room temperature. This electrode, therefore, would consist of several compositional gradations:  $\text{FeO}_x\text{-Al}_2\text{O}_3\text{-SiO}_2$  slag to  $\text{FeAl}_2\text{O}_4$  to  $\text{Fe}_3\text{O}_4$  to Fe metal. The

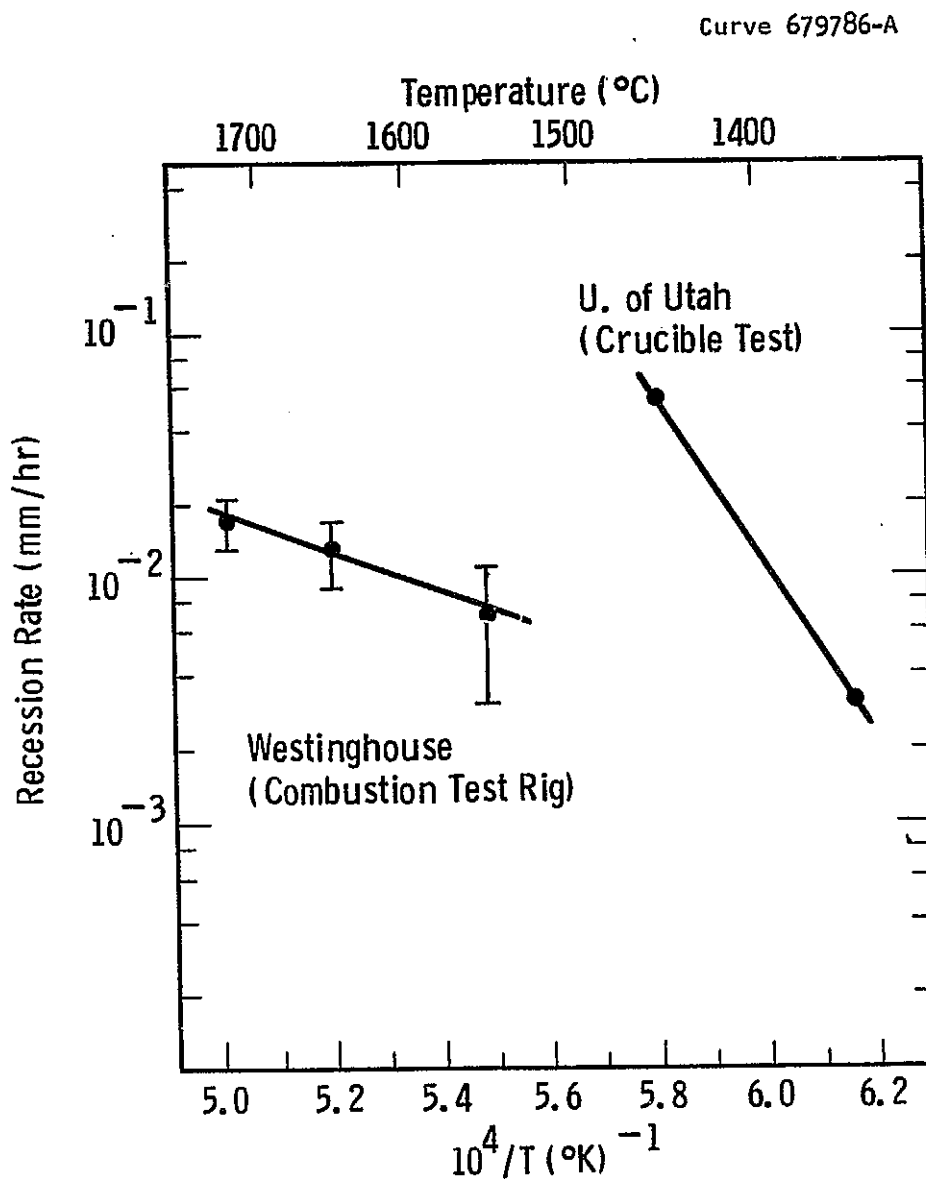


Fig. 3.35 —Recession rate of a 98% purity commercial MgO versus temperature (Ref. 9-9)

slag layer can be looked at as part of the electrode structure. Materials compatibility has been considered from the slag layer to metal current lead, in this example.

The second approach to coal-fired-generator operation is to reject most (>90%) of the slag in the combustor and to run the generator walls very hot [ $>1973^{\circ}\text{K}$  ( $3092^{\circ}\text{F}$ )] to minimize condensation of slag. The injection of gases through the generator wall to further aid in the prevention of slag condensation has also been suggested (Reference 3.199). The choice of materials that may be used under these conditions is limited to the refractory oxides, and possibly to the carbides and borides, by the injection of a neutral boundary layer gas. The presence of a continuous slag layer at this temperature is expected to result in excessive amounts of corrosion. Recent tests at Westinghouse (Reference 3.152), however, as shown in Figure 3.35, indicate that recession rates are dramatically reduced under conditions of reduced (10%) ash carry-over as compared to 100% ash carry-over. Analysis of these test samples indicates that at these ash carry-over levels and wall temperatures a continuous slag layer does not build up, but rather the slag-seed condensates are in the form of isolated droplets which cover the wall surface. These results are preliminary in nature, and further testing is required to demonstrate the effect of the amount of ash carry-over, wall temperature, and the like, before any definite conclusions are drawn.

In summary, the corrosive conditions in the coal-fired MHD duct are very severe; the identification of operation conditions, protection techniques, and materials to allow for long duration generator operation is a challenge to both materials and MHD specialists. From a materials viewpoint, coal-fired MHD generators are at the same point as clean fuel-fired MHD generators were in the early sixties: a few novel materials have been proposed, and programs to evaluate materials under real or simulated conditions have begun. When promising materials are identified they will require optimization with respect to their resistance to corrosion, erosion, and thermal stress damage (Reference 3.200). Although the selection of materials is speculative at this time, a list of possible electrode and insulator materials for the coal-fired generator

Table 3.47 — Possible Electrode and Insulator Materials for Use in Fired MHD Generators

ELECTRODES

With Slag Layer  
(T < 1500°C)

Copper

Inconel

$\text{Fe}_2\text{Al}_2\text{O}_4$

SiC

$\text{ZrB}_2/\text{SiC}$

Slag-Coated Mo or W

Graphite

High Slag Rejection-  
Hot Walls (T > 1500°C)

$\text{CeO}_2\text{-ZrO}_2$

$\text{La}_{.8}\text{Sr}_{.2}\text{CrO}_3$

$\text{MgCr}_2\text{O}_4$

SiC } with neutral  
ZrB<sub>2</sub> } gas  
          } protection

$\text{UO}_2$

INSULATORS

With Slag Layer

$\text{Al}_2\text{O}_3$

MgO

$\text{Si}_3\text{N}_4$  or Sialon

$3\text{Al}_2\text{O}_3 \cdot 2\text{SiO}_2$

$2\text{MgO} \cdot \text{SiO}_2$

High Slag Rejection  
Hot Wall

MgO

$\text{SrZrO}_3$

$\text{CaZrO}_3$



is shown in Table 3.47. With respect to several-thousand-hour lifetimes, they must be ranked, at this time, as 'D'.

### 3.9.4 Air Preheater Materials

#### 3.9.4.1 High-Temperature Air Preheaters

The air preheater is an essential auxiliary component to any MHD energy conversion system. These air preheaters provide hot air to the combustor so that high combustion temperatures can be achieved. The performance of the entire MHD cycle is dependent upon the temperature of the preheated air; in other words, a 5 to 6% increase in plant efficiency can be realized by raising the air temperature from 1273 to 1773°K (1831 to 2732°F). There are various types and designs of air preheaters. For example, the air can be heated directly by the combustion gases from the MHD channel or indirectly using a separately fired system. These two preheater types can be of two basic designs: the recuperative or the regenerative (intermittent). The recuperative heater requires an exchange of heat between two adjacent flow channels (i.e., for the exhaust gases and air). A pressure differential of 405.2 to 911.7 kPa (4 to 9 atm) exists between the two channels; this differential necessitates the use of low-permeability materials and pressure seals. Current state-of-the-art recuperators use metals and are limited to temperatures of approximately 1173°K (1652°F) because of creep, thermal fatigue, and so on. Although ceramic recuperators have been seriously considered, none has yet been built and operated. The major difficulties in using ceramics are their brittle nature, poor thermal conductivity, sealing joints, and the like. The thermal conductivity and thermal shock resistance of oxides is poor, so consideration of ceramic recuperator materials would be limited to nonoxides such as silicon carbide. A recuperator using silicon carbide could be used to temperatures approaching 1773°K (2732°F) in an atmosphere containing only combustion gases, and to temperatures less than 1573°K (2372°F) where seed or slag are present.

The regenerative air preheater has received the most attention for preheating air in MHD systems. The regenerative air preheater experiences cyclic conditions with rapid changes in flow rates, pressures, and temperatures. Switchover valves are required which also will be subjected to rapid temperature changes and large pressure changes and have moving parts. The heat storage materials in the regenerative air heater consist either of checker brick or ceramic pebbles. Multiple regenerator units are required, and the total volume of refractories is large. Lifetime and cost is, therefore, very important.

Regenerative air preheater technology is built upon the experience gained in the operation of stoves for steel plant furnaces and of ceramic stored-energy heaters for supersonic aircraft simulation facilities. Steel plant stoves operate currently at 1773°K (2732°F) for thousands of hours, and stored-energy heaters have been used as high as 2453°K (3956°F) with no major difficulties (Reference 3.201).

Several regenerative air preheaters have been built for MHD systems; the most noteworthy are those providing 1473°K (2192°F) oxygen enriched air for the U-25 facility (Reference 3.202), the pebble bed air preheater for the U-02 facility, which has operated successfully for over 25.2 Ms (7000 hr) at 1973°K (3092°F) and for shorter durations at 2273°K (3632°F) (Reference 3.185), and the moving bed preheater at Swierk, Poland (Reference 3.203). These are all separately fired preheaters which are subjected to exposure only by combustion gases (no alkali seed). While both cored brick and pebble bed preheaters have been operated over a wide range of temperatures, the latter have been found to be less satisfactory because of pressure drop, dusting, lumping of the bed, bed compaction, and low performance (Reference 3.204). These problems would be further aggravated by the presence of seed and slag.

Checker or cored brick preheaters would be constructed of more than one material in order to match the properties of certain refractories with the requirements in specific temperature ranges in the air preheater. Table 3.48 demonstrates the trade-offs encountered in the choice of these materials. The maximum use temperature is generally determined by high-

temperature mechanical strength or creep. Table 3.48 shows that combinations of different materials must be used to minimize the cost of materials.

Table 3.48 —Air Preheater Materials

<u>Material</u>	<u>Maximum Use Temperature (°C)</u>	<u>Approximate Cost Per Standard 9" Brick</u>
High $\text{Al}_2\text{O}_3$ (70-90%) Firebrick	1400	\$ 0.50
MgO (98%)	1700	1.60
$\text{Al}_2\text{O}_3$ (99%)	1700	4.20
CaO or MgO stabilized $\text{ZrO}_2$	1900	44.00
$\text{Y}_2\text{O}_3$ stabilized $\text{ZrO}_2$	2100	150.00

In addition to the heat storage materials, the walls for the air preheater will pose some serious design and material problems. The walls will be constructed of more than one material to resist corrosion, to reduce heat losses, and to contain high-pressure gases. The temperature gradient in the radial direction will be large, introducing large thermal stresses. Seed and slag penetration through cracks and joints will also be a problem (Reference 3.205).

#### 3.9.4.2 Material Requirements for MHD Air Preheater

There are a number of properties that are critical to the economical, long-term operation of MHD air preheaters. Specifically they are:

- 1) Corrosion and erosion resistance to combustion gases, seed, and slag at high temperatures
- 2) Thermal stress damage resistance during start-up, cycling, and shutdown
- 3) Resistance to creep at high temperatures
- 4) High compressive strength at high temperature

- 5) Resistance to air pressure differentials and to cyclic changes in oxygen partial pressures
- 6) Low cost due to the large quantities of refractories required.

These requirements must be maintained with respect to the demands of other requirements (e.g., compressive strength must be maintained at high temperatures after thermal cycling, after being subjected to slag and seed, to changes in oxygen partial pressure, etc.). Several of these property requirements place conflicting demands on compositions and microstructures. For example, thermal shock resistance is achieved in ceramic bodies by incorporation of 15 to 25% porosity and by a wide variation in grain size. On the other hand, a fine-grained, dense body is required for maximum compressive strength. In fact, strength is related to both grain size and porosity in an exponential fashion, as given by Equation 3.17.

$$S = S_0 e^{-\alpha p} e^{-\beta X} \quad 3.17$$

where  $S_0$ ,  $\alpha$ , and  $\beta$  are constants;  $p$  is the pore fraction; and  $X$  is the average grain size. A typical refractory oxide will lose 50% of its strength by an increase of 10% in porosity (see Figure 3.36).

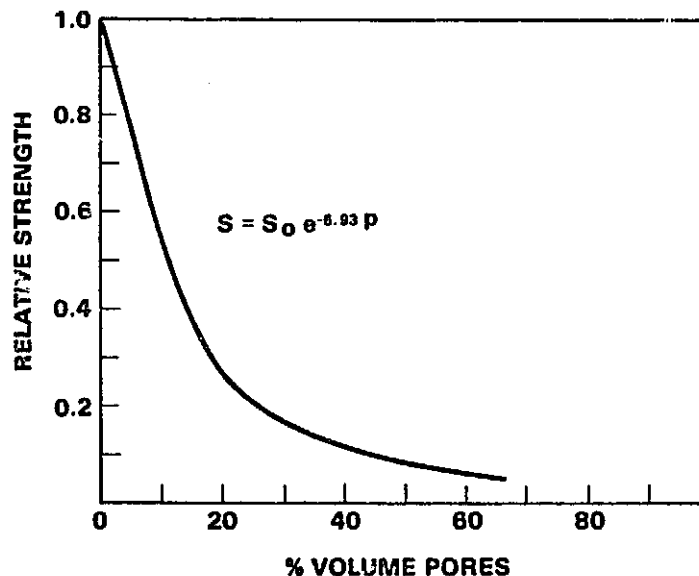


Figure 3.36 — Relative strengths of refractory oxides versus porosity (Reference 3.205).

Also, creep resistance is lowered by increased levels of porosity. It appears that tailored microstructures may be required for air preheater materials that represent a trade-off between various requirements (Reference 3.204).

#### 3.9.4.3 Mechanical Properties of Preheater Materials

In the preheater one is concerned with effects related to material mechanical properties, of both short- and long-term nature. Short-term effects are related primarily to thermal stresses on heat-up and during thermal cycling. The long-term effects are related to creep, crack growth, and corrosion-related phenomena. Thermal stress damage resistance has been discussed in a previous section (3.9.3.2). Compressive strength is related to grain size and porosity. Creep rates must be kept below  $2.8 \times 10^{-8}\%/s$  ( $1 \times 10^{-4}\%/hr$ ) for a 36 Ms (10,000 hr) preheater life (Reference 3.206). The compressive creep ratio will limit the maximum use temperature and permissible heights of most refractories, as shown in Figure 3.37, for aluminum oxide and magnesium oxide. Creep in refractories is related to strength, grain size, grain boundary compositions, phase equilibria, and refractoriness of phases present. A recent review of this subject is given by Trostel (Reference 3.207).

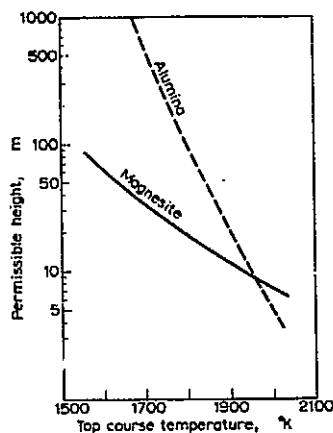


Figure 3.37 — Calculated permissible matrix height—top course temperature for alumina and magnesite refractories (Reference 3.206).

#### 3.9.4.4 Corrosion Resistance of Preheater Materials

The corrosion resistance of materials to the gases, seed, and slags is a crucial requirement for high-temperature air preheaters. Various air preheaters may be exposed to three sets of conditions:

- 1) combustion gases (clean-fuel fired, separately fired preheaters),
- 2) combustion gases plus alkali seed (clean-fuel fired, direct-fired preheaters), and
- 3) combustion gases plus alkali seed and slag (coal-fired, direct-fired preheaters).

The corrosion will vary considerably among these three cases. Separately fired air preheaters burning clean fuels have been demonstrated to operate successfully at temperatures in excess of 2273°K (3632°F) for several hundred hours in the U-02 installation (Reference 3.186) and the Arnold Engineering Test Facilities (Reference 3.201). It would be premature to extrapolate this experience to the required 36 Ms (10,000 hr) lifetimes at these temperatures. Calcia preferentially evaporates out of calcia-stabilized zirconia above 2144°K (3400°F) destabilizing this material (Reference 3.186). There is little vaporization information on yttria-stabilized zirconia in air at these temperatures. Vaporization rates of  $3 \text{ to } 6 \times 10^{-3} \text{ g/m}^2/\text{s}$  [2 to 4 cm (0.787 to 1.57 in) recession in 36 Ms (10,000 hr)] have been reported for a 10 wt%  $\text{Y}_2\text{O}_3\text{-ZrO}_2$  at 2300°K (3680°F) (Reference 3.162). Erosion tests in a combustion gas environment at a gas velocity of 500 m/s (1640 ft/s) produced a weight loss rate of  $2 \times 10^{-2} \text{ g/m}^2/\text{s}$  [14 cm (5.51 in) recession in 36 Ms (10,000 hr)] at the same temperature. The increased rate of material loss in a fast moving gas stream was attributed partly to the erosion of entire grains from the material (Reference 3.162). These data would place some caution on the extrapolation of present preheater experience to long-term performance. Creep data on yttria-stabilized zirconia are also lacking at these temperatures. Finally, the high cost of yttria [\$66.14/kg (~\$30/lb)] places a large economic penalty on the use of  $\text{Y}_2\text{O}_3\text{-ZrO}_2$  matrix materials.

While no direct-fired, high-temperature air preheaters have been built for MHD systems using clean fuels, there have been several studies of corrosion by seed compounds. Aluminum oxide has been shown

to react with potassium forming potassium  $\beta$ - $\text{Al}_2\text{O}_3$  ( $\text{K}_2\text{O} \cdot 11\text{Al}_2\text{O}_3$ ) (Reference 3.182) at temperatures as low as 1573°K (2372°F). Formation of this compound takes place both when the potassium is in the liquid and in the gaseous state. Formation of  $\beta$ - $\text{Al}_2\text{O}_3$  is noted by a weight gain, followed in time by a surface layer shelling off due to a build-up of boundary stresses (Reference 3.182). Both stabilized zirconia and magnesia are resistant to seed attack (Reference 3.182), although some dissolution of magnesium oxide by molten potassium sulfate was noted by Gannon (Reference 3.208) at 1473°K (2084°F). This dissolution is anticipated from the potassium sulfate-magnesium oxide phase diagram (Reference 3.164) which shows a single eutectic at 1340°K (1952°F). Mayauskas (Reference 3.209) also reported that a 1% potassium addition to the gas stream in erosion testing of calcium oxide-stabilized zirconium oxide increased the erosion rate by only 15% at 2273°K (3632°F). Fukui (Reference 3.181) observed potassium carbonate to be more corrosive than potassium sulfate to all ceramics.

Porosity has a profound effect on the corrosion rate. The exponential relationship between corrosion rates and porosity for magnesia as shown in Figure 3.38. Figure 3.38 illustrates that the effects of porosity overshadow those of impurities. It also indicates that the corrosion rate is increased by an order of magnitude by increasing the porosity level from 0 to 20%, as one would do to promote thermal shock resistance. The effect of porosity is related to the increased availability of surface area for reaction or dissolution by the molten potassium sulfate.

Figure 3.38 also shows the effect of other combustion products present in the potassium sulfate in the corrosion rate. This mixture called 'equilibrium seed' for an oil fuel contains 86 wt% potassium sulfate, 5 wt% potassium vanadate ( $\text{KVO}_3$ ), 4 wt% sodium sulfate, and 1 wt% each of potassium silicate, magnesium sulfate, ferrous sulfate, and nickel sulfate. These rates follow the same trend as for potassium sulfate but are almost an order of magnitude higher. It is apparent that such products of combustion will enhance the corrosion by liquid seed. In particular, vanadium is believed to contribute to increased corrosion of oxides.

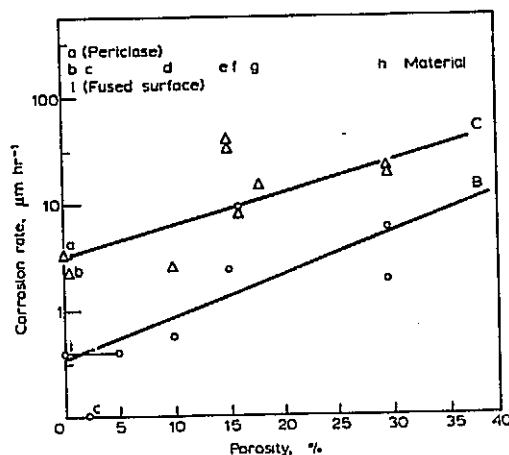


Figure 3.38 — The relationship between corrosion rate and porosity for magnesia materials. -o- Test B, 5 hours at 1700°K in  $K_2SO_4$ . -Δ- Test C, 5 hours at 1700°K in equilibrium seed. (Reference 3.206).

While studies of potassium compatibility have concentrated on aluminum oxide, magnesium oxide, and stabilized zirconium oxide, more limited studies have shown that  $MgO \cdot Al_2O_3$ , spinel, thoria, and beryllia have good resistance to seed; while silica, mullite, and titania are severely attacked at 1673 to 1773°K (2552 to 2732°F) in a few hours (Reference 3.208). While magnesium oxide and stabilized zirconium oxide show promise, there have not been extensive tests of these materials under realistic conditions for long durations. The work by Fukui comes closest to this goal. In summary, magnesia appears to be most promising as a preheater material under seed only conditions. It is favored over stabilized zirconia on the basis of cost and thermal shock resistance. It has not been demonstrated that large volumes of this material can be used with both adequate thermal shock and corrosion resistance at all locations of the preheater.

There are virtually no data on the corrosion of preheater materials by slag-seed mixtures. McCallister (Reference 3.151) reported early results of such studies being conducted at the University of Utah.



These results, which are shown in Figure 3.39, indicate that aluminum oxide has much better corrosion resistance to these mixtures than magnesia. As the most corrosion resistant material reported, aluminum oxide would lose 8 to 300 mm (0.315 to 11.81 in) of material in 31.536 Ms (1 yr) at 1723 and 1823°K (1450 and 1550°F), respectively. These rates are not encouraging when one thinks of the economics and long life required for a direct-fired air preheater. The slag-seed mixture, however, consisted of only one slag-seed composition, and the test does not truly duplicate preheater conditions. A wider range of slag and refractory compositions, as well as a more realistic type of testing, is required before a definite assessment can be made of these corrosion problems. Other candidate materials that may possess good corrosion resistance include chromium oxide, various chromites, mullite ( $3\text{Al}_2\text{O}_3 \cdot 2\text{SiO}_2$ ), spinel, and others. Again, the rejection of a large fraction (>90%) of ash in the combustor may dramatically reduce the corrosion rates in the preheater, as shown in Figure 3.39.

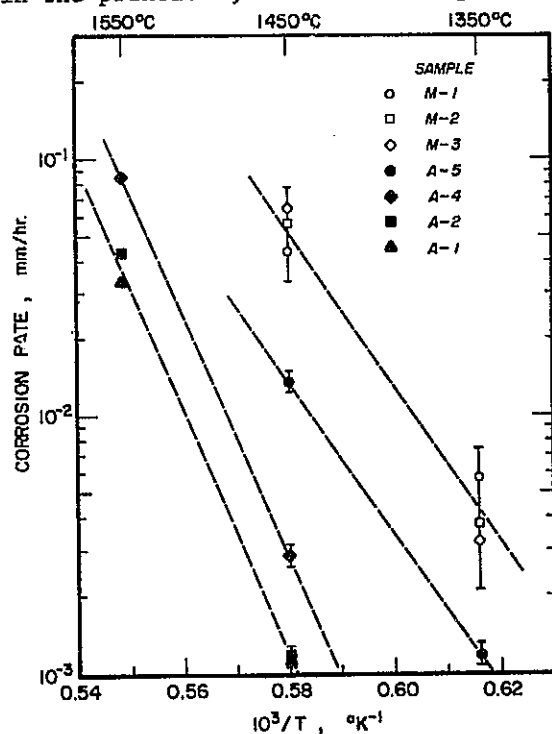


Figure 3.39 — The dependence of corrosion rate upon temperature for magnesite and alumina refractories at a constant slag shear rate of 47 in/min. (Reference 3.151.)

### 3.9.5 Other High-Temperature Components

While components such as the generator, air preheaters, and combustor command much of the attention in developing MHD materials, there are other components also that must meet similar requirements. These components include the diffuser, high-temperature ducting, and high-temperature valves.

#### 3.9.5.1 Diffuser

Although the temperatures and the gas velocities may be lower, and magnetic and electric fields are not present, the diffuser experiences many of the same conditions as are found in the generator. The differences greatly expand the list of possible high-temperature materials to be used in the diffuser. These materials need not meet the electrical requirements of either electrodes or insulators. Many materials with intermediate electrical properties can be considered for the diffuser. The lower flow velocities reduce the amount of erosion in the diffuser. Concretes with marginal erosion resistance can also be used. The diffuser will have a surface area more than an order of magnitude larger than the generator. More emphasis must be placed on the use of inexpensive materials.

For systems burning ash-free fuels, materials based on refractory oxides such as magnesia, zirconia, or alumina would be preferred. These could be in the form of brick, concrete, or castables. Less expensive, less refractory materials could be used if temperatures are low enough. Composite walls of dense brick backed up by a concrete could also be used. There is considerable flexibility here, the major goal would be to use a material or materials that are durable at the least cost.

In a coal-fired system some slag resistant compositions based on the  $\text{MgO} \cdot \text{Cr}_2\text{O}_3$ ,  $\text{Al}_2\text{O}_3 \cdot \text{SiO}_2$ ,  $\text{Al}_2\text{O}_3 \cdot \text{Cr}_2\text{O}_3$ , and  $\text{MgO} \cdot \text{Al}_2\text{O}_3 \cdot \text{Cr}_2\text{O}_3$  systems could be considered, along with other common oxides such as magnesia and alumina. These could be used in the form of brick (fused or fired), concretes, and castables. Experience gathered in coping with iron oxide-rich silicate slags in the steel-making industry could be applied here.

#### 3.9.5.2 High-Temperature Ducting

High-temperature ducting is required to move gases from one part of the MHD system to another -- in particular, from the air preheater to the combustor. A base-loaded MHD plant could incorporate several hundred meters of high-temperature ducting which is from 1 to 9 m (3.28 to 29.52 ft) in diameter (Reference 3.208). These ducts are designed to minimize both heat and friction losses. The duct construction should be simple, convenient, and inexpensive. In practice, these ducts consist of a composite of materials utilizing a refractory, corrosion resistant inner liner, low thermal conductivity insulation (porous refractories and/or fibrous insulation), and a metal pressure shell that may or may not be air or water cooled. The choice of the refractory, corrosion resistant liner is dependent upon gas temperatures and the corrosiveness of the environment. Gas temperatures could exceed 2273°K (3632°F), and the environment could vary from clean air to coal combustion products containing seed and slag. Although the materials requirements for ducts are less demanding than those for their respective preheaters and thus do not represent an obstacle in the development and use of these preheaters, the ducting is massive and subject to relatively harsh conditions. The construction of such ducting using inexpensive materials is a major concern.

#### 3.9.5.3 High-Temperature Valves

In both directly and separately fired air preheaters a number of valves are required to control the flow of air and combustion gases. The conditions to which these valves would be subjected would vary with the specific air preheater but would include rapidly changing pressures of 101.3 to 1013 kPa (1 to 10 atm), corrosion and erosion by slag and seed, high flow rates, temperatures to 2473°K (3992°F), and sudden changes in temperature. Some of these valves would be a few meters in diameter and would weigh several tons. The materials required must possess good thermal shock resistance, low creep rates, good thermal conductivity, high temperatures, mechanical strength, and good corrosion resistance.

The current state-of-the-art for high-temperature valves is represented by those used with regenerative air preheaters in the metallurgical and glass industries. Water-cooled valves up to 1.8 m (5.91 ft) in diameter are manufactured to operate at up to 1673°K (2552°F) at pressure differentials of 202.6 to 303.9 kPa (2 to 3 atm). The valves required for several of the possible MHD air preheaters are well beyond the state-of-the-art. In particular, the switchover valves for a coal-fired, direct-fired regenerative air preheater where corrosion by slag and seed in the combustion gases is encountered, and the valves for the high-temperature heat exchanger for the inert gas closed-cycle MHD system where temperatures over 2373°K (3812°F) are encountered, are particularly demanding on materials.

Water-cooled metal valves eliminate many of the high-temperature materials problems at the expense of large heat losses. Heat losses are minimized by use of ceramic valves, but the combination of requirements pose severe difficulties with these materials. Ceramic-coated water-cooled metallic valves may represent a compromise. This is clearly an area that would require much attention by both designers and materials specialists.

#### 3.9.6 Heat Recovery and Seed Recovery Materials

As the temperatures in the MHD system drop below 1500°K (2240°F), substantial amounts of potassium compounds will condense as liquids and solids. This condensation will occur in the downstream portions of the system (e.g., the low-temperature heat exchanger, boiler, superheater, etc.). These components would be constructed of various metallic alloys. The chemistry in this part of the system is both complex and undefined. The potassium will condense out as a mixture of potassium carbonate, potassium sulfate, and potassium sulfide. The prevalence of these compounds will depend on the fuel-to-air ratio (Reference 3.210). Mixtures of these three compounds will give freezing points from 1343 down to 873°K (1957 down to 1112°F). Substantial quantities of slag fly ash will be entrained in these deposits. These condensates will pose

problems of corrosion, fouling, and deposit build-up. Some of these problems are similar to those found in the boiler industry, but others are unique. Fouling of tubes, blockage of equipment passages, destruction of metal heat transfer surfaces, and so forth, can have severe operational and economic consequences.

### 3.9.6.1 Corrosion of Downstream Metallic Components

The corrosion of metallic boiler and superheater tubes by complex alkali sulfates was recognized several years ago (Reference 3.211); consequently, measures were taken to avoid the problem. Metals in the MHD environment, however, will encounter very high concentrations of both alkalis and sulfur. While both alkali and sulfur are regarded as precursors to such corrosion problems, there is very limited research under MHD conditions. There have been, however, three studies conducted under conditions close to those anticipated in an MHD system.

The British (Reference 3.212) studied the corrosion of several superheater metals under oil-fired MHD conditions. Vanadium and sodium were added to the fuel oil, and sulfur dioxide was added to give 2,000 ppm sulfur dioxide in the flue gas. The tests were for periods of 0.25, 0.9, and 3.6 Ms (70, 250, and 1000 hr) at a seeding level of 0.01% potassium. Preliminary work indicated that the deposit composition and corrosion rate were independent of seeding level. A comparison of results under these MHD conditions, and using residual oil flue gas, is shown in Figure 3.40.

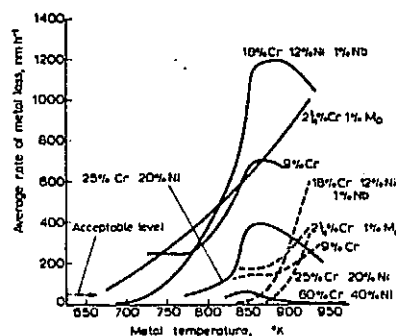


Figure 3.40 — Comparison of average rates of metal loss in 250 hour tests in MHD and residual oil flue gas (Reference 3.212).

An acceptable loss rate for 3.5 Ms (10+ yr) service would be  $\sim 13.89$  pm/s (17.2 mills/yr). These results indicate that most austenitic and ferritic stainless steels, with the exception of those with high chromium concentrations, suffer from very high corrosion rates. Only one alloy, 60 Cr-40 Ni, was found suitable for temperatures up to 870°K (1107°F). Because of the cost and low creep strength of this alloy, it was concluded that it could be used as a coating or shielding material.

In a second study, Hals et al. (Reference 3.213) studied the corrosion of various steels and high-temperature alloys used in boiler tubes and conventional heat exchangers. In this case the MHD environment was simulated by the injection of coal ash, sulfur, and potassium into the combustion products of natural gas combustion. The potassium seed level was 0.2 wt%. Metal temperatures varied from 450 to 1233°K (350 to 1760°F). Above 1116°K (1549°F) severe corrosion occurred after 0.36 Ms (100 hr) and tubes failed after 0.72 Ms (200 hr). This was attributed to the formation of liquid mixtures of sodium sulfate and potassium sulfate, a system having a eutectic at 1095°K (1511°F). The molten sulfates attacked the iron and nickel in the tubes, forming sulfides, releasing alkali oxides into the gas phase to again form alkali sulfates by reaction with sulfur dioxide and oxygen.

No corrosion was observed below 1095°K (1511°F), and no corrosion was experienced by formation of complex sulfates or pyrosulfates, which have been reported to cause severe corrosion of superheater and reheater tubes at metal temperatures of 823 to 977°K (1022 to 1299°F), and of furnace wall tubes at 584 to 644°K (592 to 700°F) in coal-fired boilers. That no such corrosion occurred was attributed to the unique operating conditions of an MHD system; in other words, near stoichiometric combustion, high combustion temperatures, rapid cooling, and uniform gases tend to suppress sulfur trioxide formation, which is a factor in formation of the pyrosulfates and complex alkali sulfates.

Finally, the corrosion behavior of general boiler tube metals was studied in a coal-fired combustion system at the Bureau of Mines (Reference 3.214). Ten different metals and alloys were subjected to

coal combustion with and without potassium seed. These tests were of 0.36 Ms (100 hr) duration, and in one set of experiments 4.4% potassium carbonate was added to the coal. The addition of seed increased the corrosion of these materials, as reported in Table 3.49.

Table 3.49 — Metal Loss of Corrosion Specimens in Combustion Gas with Unseeded Coal and in Combustion Gas with Coal Seeded with Potassium Carbonate

Material	Metal Temp., °F	Flue Gas Temp., °F	Metal Loss While Burning Unseeded Coal, in	Metal Loss While Burning Seeded Coal, in
Carbon steel (A 106)	800	1800	(1)	0.0075
Croloy 2-1/4	800	1800	0.0000	0.0015
Croloy 5	800	1800	0.0025	0.0075
446 SS	1100	2100	0.0000	0.0000
406 SS	1100	2100	0.0055	0.0035
316 SS	1100	2100	0.0000	0.0000
310 SS	1100	2100	0.0000	0.0000
310 SS	1500	2500	0.0015	(2)
Nickel	1500	2500	0.0035	(2)
Inconel	1500	2500	0.0000	(2)
Haynes 25	1500	2500	(1)	0.0005

(1) Cooling air failure caused loss of specimen.

(2) Completely oxidized after 50 hours.

At metal temperatures of 1089°K (1500°F) only the Haynes 25 alloy survived the test. At metal temperatures of 866°K (1100°F) no corrosion was found with 310, 316, and 446 SS. However, 406 SS was severely attacked in both seed and unseeded flue gas. At 700°K (800°F) metal temperatures, it was concluded that Croloy 2-1/4 might fulfill short-term use, but both carbon steel and Croloy 5 were attacked.

These studies, while providing some insights into potential problems with metallic components under these conditions, are fragmentary. The first two studies are not truly representative of coal-fired MHD conditions, and the Bureau of Mines work was limited in scope and of short duration. Clearly, more extensive corrosion studies under simulated MHD conditions are needed. A number of questions need to be

answered, such as: the effect of reduced air operation on corrosion, the enhanced destructive effects of an alkali surface containing flue gas, the role of sulfur trioxide, alkali trisulfates, and molten sulfates in metal wastage reactions, and the development of corrosion control methods (Reference 3.210).

The study of metal corrosion must be coupled with an awareness of other critical requirements for boiler and recuperator tubing, such as creep rupture, thermal fatigue, and so on. These considerations are discussed in detail in Section 3.2.

The selection of potential metals and alloys for heat transfer tubing in components such as a recuperative air preheater or steam generator can be based on experience in other coal-fired systems. This experience is summarized in Section 3.2. With the exception of the high concentration of potassium found in the MHD systems, the conditions in many of these tests are similar. In particular, Table 3.10 should be referred to for selection of heat transfer materials.

#### 3.9.7 Magnet Materials

Channel magnetic fields of 6 T were assumed for both open- and closed-cycle MHD systems. Calculations were based upon the use of a ductile intermetallic, niobium-titanium, as the superconducting material. This material is limited to peak winding fields of about 8.5 T at reasonable currents. The designs in this study indicate this is possible. Higher allowable peak fields can be achieved by use of another intermetallic material,  $\text{Nb}_3\text{Sn}$ , which has been used to generate fields well above 10 T. It is a brittle material, however, and programs have only been initiated recently to codraw this material with copper to make large conductors. Much effort will be directed toward the development of superconducting magnets for fusion devices that will also be applicable to MHD magnets.



### 3.9.8 Summary

The materials problems in the coal-fired, open-cycle MHD system can be summarized very briefly as follows. The major materials problem is the durability of materials in contact with slag and seed at elevated temperatures. This problem, while undefined, appears to be severe, and a breakthrough in terms of demonstrating that materials can survive this environment for thousands of hours is needed for successful commercial realization of open-cycle MHD. The development of an electrode which can function for thousands of hours is also critical to the successful development of open-cycle MHD. Development of such an electrode should also be regarded as a breakthrough. These materials problems and the selection of materials for coal-fired open-cycle MHD are summarized in Table 3.50.

### 3.10 Materials for Closed-Cycle MHD Systems

The current status of closed-cycle MHD may be described as experimental. Closed-cycle test facilities typically consist of small laboratory-scale generators in which short-duration experiments are conducted. At this stage studies on materials are nonexistent. The consideration of potential materials problems and materials selection both require large extrapolations from the present state-of-the-art of this energy conversion process.

Many of the primary closed-cycle components (i.e., generator, magnet, air preheater, etc.) are similar in function to those found in open-cycle MHD. Discussion of materials selection for each component, therefore, will be made in terms of compatibility with the closed-cycle environment and in satisfying requirements for each component, as discussed in Section 3.9. On this basis materials for closed-cycle MHD can be divided in three groups: 1) high-temperature ceramics for the high-temperature heat exchanger, 2) high-temperature [ $>1273^{\circ}\text{K}$  ( $1832^{\circ}\text{F}$ )] metals and ceramics for the high-temperature portion (generator, nozzle, diffuser) of the closed-cycle, and 3) low-temperature [ $<1273^{\circ}\text{K}$  ( $1832^{\circ}\text{F}$ )]

Table 3.50 — Summary of Materials Selection for Open-Cycle MHD Components

Base Case Number *	1	2	3
Fuel	Coal	Coal	Low-Btu Coal Gas
Air Preheater Type	Separately fired (2326-3519°F)** <2400°F, high $Al_2O_3$ firebrick(A) 2400 to 3100°F $Al_2O_3$ > 3100°F, CaO stabilized $ZrO_2$ (B)	Directly fired (2367°F) <1800°F, RA-333(D) <2367°F, SiC(D)	Directly fired (2556-3159°F)*** <1800°F, RA-333 (D) <2400°F, SiC (D)
Combustor	CaO stabilized $ZrO_2$ (C)	CaO stabilized $ZrO_2$ (C)	CaO stabilized $ZrO_2$ (B)
Generator Electrodes	$SiC^+$ (D)	$SiC^+$ (D)	$La_8Sr_2CrO_3$ or stabilized $ZrO_2$ (D)
Insulators	$Si_3N_4^+$ (D)	$Si_3N_4^+$ (D)	MgO (C)
Diffuser	Chromite bonded $Al_2O_3$ (C)	Chromite bonded $Al_2O_3$ (C)	MgO (B)
Finish Superheater (1100°F)	304 SS (D)	304 SS (D)	304 SS (D)
Reheater (1100°F)	2-1/4 Cr-1 Mo steel (D)	2-1/4 Cr-1 Mo steel (D)	2-1/4 Cr-1 Mo steel (C)
Evaporator (950°F)	2-1/4 Cr-1 Mo steel (D)	2-1/4 Cr-1 Mo steel (D)	2-1/4 Cr-1 Mo steel (C)
Magnet (6T)	Nb Ti (A)	Nb Ti (A)	Nb Ti (A)

\*Includes variations on base case

\*\* Point 14 exceeded 3100°F, Points 7 and 8 were less than 2400°F, all others fell between 2400 and 3100°F

\*\*\* Points 1-3 2556°F, Point 4, 3148°F and Point 5 3159°F

+ Several other equally promising electrode and insulator materials exist (See Table 3.47).

REPRODUCIBILITY OF THE  
ORIGINAL PAGE IS POOR

metals for the low-temperature portion of the closed-cycle loop. The major material problems are first, those associated with the high temperatures [ $\sim 2273^{\circ}\text{K}$  ( $3632^{\circ}\text{F}$ )] required of the high-temperature heat exchanger, and, second, cesium corrosion in the closed loop (generator, nozzle, diffuser, low-temperature heat exchanger).

### 3.10.1 High-Temperature Heat Exchanger

To efficiently use coal-derived fuels using the closed-cycle MHD process very high temperatures [ $\sim 2273^{\circ}\text{K}$  ( $3632^{\circ}\text{F}$ )] are required in the high-temperature heat exchanger. As was discussed in Section 3.9.4, successful short-term tests have been conducted both in the Soviet Union (Reference 3.186) and in this country (Reference 3.201) on air preheaters at these temperatures. These air heaters are constructed using several different matrix or pebble materials at temperatures where their properties would meet the requirements for preheater materials. Although inexpensive materials could be used at low temperatures, selection of materials above  $1973^{\circ}\text{K}$  ( $3092^{\circ}\text{F}$ ) would be restricted to a stabilized form of zirconia and above  $2173^{\circ}\text{K}$  ( $3452^{\circ}\text{F}$ ) to yttria-stabilized zirconia. Several questions arise in regard to long-term 36 Ms (10,000 hr) operation of a  $2273^{\circ}\text{K}$  ( $3632^{\circ}\text{F}$ ) heat exchanger. First, there are limited data (Reference 3.162) to indicate that loss of 2 to 14 cm (0.787 to 5.51 in) of yttria-stabilized zirconia could be expected over a 36 Ms (10,000 hr) time period due to vaporization and erosion. Also, there is some question as to thermal shock resistance, crack growth, and creep resistance of these materials over a long time period. Loss of material by thermal shock failure also could contribute to a dusting problem in the loop.

Finally, there are a number of problems associated with the ductwork and valving required for this heat exchanger. The high-temperature valves and ducts required are far beyond the current state-of-the-art (see Section 3.9.5). In particular, high-temperature valves a few meters in diameter operating at  $2273^{\circ}\text{K}$  ( $3632^{\circ}\text{F}$ ) pose a serious problem to both designer and materials specialist. Also, the heat exchanger must be tied into the metallic loop at some point [at  $2273^{\circ}\text{K}$  ( $3632^{\circ}\text{F}$ )].

This poses a serious problem in terms of chemical and mechanical compatibility.

The high-temperature heat exchanger also must be designed under the constraint of minimizing the carry-over of gaseous impurities into the cesium loop. The use of ceramic refractories with appreciable porosity for thermal stress damage resistance is no small problem in terms of gas absorption and retention. The development of a heat exchanger that can overcome both the materials and impurity carry-over problems is crucial to the success of this conversion process.

### 3.10.2 Closed-Cycle Loop Materials

#### 3.10.2.1 Cesium Compatibility of Closed-Cycle Materials

Attack of materials used in the closed-cycle loop by high-temperature cesium liquid and vapor can have at least two detrimental effects. The first is, of course, that the material under attack may in some manner fail; for example, a leak might develop in a severely corroded metal wall. Generally speaking, most structural materials are sufficiently resistant to cesium that such catastrophic symptoms of attack seldom occur.

The second and more subtle manifestation of cesium attack involves material transport of the attacked material via the cesium to other surfaces. This transport phenomenon is caused by the temperature dependence of material solubility. In this respect the oxygen level in the closed-cycle loop will be critical to the successful use of many materials.

The compatibility of cesium liquid and vapor with both metals and ceramics has been a subject of study, primarily in association with the development of high-temperature thermionic converters.

Cesium compatibility studies prior to 1967 have been critically reviewed by Klueh and Jansen (Reference 3.215). They emphasized the importance of test conditions in such exposure tests, especially the effects of impurities present in the metals and the cesium liquid.

Dissimilarity between test capsule and specimen materials and/or temperature gradients present during tests, coupled with significant (e.g., >100 ppm) impurity levels can promote mass transfer phenomena which confuse the issue of cesium corrosion per se. They concluded that earlier tests on cesium compatibility show inordinately high corrosion rates, both for conventional and for refractory metal systems, because of a strong influence of impurities in the cesium, principally oxygen. More recent and carefully conducted studies indicate that the solubilities of refractory metals in cesium are of the same low order as found in sodium and potassium. The corrosivity of cesium is intimately related to its oxygen content; primary corrosion effects are often associated with oxygen exchange-type transport reactions between zones of unlike temperature.

Structural Metals. The literature information (References 3.215 to 3.229) currently available on cesium corrosion illustrates that the majority of experimental studies have been carried out with refractory metals. As a rule, very pure refractory metals (tungsten, molybdenum, niobium, tantalum), and their alloys are not affected by exposure to pure cesium at temperatures up to at least 1773°K (2732°F).

DeMastry and Griesenauer (Reference 3.218), in a study of materials for use as thermionic converter emitters, exposed several refractory metal alloys to superheated [from 1273°K (1832°F)] cesium vapor at 1643°K (2498°F) and above for 3.6 Ms (1000 hr). Tungsten was not attacked at 1973°K (3092°F) but showed surface dissolution and grain boundary attack at 2143°K (3398°F). Such was also the case with W-15Mo, and W-25Re alloy was moderately attacked at 2143°K (3398°F). TZM alloy (Mo-0.5Ti-0.08Zr) was not attacked up to 2143°K (3398°F) but suffered from substantial grain growth at this temperature. Ta-12W showed severe surface dissolution at 1643°K (2498°F). It was suggested that carbon from the TZM containment capsule played a role in the attack. Nb-5Mo-5V-1Zr was somewhat attacked at 1643°K (2498°F).

Hargraves et al. (Reference 3.221) exposed the more cesium-resistant materials, identified by Smith et al. (Reference 3.220) in

earlier work, to long-term [36 Ms (10,000 hr)] tests at 723 and 823°K (842 and 1022°F). Tantalum and molybdenum were not attacked in these tests, although some surface scaling was observed with niobium.

Slivka (Reference 3.222) exposed various ceramics, metals, and ceramic-to-metal seals to cesium vapor at a pressure of a few mm Hg and at temperatures up to 1173°K (1652°F). Molybdenum was one of two metals that was not attacked. FS-85 niobium alloy showed a mild indication of surface reaction. Tantalum was moderately attacked, and was observed to have a matte surface, internal voids, and precipitates after exposure.

Keddy (Reference 3.216) performed rather extensive cesium exposure tests on a variety of materials. Exposures of 0.36 Ms (100 hr) to liquid cesium at 773°K (932°F) caused surface darkening on niobium, titanium, zirconium, and zircaloy; molybdenum, Nb-0.5Ti, tantalum, tungsten, and vanadium were unattacked.

Very careful work has been conducted to measure the solubility of refractory metals in alkali-metal liquids (References 3.227 to 3.229). The results showed that under very pure conditions the equilibrium solubility levels of refractory metals in potassium and lithium at high temperatures 1273°K (1832°F) are less than a few ppm by weight, but that the presence of oxygen, either in the solvent or solute, can increase measured solubilities by a factor of 10 or even 100. It was suggested that two oxygen-induced dissolution mechanisms occur. The refractory metal may dissolve into the liquid alkali metal as a simple oxide or may form complex refractory metal-alkali metal-oxygen compounds which, presumably, also dissolve. The dominating mechanism depends to a large extent upon the relative thermodynamic stabilities of the various possible oxide compounds. It was found that the presence of an oxygen gettering constituent (zirconium, titanium, and hafnium) in the refractory metal substantially reduced measured solubility of the parent metal in the alkali metal, evidently by tying up oxygen so as to remove it from the above-mentioned processes. The same general considerations are applicable to cesium-refractory metal combinations.

In summary, the refractory metals and their alloys show good corrosion resistance to cesium vapor above 1273°K (1832°F). The presence of oxygen impurities above the few ppm range, however, will lead to aggravated corrosion. The presence of oxygen gettering constituents (zirconium, titanium, and hafnium) in these metals greatly improves resistance to cesium attack by removing the oxygen from possible exchange reactions. The carry-over of other impurity gases, such as carbon monoxide, carbon dioxide, and nitrogen, and hydrocarbons from the high-temperature heat exchanger, will further complicate the corrosive effects on these materials. Formation of both carbide and nitride phases is possible, which would lead to dramatic changes in mechanical properties.

Studies on more conventional metals, such as nickel, iron, Kovar, and related alloys, show that these materials are ordinarily resistant to cesium attack to above 1273°K (1832°F). Iron and iron-based alloys such as 316 SS are moderately resistant to attack by cesium at temperatures below 1255°K (1800°F) and, in general, cesium-exposed materials exhibit a weight gain rather than a weight loss. Oxygen impurities present in the cesium are believed to be responsible for the weight gains; apparently, the cesium oxide is reduced by the stainless steel to form either chromium oxide or a complex oxide of stainless steel. In addition, experimental evidence has indicated that decarburization of stainless steels can occur at temperatures below 1255°K (1800°F). Nickel- and cobalt-based alloys behave in a similar manner (Reference 3.216). Certain steels can be attacked by cesium by processes which dissolve and transport alloying ingredients such as sulfur, selenium, and carbon (Reference 3.219).

Ceramics and Insulator Materials. Only a limited amount of experimental evidence is available concerning the compatibility of ceramic materials with cesium. All of the experimental data generated to date are the result of static cesium exposure studies; no experiments employing dynamic flowing cesium have been carried out. High-purity aluminum oxide and certain commercial grades of aluminum oxide are resistant to corrosion by static cesium to temperatures up to 1255°K (1800°F) for

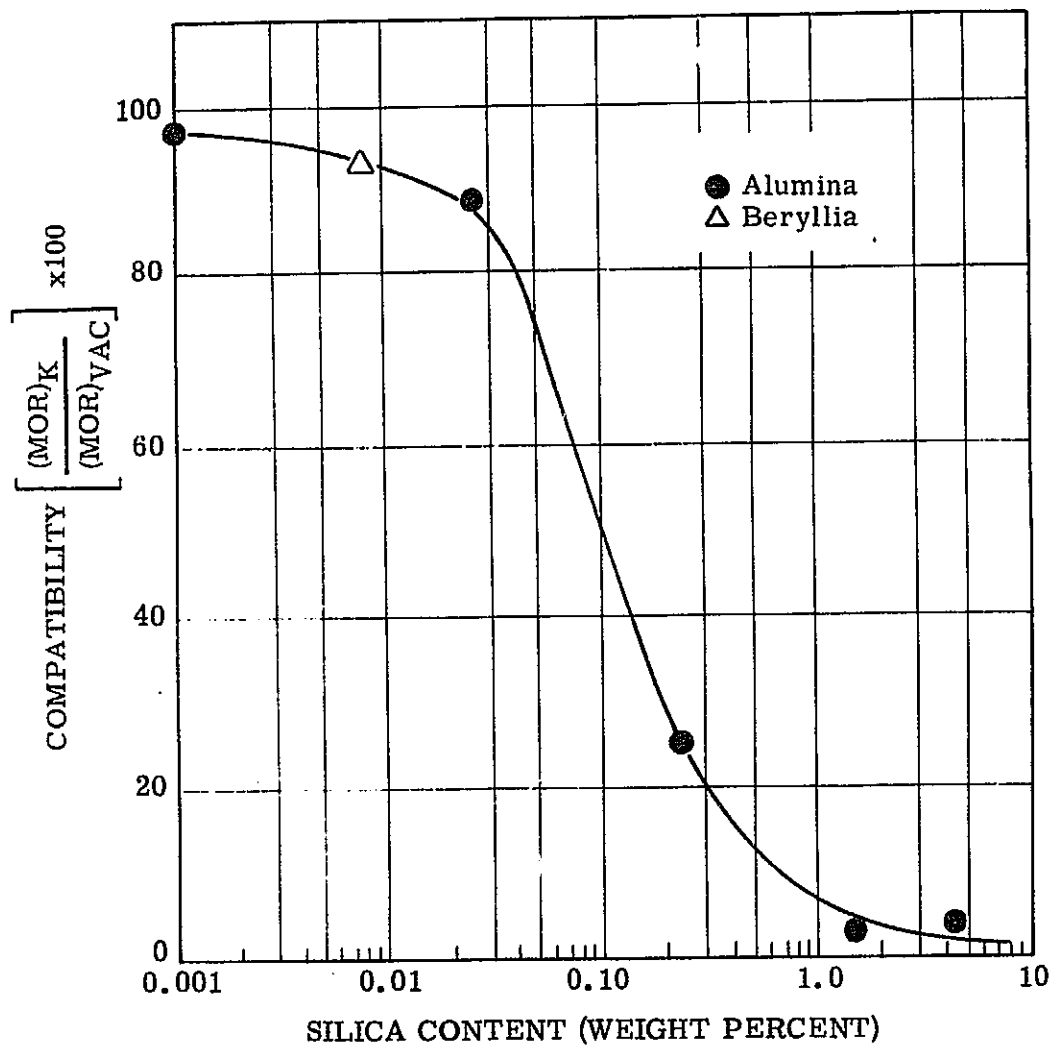


Figure 3.41 - Effect of silica content of alumina and beryllia on their compatibility with potassium at 1600°F. Determined by ratio of room temperature flexural strength of modulus-of-rupture (MOR) bars exposed to potassium vapor and to vacuum, respectively, at the exposure test temperature for 500 hours. (Reference 3,232).  
K = potassium test environment 1600°F  
VAC = vacuum test environment 1600°F



36 Ms (1000 hr) exposures. No attack was noted for hafnia and magnesia-stabilized zirconia for 14.4 ks (4 hr) (Reference 3.224) exposures to static cesium at 1922°K (3000°F). Alternatively, large material losses were noted for silicon carbide and boron nitride exposed to static cesium under similar conditions (Reference 3.226). Recently closed-cycle MHD experimental studies have shown that high-density aluminum oxide may be employed as duct insulator materials; temperatures on the order of 1700 to 2000°K (2600 to 3140°F) were maintained (References 3.230 and 3.231).

Commercial bodies which contain less stable impurity constituents such as silicon oxide will demonstrate localized attack where these impurities are present (Reference 3.216). The effect of such impurities was demonstrated in potassium compatibility studies on several commercial aluminum oxide and beryllium oxide bodies by Kueser et al. (Reference 3.232). As shown in Figure 3.41, silicon oxide contents above a few hundred ppm are sufficient to reduce alkali-metal compatibility (as evidenced by a loss in strength).

### 3.10.3 Selection of Closed-Cycle MHD Loop Materials

Generator. Closed-cycle MHD electrodes must meet the requirements outlined in Section 3.9.3.1 with the exception that corrosion resistance must be maintained with cesium vapor. As the refractory metals and their alloys appear to have good corrosion resistance to cesium at temperatures in excess of 1773°K (2732°F), they appear to be the most promising electrode materials. In fact, closed-cycle tests conducted to date use these materials. They have attractive electrical, thermal, and mechanical properties. Thorium oxide may be added to increase the thermionic emission of metals such as tungsten. A major uncertainty in using these materials centers on the amount and composition of impurity gas species such as carbon monoxide, carbon dioxide, nitrogen, and hydrocarbons that may be carried over in the high-temperature heat exchanger. These gases will react with these metals forming carbides or nitrides, thus embrittling the metals (Reference 3.234). Borosov and co-workers (Reference 3.235) studied the behavior of niobium, molybdenum,

tungsten, tantalum, and their alloys in an argon plasma at 2073 to 2273°K (3272 to 3632°F). The changes they noted were associated either with mechanical erosion of the surface by the gas flow or with chemical action by impurities in the argon -- in particular, oxygen. This study demonstrated that oxygen impurities can significantly affect the durability of these alloys during operation.

The only nonoxides considered as closed-cycle MHD electrodes to date have been zirconium and niobium carbides (Reference 3.168). Attractive properties were reported, including excellent resistance to thermal shock, resistance to reactions with potassium, and low vaporization rates ( $6 \times 10^{-6}$  g/cm<sup>2</sup> s at 2973°K (4892°F) for niobium carbide.

Insulator material requirements, with the exception of those for corrosion resistance, are the same as those outlined for open-cycle insulation in Section 3.9.3.2. As mentioned in previous discussion, high-density alumina has been used satisfactorily as an insulator at temperatures of 1700 to 2000°K (2600 to 3140°F) (References 3.230 and 3.231). No difficulties are anticipated with use of this material in high-purity form in cesium-seeded inert gases. The presence of significant amounts of oxygen in the plasma, however, could lead to formation of  $\text{Cs}_2\text{O} \cdot \text{Al}_2\text{O}_3$  compounds. Other high-purity oxides such as magnesium oxide,  $\text{SrZrO}_3$ , and  $\text{CaZrO}_3$  should also prove satisfactory.

Diffuser and Nozzle. The diffuser and nozzle represent structural components in the loop that will see both high temperatures and cesium vapor. Since corrosion problems with respect to cesium and gaseous impurities are likely to be less severe with oxide ceramics than with refractory metals, these components will be at least lined with the former. The nozzle, which operates at much higher temperatures, may require very refractory oxides such as stabilized zirconia. On the other hand, the diffuser can use alumina which is commercially available in a wide range of forms. Impurity and porosity levels of these materials must be minimized, at least at the hot surfaces, to reduce corrosive attack by cesium and to increase erosion resistance. Brick and dense plasma-sprayed coatings are possible forms that may be used.

Heat Recovery Materials. Metal tubing used in the low-temperature heat exchange subsystem must be constructed of metals that have both the necessary mechanical properties and the resistance to cesium attack at temperature. The effect of gaseous impurities in the argon on cesium compatibility is of concern with these materials. Experimental studies in flowing systems are needed to show the effect of oxygen and other impurities on corrosion of candidate metal alloys.

#### 3.10.4 Summary

The materials problems in closed-cycle, inert gas MHD can be summarized very briefly as follows. The operation of the high-temperature air heater appears to be critical in two respects to the materials problems in this system. First, can such a heater operate at such high temperatures ( $>2273^{\circ}\text{K}$  ( $3632^{\circ}\text{F}$ )) for long durations? This question is not only asked about the heater but about the associated valves and ductwork. The use of valves at these temperatures, in particular, appears to be a difficult problem. These items also appear to be very costly.

Secondly, the carry-over of gaseous impurities into the closed loop is a major question. If significant amounts of impurities, such as oxygen are present, cesium attack will be accelerated on metal components. Other impurities such as carbon monoxide, carbon dioxide, and nitrogen will react with many metals. These problems and the selection of materials for the closed-cycle MHD are summarized in Table 3.51.

#### 3.11 Materials for Fuel Cells

Fuel cells are inherently capable of converting chemical energy directly into electrical energy at high efficiencies. Many fuel cell systems have been investigated in the past to realize this potential on a commercial scale. Invariably, all have failed to meet the three minimum requisites for a commercial system: high level of performance, long life, and low cost. This is due, in large part, to inadequate materials or materials-related limitations. In this study the materials

Table 3.51 — Summary of Materials Selection for Closed-Cycle MHD Components

Component	Parametric Points 1 to 5, 7		Parametric Point 6	
	Temperature °F	Recommended Material(s)	Temperature °F	Recommended Material(s)
Heat Exchanger	3800+	< 2400°F, high $\text{Al}_2\text{O}_3$ firebrick (A) 2400 to 3100°F $\text{Al}_2\text{O}_3$ (A) 3100 to 3400°F CaO stabilized $\text{ZrO}_2$ 3400°F, $\text{Y}_2\text{O}_3$ stabilized $\text{ZrO}_2$ (C)	3100+	< 2400°F, high alumina firebrick (A) 2400 to 3100°F $\text{Al}_2\text{O}_3$ (A)
High-Temperature Valves	3800	$\text{ZrO}_2$ /metal (D)	3100	Alumina/metal (D)
Nozzle	3374	$\text{Y}_2\text{O}_3$ stabilized $\text{ZrO}_2$ (C)	2744	Alumina (C)
Electrodes	3374 (Entrance)	TZM (C) or W (C)	2744 (Entrance)	TZM (C) or W (C)
Insulators	1674 to 2397 (Exit)	$\text{Al}_2\text{O}_3$ (B)	1502 (Exit)	$\text{Al}_2\text{O}_3$ (B)
Diffusers	1674 to 2397	$\text{Al}_2\text{O}_3$ (B)	1502	$\text{Al}_2\text{O}_3$ (B)
Reheater	1250	HA-188 or HS-25 (C)	1250	HA-188 or HS-25 (C)
Full-Flow Evaporator	1150	304 SS (B)	1150	304 SS (B)
Part-Flow Evaporator	700	Croloy 2-1/4 Cr-1 Mo (B)	700	Croloy 2-1/4 Cr-1 Mo (B)
Magnet	5 or 6 T	NbTi (A)		NbTi (A)

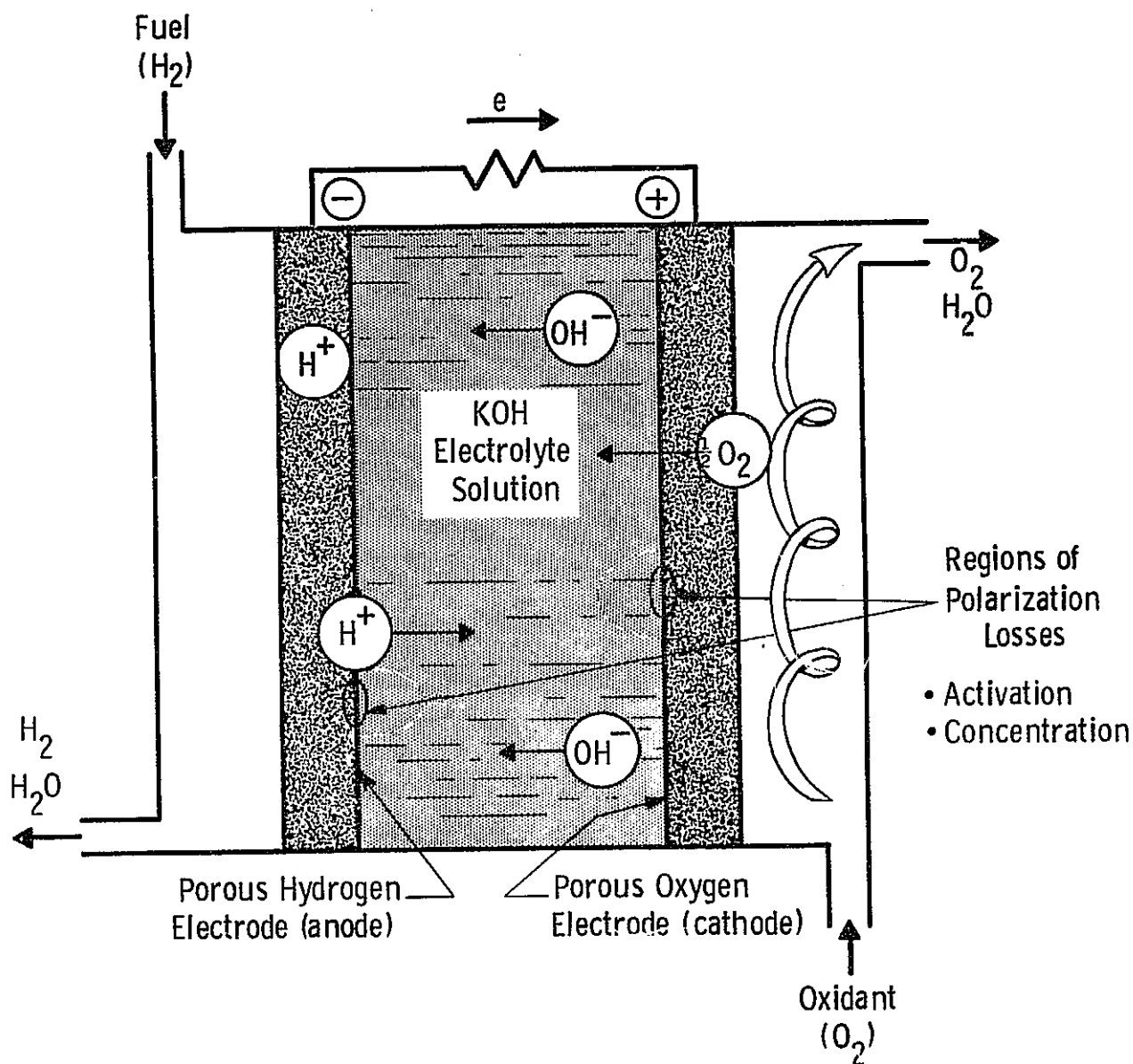
effort on fuel cells has been directed towards assessing the present state-of-the-art in fuel cell materials, in identifying critical or major materials problems, and in ascertaining the development needs for the four fuel cell systems under study:

- High-temperature solid electrolyte fuel cells
- Molten carbonate fuel cells
- Acid electrolyte fuel cells
- Alkaline electrolyte fuel cells.

In reporting the findings the first section discusses fuel cells in general, the second relates materials to performance, the next three sections discuss the four systems in particular, and the last section summarizes the results of the study.

#### 3.11.1 Background

Fuel cells (References 3.236 to 3.242) consist of electrolyte, electrodes, and electrocatalysts, if needed. Interconnections are used to series-connect individual cells into batteries, and containment vessels are used to contain the batteries or fuel cell stacks. The electrolyte may be liquid or solid, but all other components are solid. The basic components of fuel cells are shown in Figure 3.42. The electrocatalysts are applied to the internal surfaces of the porous electrodes. At the electrode/electrolyte interfaces the chemical reactions of interest occur. Low reaction kinetics lead to activation polarization losses, while slow mass transport of reactants and products to and from the interfaces leads to concentration polarization. In addition to these losses, ohmic losses occur through the cell as current is drawn. As shown in Figure 3.43, activation polarization (overpotential) losses predominate at low currents, concentration polarization (overpotential) losses at high currents, and ohmic losses at all levels of current. With increasing temperature, the activation polarization losses decrease because of a lowering of the activation barriers and, hence, so does the need for electrocatalysts.



$$\text{Usable Voltage} = \text{Open Circuit Voltage} - \text{Polarization Losses} - \text{Ohmic Losses}$$

$$\text{Power} = \text{Usable Voltage} \times \text{Current}$$

Fig. 3.42— Basic features of a hydrogen-oxygen fuel cell (Reference 3.238)

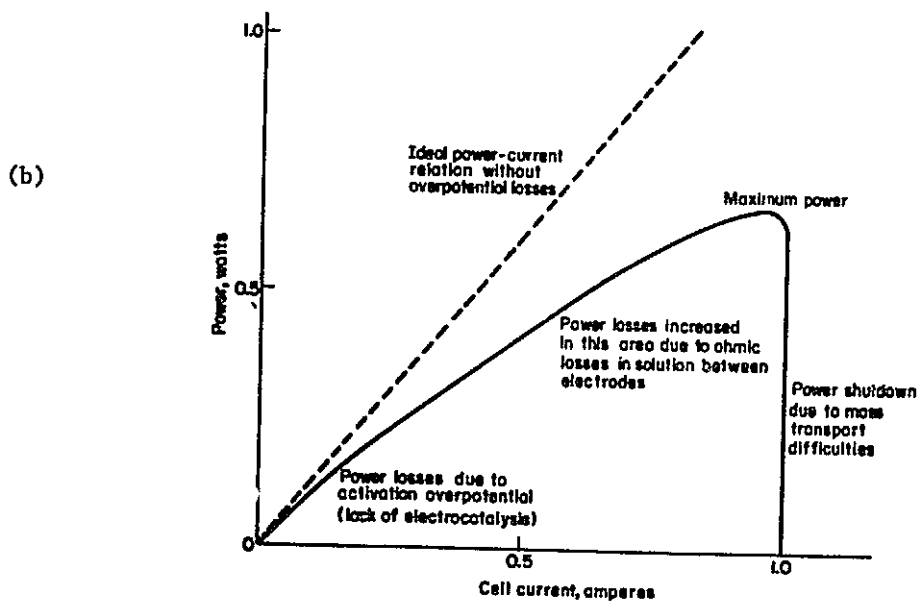
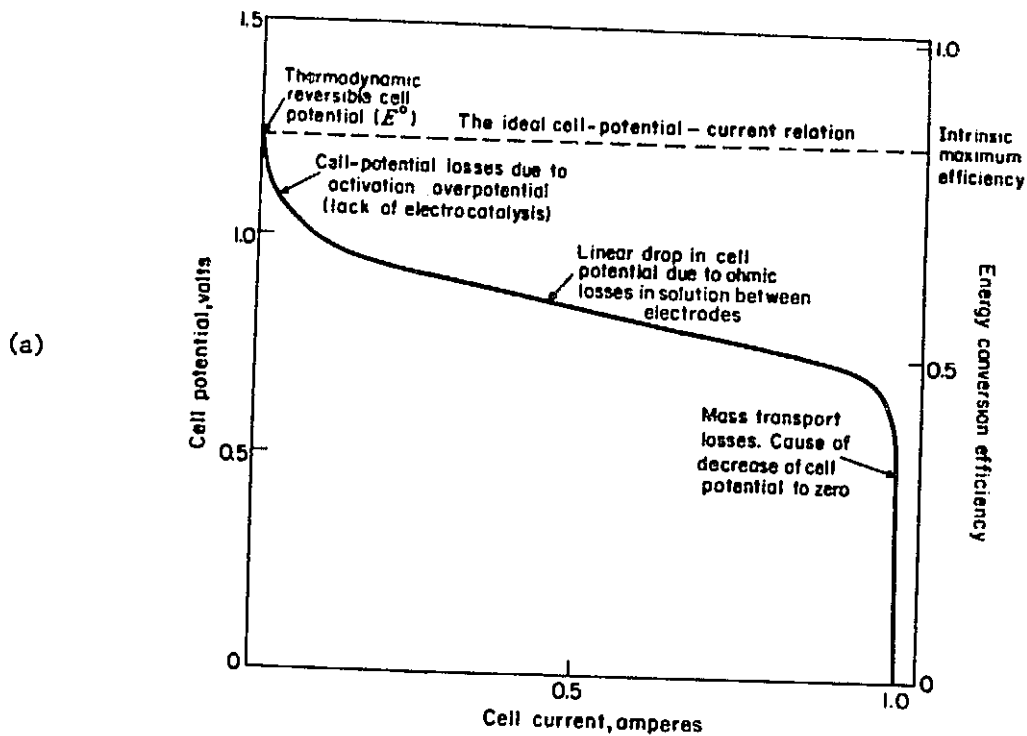


Figure 3.43 -Electrical performance of a typical fuel cell as a function of cell current: (a) cell potential and (b) power (Reference 3.241).

The usable cell voltage is the difference between the open-circuit voltage and these losses. The open-cell voltage is the thermodynamic reversible cell potential.

The polarization and ohmic losses are dependent on the materials used, the properties of the electrode/electrolyte interface, the electrode structure, cell design, and operating temperature.

### 3.11.2 Performance and Materials Requirements

In the operation of the fuel cells under consideration, using porous gas electrodes, the major loss mechanisms are:

- Polarization losses at anode and cathode
  - Activation polarization
  - Concentration polarization
- Ohmic losses in electrolyte, electrodes, and interconnection
  - Ionic in the electrolyte
  - Electronic in the electrodes and interconnection.

The choice of electrode materials, catalyst if needed, and the structure of the electrode are important materials and materials fabrication problems which can have a significant effect on the polarization losses of the fuel cell system. Ideally, highly active electrodes with many small and well-distributed pores are desirable to minimize polarization losses.

The electrode structure, however, should not be too porous, as the electrode integrity may be destroyed and/or the electronic resistance may be too high. High resistance leads to high ohmic losses. To avoid high ohmic losses while minimizing polarization losses thin electrodes with fine pores having large internal surface areas may be used with current collectors. Double porosity electrodes may also be used. Double porosity electrodes contain fine pores with large internal surface areas in contact with the electrolyte and large pores on the gas or air side to permit adequate mass transfer to and from the electrode/electrolyte interfaces. Double porosity electrodes with slight gas overpressures can contain liquid electrolytes within the fine pore structure without complete flooding of the electrodes.



The major requirements for the electrolyte, electrodes, electrocatalysts, and interconnections, and the rationale behind these requirements and the probable solutions to problems posed by the requirements, are summarized in Tables 3.52 through 3.55.

### 3.11.3 High-Temperature Solid Electrolyte Fuel Cell

The high-temperature solid electrolyte (References 3.243 to 3.250) fuel cells are based on the oxygen ion conductivity of stabilized zirconium oxide. Most solid electrolyte fuel cells operate at temperatures between 1023 and 1373°K (1382 and 2012°F). Expensive catalysts used in low-temperature fuel cells are not necessary because of the high working temperatures. Problems with creep and electrolyte vaporization losses of the molten carbonate systems are nonexistent with the solid electrolyte cells. The interconnection requirements, however, are more demanding than in low- or medium-temperature fuel cells, and the higher operating temperature places a greater demand on chemical and physical stability and inertness. In addition, thermal expansion matching between the physically joined components of the high-temperature fuel cell is very important (except for some relaxation of this requirement in the case of ductile metals).

The substitution of selected divalent or trivalent cations for the zirconium ion in monoclinic zirconium oxide stabilizes the zirconium oxide into a cubic structure with oxygen vacancies created to maintain electrical charge neutrality. The conductivity of oxygen ions through these vacancies is dependent on the type and amount of dopant and temperature, as shown in Figures 3.44 and 3.45. For a solid electrolyte zirconium oxide, stabilized with yttrium, ytterbium, or calcium, is preferred because of the high-temperature stability of the stabilized structure and the high conductivity. In fuel cell systems the electrolyte resistance predominates for electrolyte thicknesses greater than 1 mm (25 mil). In order to realize high useful power outputs, the electrolyte thickness must be reduced as in the Westinghouse thin-film design (Reference 3.248), or the temperature raised as in other designs.

Table 3.52 - Generalized Electrolyte Requirements for all Fuel Cells  
Rationale behind the Requirements and the Probable Solutions

<u>Requirement</u>	<u>Rationale</u>	<u>Solution</u>
High Ionic Conductance	Minimize ohmic losses	High alkaline or acid concentration Optimum carbonate mixture Optimum defect structure in $ZrO_2$ solid electrolyte Thin electrolyte
High Concentration of Diffusing Ions	Minimize concentration polarization losses	Concentrated acid or alkaline electrolyte Provide $CO_2$ makeup in carbonate cells
Containment of Liquid Electrolyte	Necessary for operation and prevention of electrode flooding	Free electrolyte between rigid electrodes Fixed electrolyte in matrix
Stability	Maintain performance and life	Select compatible electrodes and catalysts Clean up gases, e.g., CO and $CO_2$ for KOH systems

Table 3.53 - Generalized Electrolyte Requirements for all Fuel Cells  
Rationale behind the Requirements and the Probable Solutions

<u>Requirement</u>	<u>Rationale</u>	<u>Solution</u>
High Electronic Conductance	Minimize ohmic losses	Thick electrodes (not desired) Thin electrodes with current collectors Minimum porosity
Catalytic to Electrochemical Reactions	Minimize activation polarization losses	Catalyst coating Increase operating temperature
High Internal Catalytic Area	Minimize activation polarization losses	Fine pore structure at electrolyte-electrode interface
Porous Structure for Gas Passage	Maintain mass transfer, minimize concentration polarization losses	Thin electrodes with current collectors Double porosity electrodes
Stable Pore structure	Maintain high performance, long life	Stabilize material by preconditioning Fix material by second phase
Inert to gases and electrolyte	Maintain performance and life	Materials selection
Mechanical strength	Unit integrity	Thick electrodes (not desired) Thin electrodes with mechanical supports
Containment of liquid electrolyte	Prevent electrode flooding	Double porosity electrodes with overpressure Use hydrophobic electrodes or coatings

Table 3.54 - Generalized Catalyst Requirements, Rationale behind  
the Requirements and the Probable Solutions

<u>Requirement</u>	<u>Rationale</u>	<u>Solution</u>
Catalytic activity	Reduce activation polarization losses	Use appropriate metal or semiconductor
Inert to gases and fuel cell components	Maintain performance, life	Materials selection
High catalytic area	Minimize activation polarization losses	Finely dispersed powders Thin plating on electrodes
Stable structure	Maintain performance, life	Choice of material Stabilize material by preconditioning Fix material by second phase
Hydrogen catalysts	-----	Pt, Pd, Pt-Pd, Ni, FeNiCu, Rh, WO <sub>3</sub> , MoO <sub>3</sub>
Oxidant catalysts	-----	Pt (acid electrolyte) Pt, Ag (alkaline electrolyte) Ni, Li-NiO (molten carbonate) (Ni, Ag, and NiO stable in alkaline but not in acid cell)

3-228

REPRODUCIBILITY OF THE  
ORIGINAL PAGE IS POOR

Table 3.55 - Generalized Interconnection Requirements, Rationale  
behind the Requirements and the Probable Solutions

<u>Requirement</u>	<u>Rationale</u>	<u>Solution</u>
Low electronic resistance	Minimize ohmic losses	<p>Acid and alkaline systems and molten carbonate systems use metal wires, screens, or plates</p> <p>High-temperature solid electrolyte system uses conductive oxides</p>
Stability	Maintain performance, life	Choice of material. Most critical to high-temperature solid electrolyte systems and molten carbonate systems

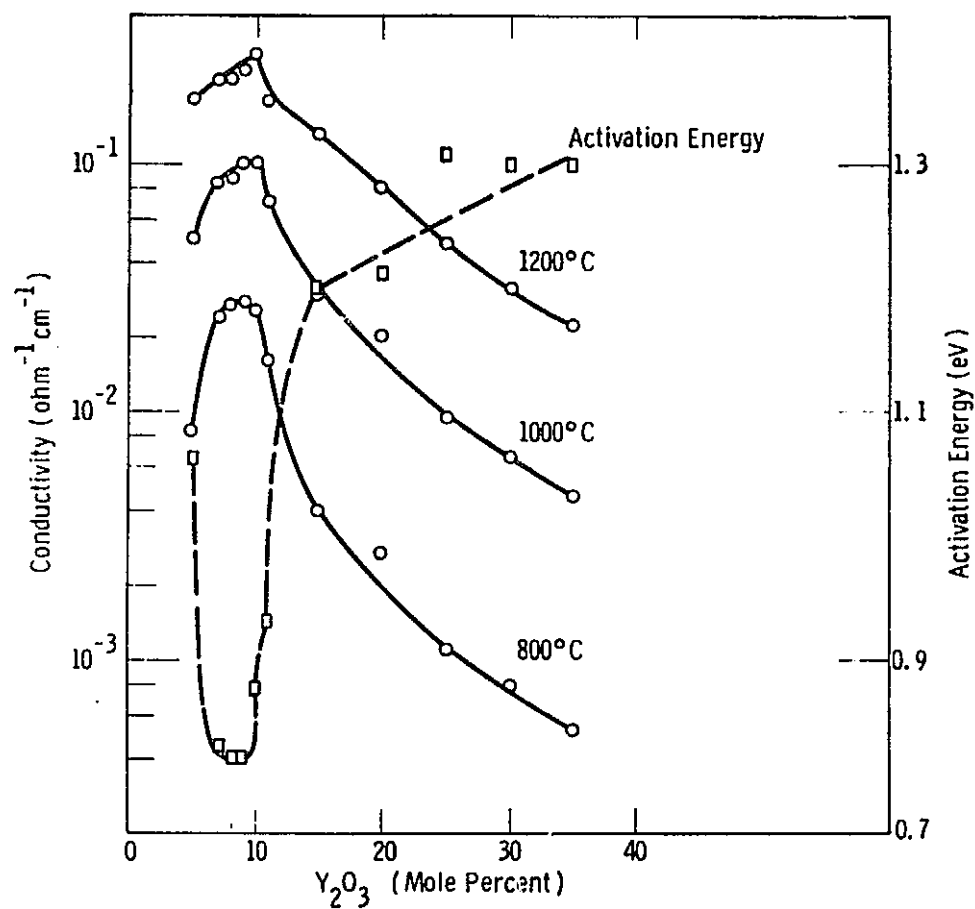


Figure 3.44 — Conductivity isotherms and activation energies for the system  $Y_2O_3-ZrO_2$  (Reference 3.251).

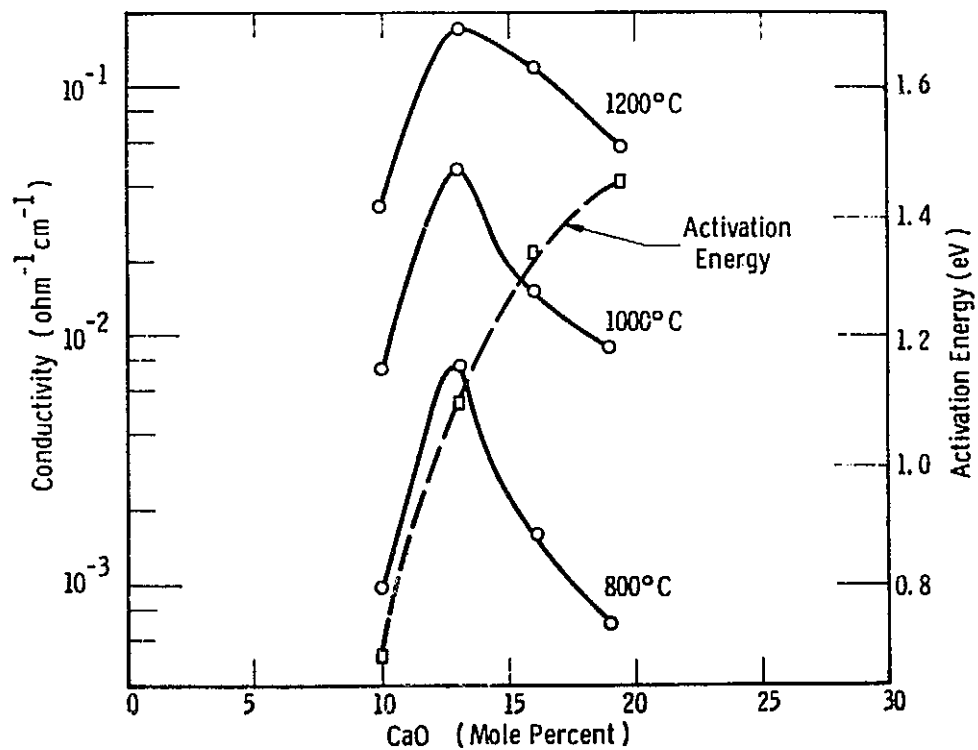


Figure 3.45 — Conductivity isotherms and activation energies for the system  $\text{CaO-ZrO}_2$  (Reference 3.251).

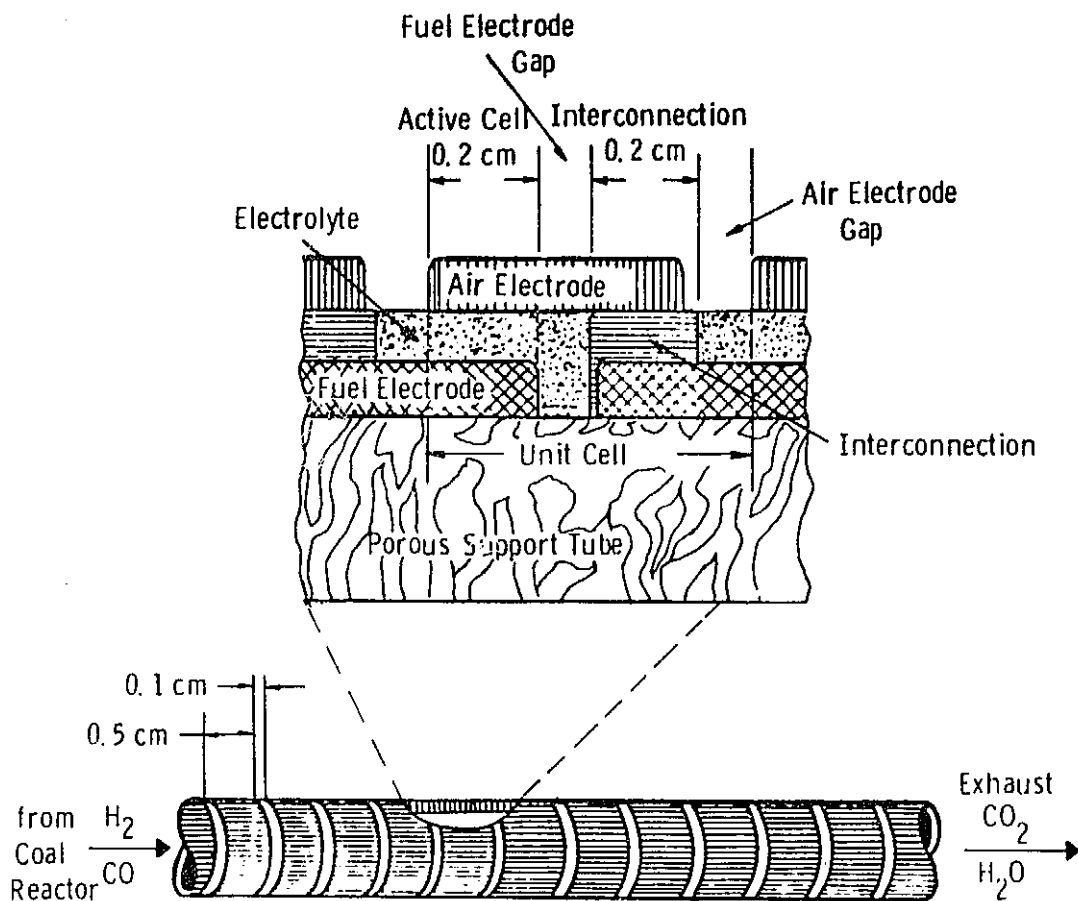


Figure 3.46 — Cross section through the wall of a thin film fuel cell battery (Reference 3.249). Note vertical scale exaggerated.

REPRODUCIBILITY OF THE  
ORIGINAL IMAGE IS POOR



The electrodes and interconnections must have adequate conductivity and also meet certain minimum chemical and physical requirements including:

- Chemical stability
- Physical stability
- Low vapor pressure
- Chemical compatibility with other components
- Mechanical strength
- Minimum thermal expansion mismatch.

Other requirements include: stable structure for the electrode and a high electronic conductivity for the interconnections under oxygen partial pressure ranging from oxidizing (air) to reducing (fuel).

The selected baseline case for the high-temperature solid electrolyte fuel is:

Fuel Cell	Thin-film solid electrolyte on porous support tube
Electrolyte	Y-stabilized $ZrO_2$
Electrolyte Thickness	40 $\mu m$
Anode	Ni- $ZrO_2$ cermet
Cathode	$In_2O_3$ - $PrCoO_{3-x}$
Interconnection	$Cr_2O_3$

The components (Reference 3.249) of a thin-film solid electrolyte fuel cell battery are shown in Figure 3.46. It consists of five components.

1) Porous support tube - a tube functioning as the mechanical support for the battery - porous enough to allow countercurrent diffusion of the fuel gases and their reaction products.

2) Fuel electrodes - porous films of electronically conductive material, providing a large three-phase contact area between fuel gas, electrolyte, and electronic conductor.

3) Electrolyte - gas-tight films of stabilized zirconia having high ionic but negligible electronic conductivity.

Table 3.56 — Materials Investigated for the Cathodes  
of Solid Electrolyte Fuel Cells  
(References 3.244 and 3.246 to 3.248)

Material	Remarks
Pt, Pd, Ag	Pt and Pd - too expensive Pd and Ag - excessive volatilization
$\text{Li}_{0.1}\text{Ni}_{0.9}\text{O}$	Li vaporization leading to loss of conductivity
Doped ZnO	Satisfactory at temperatures < 800°C; marginal conductivity
ZnO	Reacted with electrolyte
Sn-doped $\text{In}_2\text{O}_3$	Satisfactory; requires very thin films
Sn-doped $\text{In}_2\text{O}_3$ with $\text{PrCoO}_{3-x}$	Improved performance
$\text{PrCoO}_3$	Satisfactory performance; capable of long-term stable performance; thermal expansion mismatch
$\text{LaCoO}_3$	Reacts with electrolyte; thermal expansion mismatch
$\text{Sr}_{0.1}\text{La}_{0.9}\text{CoO}_3$	Reacts with electrolyte; thermal expansion mismatch
Sb-doped $\text{SnO}_2$	Satisfactory if applied in thin coatings; thermal expansion mismatch

4) Air electrodes - highly permeable, electronically conductive layers, stable in air at 1273°K (1832°F), and providing a large contact area between oxygen from the air stream, electrons, and the zirconia electrolyte.

5) Cell interconnections - thin gas-tight films of an electronic conductor which serves to connect adjacent cells in series by connecting the fuel electrode of one cell to the air electrode of the adjoining cell.

Insulation between adjacent cell units of the battery is provided by the gaps in the fuel and air electrodes, and by the relatively long paths through the thin electrolyte film. This is evident if the scale of the design is considered -- the film thicknesses lie in the range of 20 to 80  $\mu\text{m}$  (39.3 and 78.7 mil), while the gap lengths are between 0.1 and 0.2 cm (0.039 to 0.078 in).

Both  $\text{Co-ZrO}_2$  and  $\text{Ni-ZrO}_2$  (Reference 3.248) cermet electrodes have been successfully used for the anode in this type of fuel cell. The  $\text{Ni-ZrO}_2$  electrode is preferred because of its ability to function in a fuel gas with slightly higher oxygen partial pressures.

The major materials investigated as cathodes for solid electrolyte fuel cells are shown in Table 3.56. The noble metals, platinum, palladium, and silver can be used, but prohibitive cost (platinum and palladium) or excessive vaporization (palladium and silver) precludes their use in practical systems designed for long-term operation. Lithiated nickel undergoes excessive vaporization of the lithium ion; zinc oxide reacts with the electrolyte as does  $\text{Sr}_{0.1}\text{La}_{0.9}\text{CoO}_3$ . Antimony-doped tin oxide is limited to thin layers and has a large thermal expansion mismatch with the electrolyte. Most promising electrodes include tin-doped indium oxide,  $\text{PrCoO}_3$ , or a composite structure of  $\text{PrCoO}_{3-x}$  and tin-doped indium oxide.

The interconnection materials investigated have included a large number of oxides and cermets. Many of the materials investigated meet most of the requirements for interconnections, but only a few meet all of the requirements. The most promising interconnections include

nickel-doped chromium oxide, manganese-doped  $\text{NiCr}_2\text{O}_4$  and  $\text{La}_{0.8}\text{Sr}_{0.2}\text{CrO}_3$ . The first two have been investigated (Reference 3.248) and have shown satisfactory short-term performance in thin-film solid electrolyte cells. The third appears to be an acceptable alternative.

The porous support tube of the thin-film design may be made with calcium-stabilized zirconium oxide (partially stabilized) or with yttrium-stabilized zirconium oxide (fully stabilized). The partially-stabilized calcium-zirconium oxide tubes offer better thermal shock resistance and the yttrium-zirconium oxide tubes better thermal expansion match with the yttrium-zirconium oxide thin-film electrolyte.

The electrodes, electrolyte, and interconnections have been made by several techniques (References 3.247 to 3.249): chemical vapor deposition, sputtering, or slurry sintering: the fuel electrodes by co-sintering of mixed zirconium oxide and nickel oxide followed by reducing in hydrogen to form the porous nickel-zirconium oxide cermet; the air electrode by chemical vapor deposition or slurry sintering; the electrolyte by sputtering, chemical vapor deposition, or in the case of thin-film calcium-stabilized zirconium oxide, by reactive sintering using  $\text{CaZrO}_3$  and zirconium oxide powders; and the interconnection by chemical vapor deposition (chromium oxide) or slurry sintering ( $\text{NiCr}_2\text{O}_4$ ).

#### 3.11.3.1 Materials Problems

The cathode and interconnection represent the major problems in the high-temperature solid electrolyte fuel cells. The choice of materials is greatly limited by the requirements which must be met. The fabrication of these materials in the thin-film design restricts them even further. The materials and structure are the primary limiting factors with the cathode. Polarization losses in the high-temperature fuel cell are almost completely associated with the cathode. The structure and the poor oxygen transport in many of the cathode oxide materials account for failure of the cathode. The incorporation of a perovskite ( $\text{PrCoO}_{3-x}$ ) with a higher oxygen ion conductivity than tin-

doped indium oxide can improve the performance of the cathode over that of tin-doped indium oxide, but additional improvements are needed.

The interconnection represents the most severe materials problem because of its requirement for chemical, physical, and electrical stability while exposed to the fuel gas on one side and air on the other side. The long-term performance of chromium oxide ( $\text{Cr}_2\text{O}_3$ ) and  $\text{NiCr}_2\text{O}_4$  interconnections has not been determined under these conditions. The fabrication of the thin-film interconnections and electrolyte and dense films correctly positioned on the fuel cell battery is critical to prevent direct gas diffusion between the air and fuel streams.

The long-term stability of the dissimilar components in intimate contact at high temperatures represents a potentially severe problem. Changes in the interface between these materials through reactions and interdiffusion can change the electrical characteristics of the interfaces and, in turn, the performance.

#### 3.11.3.2 Development Needs

Improved cathodes and interconnections are critical to the successful development of commercial thin-film solid electrolyte cells. The techniques for fabricating these components in the battery also pose a critical problem for investigation. The development of improved structures in the cathode should be pursued. The improvements in cathode performance by incorporation of  $\text{PrCoC}_3$  into the tin-doped indium oxide cathode demonstrates one way in which cell performance may be improved. The interconnection material should be fully determined in the air and fuel gas environment to define its performance and from this to design improved interconnections.

#### 3.11.4 Molten Carbonate Fuel Cells

Molten carbonate fuel cells (References 3.237 and 3.252 to 3.257) are based on molten electrolytes from the  $\text{Li}_2\text{CO}_3$ - $\text{Na}_2\text{CO}_3$ - $\text{K}_2\text{CO}_3$  ternary system. Both binary and ternary mixtures have been used as electrolytes. The various fuel cells investigated in the past may be

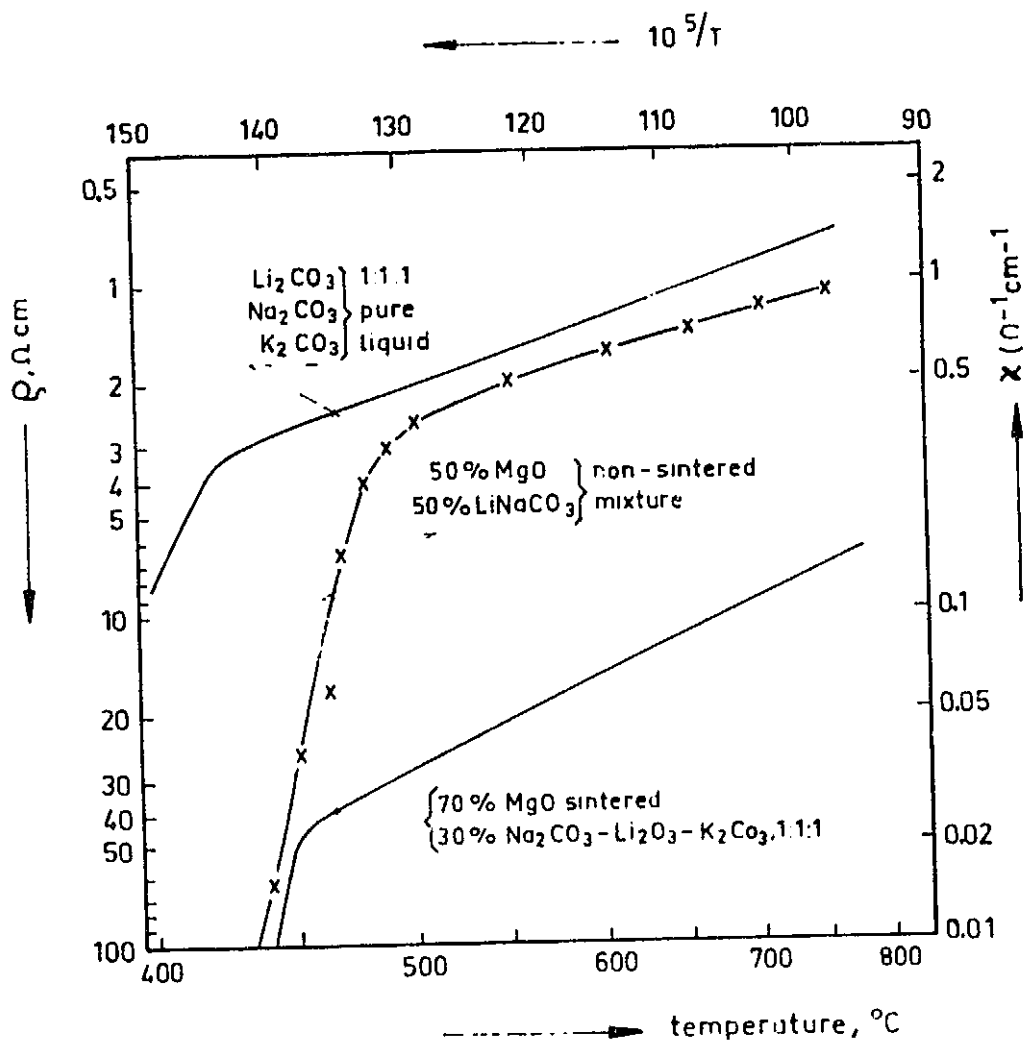


Figure 3.47 — Specific resistance (conductivity) of liquid, paste, and sintered matrix electrolytes. (Reference 3.255.)

REPRODUCIBILITY OF THE  
ORIGINAL PAGE IS POOR

classified according to the electrolyte:

- Free electrolyte cells
- Trapped electrolyte cells
  - Porous refractory diaphragms (e.g., magnesium oxide)
  - Paste (or slurry) electrolyte diaphragms
    - Noneutectic type
    - Eutectic type.

In practical cells double-porosity sintered electrodes have been used with the free electrolyte, and powder electrodes and single-porosity sintered electrodes have been used with the trapped electrolyte. The free electrolyte cell, however, is of little interest because of difficulties in manufacturing the double-porosity electrodes and because of unsatisfactory electrolyte containment. As an alternative the electrolyte may be trapped by impregnating it into the pore structure of a porous refractory magnesium oxide or by mixing it with magnesium oxide or alkali-aluminate powders to form a cohesive paste when the carbonate is molten. Entrapment in the porous refractory is unsatisfactory because of electrolyte creep out of the pore structure but entrapment in the paste electrolyte works well. As a result, the paste electrolytes are considered to be best for molten carbonate fuel cells. The paste electrolytes consist of a mixture of inert solid magnesium oxide or alkali-aluminate filler and a noneutectic or eutectic carbonate phase. The use of magnesium oxide has been discontinued in the most recent cells because alkali aluminates perform better. The noneutectics are characterized by a narrow working-temperature range and poorly defined solid/liquid interfaces which are dependent on temperature. The eutectics have a broader temperature range above the eutectic temperature and better defined solid/liquid interfaces. The specific resistances of a free eutectic, of eutectic impregnated in a magnesium oxide frame, and of 50/50 magnesium oxide/binary paste electrolyte are shown in Figure 3.47. The superiority of the paste electrolyte compared with impregnated magnesium oxide is obvious. The paste electrolyte offers further advantages in fabricability, as the paste can be molded into any shape, using cold pressing and sintering, hot pressing, or flame spraying.

Materials which have been used as anodes include nickel, iron, iron + nickel + copper, silverized zinc oxide, palladium foil, silver-palladium foil, and stainless steel; while lithiated nickel oxide (Li-NiO), silverized zinc oxide, gold, copper oxide, and stainless steel have been used as cathodes. Nickel anodes and lithiated nickel oxide cathodes offer minimum corrosion and metal ion migration between the electrodes, coupled with good catalytic activity and moderate costs. Silver cathodes have been extensively investigated, but difficulties with silver migration and dendritic growth through the electrolyte have been observed frequently. Although the use of paste electrolytes has reduced the dendritic growth problem, the preferred anode is still nickel (based on other considerations). The other anodes and cathode materials investigated are not considered comparable overall with nickel or lithiated nickel oxide.

The interconnections between the single molten carbonate cells have not received the attention warranted by their importance in making practical cells work. Little reference to interconnection materials is made in the literature. It is believed that interconnections between cells may be in the form of sheets, wires, screens, or other forms, with nickel appearing to be a good candidate because of its stability in the fuel gas and because of the compatibility of the oxide found on nickel in air with the lithiated nickel oxide cathodes. The use of leads incompatible with either electrode can result in corrosion and/or high contact resistance.

#### 3.11.4.1 Materials Problems

Changes in the chemistry and physical properties of the electrode and electrolyte, corrosion, and electrolyte creep are the major materials problems with molten carbonate fuel cells. Chemistry changes, such as the oxidation of metal electrodes and interconnections, reduction in oxides, and corrosion of the various components by the molten electrolyte or by reaction between components, can be serious. The surface layers of nickel electrodes may undergo oxidation and reduction under varying anodic polarization; nonnoble metallic interconnections will undergo



oxidation on the oxidant side; dissolution of atomic hydrogen into metal may alter lattice constants; and heterogeneous potential distributions can cause local bulk oxidation of the nickel anodes. At the high temperatures [ $>773^{\circ}\text{K}$  ( $932^{\circ}\text{F}$ )] used with molten carbonate cells, materials undergo recrystallization or sintering. As a result, the initial structure of the electrodes, pore size and distribution, and internal surface area may change. The small pores will grow into large pores, and the internal surface area will decrease. Cell performance, thus, will degrade rather rapidly at first, then slower, during the life of the cells.

The recrystallization phenomenon is more pronounced on the anode side because of the higher sintering rate of the fine metal particles or grains as compared with that of the oxide cathodes. In a long-term test (Reference 3.253) with silver screen cathodes, commercial nickel anodes, and paste electrolyte, excessive sintering of the nickel screen and some vaporization of the carbonate was observed after 16.56 Ms (4600 hr) at  $973^{\circ}\text{K}$  ( $1292^{\circ}\text{F}$ ). The surface area of the nickel screen was reduced by 30% and its thickness by 40% after 2.25 Ms (625 hr) of operation. The electrolyte lost 50 mole % of the carbonate content during the test. The cell initially showed an increase in polarization due to sintering effects of the porous nickel anodes and a gradual decrease in terminal voltage over the test period as vaporization of the electrolyte occurred, thus demonstrating the need to precondition the electrodes and to minimize vaporization of the electrolyte.

#### 3.11.4.2 Development Needs

New and more stable electrodes and electrolytes need to be developed or present ones improved. Stable electrode structures not prone to changes due to recrystallization or other phenomena at the operating temperatures and environment are needed. The use of very high pretreatment temperatures or the inclusion of inert and stable phases in the electrode to deter grain growth should be explored and techniques

developed to do this. Suitable interconnections compatible with the electrodes and meeting all the requirements for good electrical contact to the electrodes, low resistance, long life, and low cost are needed. Not much work has been done with interconnections. Corrosion of the electrodes, and possibly the interconnections by the electrolyte, should be determined; and materials substitution, design, or operating changes to obviate this problem should be identified and evaluated.

#### 3.11.5 Acid and Alkaline Fuel Cells

The acid and alkaline fuel cells (References 3.236 to 3.239 and 3.258) have used a variety of porous carbon, porous metal, and porous plastic-bonded electrodes. For free electrolyte cells thick, rigid electrodes with double porosity structures have been used; for immobilized electrolyte cells flexible and thin electrodes have been used. The electrode structure may consist of random, graded, or double porosities. Self-supporting porous carbon electrodes are made by machining porous carbon stock or by powder-sintering techniques. The latter is preferred for producing double-porosity electrodes.

One method (Union Carbide) of preparing free-standing porous carbon electrodes for fuel cells is to mix filler (petroleum coke flour) with binder (coal-tar pitch), bake to carbonize the pitch, and fire at 1173°K (1652°F) or above. The pore structure is controlled by the filler size and amount and by the holes produced by gas escape during carbonization. The electrodes are activated by burnout in air, steam, or carbon dioxide to increase the internal surface area. Other variations of this procedure include the use of petroleum pitches and resins as binders instead of the coal-tar pitch. Electrodes may be formed by molding or extrusion. The electrodes are catalyzed by plating or by impregnation with metal or metal-oxide catalysts. The electrodes are wet proofed by coatings of waxes, silicones, or other agents. Major disadvantages of porous carbon electrodes used with free electrolyte cells are their brittle nature (requiring thick electrodes) and their tendency to flooding, with the flooding rate increasing with current densities.

With fixed electrolyte cells, where the electrolyte is immobilized in a porous inert matrix flexible porous carbon or other electrodes, may be used. In this type of cell the electrolyte retention in the matrix reduces the tendency for electrode flooding, permits the use of flexible electrodes such as porous carbon cloth, and reduces the cell size. The Pratt and Whitney acid fuel cell now undergoing field testing uses immobilized hot phosphoric acid electrolyte with carbon cloth electrodes catalyzed with a mixture of platinum-rhodium, molybdenum and tungsten oxides, and tungsten carbides.

Sintered metal electrodes (References 3.237 and 3.258 to 3.260) have been made by sintering metal powders onto compatible metal screens or by sintering or hot pressing metal powders to form self-supporting structures. The catalyst (platinum, palladium, nickel, silver, or semi-conducting oxides) may be mixed and sintered with the metal powders. Raney-type metal powders (e.g., nickel-aluminum, silver-aluminum, platinum-aluminum) may also be included with these metal powders or used alone to form a highly porous structure. The Raney metals are sintered on screens or as free-standing shapes, then chemically or electrochemically etched in caustic to remove the aluminum phase of the metal.

Plastic-bonded electrodes (References 3.237 and 3.238) consisting of carbon, metal powders, and/or catalyst powders bonded to wire screen with Teflon or polyethylene particles have been used. The hydrophobic nature of the plastic bond prevents electrode flooding and eliminates the necessity for double-porosity electrodes or for hydrophobic coatings which have been used for carbon or metal electrodes. A novel air electrode for use with free or fixed acid or alkaline electrolyte is described by Landi et al. (Reference 3.261). The electrode was fabricated with conventional plastics-processing equipment using a thermoplastic molding compound, a polytetrafluoroethylene (PTFE) latex, and a graphitic carbon or metallized graphitic carbon filler. The electrode was made by coating long fibers of the PTFE, then molding to form a cohesive sheet of graphitic carbon catalyst bonded by the PTFE

fibers. No sintering was required. The electrodes were used as is or bonded to metal screens under moderate heat and pressure. Plastic-bonded electrodes may also be made by other similar techniques, including sintering or pressing mixtures of Teflon or other plastic, platinum-black catalysts, and metal and metal oxide powders under moderate temperatures and pressures.

The selected base line cases for the acid and alkaline fuel cells are given in Table 3.57.

Table 3.57 — Materials - Base Line Cases

<u>Fuel Cell</u>	<u>Acid</u>	<u>Alkaline</u>
Electrolyte	85 wt% $\text{H}_3\text{PO}_4$	30 wt% KOH
Anode	Porous carbon	Porous carbon
Anode Catalyst	Pt ( $1 \text{ mg/cm}^2$ )	Pt ( $1 \text{ mg/cm}^2$ )
Cathode	Porous carbon	Porous carbon
Cathode Catalyst	Pt ( $1 \text{ mg/cm}^2$ )	Ag ( $5 \text{ mg/cm}^2$ )
Operating Temperature	190°C	70°C

The interconnections used in either cell may be metal wire, screen, or plates which are compatible in the acid or alkaline environment. The alkaline (References 3.238 and 3.262) fuel cells are technologically the most developed fuel cell type because of their early selection for space and military applications. The advantages of the alkaline system include:

- High power output at ambient temperatures and low pressures
- Use of conventional materials (carbon, nickel, silver, plastics)
- Available catalysts (noble metals, Raney alloys)
- Use of easily oxidizable fuels such as hydrogen and hydrazine
- Possible air operation with no precious metal catalyst.

The alkaline cells also possess the following disadvantages:

- Hydrocarbons cannot be used directly in fuels
- Air operation requires a  $\text{CO}_2$ -scrubbing system.

The acid fuel cell also has many of the same advantages but is tolerant of carbon dioxide in the fuel gas, which the alkaline fuel cell is not. The acid fuel cell, however, cannot use silver catalysts on the air side because of their solubility in the acid; the platinum catalyst used on the fuel side may need to be more heavily loaded to compensate for the slow catalytic activity with carbon monoxide gases, or other catalysts more active to carbon monoxide may be added. The higher platinum loading is also required by the loss of active platinum surface area due to recrystallization at the higher [463°K (374°F)] operating temperature.

For the alkaline system (Reference 3.237 and 3.239) high-area nickel, Raney nickel, and nickel boride have been successfully substituted for the platinum catalyst on the anode. But the cells with nickel and nickel boride had to be run at lower current densities to prevent electrochemical oxidation of nickel and nickel boride due to polarization. Nickel is more sensitive to oxidation than the boride. This sensitivity to oxidation places a further requirement to maintain a uniform electrode structure throughout the electrode, as localized high current densities can lead to oxidation of the electrode with subsequent degradation in performance. As an alternative to the silver cathode catalyst of the alkaline cell, a  $\text{CoAl}_2\text{O}_4$  spinel catalyst has been successfully used, but, again, at a slight penalty in performance. At the lower current densities typically used in this type of cell the polarization was higher than platinum- or silver-catalyzed carbon electrodes, but at very high current densities the spinel catalysts performed better, as shown in Figure 3.48. The effect of electrode thickness on cell performance can also be seen in comparing the thick and thin platinum-catalyzed air electrodes using air as the oxidant.

In the acid cells the thin-screen electrodes developed by American Cyanamid (References 3.237 and 3.260) have been used in cells with phosphoric acid immobilized in a glass-fiber matrix. These electrodes are reported (Reference 3.260) to be long-lived in a low-current cell operating at 363°K (194°F) using reformed natural gas over

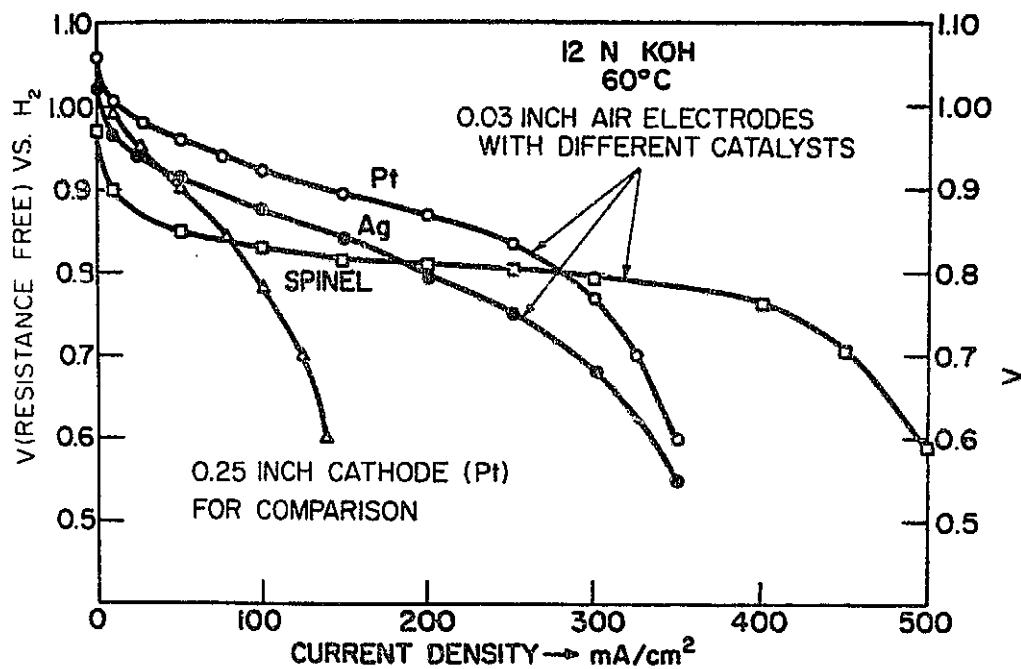


Figure 3.48 — Electrode polarization curves employing different catalysts (linear diagram).

a two-year period. The glass-fiber matrix however was slowly attacked by phosphoric acid, changing to a gel and losing its wet strength over the test period. Periodic replacement of the matrix was required. Stable electrodes (Reference 3.237) for use with acid cells based on Teflon bonding have been successfully used with platinum black on a tantalum substrate.

### 3.11.6 Summary

The materials selected for the electrodes, electrocatalysts, electrolyte, and interconnections for the base line cases of the four fuel cell systems are summarized in Table 3.58. The high-temperature solid electrolyte cell uses a Ni-ZrO<sub>2</sub> cermet as the anode, mixed oxides (In<sub>2</sub>O<sub>3</sub> and PrCoO<sub>3-x</sub>) as the cathode, chromium oxide as the interconnection, and yttrium-stabilized zirconium oxide as the electrolyte -- all as thin films positioned on a porous, partially stabilized, calcia-zirconia tube. The molten carbonate cell uses nickel anodes, lithiated nickel oxide, nickel interconnections, and a paste electrolyte consisting of molten carbonates in an inert alkali-aluminate powder. No electrocatalysts are required for either type of cell. The acid electrolyte cell uses carbon anodes and cathodes, platinum anode and cathode catalysts, and 85 wt% phosphoric acid immobilized in a glass fiber or other matrix. The alkaline electrolyte cell uses carbon anodes and cathodes, platinum anode catalyst, silver cathode catalyst, and 30 wt% potassium hydroxide electrolyte. Bipolar designs may be used with the acid and alkaline cells and, thus, obviate the need for interconnections.

The materials and fabrication requirements for the four fuel cell systems were considered for the parametric points selected for each system. The materials and fabrication were given an A, B, C, or D rating depending on their status as: A - established materials, B - near-term materials, C - developmental materials, and D - speculative materials. In these ratings qualitative estimates on the materials-related performance and lifetimes of the cell components were made. These ratings are reported in Tables 3.59 through 3.62 for the parametric points

Table 3.58 — Summary of the Base-line Cases for the  
Four Fuel Cell Systems

Parameter	High-Temperature Solid Electrolyte Fuel Cell	Molten Carbonate Fuel Cell	Acid Electrolyte Fuel Cell	Alkaline Electrolyte Fuel Cell
Temperature	1000°C	650°C	190°C	70°C
Current Density	400 mA/cm <sup>2</sup>	200 mA/cm <sup>2</sup>	200 mA/cm <sup>2</sup>	100 mA/cm <sup>2</sup>
Cell Voltage	0.66 V	0.80 V	0.70 V	0.80 V
Electrolyte	(Y <sub>2</sub> O <sub>3</sub> ) <sub>x</sub> (ZrO <sub>2</sub> ) <sub>1-x</sub>	Paste: Li, Na, K carbonates, and alkali aluminates	85 wt% H <sub>3</sub> PO <sub>4</sub>	30 wt% KOH
Electrolyte State	Solid	Molten	Immobilized Liquid	Liquid
Electrolyte Thickness	4 x 10 <sup>-3</sup> cm	0.10 cm	0.05 cm	0.05 cm
Anode	Ni-ZrO <sub>2</sub>	Ni	Carbon	Carbon
Anode Catalyst	None	None	Platinum 1 mg/cm <sup>2</sup>	Platinum 1 mg/cm <sup>2</sup>
Cathode	In <sub>2</sub> O <sub>3</sub> - PrCoO <sub>3-x</sub>	Li-NiO	Carbon	Carbon
Cathode Catalyst	None	None	Platinum 1 mg/cm <sup>2</sup>	Silver 5 mg/cm <sup>2</sup>
Interconnection	Cr <sub>2</sub> O <sub>3</sub>	Ni Specified	Bipolar	Bipolar

3-248

REPRODUCIBILITY OF THE  
ORIGINAL PAGE IS POOR



Table 3.59 —Summary of Materials Selection and Ratings for High-Temperature Solid Electrolyte Fuel Cells

Case No:	1,2,3 4,5,10, 11,12	6	7	8,9	13	14	15	16	17	18,20	19	Remarks
Condition:												(1) $(\text{CaO})_x(\text{ZrO}_2)_{1-x}$ (2) $\text{SnO}_2$ (Sb doped) (3) $\text{CoCr}_2\text{O}_4$ (Mn doped)
Fuel Type: Low-Btu											X	
Med. -Btu	X	X	X	X	X	X	X	X	X			
High-Btu										X		
Fuel Cell Life: 10,000 hr	X				X	X	X	X	X	X	X	
30,000 hr		X										
50,000 hr			X									
100,000 hr				X								
Temperature: 900°C								X				
1000°C	X	X	X	X	X	X	X			X	X	
1100°C									X			
Components:												
Electrolyte: $(\text{Y}_2\text{O}_3)_x(\text{ZrO}_2)_{1-x}$	A	B	b	C	A	B(1)	A	A	A	A	A	
Anode: Ni-ZrO <sub>2</sub>	A	B	B	C	A	A	A	A	B	A	A	
Catalyst: None												
Cathode: In <sub>2</sub> O <sub>3</sub> -PrCoO <sub>3-x</sub>	B	B	C	C	B	B	B(2)	B	B	B	B	
Catalyst: None												
Interconnection: Cr <sub>2</sub> O <sub>3</sub>	C	D	D	D	C(3)	C	C	C	D	C	C	

Table 3.60 — Summary of Materials Selection and Ratings for Molten  
Carbonate Electrolyte Fuel Cells

Case No:	1,2 3,5 10,11 16	4	6	7	8,9	12	13	15
<u>Condition:</u>								
Fuel Type: Med.-Btu		X						
High-Btu	X		X	X	X	X	X	
Methanol								X
Fuel Cell Life: 10,000 hr	X	X				X	X	X
30,000 hr			X					
50,000 hr				X				
100,000 hr					X			
Temperature: 650°C	X	X	X	X	X			X
700°C						X		
750°C							X	
<u>Components:</u>								
Electrolyte: Paste <sup>(1)</sup>	A	A	B	B	C	B	B	A
Anode: Ni	A	A	A	B	C	B	B	A
Catalyst: None								
Cathode: Lithiated NiO	B	B	C	C	C	C	C	B
Catalyst: None								
Interconnection: Ni	C	C	C	C	C	C	C	C

(1) Paste electrolyte of Li, Na, K carbonates and alkali aluminates.

Table 3.61 — Summary of Materials Selection and Ratings for Acid  
Electrolyte Fuel Cells

<u>Case No:</u>	1,2	4	6	7	8,9	12	13	14	<u>Remarks</u>
	3,5 10,11 15								
<u>Condition:</u>									(1) Pt 0.3 mg/cm <sup>2</sup> (2) Pt 0.1 mg/cm <sup>2</sup>
Fuel Type: Med-Btu		X							
High-Btu	X		X	X	X	X	X		
Methanol								X	
Fuel Cell Life: 10,000 hr	X	X				X	X	X	
30,000 hr			X						
50,000 hr				X					
100,000 hr					X				
<u>Components:</u>									
Electrolyte: 85 wt% H <sub>3</sub> PO <sub>4</sub>	A	A	B	C	C	A	A	A	
Anode: Carbon	A	A	A	B	C	A	A	A	
Catalyst: Pt 1 mg/cm <sup>2</sup>	A	A	B	C	C	B(1)	C(2)	A	
Cathode: Carbon	A	A	B	B	C	A	A	A	
Catalyst: Pt 1 mg/cm <sup>2</sup>	A	A	B	C	C	B(1)	C(2)	A	
Interconnection: Bipolar	A	A	A	A	A	A	A	A	

Table 3.62 — Summary of Materials Selections and Ratings for Alkaline Electrolyte Fuel Cells

Case No:	1,2,3 5,10 11,16	4	6	7	8,9	12	13	14	15	Remarks:
Condition:										(1) Raney Ni (2) Pt 0.1 mg/cm <sup>2</sup> (3) Pt 0.01 mg/cm <sup>2</sup> (4) Ag 1 mg/cm <sup>2</sup>
Fuel Type: Med.-Btu High-Btu	X	X	X	X	X	X	X	X	X	
Fuel Cell Life(hr): 10,000 hr	X	X				X	X	X	X	
30,000 hr			X							
50,000 hr				X						
100,000 hr					X					
Components:										
Electrolyte: 30 wt% KOH	B	B	B	C	C	B	B	B	B	
Anode: Carbon	A	A	A	B	C	A	A	A(1)	A	
Catalyst: Pt 1 mg/cm <sup>2</sup>	A	A	A	A	B	B(2)	C(3)	None	A	
Cathode: Carbon	A	A	B	C	D	A	A	A(1)	A	
Catalyst: Pt 1 mg/cm <sup>2</sup>	A	A	A	B	C	A	A	A(4)	A(4)	
Interconnection: Bipolar	A	A	A	A	A	A	A	A	A	

3-252

REPRODUCIBILITY OF THE  
ORIGINAL PAGE IS 100%

of the four fuel cell systems. These ratings are of a preliminary nature and will be refined and possibly modified under Tasks II and III of the program. On the basis of these preliminary ratings some conclusions may be drawn for each of the fuel cell systems:

For the high-temperature solid electrolyte cells the nickel-zirconium oxide anode, 36 Ms (10,000 hr) life may be easily achieved, while 360 Ms (100,000 hr) life would require development. The yttrium-stabilized zirconium oxide electrolyte may undergo some changes in structure and resistance over the longer time periods or higher current densities. Replacement of the yttrium-stabilized zirconium oxide electrolyte with calcium-stabilized zirconium oxide could be developed with a moderate level of effort. The cathode material and structure could be developed to handle current densities up to  $800 \text{ mA/cm}^2$  with moderate polarization losses and lifetimes up to 360 Ms (100,000 hr). Extensive development would be required, however. The interconnection represents the most significant problem with the solid electrolyte cell. The interconnection needs extensive development to function properly in the thin-film cells. Lifetimes up to 36 Ms (10,000 hr) may be achieved, but longer lifetimes or operation at  $1373^\circ\text{K}$  ( $2012^\circ\text{F}$ ) are highly speculative at this time.

For the molten carbonate cells the lifetime of the electrolyte is considered within the state-of-the-art up to 36 Ms (10,000 hr) and questionable above 36 Ms (10,000 hr). Lifetimes up to 180 Ms (50,000 hr) may be achieved with some development, while lifetimes up to 360 Ms (100,000 hr) represent a serious problem. Similar estimates apply for the anodes and cathodes. Interconnections made of nickel or other material need extensive development and evaluation.

For the acid cells the lifetime of the electrolyte (and its matrix) is in excess of 108 Ms (30,000 hr). Development of improved matrix materials is expected to extend the probable lifetime to as high as 180 to 360 Ms (50,000 to 100,000 hr). The carbon anodes and cathodes may exhibit satisfactory lifetimes up to 108 Ms (30,000 hr) but require development to extend the lifetime to in excess of 180 Ms (50,000 hr).

Table 3.63 — Composition of Alloys Included in Study

CORALIT BASED	C	Mn	Si	Cr	Ni	Co	Mo	W	Cb	Fe	Ti	Al	B	Zr	Ta	Other
Mar M509	0.60			24.0	10.0	Bal		7.0			0.2			0.5	0.50	
X-40	0.50	1.0	0.5	25.5	10.5	Bal		7.5		2.0			0.01			
X-45	0.25	1.0		25.5	10.5	Bal		7.5		2.0			0.01			
HA188	0.10	0.75	0.40	22.0	22.0	Bal		14.0		1.5						0.08La
L605/HA25	0.10	1.50	0.50	20.0	10.0	Bal		15.0								
S816	0.38	1.20	0.40	20.0	20.0	Bal	4.0	4.0	4.0	4.0						
(Co,Cr)-(Co,Cr) <sub>7</sub> C <sub>3</sub>	2.4			41.0		Bal										
Co-TaC	0.85			15.0		Bal									12.2	
<b>IRON BASED</b>																
2-1/4 Cr-1 Mo	0.1	0.40	0.3	2.3			1.0			Bal						
Cr-Mo-V	0.3	0.92	0.34	1.16			1.22			Bal						0.23V
AISI 304	0.7	1.70	0.57	18.6	10.5	0.12	0.18			Bal						
AISI 316	0.5	1.53	0.32	16.9	10.4		2.13			Bal						
AISI 347	0.05			18.0	11.0	0.2				Bal				0.8		
INCOLOY 801	0.1 max	1.5 max	1.0 max	20.0	32.0					Bal	1.0					
INCOLOY 802	0.2-0.5	1.5 max	.75 max	20.0	32.0					Bal						
INCOLOY 800H	.06-.10			20.0	32.0					Bal	0.38	0.38				
KROMARC 58	0.04	10.0	0.25	16.0	20.0		2.25			Bal			0.01	0.01		0.2V, 0.17N
17-14 Cu-Mo	0.1	0.9		16.0	14.0		2.3		0.55	Bal	0.26					
A286	0.05	1.4	0.40	15.0	26.0		1.25			Bal	2.15	0.2	0.003			0.3V
DISCALOY	0.04	0.5	0.40	13.5	25.0		3.0			Bal	1.75					
<b>NICKEL BASED</b>																
γ'-δ					Bal				23.0			4.4				
TRW-NASA VIA	0.13			6.1	Bal	7.5	2.0	5.5	0.5		1.0	5.4	0.02	0.13	9.0	
IN792	0.21			12.7	Bal	9.0	2.0	3.9			4.2	3.2				
UDIMET 710	0.07			18.0	Bal	15.0	3.0	1.5			5.0	2.5	0.2			
UDIMET 520	0.05			19.0	Bal	12.0	6.0	1.0			3.0	2.0	0.005			
UDIMET 500	0.08			19.0	Bal	18.0	4.1			4.0	2.9	2.9	0.005			
TD-Ni					Bal											2 ThO <sub>2</sub>
AVCO-LY E2	0.11			14.83	Bal			3.85		0.31	2.66	2.67			3.78	1.17 Y <sub>2</sub> O <sub>3</sub>
IN617	0.07			22.0	Bal	12.5	9.0					1.0				
HASTELLOY-X	0.10	0.5	0.5	22.0	Bal	1.5	9.0	0.6		18.5						
<b>REFRACTORY BASED</b>																
Cb-1 Zr	0.005									Bal				1.0		
B66	0.006						5.0			Bal				1.0		5V
B88	0.067							28.0		Bal						2Hf
Mo-TZM	0.03						Bal				0.5			0.1		
T-111								8.0							Bal	2Hf
Chromium alloy				Bal			7.0		1.0				0.08			0.1Y

Similar estimates are applicable to the catalysts except that the lifetimes of the catalysts are considered to be shorter and, thus, represent a more serious obstacle to long-term life. Reducing the catalyst loading to  $0.1 \text{ mg/cm}^2$  (compared to  $0.3 - 1.0 \text{ mg/cm}$  for the present state-of-the-art) is considered possible but would require development.

For the alkaline cells the electrolyte lifetime represents a problem, especially for long-time operation. The anode catalysts should be capable of 180 Ms (50,000 hr) operation with present materials and technology, but some development would be required to extend the lifetime or to reduce the catalyst loading. The carbon anode lifetime should be similar to that of the anode catalyst except that the achievement of the longer lifetime is expected to be more difficult. The life of the carbon cathodes is expected to be less than that of the carbon anodes, and lifetimes on the order of 360 Ms (100,000 hr) must be considered speculative. The substitution of Raney nickel for the carbon anodes and cathodes can be made with little difficulty, as the technology is within the state-of-the-art.

These ratings are of a qualitative nature and are presented here to identify the most serious materials problems for the four systems and to show trends on expected lifetimes under various conditions. Further refinements are needed to establish the development necessary to achieve the three requisites for a commercial system: high level of performance, long life, and low costs.

### 3.12 Compilation of Composition and Mechanical Properties

In this section the nominal chemical composition and mechanical properties of the materials discussed in Section 3 of this report are compiled (Table 3.63). Most of the designs being considered in this study are limited by the high-temperature strength of the materials. Design stress allowables for these applications are usually derived from specified

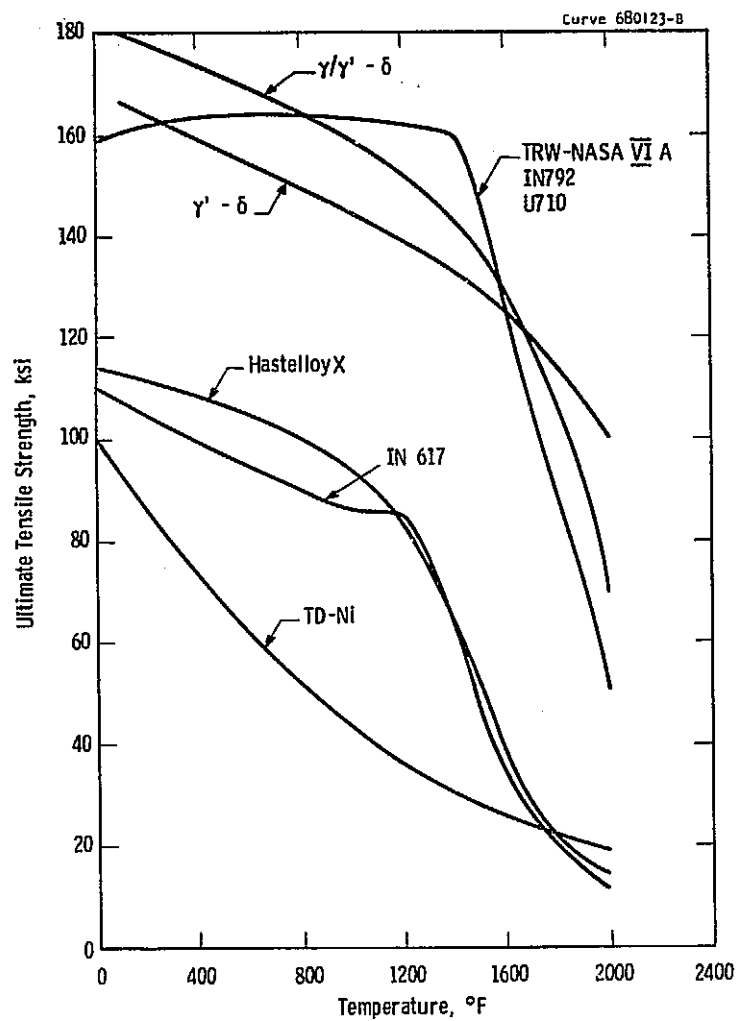


Fig. 3. 49 -Ultimate strength - temperature plot for selected nickel base alloys



fractions of the yield strength and 360 Ms (100,000 hr) stress rupture strength, in addition to other concerns, such as low-cycle fatigue and plastic strains below 1%.

Since most of the conceptual type designs in Task I were derived from yield and rupture strength considerations, only these properties are included in this section. The yield strength has been plotted (Figures 3.49 to 3.52) as a function of temperature for all alloy systems except the nickel-based alloys, where only a complete collection of ultimate tensile strengths could be located. The stress rupture strengths have been presented in the form of Larson-Miller parameter plots (Figures 3.53 to 3.56). This format was used since very little long-time stress rupture data are available for the material being considered, and this parameter was used to extrapolate existing data to 360 Ms (100,000 hr) strength. A parameter of 20 was used for all systems except the refractory metals, where a factor of 15 is generally found to better represent the data. In the case of silicon nitride, where insufficient data exist to establish a correct parameter, a value of 20 was used.

### 3.13 Comparison of Materials Problems Associated with the Advanced Energy Conversion Systems

In the foregoing subsections the materials problems associated with each of the advanced energy conversion systems have been discussed, and in each case a summary chart has been included which identifies the materials selections, the system parametric points to which they apply, and materials application ratings. It is the purpose of this subsection to further analyze these ratings and to compare the materials aspects of the advanced energy conversion systems.

#### 3.13.1 Summary Materials Application Evaluations

The basis for the materials application ratings was set forth in Subsection 3.1. The rating system is seen primarily as a qualitative measure of the difficulty of demonstrating the utility of a particular

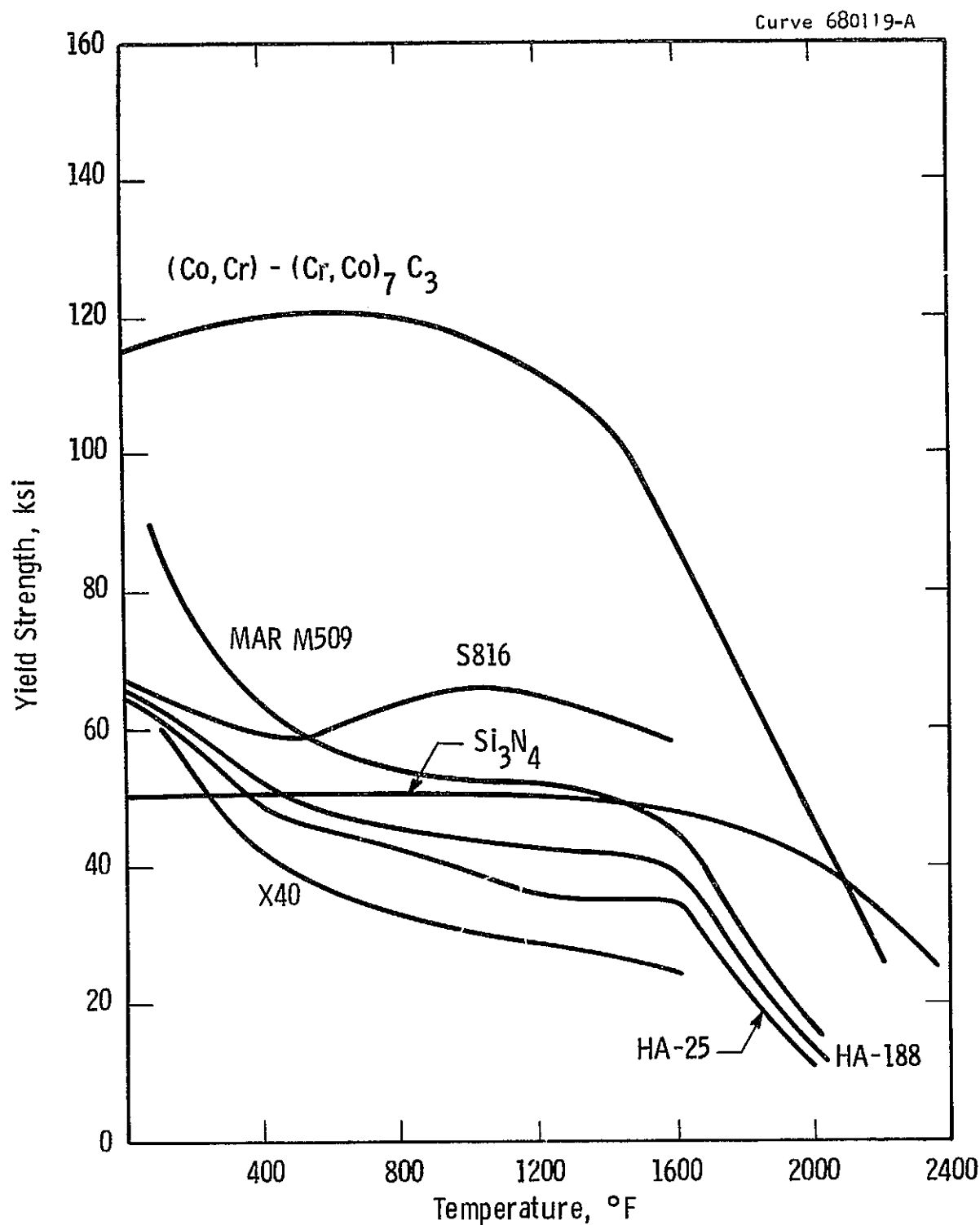


Fig. 3.50—Yield strength - temperature plot for selected cobalt base alloys and Si<sub>3</sub>N<sub>4</sub>

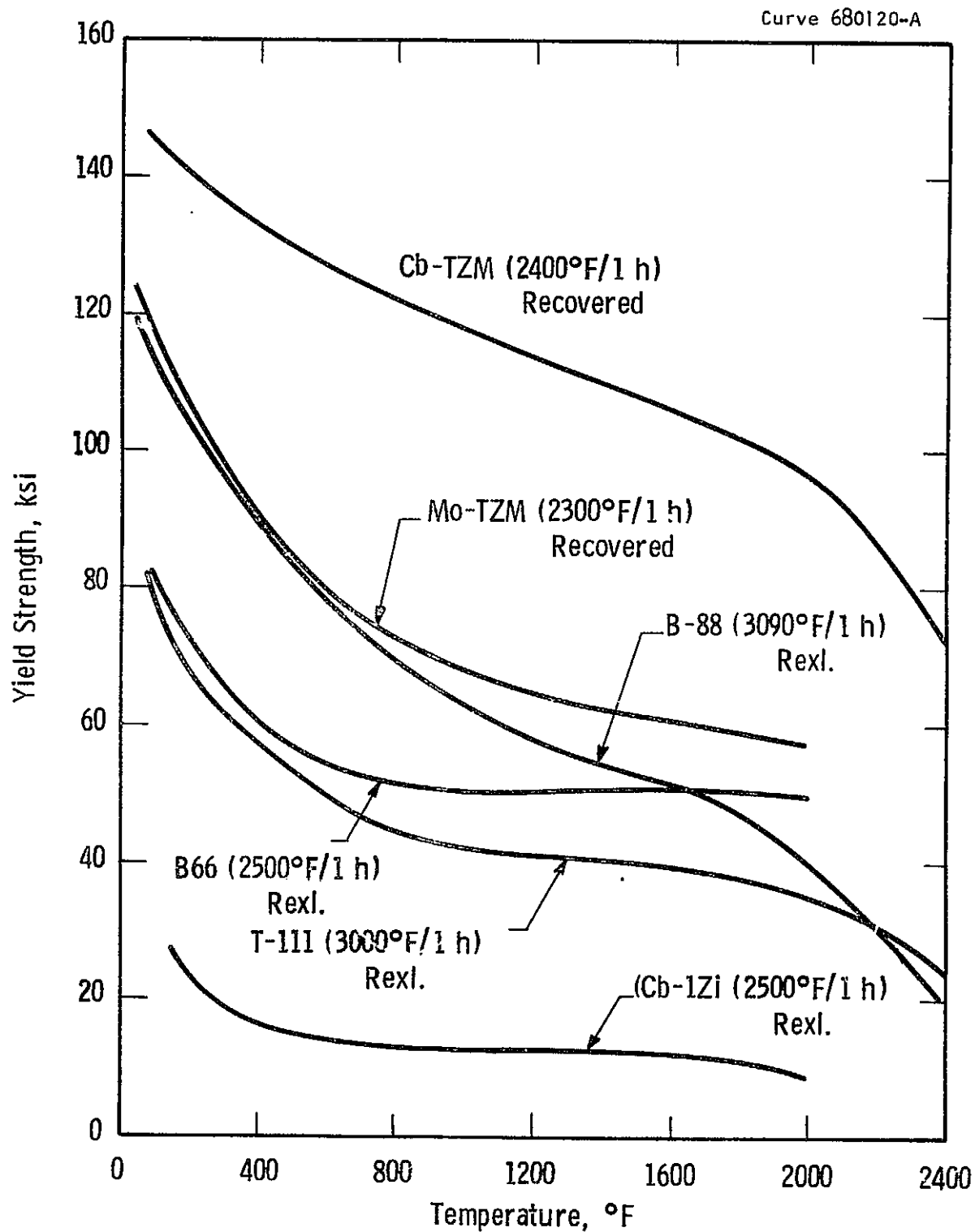


Fig. 3.51—Yield strength - temperature plot for selected refractory metals

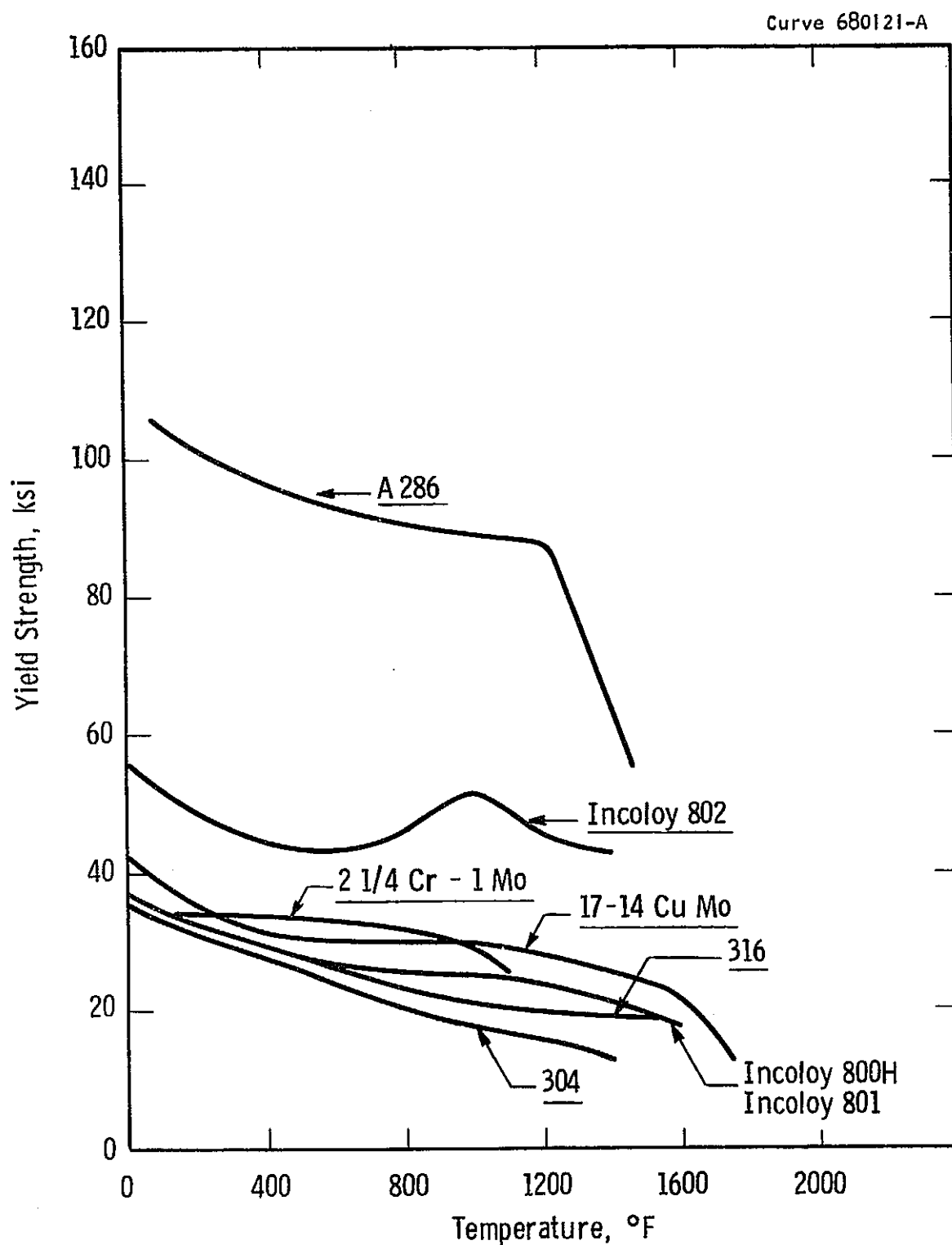


Fig. 3. 52—Yield strength-temperature plot for selected iron-base alloys

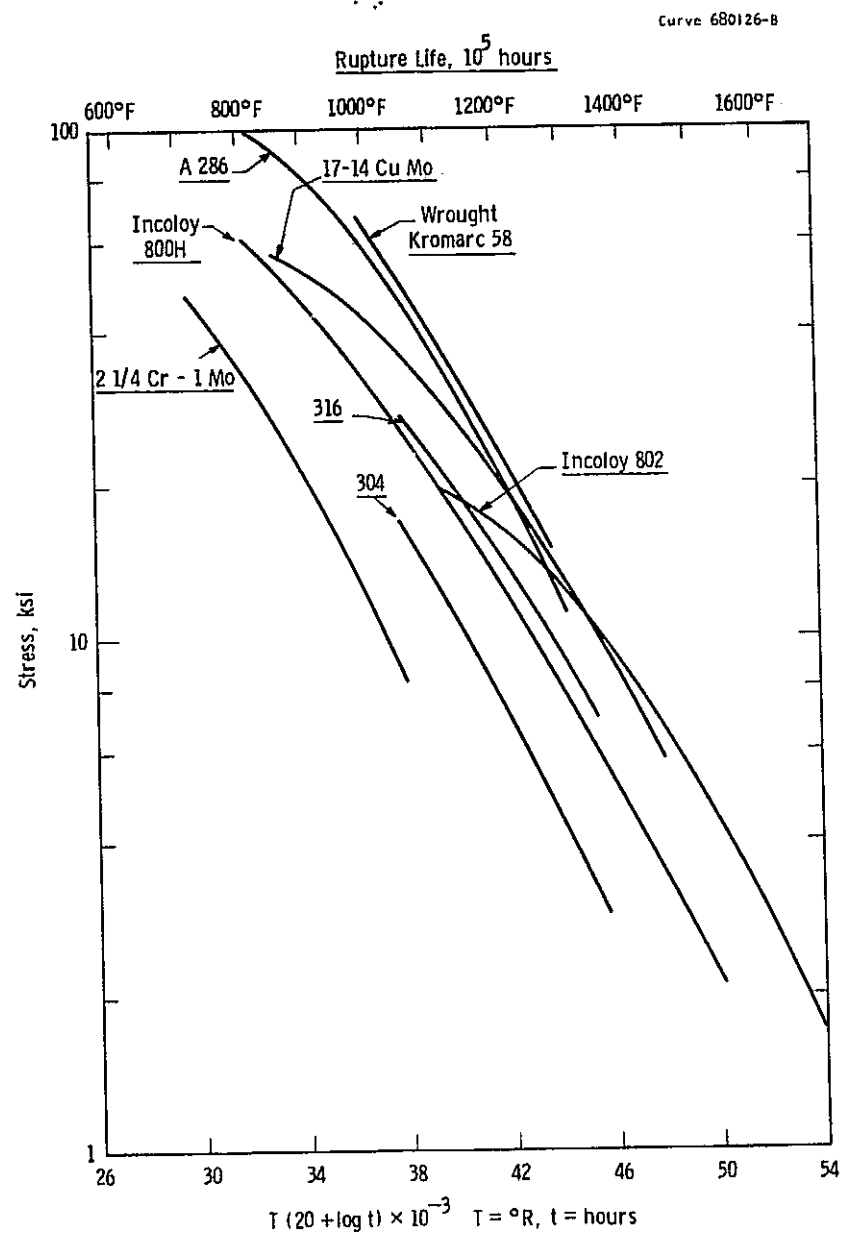


Fig. 3. 53 -Stress rupture data (Larson-Miller plot) for selected iron-base alloys

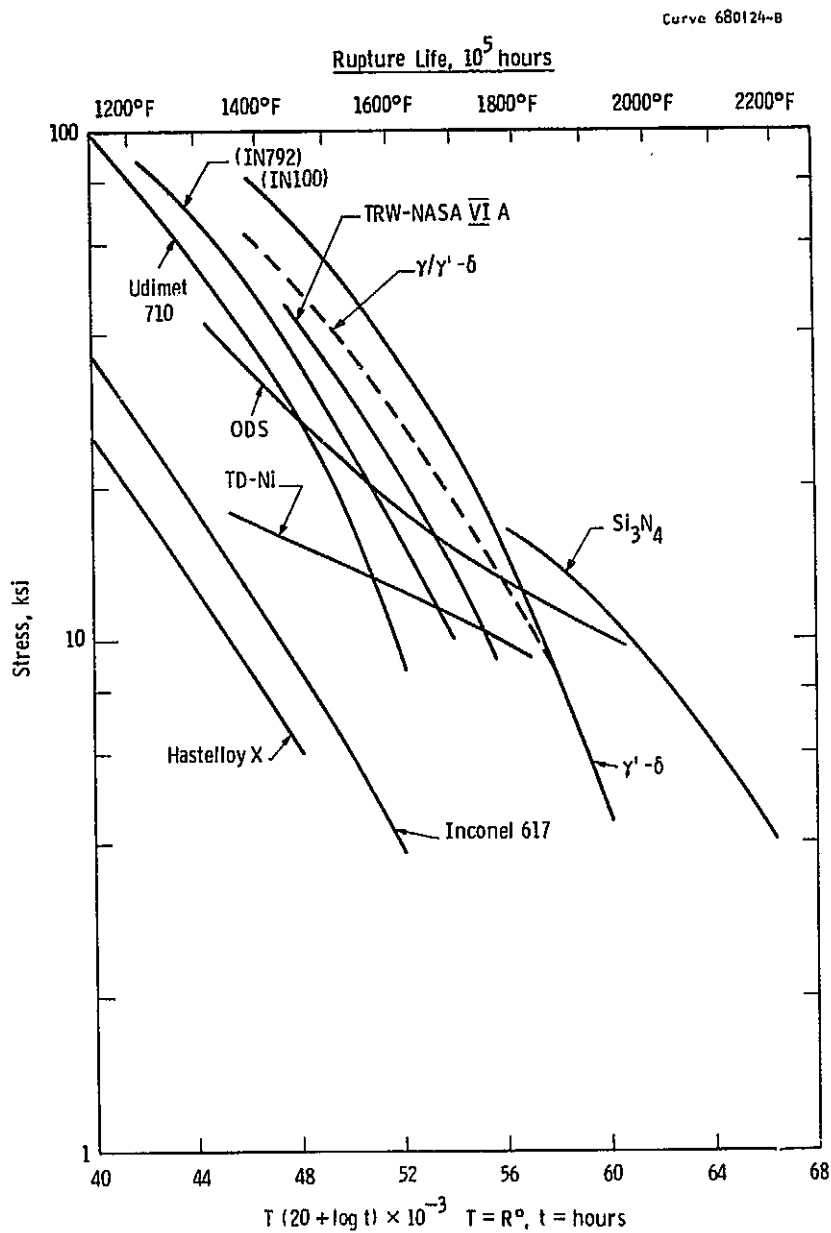


Fig. 3.54—Stress rupture data (Larson-Miller plot) for selected nickel base alloys

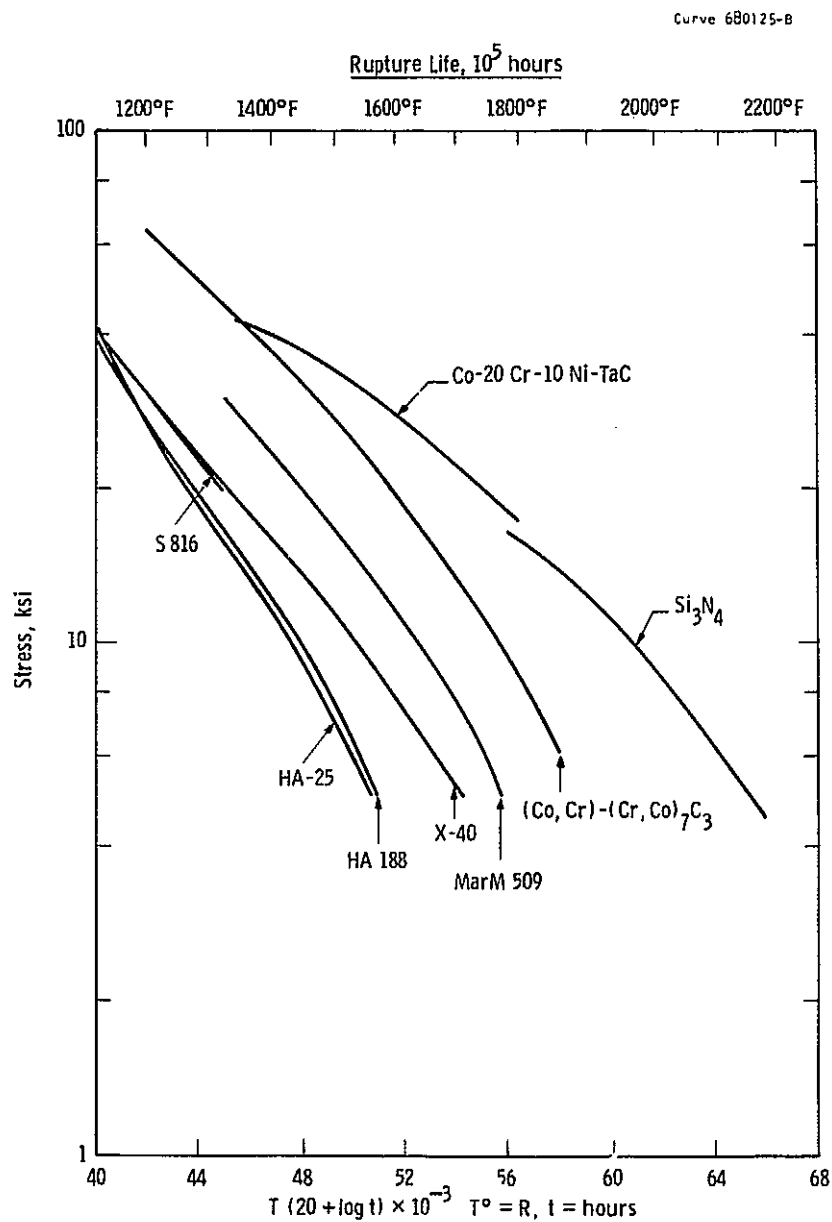


Fig. 3.55—Stress rupture data (Larson-Miller plot) for selected cobalt base alloy and  $\text{Si}_3\text{N}_4$

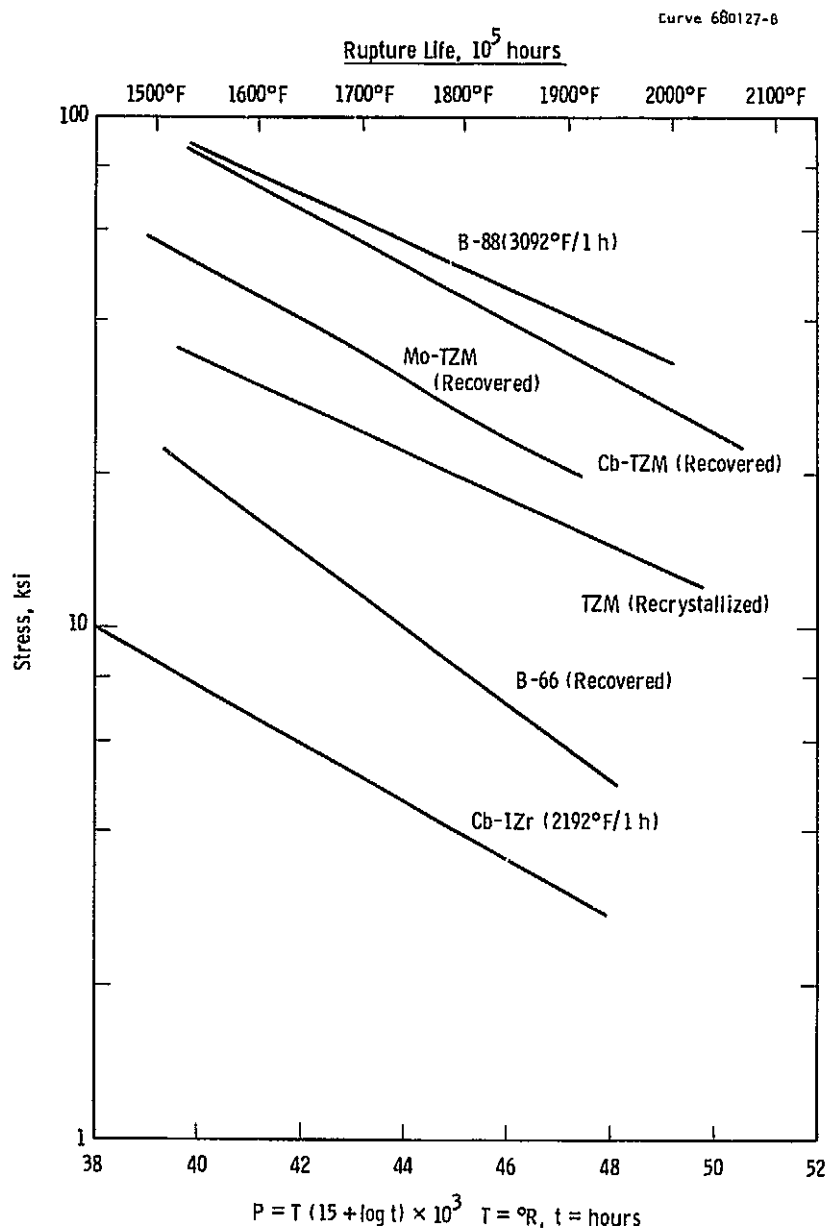


Fig. 3.56—Stress rupture data (Larson-Miller plot) for selected refractory alloys



material in a particular application. Increasingly difficult materials problems imply that the program time and the cost to solve the problem also increase and that the probability of program success decreases.

Summary materials application evaluations are presented for the various advanced systems in Tables 3.64 to 3.72, inclusive, which represent, in part, condensations of the data given in the summary tables in the subsections dealing with materials for the corresponding advanced system. In each table the contents are arranged according to the principal system parameters which are most important from the point of view of materials--for example, turbine inlet temperature. A compilation of the number of items (materials applications) having a given rating, A, B, C, or D, is entered into each table. In compiling this information an attempt was made to avoid counting the same problem twice. Thus, for example, in the subsection on fuel cells there are separate ratings for anode material and anode catalyst for the low-temperature fuel cells. Since the catalyst is actually incorporated into the anode material, however, they represent one problem and have been treated as such in Table 3.72. Similarly, the turbine disk and shaft in the case of the liquid-metal vapor cycle are interpreted as one problem.

In addition, a composite rating is included which is intended to represent the overall difficulty of the materials application problems involved in a particular system. The composite rating is computed from Equation 3.18.

$$\text{Composite Rating} = N_B + 5 N_C + 10 N_D \quad (3.18)$$

where  $N_B$  is the number of B-rated items,  $N_C$  is the number of C-rated items, and  $N_D$  is the number of D-rated items. The weighting factors are based on the opinion that the total effort or cost to solve B-rated, C-rated, and D-rated materials application problems is in the ratio 1:5:10, respectively. The weighting factor for A-rated materials applications is taken as zero, reflecting the fact that only minimal routine materials applications engineering would be involved, which in the present context does not constitute a materials problems relevant to a particular type of system.

Table 3.64 — Materials for Advanced Steam Cycle Components

Turbine Inlet Cond. °F, psi)	Number of Items Having a Given Rating				Most Critical Materials Application		
	<u>A</u>	<u>B</u>	<u>C</u>	<u>D</u>	<u>Lowest Rating</u>	<u>Composite Rating</u>	<u>Critical Items (C &amp; D)</u>
1200/2400	3	1			B	1	--
1200/3500	2	2			B	2	--
1200/5000	2	1	1		C	6	Inconel 802 or 617 Boiler Tubes (C)
1400/3500	1	1	2		C	11	. Waspalloy Rotor (C) . Inconel 617 or HA188 Boiler Tubes (C)
1400/5000	1		2	1	D	20	. Waspalloy Rotor (C) . S816 Inlet Piping & Inner Cylinder (C) . S816 Boiler Tubes (D)

### 3.13.2 Comparison of Materials Ratings

Using the information compiled in Tables 3.64 through 3.72, composite materials application ratings for all of the advanced systems are displayed together in Table 3.73. The principal system parameters shown are easily relatable to most system parametric cases. An exception exists in the entries for gas turbines in that the amount of blade or vane cooling is not treated parametrically in the system study, while in the materials analysis it was recognized that increased temperature capability of blade or vane materials represents a performance improvement resulting from a reduced cooling requirement for a given turbine inlet temperature. The entries in the table labeled "max. cooling" or "no cooling" correspond to the system study assumptions.

The systems are listed in Table 3.72 in the order of increasing severity of materials problems, considering each type of system as a single entity. The materials problems associated with the gas turbine systems using blade and/or vane cooling are considered to be less than with any of the other systems. The closed-cycle gas turbine and liquid sodium-argon metal MHD materials problems are slightly more severe than those of the gas turbine systems. (The lithium-helium liquid-metal MHD system is markedly more difficult from a materials point of view than the sodium-argon liquid-metal MHD system, and perhaps should be ranked separately.) The ranking order continues with advanced steam systems, liquid-metal vapor rankine, fuel cells, closed-cycle MHD, and open-cycle MHD systems.

It is inappropriate to speculate further upon the materials application ratings and the ranking of systems materials development requirements. In Tasks II and III detailed development program descriptions, costs, and schedules will be worked out for the systems which are to be continued.

Table 3.65 — Materials for Recuperated Open-Cycle Turbine Cycle Components  
(Fuel: Coal Distillate)

Turbine Conditions (T.I.T. - °F) (Cooling)	Number of Items Having a Given Rating				Most Critical Materials Applications		
	A	B	C	D	Lowest Rating	Composite Rating	Critical Items (C's & D's)
<u>1800-2500</u>							
Max. Blade & Vane Cooling	3				A	0	--
Int. Blade & Vane Cooling	1	2			B	2	--
Min. Blade & Vane Cooling	1		2		C	10	. W-reinforced superalloy or Cr-alloy first-row blades (C) . Mo-reinforced superalloy last- row blades (C)
<u>2200-2500</u>							
Max. Blade Cooling	2	1			B	1	--
Int. Blade Cooling		3			B	3	--
Min. Blade Cooling		1	2		C	11	. W-reinforced superalloy or Cr-alloy first-row blades (C) . Mo-reinforced superalloy last- blades (C)
<u>2200-2500</u>							
No Cooling	1	1	1		C	6	Si <sub>3</sub> N <sub>4</sub> or SiC first-row blades (C)

Table 3.66 — Materials for Combined Cycle Gas Turbine Components

Turbine Conditions (T.I.T. °F) (Cooling)	Fuel	Number of Items Having a Given Rating				Most Critical Materials Applications		
						Lowest	Composite	Critical Items
		A	B	C	D	Rating	Rating	(C's & D's)
1800-2500	Coal Distillate	--- Same as Recuperated Open Cycle Gas Turbine ---						
<u>2200</u>								
Max. Blade & Vane Cooling	High- or Low-Btu Gas	3				A	0	--
Int. Blade & Vane Cooling	"	1	2			B	2	--
Min. Blade & Vane Cooling	"	1		2		C	10	. W-reinforced superalloy or Cr alloy first-row blades (C) . Mo-reinforced superalloy last-row blades (C)
<u>2200</u>	Coal Distillate							
H <sub>2</sub> O-cooled Blades Max. Cooling		2	1			B	1	
Int. Cooling		1	2			B	2	
Min. Cooling		1	1	1		C	6	. Mo-reinforced last-row blades (C)

Table 3.67 — Materials for Closed-Cycle Gas Turbine Components

Turbine Inlet Temp., °F	Number of Items Having a Given Rating				Most Critical Materials Applications		
					Lowest Rating	Composite Rating	Critical Items (C & D)
	<u>A</u>	<u>B</u>	<u>C</u>	<u>D</u>			
1200	6				A	0	--
1500	4	2			B	2	--
1800	2	3	1		C	8	Inco Clad 671 on HA-188 or Inco Clad on S816 Heat Exchanger (C)

Table 3.68 — Materials for Potassium and Cesium Vapor Rankine  
Cycle Components

<u>Turbine Inlet Temperature, °F</u>	<u>Number of Items Receiving a Given Rating</u>				<u>Most Critical Materials Applications</u>		
	<u>A</u>	<u>B</u>	<u>C</u>	<u>D</u>	<u>Lowest Rating</u>	<u>Composite Rating</u>	<u>Critical Items (C &amp; D)</u>
1400		3	3		C	18	Incoloy 800 boiler (C) Incoloy turbine shaft & disk (C) U700 turbine blades and tie bolts (C)
1500	1	2	2	1	D	22	Incoloy 800 boiler (C) Waspalloy disk and shaft (D) Inlet casing (Incoloy 801) case and scroll (HA 188) (C)
1600	1	2	2	1	D	22	HA-188 boiler (C) Waspalloy disk & shaft (D) HA-188 inlet casing, case, and scroll (C)

Table 3.69 — Materials for Sodium and Lithium MHD System Components

Duct Inlet Temperature °F	Number of Items Receiving a Given Rating				Most Critical Materials Applications		
	<u>A</u>	<u>B</u>	<u>C</u>	<u>D</u>	<u>Lowest Rating</u>	<u>Composite Rating</u>	<u>Critical Items (C's &amp; D's)</u>
1200 (Na-Ar)	7		1		C	5	. Al <sub>2</sub> O <sub>3</sub> or MgO Insulators (C)
1500 (Na-Ar)	1	4	2		C	14	. Al <sub>2</sub> O <sub>3</sub> or MgO Insulators (C) . HA-188 Steam Generator (C)
1500 (Li-He)	1		6		C	30	. Cb Alloy Heat Source (C) . Cb Alloy Generator (C) . MgO or BeO Insulators (C) . Cb Alloy Electrodes (C) . Cb Alloy Loop (C) . Cb Alloy Duplex Tubes (C) for Steam Generator

3-272

REPRODUCIBILITY OF THE  
ORIGINAL PAGE IS POOR



Table 3.70 --- Materials for Open-Cycle MHD Components

Duct Temperature Fuel Firing	Number of Items Having a Given Rating				Most Critical Materials Application		
	<u>A</u>	<u>B</u>	<u>C</u>	<u>D</u>	<u>Lowest Rating</u>	<u>Composite Rating</u>	<u>Critical Items (C &amp; D)</u>
2380 - 3700°F Coal Separately Fired Preheat.	3	1	2	4	D	51	. SiC Combustor (C) ."SiC" Electrodes (D) ."Si <sub>3</sub> N <sub>4</sub> " Insulators (D) . Chromite Bonded Al <sub>2</sub> O <sub>3</sub> Diffuser (C) . 304 SS Superheater (D) . 2-1/4Cr - 1 Mo Reheater & Evaporator (D)
2400°F Coal Direct Firing	1		2	6	D	70	. SiC Preheater Tubes (D) . RA333 Preheater Tubes (D) . SiC Combustor (C) ."SiC" Electrodes (D) ."Si <sub>3</sub> N <sub>4</sub> " Insulators (D) . Chromite Bonded Al <sub>2</sub> O <sub>3</sub> Diffuser (C) . 304 SS Superheater (D) . 2-1/4Cr - 1 Mo Reheater & Evaporator (D)
2590 - 3190 Low BTU Gas Direct Firing	1	2	2	4	D	52	. SiC Preheater Tubes (D) . RA 333 Preheater Tubes (D) . La-Sr CrO <sub>3</sub> Electrodes (D) . MgO Insulators (C) . 304 SS Superheater (D) . 2-1/4 Cr- 1Mo Reheater (C)

Table 3.71 — Materials for Closed-Cycle MHD Components

Duct Temperature °F	Number of Items Having a Given Rating				Most Critical Materials Applications		
	<u>A</u>	<u>B</u>	<u>C</u>	<u>D</u>	<u>Lowest Rating</u>	<u>Composite Rating</u>	<u>Critical Items (C's &amp; D's)</u>
3100	3	4	3	1	D	29	. Y <sub>2</sub> O <sub>3</sub> Stab. ZrO <sub>2</sub> Valves (D) . Al <sub>2</sub> O <sub>3</sub> Nozzle (C) . TZM Electrodes (C) . HA-188 Reheater Tubes(C)
3800	4	4	3	1	D	29	. Y <sub>2</sub> O <sub>3</sub> Stab. ZrO <sub>2</sub> Valves (D) . Y <sub>2</sub> O <sub>3</sub> Stab. ZrO <sub>2</sub> or TZM Nozzle (C) . TZM Electrodes (C) . HA-188 Reheater (C)

Table 3.72 — Materials for Fuel Cells (100,000 hr life)

Cell Type	Number of Items Having a Given Rating				Most Critical Materials		Applications
	A	B	C	D	Lowest Rating	Composite Rating	Critical Items (C & D)
Alkaline Electrolyte	1		2	1	D	20	. "Carbon" anode (C) . "Carbon" cathode (D) . Electrolyte (C)
Acid Electrolyte	1		3		C	15	. "Carbon" anode (C) . "Carbon" cathode (D) . Electrolyte (C)
Molten Carbonate Electrolyte			4		C	20	. Aluminates in electrolyte paste (C) . "Ni" anode (C) . Lithiated NiO cathode (C) . Interconnections (C)
Solid Electrolyte			3	1	D	25	. "Cr <sub>2</sub> O <sub>3</sub> " interconnection (D) . Ni-ZrO <sub>2</sub> anode (C) . In <sub>2</sub> O <sub>3</sub> - PrCoO <sub>3-x</sub> cathode (C) . (Y <sub>2</sub> O <sub>3</sub> ) <sub>x</sub> (ZrO <sub>2</sub> ) <sub>1-x</sub> Electrolyte (C)

Table 3.73 — Summary of Materials Application Ratings

SYSTEM			Composite Materials Application Rating							
			0	10	20	30	40	50	60	70
Open-Cycle G.T.	1800-2500°F	Max Cooling B/V								
and Combined	"	Min "								
G.T. Cycle	2200-2500°F	Max Cooling B								
Fuel Distillate	"	Min. "								
	"	No Cooling								
Comb.G.T.Cycles	2200°F	Max Cooling B/V								
Hi&Lo Btu Gas	"	Min Cooling B/V								
Comb.G.T.Cycles	2200°F	Max H <sub>2</sub> O B Cooling								
Fuel: Distillate	"	Min H <sub>2</sub> O B Cooling								
Closed-Cycle G.T.	1200°F									
	1500°F									
	1800°F									
Liquid-Metal MHD	1400°F	Na-Ar								
	1500°F	Na-Ar								
	1500°F	Li-He								
Advanced Steam	1200°F/2400 psi									
	1200/3500									
	1200/5000									
	1400/3500									
	1400/5000									
Liquid-Metal Vapor Rankine	1400°F	K or Cs								
	1500°F	"								
	1600°F	"								
Fuel Cells	Acid									
	Alkaline									
	Molten Carbonate									
	Solid Electrolyte									
Closed-Cycle MHD	3100°F									
	3800°F									
Open-Cycle MHD	2380-3700°F	Coal, Sep. Firing								
	2400°F	Coal, Direct Firing								
	2590-3190°F	Low Btu Gas								
	Direct									

REPRODUCIBILITY OF THE  
ORIGINAL PAGE IS POOR

### 3.14 References

- 3.1 E.V. Somers and L.E. Brecher, "Coal-Derived Liquid and Gaseous Fuels for Power Plants #1: Fuel Composition," W Research Memo 74-9EO-ECAS-M1, (1974).
- 3.2 J.R. Hamm, W Research Labs, Private Communication.
- 3.3 S.A. Jansson and E.F. Sverdrup, Work performed on OCR Contract No. 14-32-0001-1514-26, (1973).
- 3.4 M.A. Alvin, W Research Labs., Work performed on OCR Contract No. 14-32-0001-1514-26, (1974).
- 3.5 J.W. Clark, "Clean Power Generation from Coal," OCR Contract No. 14-32-0001-1223.
- 3.6 R.C. Hurst, J.B. Johnson, M. Davies and P. Hancock, "Sulfate and Chloride Attack of Nickel-Based Alloys and Mild Steels," in Deposition and Corrosion in Gas Turbines, (A.B. Hart and A.J.B. Cutler, Eds.) John Wiley & Sons, New York, (1973).
- 3.7 S.C. Singhal, "Oxidation and Corrosion/Erosion Behavior of Hot Pressed  $\text{Si}_3\text{N}_4$  and  $\text{SiC}$ ," in Ceramics for High Performance Applications, (J.J. Burke, A.E. Gorum and R.N. Katz, Eds.) Brook Hill Publishing Co., (1974).
- 3.8 S.C. Singhal, Work Performed on ARPA Contract No. DAAG 46-71-C-0162, (1974).
- 3.9 J.W. Clark, "Development of  $\text{Cr-Li-Y}_2\text{O}_3$  Coatings for Chromium-base Alloys," NASA CR-72763, (1971).
- 3.10 J.W. Clark, Private Communication
- 3.11 A.M. Beltran, Cobalt, Vol. 46, (1970).
- 3.12 C.J. Spengler, S.Y. Lee, and W.E. Young, "The Pressurized Passage, A Laboratory Rig for Gas Turbine Simulation," in Deposition and Corrosion in Gas Turbines (A.B. Hart and A.J.B. Cutler, Eds.) John Wiley & Sons, (1973).
- 3.13 "Hot Corrosion in Gas Turbines," National Materials Advisory Board NMAB-260, (1970).

- 3.14 S.Y. Lee, S.M. DeCorso, and W.E. Young, "Laboratory Procedures for Evaluating High-Temperature Corrosion Resistance of Gas Turbine Alloys," J. Engrg. for Power, (1971) p. 313.
- 3.15 C.T. Sims and W.C. Hagel, "The Superalloys," John Wiley & Sons, New York, (1972).
- 3.16 I.G. Wright, "Oxidation of Iron-Nickel-and Cobalt-Base Alloys," MCIC 72-07, (1972).
- 3.17 J. Stringer and D.P. Whittle, "High Temperature Corrosion and Coating of Superalloys," in High Temperature Materials in Gas Turbines, (P.R. Sahm and M.O. Speidel, Eds.), Elsevier Scientific Publishing Co., 1974.
- 3.18 Kobe Technical Institute, Mitsubishi Heavy Industries, Ltd., (1973).
- 3.19 C.M. Jackson and A.M. Hall, NASA TMX-53448, 1966.
- 3.20 "High Temperature Oxidation Resistant Coatings," ISBN-2-309-01769-6, NAC-NMAB, (1970).
- 3.21 N.R. Lindblad, Oxidation of Metals, Vol. 1, 1969.
- 3.22 G.W. Goward, J. Metals, (1970), p. 31
- 3.23 S.J. Grisaffe, "Coatings and Protection," in the Superalloys, (C.T. Sims and W.C. Hagel, Eds.) John Wiley & Sons, (1972).
- 3.24 E.J. Felten, T.E. Strangman, and N.E. Ulion, "Coatings for Directional Eutectics," NASA-CR-134735, (1974).
- 3.25 D.L. Keairns et al, "Evaluation of the Fluidized Bed Combustion Process," Vols. I, II, and III; EPA-650/2-73-048 a,b and c, (1973).
- 3.26 "Corrosion and Deposits from Combustion Gases," Abstracts and Index 1970; Battelle Memorial Institute, Columbus, Ohio, (1970).
- 3.27 W.T. Reid, "External Corrosion and Deposits, Boilers and Gas Turbines," Elsevier, (1971).
- 3.28 R.J. Bishop, "The Formation of Alkali-rich Deposit by a High-Chlorine Coal," J. of the Institute of Fuel, Vol. 51, (1968), p. 51.
- 3.29 B.J. Glidden, C.E.G.B. Research Report.
- 3.30 "Reduction of Atmospheric Pollution," National Coal Board, London, Report for EPA, (1971).

- 3.31 Pope, Evans and Robbins, Monthly Reports prepared under Contract No. CPA70-10 for National Air Pollution Control Administration.
- 3.32 A.D. Dainton and D.E. Elliot, Seventh World Power Conference, Moscow, (1968).
- 3.33 National Research Development Corp., London, R&D Report No. 85, for Office of Coal Research Contract No. 14-32-0001-1511, (August 1972 - September 1973).
- 3.34 C.A. Barrett and C.E. Lowell, "Comparison of Isothermal and Cyclic Oxidation Behavior of Twenty-Five Commercial Sheet Alloys at 1150°C, NASA TN D-7615, April, (1974).
- 3.35 R.F. Decker and E.G. Richards, Paper No. 3, International Nickel Power Conference, Lausanne, (1967).
- 3.36 W.K. Armitage and D.F. Plowman, "High Temperature Corrosion-Resistant Alloys for Fossil-Fired Boilers," International Nickel Power Conference, Lausanne, (1972).
- 3.37 International Nickel Publication 2942, "Chromium Nickel Alloys that Overcome Fuel-Ash Corrosion.
- 3.38 D.W. Rahoï, "Controlling Fuel Ash Corrosion with Nickel Alloys," Materials Engineering Quarterly, February, 1974.
- 3.39 "Haynes Alloy 188- A New Oxidation Resistant High Strength Ductile Cobalt Base Alloy," Stellite Division, Cabot Corp., publication.
- 3.40 H.S. Blumberg, "Metallurgical Considerations of Main Steam Piping for High-Temperature, High-Pressure Service," Trans. of ASME, Vol. 79, pp. 1377-1409 (1957).
- 3.41 ASME Boiler and Pressure Vessel Code, Section 1, 1974 Edition.
- 3.42 Material Selector 1975, Materials Engrg., Vol. 80, No. 4.
- 3.43 Metals Progress Data Book, 1974, ASM, Vol. 106, No. 1
- 3.44 Alloy Digest, Engrg. Alloy Digest, Inc.
- 3.45 Technical Bulletins
- 3.46 I.L.W. Wilson, Unpublished Letter, Westinghouse R&D.

- 3.47 "Behavior of Superheated Alloys in High Temperature, High Pressure Steam," Ed. G.E. Lien, Pub. ASME (1968).
- 3.48 S. Jansson, W. Hubner, G. Ostberg, M. dePourbaix, "Oxidation Resistance of Some Stainless Steels and Nickel Based Alloys in High Temperature Water and Steam," Br. Corros. J. 4, p. 21 (1969).
- 3.49 "Incoloy Alloys," Huntington Alloys Publication of the International Nickel Co., (1973).
- 3.50 Inconel 601 publication of HAPD, INCO, (1969).
- 3.51 Inconel X-750 publication of HAPD, INCO (1970).
- 3.52 Inconel 625 publication of HAPD, INCO (1970).
- 3.53 F. Eberle, F.G. Ely, J.A. Dillon, "Experimental Superheater Report After 12,000 hrs of Operation," Trans. ASME 76, p. 665 (1954).
- 3.54 D.A. Hawkes, S.B. Hosegood, "The High Temperature Gas Reactor: A Process Heat/Electrical Energy Source for a Large Steelworks," J.B.N.E.S. 10, p. 308 (1971).
- 3.55 R.H. Caughey and W.G. Benz, Jr., "Material Selection and Fabrication, Main Steam Piping For Eddystone No. 1, 1200°F and 5000 psi Service," Trans. ASME, 82, p. 293 (1960).
- 3.56 W.E. Trumpler, A.F. Le Breton, E.A. Fox and R.B. Williamson, "Development Associated with the Superpressure Turbine for Eddystone Station Unit No. 1," Trans. ASME, 82, p. 286 (1960).
- 3.57 ASME Boiler and Pressure Vessel Code, Sec. 1, 1974 Edition.
- 3.58 F.C. Hull, "A High-Strength Weldable Steel for Elevated Temperature Service," Advances in the Technology of Stainless Steels and Related Alloys, STP 369, p. 88 (1965).
- 3.59 R.S. Cremisio, "Melting," The Superalloys, (C.T. Sims and W.C. Hagel, Eds.) p. 373 (1972).
- 3.60 R. Viswanathan and T.P. Sherlock, Met. Trans. 3, p. 459 (1972).
- 3.61 A. Cochardt, "The Origin of Damping in High Strength Ferromagnetic Alloys," Trans. ASME, J. of Appl. Mech., 75, p. 196 (1953).



C-4

- 3.62 Special Metals, Technical Data Sheet on U710.
- 3.63 Preliminary Data. Based on Rupture Strength of IN100.
- 3.64 G.E. Wasielewski and N.R. Lindblad, Proc. Second International Conf. on Superalloys-Processing MCIC Report 72-10.
- 3.65 H.E. Collins, Development of High Temperature Nickel-Base Alloys for Jet Engine Turbine Bucket Applications, NASA CR-54507 (1967).
- 3.66 J.S. Benjamin, Met. Trans. 1, pp. 2943-2951 (1970).
- 3.67 R.P. Dalal and R.J. Fiedler, "Conference on Hot Corrosion of Superalloys," Castine, Maine, (1974)
- 3.68 F.D. Lemkey and E.R. Thompson, "Proc. Conference on In-Situ Composite," Lakeview, Conn., September (1972).
- 3.69 H. Bibring, G. Seibel and M. Raninovitch, Second International Conference on Strength of Met. and Alloys, Asilomar, Vol. III, p. 1178 (1970).
- 3.70 E.R. Thompson, D.A. Koss and J.C. Chesnutt, Met. Trans., 1, p. 2807 (1970).
- 3.71 D.W. Petrasek, R.A. Signorelli, J.W. Weeton, NASA Report.
- 3.72 Private Communication, J.A. Cornie
- 3.73 J.W. Clark, "Development of High Temperature Chromium Alloys," NASA Contract Reports 92619 and 72731, June (1967) and November (1970).
- 3.74 A.M. Filippi, "Development of Ductile High Strength Chromium Alloys," NASA Contract Report 134522, September (1973).
- 3.75 A.F. McLean, E.A. Fisher and R.J. Bratton, "Brittle Materials Design, High Temperature Gas Turbine, AMMRC CTR-74-26, p. 109, April (1974).
- 3.76 R. Kossowsky, D.G. Miller and E.S. Diaz, Westinghouse Scientific Paper 74-9D4-FORAM-P8, August 7, 1974.
- 3.77 E.R. Thompson and F.D. Lemkey, Met. Trans., 1, p. 2799, (1970).

- 3.78 E.R. Thompson, D.A. Koss and J.C. Chesnutt, Met. Trans., 1, p. 2807 (1970).
- 3.79 See Reference 5.14, September (1974).
- 3.80 J.C. Bokros and H.E. Shoemaker, "Reactor Materials Compatibility with Impurities in Helium," (1961) USAEC Report GA-1508.
- 3.81 J.W. Wunderlich and W.E. Baker, "Exposure of HTGR Candidate Core Plate and Thermal Materials to Impure Helium at 1650°F to 1850°F for 3,000 Hours," (1966) USAEC Report GAMD-7377.
- 3.82 A.F. Weinberg and J.M. Scoffin, "Exposure of Reactor Materials to Impure Helium at Elevated Temperatures," (1962) USAEC Report GA-2998.
- 3.83 T.T. Claudson and R.E. Westerman, "An Evaluation of the Corrosion Resistance of Several High Temperature Alloys for Nuclear Appl.," (1965) USAEC Report BNWL-155.
- 3.84 L.A. Charlot and R.E. Westerman, "High Temperature Corrosion of Candidate ATR Structural Materials," (1965) USAEC Report BNWL-100.
- 3.85 T.T. Claudson and H.J. Pessl, "Evaluation of Iron and Nickel-Based Alloys for Medium and High Temperature Reactor Applications, Part II," (1965) USAEC Report BNWL-154.
- 3.86 S. Sekino, "Studies of Heat-Resistant Materials for High Temperature Gas Reactors," NASA Technical Translation, NASA TT F-15, 576.
- 3.87 A.B. Knutsen, J.F.G. Conde and K. Pierce, "High Temperature Corrosion of Nimonic-75 and Various Steels in Gases at Low Partial Pressures," (1969), Br. Corros. J., 4, p. 94-103.
- 3.88 H.I. Inouye, "High Temperature Reactions of Type 304 Stainless Steel in Low Concentrations of Carbon Dioxide and Carbon Monoxide," Proc. IAEA Conf. on Corrosion of Reactor Materials, (1962), 1, p. 317-342.
- 3.89 J. Board, "The Effect of Helium Environment on the High Temperature Properties of Structural Materials, J. BNES, (1970), p. 101-112.
- 3.90 R.J. Pearce and R.P. Sperry, "Electron Probe Microanalysis of Certain Metallic Specimens Exposed in Fuel Element Assemblies of the Dragon Reactor, Gen. Electr. Gen. Board, Report No. RD/B/N2277.
- 3.91 D.S. Wood, M. Farrow, and W.T. Burke, "A Preliminary Study of the Effect of Helium Environment on the Creep and Rupture Behavior of Type 316 SS and Incoloy 800," Eff. Environ. Mater. Prop. Nucl. Syst. Proc. Int. Conf. Corros., (1971), pp. 203-12.

- 3.92 D.S. Wood, M. Farrow, A.B. Baldwin, W.T. Burke, "Creep Rupture Properties of Some High Temperature Reactor Circuit Materials in Helium," Int'l Conf. on Creep and Fatigue in Elevated Temperature Applications, Inst. Mech. Engrs. Conf., Publ.13 (1973).
- 3.93 R.A.U. Huddle, See Reference 6.12
- 3.94 R.A.U. Huddle, "The Surface Reactions of HTR Helium with Turbine Materials and Their Influence on Creep Behavior," Deposition and Corrosion in Gas Turbines, (A.B. Hart and A.J.B. Cutler, Eds.), J. Wiley & Sons, New York (1973, pp. 158-177).
- 3.95 ASME Boiler and Pressure Vessel Code, Section 1, (1974).
- 3.96 E.O. Miller and W. Jackobeit, "Super" Superalloys for Temperatures over 900°C" Gas Turbine International, March-April (1970).
- 3.97 W. Jackobeit, "Molybdenum-based Alloys as Materials for Helium Gas Turbines," High Temperature Materials in Gas Turbines, (P.R. Sahm and M.O. Speidel, Eds.) (1974).
- 3.98 A.W. Goldenstein, "Molybdenum Forging Process Development," ML-TDR-64-6)February, (1964).
- 3.99 B.L. Moor and E. Schnetzer, "Three-Stage Potassium Vapor Turbine Test," Final Report, NASA-CR-1815, May (1971). (Also under GESP-547, August, (1970).
- 3.100 Mine Safety Appliance Research, Evans City, Pa., Personal Communication.
- 3.101 G.G. Lessmann, et al., "Material Considerations for Design of the Potassium Turboalternator (KTA)" WANL-TME-1889, January 3, 1969.
- 3.102 J.H. Stang, et al., "Compatibility of Liquid and Vapor Alkali Metals with Construction Materials," DMIC Report 227, April (1966)
- 3.103 E.E. Hoffman, (Ed.) "Potassium Corrosion Test Loop Development," NASA-CR-54843 (1965).
- 3.104 E.M. Simons and J.F. Lagedrost, "Mass Transfer of TZM Alloy by Potassium in Boiling-Refluxing Capsules," CONF-650411 (1966), AEC-NASA Liquid Metals Information Meeting, April (1965).
- 3.105 C.M. Scheuerman and C.A. Barrett, "Compatibility of Columbium and Tantalum Tubing Alloys with Refluxing Potassium," NASA-TN-D-3429 (1966).

- 3.106 J.H. DeVan, J.R. DiStefano, and D.H. Jansen, "Compatibility of Refractory Metals with Boiling Alkali Metals," Trans. Amer. Nucl. Soc., 8, 2 (1965).
- 3.107 L.B. Engle and R.G. Frank, "Evaluation of High-Strength Columbium Alloys for Alkali Metal Containment," NASA-CR-54226 (1964).
- 3.108 J.W. Semmel, et al, "Alkali Metals Boiling and Condensing Investigations, Vol. II, Materials Support," Final Report from January 1, 1961 to June 30, 1962. G.E. -63-FPD-66, June (1963).
- 3.109 W.T. Chandler, "Alkali Metal Corrosion Studies at Rocketdyne," AEC-NASA Liquid Metals Corrosion Meeting, TID-7626 (Part 1) April (1962).
- 3.110 E.E. Hoffman and R.W. Harrison, "The Compatibility of Refractory Metals with Liquid Metals," pp. 251-288, in Refractory Metal Alloys, Metallurgy and Technology by I. Machlin, R.T. Begley and E.D. Weisert, (Eds.) TMS AIME, Plenum Press, New York (1968).
- 3.111 D.H. Jansen and J.H. DeVan, "Niobium-1% Zirconium Boiling Potassium Forced-Convection Loop Test," ORNL-4301, December (1968).
- 3.112 E. Schnetzer (Ed.), "3000-Hour Test Two-Stage Potassium Turbine," NASA-CR-72273, July, (1967).
- 3.113 H.G. Young and A.G. Grindell, "Summary of Design and Test Experience with Cesium and Potassium Components and Systems for Space Power Plants," ORNL-TM-1833, June (1967).
- 3.114 J.H. DeVan, et al., "Compatibility of Boiling Potassium with Refractory Metal Alloys," pp. 124-129, ORNL-3870, Metals and Ceramics Division Annual Progress Report for Period Ending June 30, 1965, November (1965).
- 3.115 R.C. Andrews, "The Effect of Sodium on the Mechanical Properties of Austenitic and Ferritic Steels," AEC-NASA Liquid Metals Information Meeting, Gatlinburg, Tenn., April (1965), CONF-650411, p. 108 (1966).
- 3.116 S.S. Blecherman and J. Hodel, "The Compatibility of Structural and Turbo-Machinery Alloys in Boiling Potassium," AEC Report PWAC-501 (1965).
- 3.117 K.J. Kelly, S.S. Blecherman, and J. Hodel, "Corrosion Studies of Refractory Metal Alloys in Boiling Potassium and Liquid NaK," AEC Report CNLM-6246 (1965).

- 3.118 E.A. Kovacevich and R.L. Salley, "Materials Investigation, SNAP 50? SPUR Program, Mechanical Properties of TZM," AFAPL-TR-65-51, June (1965).
- 3.119 E.A. Kovacevich, "Materials Investigation, SNAP 50/SPUR Program, Elevated Temperature Fatigue Studies of Wrought, Stress-Relieved TZM Alloy," AFAPL-TR-66-134, December (1966).
- 3.120 V.R. Degner, "Research in the Field of Liquid-Metal-Lubricated Bearings," Rocketdyne Report R-5086-7, June (1965).
- 3.121 R.A. Burton, et al., "Fundamental Investigation of Liquid-Metal Lubricated Journal Bearings," Southwest Research Institute, SWRI-1228-60, April (1965).
- 3.122 E.B. Arwas (Ed.), "Proc. of the Technical Meeting on: Super-Laminar Flow Bearings and Seals for Process Fluid Lubricated Turbomachinery," Report No. NYO-1363-6 and MTI-66TR66, December, 1966.
- 3.123 R.G. Frank, "Potassium Corrosion Studies," in AEC-NASA Liquid Metals Information Meeting, Gatlinburg, Tenn. April (1965) CONF-650411, p. 302 (1966).
- 3.124 C.J. Mole et al., "Design and Development of a Segmented Magnet Homopolar Torque Converter," EM 4602, July (1974).
- 3.125 MHD Electrical Power Generation 1972 Status Report, Section 4, pp. 350-377. Reprinted from Atomic Energy Review, Vol. 10, No. 3, IAEA, Vienna (1972).
- 3.126 D.T. Beecher, Study of Advanced Energy Conversion Techniques for Utility Applications Using Coal and Coal-Derived Fuels, February Monthly Progress Narrative, NASA Contract No. NAS 3-19407, March (1975).
- 3.127 J.H. Stang, J.A. Simons, J.A. Demastry and J.M. Genco, Compatibility of Liquid and Vapor Alkali Metals with Construction Materials, DMIC Report 227, April (1966).
- 3.128 F.J. Hetzler and R.S. Young, "Sodium Mass Transfer: II Screening Test Data and Analysis, Volume 2 - Metallurgy," Report No. GEAP-3726 (Vol. 2), General Electric Co., Atomic Power Equipment Department, San Jose, Calif., USAEC Contract AT(04-3)-189, June (1962).

- 3.129 S.L. Schrock and G.A. Whitlow, "Corrosion Studies for the Sodium Cooled Fast Breeder Reactor Program," Reprinted from Corrosion Problems in Energy Conversion and Generation, pp. 225-239.
- 3.130 W.E. Berry, Corrosion in Nuclear Applications, Chapter 4, "Corrosion by Liquid Metals," J. Wiley & Sons Inc., New York (1971).
- 3.131 R.N. Lyon, Liquid Metals Handbook, Second Edition, Sponsored by the Committee on Basic Properties of Liquid Metals, Office of Naval Research, Department of the Navy in Collaboration with the Atomic Energy Commission and the Bureau of Ships, Department of the Navy, pp. 158-161, June (1952).
- 3.132 W.D. Tuohig, J.T.A. Robers and R.N. Singh, "Materials Studies in Support of Liquid Metal MHD Systems, 14th Symposium - Engineering Aspects of Magnetohydrodynamics, Tullahoma, Tenn., April (1974) p. IV.10.1
- 3.133 J.W. Mausteller, F. Tepper and S.J. Rodgers, Alkali Metal Handling and System Operating Techniques, Chapter 7, "System Operation," Gordon and Breach, Science Publishers, New York (1967).
- 3.134 D.W. Shannon and W.R. Wykoff, Sodium Technology, Nuclear Engineering International, August (1972) pp. 627-628.
- 3.135 O.J. Faust (Ed.), Sodium-NaK Engineering Handbook, Vol. 1, Sodium Chemistry and Physical Properties, Gordon and Breach, Science Publishers, New York (1972) pp. 237-243.
- 3.136 P.A.F. White and S.E. Smith, Inert Atmospheres, Butterworth & Co., Ltd. London (1962).
- 3.137 Westinghouse Letter Contract AT(04-3)-962 under General Electric Contract AT(04-3)-893 Task 10 LMFBR Steam Generator Development Program.
- 3.138 J.M. McKee, D.R. Vissers, P.A. Nelson, B.R. Grundy, E. Berkey and G.R. Taylor, "Calibration Stability of Oxygen Meters for LMFBR Sodium Systems," to be published in Nuclear Technology, (1974).
- 3.139 R.E. Witkowski, E. Berkey and B.R. Grundy, "An On-Line Meter for the Measurement of Hydrogen in Liquid Sodium Systems," ANS Trans., 14, No. 1, p. 234, June (1972).
- 3.140 R.E. Witkowski, W.H. Reed, J.E. Bauerle and E. Berkey, "On-Line Analytical Instrumentation for Monitoring the Oxygen and Hydrogen Levels in the Sodium Coolant of Liquid Metal Fast Breeder Reactors," Westinghouse Research Labs Unrestricted Scientific Paper 73-1B6-HYMET-P1, November (1973).

- 3.141 W.H. Reed, J.E. Bauerle, E. Berkey, "A Thermal Ionization-Type Leak Detector for Sodium Vapor and Aerosol," ANS Trans., Vol. 18, pp. 102-103, June (1974).
- 3.142 A. Pebler, "Mass Spectrometric Trace Gas Analysis in Steam," Paper No. 381, 1974 Pittsburgh Conference on Analytical Chemistry and Applied Spectroscopy, March (1974), Cleveland, Ohio.
- 3.143 D.L. Smith and K. Natesan, "Influence of Nonmetallic Impurity Elements on the Compatibility of Liquid Lithium with Potential CTR Containment Materials," Nuclear Technology, Vol. 22, pp. 392-404, June (1974).
- 3.144 J.B. Dicks et al, "The Direct-Coal-Fired MHD Generator System," 14th Symposium on Engineering Aspects of MHD, April (1974).
- 3.145 AVCO Everett Laboratories, "Development Program for MHD Power Generation," Monthly Progress Report, OCR Contract 14-32-0001-1208, February (1974).
- 3.146 C.D. Maxwell, S.T. Demetriodes and S.R. Davis, "Resistive Coatings Over MHD Electrodes - Theoretical and Experimental Studies," 14th Symposium on Engineering Aspects of MHD, April (1974).
- 3.147 H.K. Bowen, J.W. Halloran and W.T. Petuskey, "Chemical Stability and Degradation of MHD Electrodes," in Corrosion Problems in Energy Conversion and Generation, Electrochemical Society, October (1974).
- 3.148 S.J. Schneider, "Materials Properties Determination: Transport Properties, Phase Equilibria and Slag Properties," NSF-OCR Workshop on MHD Materials, November (1974).
- 3.149 S.J. Schneider et al., "High Temperature MHD Materials," NBSIR 74-543, September (1974).
- 3.150 J.L. Bates, "Properties of Molten Coal Slags Relating to Open Cycle MHD," Progress Report No. 1, NSF Grant GI-44100, (1975).
- 3.151 W.D. Callister, Jr., M. Fisher, I.B. Cutler and R.W. Ure, Jr. "Corrosion of MHD Preheater Materials in Coal Slag-Seed Mixtures, 14th Symposium on Engineering Aspects of MHD, April (1974).

- 3.152 B.R. Rossing, J.A. Dilmore, S. Way and W.E. Young, "Corrosion Resistance of MHD Generator Materials to Slag-Seed Mixtures, 6th Int'l Conf on MHD Electrical Power Generation, June (1975).
- 3.153 H.P.R. Frederikse, W.R. Hosler, and N.L. Loeffler, "Testing and Test Analysis of MHD Materials," NSF-OCR Workshop on MHD Materials.
- 3.154 J.F. Louis, (Ed.) "Open Cycle Coal Burning MHD Power Generation: An Assessment and a Plan for Action," MIT Report prepared for OCR, Juen (1971).
- 3.155 H.P. Hoy, A.G. Roberts and D.M. Wilkins, "Coal Combustion," Chapter 4 in Open Cycle MHD Power Generation, (J.B. Heywood and G.J. Womack, Eds.), (1969)
- 3.156 J.J. Laeey, J.J. Demeter and D. Bienstock, "Production of a Clean Working Fluid for Coal-Burning Open Cycle MHD Power Generation," 12th Symposium on the Engineering Aspects of MHD (1972).
- 3.157 S.A. Tager, E.V. Samuilov, I.B. Rozhestvensky, R.V. Talumaer, and F.M. Jakhalevich, "Development and Investigation of High Temperature Combustor to be Used for a Solid Fuel MHD Generator and Thermodynamic Analysis of Combustion Conditions," 5th Int'l Conf. on MHD Electrical Power Generation (1971).
- 3.158 S.A. Tager, 1st US-USSR Colloquium on MHD, Moscow, February (1974).
- 3.159 J.B. Heywood, W.T. Norris and A.C. Warren, "Electrodes and Insulators," Chapter 5 in Open Cycle MHD Power Generation, J.B. Heywood and G. J. Womack, Eds.), (1969)
- 3.160 M. Berberian and R.W. Ure, Jr., "MHD Materials: Electrode and Insulator Materials - A Literature Survey," Univ. of Utah College of Engineering Report UTEC MSE 73-068, March (1973).
- 3.161 L.L. Fehrenbacher and N.M. Tallen, "Electrode and Insulation Materials in Magnetohydrodynamic Generators," in Ceramics in Severe Environments, (W.W. Kriegel and H. Palmovr III, Eds.) (1971).
- 3.162 A.I. Rekov, Materials for MHD Generator Channels (1960) (Translation available through NTIS as report # JPRS 53939).
- 3.163 C.L. McDaniel and E.R. Plante, "Phase Relations Involving Seed-Electrode-Insulator Materials in MHD," 14th Symposium on Engineering Aspects of MHD, April (1974).



- 3.164 J.F. Louis, J. Lothrop and T.R. Brogan, "Fluidynamic Studies with and MHD Generator," *Physics of Fluids* 1, (1964) p. 62
- 3.165 T. Bone et al, "Experiences with the Open Cycle MHD Facility VEGAS," 12th Symposium on Engineering Aspects of MHD, April (1972).
- 3.166 A. Sheyndlin, 1st US-USSR Colloquium on MHD, Moscow, February (1974).
- 3.167 P. Goolsby, Reynolds Aluminum Co., U.S. Patent # 3,710,152.
- 3.168 V.G. Gordon et al., "Oxide and Carbide Materials as MHD Electrodes," 4th Int'l. Conf. on MHD Electrical Power Generation, Warsaw (1968).
- 3.169 D.B. Meadowcroft, "Electronically-Conducting Refractory Ceramic Electrodes for Open Cycle MHD Power Generation," *Energy Conversion* 8, 1968, p. 185.
- 3.170 D.B. Meadowcroft, "Some Properties of Strontium-Doped Lanthanum Chromite," *Brit. J. Appl. Phys.* 2, (1969) p. 1225.
- 3.171 G.P. Gokhshteyn, A.A. Safanov and V.P. Lyubimov, "On the Physical and Chemical Behavior of the Electrodes of an MHD Generator Made of  $ZrO_2-Y_2O_3$  and  $ZrO_2-CeO_2$ , in MHD Method of Producing Electrical Energy, (V.A. Kirillin and A. Y. Sheyndlin, Eds.) (1972).
- 3.172 R.S. Skibitskaya and Y.I. Aleksandrova, (Eds.), 1973 Annual Report of the Institute of High Temperatures of the USSR Academy of Sciences (1974). (English Translation available from NTIS as Report SPRS 64042).
- 3.173 G.P. Gokhshteyn and A.A. Safonov, "Operation of a Refractory Ceramic Electrode in an MHD Generator," *Inorganic Materials*, 7, (1971) p. 582.
- 3.174 R.E.W. Casselton, "Blackening in Yttria Stabilized Zirconia Due to Cathodic Processes at Solid Platinum Electrodes," *J. Applied Electrochemistry*, 4, (1974) p. 25
- 3.175 G. Johnson, E.P. Tuffy and D. Balfour, "Development and Testing of High Temperature Electrodes Based on Stabilized Zirconia," 4th Symposium on MHD Power Generation, Warsaw, (1968).
- 3.176 G. Telegin, High Temperature Institute, US/USSR Cooperative Exchange in MHD Power Generation, Washington, D.C., April (1975).
- 3.177 1972 Annual Report of the Institute of High Temperatures of the USSR Academy of Sciences, 1973. (English Translation available from NTIS as Report JPRS 983).

- 3.178 D.B. Meadowcroft and J. Wimmer, "Volatile Oxidation of Lanthanum Chromite," Paper 87-B-73, 75th Annual Meeting of the American Ceramic Society, April (1973).
- 3.179 D.B. Meadowcroft and J. Wimmer, U.S. Air Force Materials Laboratory, Private Communication (1973).
- 3.180 S. Rohatgi, Indian Atomic Energy Commission, Private Communication (1974).
- 3.181 T. Fukui et al., "Corrosion Resistance of Refractory Materials for High Temperature Regenerators" 5th Int. Conf. on Elect. Power Generation, Munich (1971).
- 3.182 A. Nagahiro et al., "Preparation and Test of Refractory Materials for Heater Bed in Regenerator of MHD Power Plant," 4th Int'l. Conf. on MHD Electrical Power Generation, Warsaw, (1968).
- 3.183 A. Dubois and M. Hamar, "Corrosion of Refractories by Potassium Seed Combustion Gases," Int'l. Conf. on MHD Electrical Power Generation, Paris (1964).
- 3.184 Y. Furuse et al, "Study on Refractory Materials for the MHD Electric Power Generation; Part 3: Electrical Behavior of Various Types of MgO Refractories, Reports Res. Lab Asahi Glass Co., Ltd., 20 (1970) p. 33.
- 3.185 D.A. Vysotskiy et al., "Materials Based on High Melting Oxides in the Insulating Walls of the Channel of an MHD Generator," in The MHD Method of Producing Electrical Energy, (V.A. Kirillin and A. Y. Sheyndlin, Eds.) (1972).
- 3.186 Experimental Research on Model MHD Generator U-02, Institute of High Temperatures of the USSR Academy of Science, Moscow (1973) (English translation available from NTIS as Report JPRS 60972).
- 3.187 Y. P. Kukota, V.K. Osadchy and G.M. Stschegolev, "MHD Generator with Channel Walls Protection by Blowing In," 5th Int'l Conf. on MHD Electrical Power Generation, Munich (1971).
- 3.188 G.V. Samsonov, et al., "Research On Materials for Open-Cycle MHD Generator Electrodes," 5th Int'l Conf. on MHD Electric Power Generation, Munich (1971)
- 3.189 F.A. Hals, "Magnetohydrodynamic Power Generation," Paper 67 PWR-12, ASME-IEEE Joint Power Generation Conference, Detroit, Michigan September(1967).
- 3.190 D.P.H. Hasselman, "Unified Theory of Thermal Shock Fracture Initiation and Crack Propagation in Brittle Ceramics," J. Amer. Cer. Soc., 52, (1969) p. 600.

- 3.191 D.R. Larson, J.A. Coppola, and D.P.H. Hasselman, "Fracture Toughness and Spalling Behavior of High -  $\text{Al}_2\text{O}_3$  Refractories," J. Amer. Ceramic Society, 57, (1974) p. 417.
- 3.192 F.H. Norton, Refractories, (1968).
- 3.193 R. Goodof and D.R. Uhlmann, "Thermal Shock Resistance of Air Preheater Materials," 14th Symposium on Engineering Aspects of MHD, April (1974).
- 3.194 R.J. Rosa, "Design Considerations for Coal Fired MHD Generator Ducts," 5th Int'l. Conf. on MHD Electrical Power Generation, Munich (1971).
- 3.195 Phase Diagrams for Ceramists, (E.M. Levin, C.R. Robbins, and H.F. McMurdie, Eds.) (1966 and 1969).
- 3.196 W.D. Kingery, "Corrosion of Refractories by Liquid Melts," in High Temperature: A Tool for the Future, (1956).
- 3.197 H.K. Bowen, "MHD Channel Materials Development Goals," NSF-OCR Workshop on MHD Materials, November (1974).
- 3.198 H.P.R. Frederikse and W.R. Hosler, "Electrical Conductivity of Coal-Slag," J. Amer. Ceramic Soc., 54, (1973), p. 418.
- 3.199 S. Way, Westinghouse Electric Corp., Private Communication (1972).
- 3.200 B.R. Rossing and T.K. Gupta, "The Role of Processing in the Development of Generator Components," NSF-OCR Workshop on MHD Materials, November (1974).
- 3.201 C.R. Tinsley, "R&D Testing of  $\text{Y}_2\text{O}_3$  Stabilized Matrix Bricks in the Pilot Test Unit (PTU) at AEDC," Report AEDC-TR-72-161, November (1972).
- 3.202 Research on the U-25 Apparatus (1972), (Translation available from NTIS as Report JPRS 59983.)
- 3.203 W. Brzozowski, et al., "The Results of Initial Experiments on the 3MW MHD Installation at Swierk," 5th Int'l Conf. on MHD Power Generation, Munich (1971).
- 3.204 N. Ault, "Product Definition and Processing for Air Preheaters," NSF-OCR Workshop on MHD Materials, November (1974).
- 3.205 J.L. Bates, "Material Development Goals for Open-Cycle, MHD Air Preheaters," NSF-OCR Workshop on MHD Materials, November (1974).

- 3.206 G.J. Womack, "Directly Fired Air Heaters, Chapter 2, in Open Cycle MHD Power Generation, (J.B. Heywood and G.J. Womack, Eds.) (1969)
- 3.207 L.J. Trostel, "Deformation of Oxide Refractories," Symposium on Deformation of Oxide Materials, Pennsylvania State University, July (1974).
- 3.208 R.E. Gannon, F.A. Hals, and H.H. Reynolds, "Corrosion Studies in Materials for Auxiliary Equipment in MHD Power Plants," in Corrosion Problems in Energy Conversion and Generation, Electrochemical Society, October (1974).
- 3.209 I.S. Mayauskas, R. I. Abraitis, A.G. Karaulov and A.A. Grebenyuk, "Action of High Temperature Gas Streams of Zirconia Refractories,"
- 3.210 P.D. Bergman, J.I. Bergman, R.J. Joubert, R.J. Demski and D. Bienstock, "Design of Heat Recovery and Seed Recovery Units in MHD Power Generation," NSF-OCR- Workshop on MHD Materials, November (1974).
- 3.211 W.T. Reid, External Corrosion and Deposition, (1971).
- 3.212 J.W. Laxton and C.G. Stevens, "Steam Plant Equipment," Chapter 10, in Open Cycle MHD Power Generation, (J.B. Heywood and G.J. Womack, Eds.) (1969).
- 3.213 F. A. Hals, L. Keefe and A. ElBindari, "Studies of Seed Recovery and Corrosion in Coal Fired MHD Power Plants," Presented at Winter Annual Meeting ASME, Nov-Dec (1964), Paper No. 64-AA/Ener-5.
- 3.214 D. Bienstock, R.J. Demski and R.C. Corey, "Corrosion of Heat Exchanger Tubes in a Simulated Coal-Fired MHD System" Trans. ASME, J. Engr. for Power, 93, Series A, No. 2, April (1971), p. 249.
- 3.215 R.L. Klueh and D.H. Jansen, "Effects of Liquid and Vapor Cesium on Structural Materials," ORNL-TM-1813, (1967).
- 3.216 E.S. Keddy, "Compatibility Evaluation of Materials with Cesium," LAMS Report 2948, (1963).
- 3.217 J.H. Stang, E.M. Simons, J.A. DeMastry and J.M. Geneo, "Compatibility of Liquid and Vapor Alkali Metals with Construction Materials," DMIC Report 227, (1966).

- 3.218 J.A. DeMastry and N.M. Griesenauer, "Refractory Metals in 1370 to 1870°C Cesium Vapor," presented at the AEC-NASA Liquid Metal Corrosion Meeting, Gatlinburg, Tenn. (1965).
- 3.219 P.M. Winslow, "Synopsis of Cesium Compatibility Studies," Presented at AEC-NASA Liquid Metal Corrosion Meeting, Gatlinburg, Tenn. (1965).
- 3.220 R.G. Smith, F. Hargreeves, G.T.J. Mayo and A.G. Thomas, "A Study of the Compatibility of Thermionic Converter Materials with Cesium," J. of Nuclear Materials, 10, (1963) 191.
- 3.221 F. Hargreeves, G.T.J. Mayo, and A.G. Thomas, "A Study of the Long Term Compatibility of Thermionic Converter Materials with Cesium," J. of Nuclear Materials, 18, (1966) 212.
- 3.222 M.J. Slivka, "A Study of Cesium Vapor Attack on Thermionic Converter Construction Materials," Advanced Energy Conversion, 3, (1963) p. 157.
- 3.223 W.B. Hall and S.W. Kessler, "Cesium Compatibility of Thermionic Converter Structural Materials," N65-33774 (1963).
- 3.224 F. Tepper and J. Greer, "Factors Affecting the Compatibility of Liquid Cesium with Containment Metals," AFML-TR-64-327 (1964).
- 3.225 W.T. Chandler and N.J. Hoffman, "Effects of Liquid and Vapor Cesium on Container Metals, ASD-TDR-62-965 (1963).
- 3.226 W.E. Berry, Corrosion in Nuclear Applications, J. Wiley & Sons, Inc., (1971).
- 3.227 R.L. McKisson, R.L. Eichelberger, R.C. Dahleen, J.M. Scarborough and G.R. Argue, "Solubility Studies of Ultra-Pure Transition Elements in Ultra Pure Alkali Metals," NASA-CR-610 (1966).
- 3.228 S. Stecura, "Solubilities of Molybdenum and Tungsten in Liquid Potassium," NASA Tech. Note D-5504 (1969).
- 3.229 R.L. Eichelberger, R.L. McKisson and B.G. Johnson, "Solubility of Refractory Metals and Alloys in Potassium and in Lithium," NASA CR-1371 (1969).
- 3.230 I.R. McNab, J.S. Dolby, and M.G. Haines, "Ionization, Recombinations and Voltage Drop Measurements in a Closed Cycle MHD Generator," 14th Symposium on Engineering Aspects of Magnetohydrodynamics, Tullahoma, Tenn. pp. VII.3.1 - VII.3.6, April (1974).

- 3.231 R.J. Sovie and L.D. Nichols, "Closed Cycle MHD Power Generator Experiments in the NASA Lewis Facility," 14th Symposium on Engineering Aspects of Magnetohydrodynamics, Tullahoma, Tenn., pp. VII.6.1 - VII.6.5, April (1974).
- 3.232 P.E. Kueser, et al., "Bore Seal Technology Topical Report," NASA CR-54093, December (1964).
- 3.233 T. Bohn, S. Forster, K. Grawatsch and S.W. Angewante, Magnetohydrodynamik, No. 3 (1967).
- 3.234 N.N. Gribov, Y.A. Dushin, L.I. Emel'yanova and Y.V. Solomko, "Performance of Molybdenum Alloys in a High Temperature Closed Cycle Plant with an Inert Gas," High Temperature, 12 (1974). p. 555.
- 3.235 A. Y. Borisov, et al., "Behavior of Refractory Metal Electrodes in an Argon Plasma," 5th Int'l. Conf. on MHD Electrical Power Generation, Warsaw, (1968).
- 3.236 W.T. Grubb and L.W. Niedrach, "Fuel Cells," in Direct Energy Conversion, (G.W. Sutton Ed.) McGraw-Hill Co., New York (1966).
- 3.237 L.G. Austin, "Fuel Cells," A Review of Government-Sponsored Research, (1950-1964) NASA SP-120 (1967).
- 3.238 L.G. Austin, "Fuel Cells: A Progress Report," Chem. Engr. June (1969) p. 81-85.
- 3.239 E.J. Cairns and H. Shimutake, "Recent Advances in Fuel Cells and Their Application to New Hybrid Systems," in Fuel Cell Systems-II, Adv. in Chem. Ser. 90, pp. 392-425, Am. Chem. Soc. (1969).
- 3.240 G. Sandstede, "Introduction: Types of Fuel Cells," in From Electrocatalysis to Fuel Cells, (G. Sandstede, Ed.) p. xiii to xxv, University of Washington Press (1972).
- 3.241 J.D.M. Bockris, J. McHardy and R. Sen, "Some Basic Aspects of Electrocatalysis," in "From Electrocatalysis to Fuel Cells (G. Sandstede, Ed.) p. 385-409, University of Washington Press (1972).
- 3.242 M.I. Gillibrand and G.R. Lomax, "Factors Affecting the Life of Fuel Cells," in Proc. of the 20th Annual Power Sources Conf. May (1966) pp. 24-28.

- 3.243 D.H. Archer, L. Elikan and R.L. Zahradnik, Proc. Symp. on Hydrocarbon Air Fuel Cells, 9, No. 3, Part I (1965).
- 3.244 C.S. Tedman, Jr., H.S. Spacil and S.P. Mitoff, "Cathode Materials and Performance in High-Temperature Zirconia Electrolyte Fuel Cells," J. Electrochem. Soc., Electrochemical Science, September (1969) Vol. 116, No. 7, pp. 1170-1175.
- 3.245 J. Weissbart and R. Ruka, "Solid Oxide Electrolyte Fuel Cells," in Fuel Cells (G.J. Young, Ed.) Reinhold Publ. Corp. (1963). pp. 37-49.
- 3.246 H. Tannenberger and H. Siegert, "The Behavior of Silver Cathodes in Solid Electrolyte Fuel Cells," in Fuel Cell Systems-II, Adv. in Chem. Ser. 90, pp. 281-300, Am. Chem. Soc., (1969).
- 3.247 E.F. Sverdrup, D.H. Archer and A.D. Glasser, "Stannic Oxide and Indium Oxide Films as Air Electrodes for High Temperature Coal Reacting Fuel Cells," in Fuel Cell Systems-II, Adv. in Chem. Ser. 90, pp. 301-314, Am. Chem. Soc. (1969).
- 3.248 Final Report Project Fuel Cell, Research & Development Report No. 57, Contract No. 14-01-0001-303 OCR, Department of the Interior, (1970).
- 3.249 E.F. Sverdrup, C.J. Warde, and A.D. Glasser, "A Fuel-Cell Power System for Central-Station Power Generation Using Coal as a Fuel," in From Electrocatalysis to Fuel Cells," (G. Sandstedt, Ed.) pp. 255-277, University of Washington Press (1972).
- 3.250 H. Tannenberger, "Problems of High Temperature  $ZrO_2$  - Solid Electrolyte Fuel Cells," in From Electrocatalysis to Fuel Cells, (G. Sandstedt, Ed.), pp. 235-246, University of Washington Press (1972).
- 3.251 D.W. Strickler and W.G. Carlson, "Ionic Conductivity of Cubic Solid Solutions in the System  $CaO-Y_2O_3-ZrO_2$ ," J. Am. Cer. Soc., Vol. 47, No. 3, (1964) pp. 122-127.
- 3.252 A.D.S. Tantram, A.C.C. Tseung, and B.S. Harris, "Some Aspects of Molten Carbonate Fuel Cells," in Hydrocarbon Fuel Cell Tech., (B.S. Baker, Ed.) Academic Press, New York, (1965), pp. 187-212.
- 3.253 G.H.J. Broers and M. Schenke, "Long-Run Experiments on High-Temperature Molten Carbonate Fuel Cells," in Hydrocarbon Fuel Cell Technology, (B.S. Baker, Ed.) Academic Press, New York (1965), pp. 225-250.

- 3.254 I. Trachtenberg, "Hydrocarbon-Air Fuel Cells Employing Slurried Molten Carbonate Electrolyte," in Hydrocarbon Fuel Cell Technology, (B.S. Baker, Ed.), Academic Press, New York (1965). pp. 251-265.
- 3.255 G.H.J. Broers and M. Schenke, "Recent Developments in High-Temperature Fuel Cell Research in the Netherlands," in Fuel Cells (G.J. Young, Ed.), Reinhold Publ. Corp., (1963), pp. 6-23.
- 3.256 A. Burucka, "Single Gas Electrodes in Molten Carbonates," in Fuel Cell Systems-II, Adv. in Chem. Ser. 90, pp. 242-248, Am. Chem. Soc. (1969).
- 3.257 I. Trachtenberg and D.F. Cole, "Electrolyte Studies for Molten Carbonate Fuel Cells," in Fuel Cell Systems-II, Adv. in Chem. Ser. 90, pp. 354-365, Am.Chem. Soc. (1969).
- 3.258 D.Y.C. Ng and D.K. Fleming, "Reformed Natural Gas, Acid Matrix Fuel Cell Batteries," in Fuel Cell Systems-II, Adv. in Chem. Ser. 90, pp. 354-365, Am. Chem. Soc. (1969).
- 3.259 H. Binder, A. Kohling, W.H. Kuhn, W. Lindner, and G. Sandstede, "Hydrogen and Methanol Fuel Cells with Air Electrodes in Alkaline Electrolyte," in From Electrocatalysis to Fuel Cells, (G. Sandstede, Ed.), pp. 131-141-, Univ. of Washington Press (1972).
- 3.260 H. Binder, A. Kohling, and G. Sandstede, "Raney Catalysts," in From Electrocatalysis to Fuel Cells (G. Sandstede, Ed.) pp. 15-31, Univ. of Washington Press, (1972).
- 3.261 H.P. Landi, J.D. Voorhies, and W.A. Barber, "A Novel Air Electrode," Fuel Cell Systems-II, p. 13-23, Adv. in Chem. Ser. 90, Am. Chem. Soc., Wash. D.C., (1969)
- 3.262 K.V. Kordesch, "Outlook for Alkaline Fuel Cell Batteries," in From Electrocatalysts to Fuel Cells, (G. Sandstede, Ed.) pp. 157-167, Univ. of Washington Press, (1971)
- 3.263 K.V. Kordesch, "Carbon-Air Electrode for Low Temperature Fuel Cells," in Hydrocarbon Fuel Cell Technology, (B.S. Baker, Ed.) Academic Press, New York (1965) pp. 17-23.